UC Berkeley
UC Berkeley Electronic Theses and Dissertations

Title
Establishment of Human Brain Organoid Models of Tuberous Sclerosis

Permalink
https://escholarship.org/uc/item/1hg258hj

Author
Blair, John Donald

Publication Date
2020

Peer reviewed|Thesis/dissertation

eScholarship.org Powered by the California Digital Library
University of California

Establishment of Human Brain Organoid Models of Tuberous Sclerosis

By

John Donald Blair

A dissertation submitted in partial satisfaction of the
requirements for the degree of
Doctor of Philosophy
in
Molecular and Cell Biology
in the
Graduate Division
of the
University of California, Berkeley

Committee in Charge:

Professor Helen Bateup, Chair
Professor John Ngai
Professor David Schaffer
Professor Roberto Zoncu

Summer 2020

ABSTRACT

Establishment of Human Brain Organoid Models of Tuberous Sclerosis

By

John Donald Blair

Doctor of Philosophy in Molecular and Cell Biology

University of California, Berkeley

Professor Helen Bateup, Chair

Tuberous Sclerosis (TSC) is a multisystem developmental disorder, which is associated with early-onset epilepsy, varying degrees of intellectual disability and high risk for psychiatric conditions including autism. It is defined by the presence of “cortical tubers”, which are focal cortical malformations composed of dysplastic neurons and astrocytes that can become seizure foci. TSC is caused by mutations in either *TSC1* or *TSC2*, which encode for proteins forming a complex that is a negative regulator of mTORC1, a key cellular signaling node controlling cell growth and metabolism. Animal models have greatly increased our understanding of TSC; however they fail to recapitulate some of the key neuropathological features, namely the cortical tubers. This may be due to the contracted timeframe over which rodent cortical development occurs (days) compared to human cortical development (months) as well as the presence of human-specific progenitor cells. My research goal was to overcome these limitations by creating a human neuronal model of TSC that develops on a human timescale and recapitulates key features of early human cortical development.

I used CRISPR/Cas9 to create an isogenic panel of human embryonic stem cell lines harboring heterozygous or homozygous loss-of-function mutations in *TSC1* or *TSC2*. I differentiated these cells into 3D cortical spheroids over five months in culture to model mid-gestational human fetal development. I found that while early forebrain development was largely normal, *TSC1*$^{-/-}$ or *TSC2*$^{-/-}$ cells in five-month-old spheroids were highly abnormal. Specifically, loss of function of TSC1/2 led to the formation of highly enlarged, dysplastic cells that strongly resembled the cortical tuber cells seen in patients. Furthermore, I revealed a significant differentiation bias of *TSC1/2* mutant cells towards glial cell fates and away from neuronal fates, again reflecting what is seen in patient cortical tubers.

Cortical tubers are thought to arise due to a “second-hit” somatic mutation during progenitor cell proliferation that results in loss of heterozygosity. I further refined our human TSC model to mimic a somatic second-hit event, by generating a *TSC2*$^{c/-}$ stem cell line, in which all cells were heterozygous for *TSC2* but would undergo biallelic inactivation in the presence of Cre recombinase. I also engineered a fluorescent Cre-reporter into these cells to enable lineage tracing of *TSC2*$^{-/-}$ cells over time. I found that cells with a second-hit mutation in *TSC2* were large, dysplastic and primarily expressed

glial markers, while the adjacent *TSC2*$^{+/-}$ cells showed normal morphology and development, mimicking a cortical tuber. Chronic treatment with rapamycin, a potent mTOR inhibitor, starting early in development rescued tuber cell morphology and caused marked shifts of differentiation towards a neuronal fate in both *TSC2*$^{+/-}$ and *TSC2*$^{-/-}$ cells, demonstrating mTORC1's bidirectional control over human neuronal differentiation.

To elucidate the developmental programs of normal human corticogenesis and how these are altered by loss of TSC2, I have performed an in-depth single cell RNA-sequencing analysis across development in *TSC2*$^{c/-}$ spheroids. My analysis has confirmed the differentiation bias of *TSC2*$^{-/-}$ cells away from neuronal cell fates and revealed that this becomes pronounced primarily after two months of differentiation, before which *TSC2*$^{+/-}$ and *TSC2*$^{-/-}$ cells share similar identities. Furthermore, I discovered novel genetic markers of *TSC2*$^{-/-}$ cells: CLU, PTGDS, APOE, B2M that may contribute to their aberrant differentiation. Together, my thesis research has established novel, validated human brain spheroid models for TSC, which have generated new insights into the early molecular, cellular, and developmental mechanisms contributing to both normal and abnormal human brain development.

Acknowledgments

I would like to acknowledge and thank all the individuals that have guided me, commiserated with me, comforted me and pushed me throughout my time at Berkeley.

Firstly, thank you to Helen for being such a wonderful mentor and taking a chance on me by hiring me in 2013 and by taking an even further chance by keeping me on as a graduate student in 2015. You have treated me with respect, collegiality and kindness since day one, and it is an honor to be one of your first students and to help lay the groundwork for some of your great scientific ideas. You started out as a great mentor and continue to be so – your future students are very lucky!

Secondly, to Dirk for being an excellent "unofficial" mentor. The techniques and expertise that you have shared with me will likely be the basis of my research for years to come and I cannot fully describe how much I have learned from you.

To the members of my committee – thank you for the very fruitful discussions we have at and outside of our official meetings. They have been tremendously helpful and enlightening.

To all the members of the Bateup Lab – thank you for putting up with my rants about trash, ordering, kitchen mess and everything in between. I swear I was just trying to make all our lives better. To DK, no matter where you are, whether it's one bench away or all the way across the bay, you'll always be with me and you'll always be my brother.

To the members of the Hockemeyer Lab, thank you for letting me take up TC time and incubator space and feeders (SR, JB, KH + more) for 7 years and letting me come to your happy hours and giving me a lab away from lab, while still not making me study telomeres. Chiba and Franzi in particular – thank you for the one million beers – let's have one million more.

To the class of 2015 and the broader MCB community, thank you for being engaging and thoughtful, it's a great privilege to consider myself a part of this community. Thank you for inventing follies and pushing people to make better and better follies each year. While I never won a golden pipette, I am glad to have contributed to what was always the highlight of the year. To Avi, thank you for introducing me to follies when I was "just a tech" and continuing to be my follies partner for the subsequent years. When you graduated, my follies creativity died.

To all the non-science friends in my life, thank you for recognizing that yes I do have to go to work every day and that is perfectly normal (right?) and for giving me a refuge away from science, allowing me to develop a multi-dimensional personality.

To my parents, thank you for giving me a life without hardship while simultaneously, raising me to not ignore the hardship of others.

To my brothers, thank you for all the support and the visits, it is a huge advantage to know that you are on my team.

And finally, to Ellen – from when you professionally edited my grad school applications until our move across the country, you have always been there for me and I appreciate and love you so much. You give me a confidence every day that even if I fail, you will still support me regardless. From vacations, to quarantine to just generally spending our lives together, I have so much fun with you and am excited to spend my future with you as well.

Table of Contents

Chapter 1: **The Molecular Landscape of Tuberous Sclerosis**

Portions of this chapter were published as “New frontiers in modeling tuberous sclerosis with human stem cell-derived neurons and brain organoids” in *Developmental Dynamics*, 2020 Jan;249(1):46-55, by John D. Blair and Helen S. Bateup [2]. It has been reproduced in part here with full permission of the authors.

Prevalence and Pathology of TSC

Tuberous Sclerosis (TSC) is a multisystem developmental disorder that affects approximately 7-12 births per 100,000 in Western Europe and slightly fewer births elsewhere [3-5]. The most common manifestations of TSC include renal angiomyolipoma and renal cysts in the kidneys, lymphangioleiomyomatosis in the lungs, angiofibromas on the skin and subependymal giant astrocytomas (SEGAs), subependymal nodes and cortical tubers in the brain [6]. Individuals with TSC are likely to have neurological symptoms including intellectual disability (~55% of cases) [7] and epilepsy (~85% of cases) [8]. The epileptic seizures that affect individuals with TSC are often focal seizures that originate from cortical tubers. Cortical tubers, from which TSC gets its name, are regions of dysplastic and dysmorphic astrocytes and neurons that appear stochastically during neurodevelopment and are detectable on an MRI [9].

mTORC1 signaling and the TSC complex

Genetically, TSC is caused by mutations in *TSC1* [10] or *TSC2* [11], genes which encode for proteins that, along with TBC1D7 [12], form a heterotrimeric regulatory protein complex that represses mTOR Complex 1 (mTORC1) signaling [13] (Fig. 1). Within the complex, TBC1D7 binds to TSC1 and TSC1 binds to TSC2. TBC1D7 and TSC1 primarily function to stabilize the respective proteins they are bound to and thus stabilize the whole complex, permitting its activity [14, 15]. TSC2 is the catalytically active protein within the TSC complex, as well as the target for post-translational modifications that affect its activity. It acts as a signal integration hub and its activity can be modulated through phosphorylation by AKT (repressing), ERK1/2 (repressing), AMPK (activating) and GSK3-β (activating), among others [16]. When active, TSC2 acts as a GTPase activating protein (GAP) on the small GTPase, RHEB. RHEB is active in its GTP-bound form but interacting with TSC2 causes its GTP to be catalyzed into a GDP, inactivating it. In its GTP-bound form, RHEB activates mTORC1 [16].

mTORC1 is a key cellular signaling node whose primary role is to activate anabolic processes and repress catabolic processes through the serine/threonine kinase activity of requisite protein mTOR. The protein components of mTORC1 include RAPTOR (scaffolding protein), DEPTOR, PRAS40 (inhibitory proteins) and MLST8 [16]. When amino acids are abundant, mTORC1 is translocated to the lysosomal surface where it can be activated by RHEB. This process is mediated by a set of amino acid sensing proteins, Rag proteins and the Ragulator complex [17]. One key function of mTORC1 is to control protein synthesis, which it does through the phosphorylation of EIF4EBP1 and p70-S6K. In its unphosphorylated state, EIF4EBP1 binds to the

translation initiation factor EIF4E, preventing it from binding to the 5' end of mRNA transcripts, particularly those with a 5' TOP motif, and initiating translation [18]. The phosphorylated EIF4EBP1 cannot bind to EIF4E, allowing translation to be initiated. p70-S6K is a kinase that itself has many targets, among them, factors that initiate rRNA and tRNA transcription as well as other initiation factors and elongation factors [16]. A particularly robust target of p70-S6K is RPS6, a small subunit ribosomal protein, however the consequences phosphorylating RPS6 (p-S6) are unclear as mutations of the phosphorylation site do not appear to affect translation [19]. Complementary to promoting the anabolic process of protein synthesis, mTORC1 also represses the catabolic process of autophagy. Autophagy is the mechanism by which cellular material is broken down to its component parts for reuse. mTORC1 perturbs autophagy through the phosphorylation of ULK1 [20], which prevents ULK1's ability to promote autophagosome maturation [21]. It should also be noted that mTOR is the requisite protein of another complex, mTORC2, which shares the proteins DEPTOR and MLST8 with mTORC1 and uniquely possesses RICTOR, mSIN1 and PROTOR1/2 [16]. mTORC2 functions include phosphorylating AKT and actin cytoskeleton remodeling [22].

Much of mTORC1 activity under normal conditions comes from its role as a central signaling hub, receiving anabolic activating signals from growth factors and nutrients [16]. Perturbations of this activity can have major effects. One hallmark of high mTORC1 activity is increased cell size, likely due to increased cellular anabolic activity [23]. As much of growth factor signaling is integrated at the level of the TSC complex, mutations within TSC complex genes are especially potent in their ability to deregulate mTORC1 signaling. Neurological disorders caused by mutations in genes that feed into the mTORC1 signaling pathway are collectively known as "mTOR-opathies" and many of them have similar disease profiles [24]. For instance, some patients with focal cortical dysplasia (FCD) have somatic activating mutations in *MTOR* and present with cortical malformations that resemble cortical tubers and often have epileptic seizures [25]. Correspondingly, gain-of-function mutations in *RHEB* lead to similar pathologies [26]. Non-neurologically, mutations leading to increased mTORC1 activity often manifest as tumors [27], highlighting the importance of keeping mTORC1 well-regulated even outside of a developmental context.

The genetics of TSC and the second-hit hypothesis

The genetic mechanism leading to TSC and the formation of cortical tubers is still controversial. It is known that >95% of TSC patients have heterozygous mutations in either *TSC1* or *TSC2*, either germline or mosaic [28]. Hundreds of individual mutations have been identified, with most hypothesized to be loss-of-function mutations [29]; however this may be biased in that individuals with silent mutations in *TSC1/2* are not likely to have TSC and thus not be screened. Most mutations identified are in *TSC2*, (84.9% vs 12.1% in one study [28]) and *TSC2* mutations are generally associated with more severe phenotypes [29]. Due to the lack of uniformity in location, size or even presence of cortical tubers in TSC patients, it has been hypothesized that there must be an additional genetic insult (a "second-hit") in a subset of neural precursor cells that leads to cortical tubers [30]. A second-hit mechanism for TSC-associated tumors has

been verified through the sequencing of renal angiomyolipomas (RAs) found in the kidneys of TSC patients and SEGAs [28] where >85% of samples had mutations in both alleles of either *TSC1* or *TSC2*. In the same study, only 35% of cortical tubers had detectable second-hit mutations, an observation that was also reported in a prior study [31]. This could be due to technical reasons, such as focusing only on protein coding regions of the gene, or due to the nature of cortical tubers wherein only a small subset of cells within them have second-hit mutations. Thus, when performing bulk sequencing analysis, that signal gets masked by the heterozygous cells. Additionally, there may be cases where the second genetic mutation leading to cortical tuber formation occurs in a different gene within the mTORC1 pathway than the germline mutation, but still leads to a similar pathology. As a result, there is still an open question as to whether single, heterozygous mutations in *TSC1* or *TSC2* can lead to the formation of cortical tubers. Further support for the second-hit hypothesis comes from germline heterozygous rodent models that do not show cortical tuber-like pathologies, while animals that receive an *in utero* second-hit mutation produce dysplastic cortical cells that resemble those found in patient tubers [32].

Human Cortical Differentiation

To understand how mutations in *TSC1* or *TSC2* can lead to cortical tubers, it is important to understand how human cortical development occurs (Fig. 2). In the developing embryo, after the neural tube has developed and closed, multipotent neuroectodermal cells line up at the ventricular zone (VZ). These neuroectodermal cells are known as ventral radial glia (vRG), cells with long processes that reach from the ventricle, through the sub-ventricular zone (SVZ), all the way to the pial surface, creating a scaffold-like architecture [33]. In primates, these vRG can directly lead to outer radial glia (oRG), similar progenitor cells that migrate to the outer subventricular zone (oSVZ), but lose contact with the ventricle [34]. A key feature of RG is their ability to undergo asymmetric division, a mitotic process that maintains the identity of the parent cell, but also produces a daughter cell with a new identity. In early neurodevelopment, this is an intermediate progenitor cell (IPC). IPCs derived from vRG first migrate away from the VZ to the SVZ and then undergo several rounds of symmetric division before differentiating into neurons (or in a minority of cases, oligodendrocyte precursor cells (OPCs) [35]), while IPCs from the oRGs in the oSVZ remain in place, and undergo symmetric divisions. The number of rounds of division vary from species to species, and a greater number of divisions is one of the reasons for an enlarged cortex in primates compared to other mammals [34]. After the IPCs have undergone their terminal differentiation into neurons, the neurons migrate up the radial glial scaffold towards the pial surface, embedding themselves in the appropriate cortical layer depending on their time of birth [33]. During early and mid-development, some RGs also terminally differentiate into neurons, while later in development they terminally differentiate into astrocytes, non-neuronal cells that provide support, help maintain a homeostatic environment within the brain, and shape developing synapses and circuits [35]. It is presumed that all the neurons born during this process of forebrain cortical development are excitatory glutamatergic neurons, however there may be a small population of inhibitory, GABAergic neurons born as well [36]. Most cortical

inhibitory neurons, which are an integral part of the mature cortex, are born elsewhere (the preoptic area and Medial and Caudal Ganglionic Eminences) and later migrate into the cortex [37]. The timing of cortical development has been well documented in mice, with the first neurons being born at E11, the last neurons at E16 [38], while OPC differentiation (E11.5-E14.5 [35]) happens concurrently and astrocyte differentiation (E16 [39]) and cortical interneuron migration (E14.5-P2 [37]) happen later. In humans, this process takes several months, with only the approximate number of weeks describable for each milestone: first neurons (GW7), last neurons (GW15 [40]) and astrocytes (GW15 [41]).

Because newly born cortical neurons and astrocytes tend to mostly move radially away from the ventricle and not laterally [33, 35], it can be surmised that the thousands of cells in one small cortical area have likely come from the same progenitor cell pool. Per the second-hit hypothesis of cortical tuber formation, the second-hit happens in an RG sometime early in cortical development, giving rise to the population of cortical neurons and astrocytes that comprise the cortical tuber [30]. In this scenario, the number and developmental timing of second-hit mutations then dictates how numerous and large the tubers are in each patient. If the mutations happen very early or in a large number of progenitor cells, this is likely not compatible with a viable pregnancy, as it is known that germline loss of *Tsc1* or *Tsc2* in mice is embryonic lethal [42, 43]. The stochastic nature of cortical tubers makes it unlikely that they arise from the same heterozygous cells that lead to pathologically normal adjacent cortical tissue; however it is still unexplained why the *TSC1/2* genes are hotspots for genetic mutations.

Cortical tuber composition and pathology

The cellular composition of cortical tubers can be varied, however there are several pathological cell types that have been identified in tuber samples. Among these cell types there are dysplastic neurons, dysplastic astrocytes and giant cells, which all share the distinct quality of having greatly increased mTORC1 signaling as defined by increased p-S6 [44]. Variably interspersed amongst these cells are normal-appearing neurons, astrocytes and reactive astrocytes [45, 46]. Dysplastic neurons express the normal neuronal markers NeuN and synapsin, however their morphology is different from normal neurons, with larger cell bodies and thicker, larger and more branched cellular processes (dendrites and axons). Combined with their altered morphology, they also have differing expression of the postsynaptic AMPA and NMDA receptors, which may lead electrophysiological changes within the cells, potentially contributing to the seizures seen in TSC patients [44]. Dysplastic astrocytes also have altered morphology, however the effect of this on the activity of neighboring neurons is not clear and unlike morphologically similar “reactive” astrocytes, they do not express GFAP [44, 45]. The final pathological cell type, giant cells, are like dysplastic astrocytes in that they both express the neurofilament protein Vimentin, have altered expression of neurotransmitter receptors and do not express GFAP. Unlike dysplastic astrocytes, however, giant cells are often multinucleated and balloon-like in their morphology, with their effect on cortical activity also unknown [44].

Treatment of Tuberous Sclerosis

Currently, one of the most effective treatments for retractable TSC-associated epilepsy is surgical removal of the cortical tubers that lead to seizures. As this is a very invasive procedure with a good but still limited success rate [47], pharmacological interventions have been the focus of much research. The most studied pharmaceuticals have been general anti-epileptic drugs [48]; however another compound with promise is the potent mTORC1 inhibitor, rapamycin (trade name Sirolimus, and its chemically similar rapalogue, Everolimus. These are FDA approved drugs that are commonly used as immunosuppressants in preparation for organ transplant surgery [49]. To function as an mTORC1 inhibitor, rapamycin must first bind the endogenous protein FKBP12 which then binds to mTOR, preventing its ability to activate further substrates [50]. Rapamycin has shown promise as a topical treatment for angiofibromas in TSC patients [51], as well as a treatment paradigm for seizures TSC with a 40% seizure reduction in 40% of individuals with TSC-associated epilepsy [52]. In contrast, rapalogue treatment for neuropsychiatric symptoms of TSC has failed to show meaningful improvements, hypothesized to be due to the developmentally late commencement of the treatment and the restricted treatment time [53]. Other reasons may be the large chemical size of rapamycin, reducing its ability to cross the blood-brain barrier, necessitating either large oral doses or intracranial injections, and its limited temporal activity, necessitating chronic treatment which may have side effects [54]. Other pharmacological compounds have shown abilities to effectively repress mTORC1 activity including but not limited to Torin1 [55], an ATP competitor that also repressed mTORC2, and EN6, a lysosomal v-ATPase inhibitor [56], however these have yet to be included in clinical studies of TSC.

Rodent models of Tuberous Sclerosis

While much fundamental work in basic cellular biology of TOR signaling has been done in yeast and fruit flies [57, 58], the predominant models for studying neurological aspects of TSC have been mice and rats. Rodent models have provided key insights into the consequences of *Tsc1/2* loss on brain development and function. As germline knock-out mouse models demonstrated that complete loss of *Tsc1* or *Tsc2* is embryonic lethal [43] [42], subsequent conditional knock-out models of *Tsc1* [42] and *Tsc2* [59] have been developed. Different applications of Cre-recombinase using viral injections, in utero electroporation, or Cre-expressing mouse lines, have illuminated the effects of Tsc1 or Tsc2 loss on multiple neural cell types. Somatic mTOR-activating mutations have also been modeled in mice by sparse expression of mutant *Mtor*, constitutively active Rheb, or CRISPR/Cas9 constructs targeting *Tsc1* or *Tsc2* [60-63]. The Eker rat model of TSC, carrying a spontaneous loss-of-function mutation in *Tsc2* was shown to develop sporadic cytomegalic neurons, glia, and SEGAs in aged or irradiated young animals to induce a “second-hit” [32, 64, 65]. Collectively, these rodent studies have shown that loss of Tsc1/2 function impacts multiple processes happening at different developmental time points. These include altered neuronal differentiation, survival, migration, morphology, excitability, synaptic plasticity, glial function, and behavior [66-70]. In general, complete loss of *Tsc1* or *Tsc2* is required to observe strong disease-related phenotypes, however, heterozygous animals do exhibit some

changes in synaptic function, neuronal excitability, and behavior [71-74]. While these rodent models have been, and will continue to be powerful research tools, it is important to note that bona fide cortical tuber regions are not readily observed in animal models, suggesting that this pathology may result from unique aspects of human brain development.

Human pluripotent stem cell based neuronal disease modeling

Researching the molecular mechanisms of human neurological disorders can be difficult given the dearth of available human brain tissue and the difficulty of culturing primary human neurons. Currently the best way to approximate live human neuronal tissue is to culture human pluripotent stem cells (hPSCs) and differentiate them into a neuronal lineage. To create the genetic models of neurological disorders, one can either obtain somatic cells from patients and de-differentiate them back into pluripotent stem cells (induced pluripotent stem cells; iPSCs [75]) or genetically engineer known mutations into wild-type hPSCs. Genetically engineered hPSCs have an advantage in that it is possible to use the parent cell-line as an isogenic control, while the advantage of iPSCs is that their specific genetic background is known to lead to a disease state that can be directly tied to clinical data.

CRISPR/Cas9 gene editing technology is currently the most efficient way to genetically engineer hPSCs [76]. Targeted, but non-specific, gene disruptions can be achieved by using a single guide RNA expressed with the Cas9 protein and associated machinery. Alternatively, specific exon deletions leading to predictable gene disruptions can be created by using two guide RNAs, which cut out a specific piece of a gene [77, 78]. These methods require the isolation of single-cell derived colonies and subsequent PCR genotyping of those colonies to verify and establish the properly targeted new cell line [79]. Modeling the second-hit hypothesis in a disorder like TSC requires a more complex system than constitutive genetic mutations. To specifically address this, CRISPR/Cas9 can be used to add genetic constructs such as LoxP sites on either side of an exon, creating a conditional knockout [77, 80]. Additional genetic constructs, like fluorophores [76], differentiation factor cassettes [81] or even CRISPR constructs [82] themselves can also be added by including the gene-encoding template flanked by homologous DNA with the Cas9 and guide-RNA constructs. This approach uses the endogenous cellular homology-directed repair mechanism to incorporate the construct of interest into the desired site [83]. Screening for hPSCs that have incorporated the constructs can be done by including an antibiotic resistance cassette with the gene of interest and subjecting the targeted cells to antibiotic selection followed by PCR genotyping.

From hPSCs, two- (2-D) or three-dimensional (3-D) cultures comprising different lineages of neurons and glia can be established depending on the differentiation protocol employed. Cortical excitatory neurons and astrocytes of the telencephalic lineage are key cell types of relevance for TSC as the dysplastic cells in tubers are positive for glutamatergic and astrocytic markers [70]. These cell types can be generated through manipulation of endogenous neuro-ectodermal differentiation pathways either via inhibition of the dual-SMAD pathway [84] or overexpression of transcription factors [85]. Studies with cell type-specific conditional knock-out mice have

also highlighted cerebellar Purkinje cells as relevant to TSC pathophysiology, particularly the behavioral symptoms of autism [74, 86, 87]. A human cellular differentiation protocol based on the addition of specific growth factors has recently been established for cerebellar Purkinje cells and specifically applied to disease modeling in TSC [88].

While differentiation has traditionally been done in 2-D monolayer cultures, protocols have recently been adapted for 3-D differentiation to generate brain spheroids or organoids (collectively called spheroids here) [1, 89-91]. An advantage that 3-D brain models have over 2-D models include more complex cytoarchitecture and cellular niches that preserve cell-cell and cell-matrix interactions [92].

The approach of differentiating neurons and glia from human pluripotent stem cells generally operates on a human developmental timescale. For example, by transcriptional profiling, a 10-week-old human brain organoid is roughly equivalent to a 16-19 post-conception week human brain [1]. This enables the observation and manipulation of human neural development in approximately real-time. For this reason, neurodevelopmental disorders such as TSC are particularly well-suited to this disease modeling approach.

Human 2-D neuronal models of TSC

Forebrain excitatory neurons and glia

Alterations in differentiation, signaling, and gene expression

Initial work in developing human neural models of TSC has focused on the differentiation of genetically engineered hESCs [77, 93, 94], TSC patient-derived iPSCs [95-97] or gene edited TSC iPSCs [98] into 2-D forebrain cultures. These studies were undertaken using a variety of differentiation methods, investigating the effects of *TSC1* or *2* reduction on neural precursors, neurons, astrocytes and, in one case, oligodendrocytes [96].

Differentiation into neural precursors proceeded normally in each study with only minor differences observed such as increased neural rosette size in *TSC2*$^{-/-}$ cultures [93] and increased proliferation rate in *TSC2*$^{+/-}$ cultures [95], although this was not observed in other studies [97]. In contrast to this normal early neural differentiation, terminal differentiation into neurons proved highly problematic for cells with complete loss of TSC1/2 complex function. Specifically, *TSC2*$^{-/-}$ cultures produced significantly lower numbers of cells expressing the neuronal markers HuC/D [93]. Notably, loss of one copy of *TSC1* or *TSC2* was much less deleterious with cultures exhibiting either a minor decrease in HuC/D-positive cells [93, 97], or no decrease at all [96]. The differentiation defects in cells with loss of TSC1/2 may be due to a combination of increased neuronal death [93], delayed neuronal differentiation [97], or a shift towards astro-glial fate [93, 94]. Dissecting the potential mechanisms of altered differentiation will be an interesting avenue for future investigation with these models.

The expected hyperactivation of mTORC1, as indicated by increased p-S6, was observed in all studies, however the strong effects seen at every developmental stage in *TSC2*$^{-/-}$ cultures [93] were not consistently seen at the NPC stage in *TSC2*$^{+/-}$ cultures [77, 97]. Transcriptome analysis through RNA sequencing of patient iPSC-derived heterozygous NPCs found 513 differentially expressed transcripts compared to a sibling

control line. Gene ontology analysis indicated that these transcripts were primarily involved in neuron migration and development [97]. Independent RNA sequencing of isogenic, gene-edited *TSC2* heterozygous and homozygous cultures found very few differences between *TSC2*$^{+/-}$ and *TSC2*$^{+/+}$ cells (10 transcripts) but large differences between *TSC2*$^{-/-}$ and *TSC2*$^{+/+}$ with over 2000 transcripts differentially expressed [94]. It is possible that some of the differences between the patient iPSC and control line in the study by Zucco et al could be driven by genetic differences independent of the *TSC2* mutation. Analysis of additional TSC patient and control cell lines would be helpful to resolve this. In the *TSC2*$^{-/-}$ cultures in the Grabole et al study, groups of transcripts involved in astrogliosis, inflammation, and glycolysis were all upregulated, which corresponds to observations of poor mitochondrial function in gene edited iPSC-derived *TSC2*$^{-/-}$ neurons [98]. The transcriptome of *TSC2*$^{-/-}$ cultures also closely corresponded with previous microarray studies of cortical tubers and SEGAs [99, 100].

Given the key involvement of mTORC1 signaling in mRNA translation, translational profiling may reveal further differences in TSC neural cultures that may occur independently of transcriptional changes. This will be an interesting avenue for future exploration. Related to this, our recent study showed that mTORC1 signaling and translation of the translational machinery is high in human pluripotent stem cells but is suppressed during neural differentiation [101]. In addition, numerous changes in mRNA translation without a corresponding change in mRNA levels were observed across human neuronal development, highlighting the importance of translational control for developing neurons [101].

Impact on neuronal morphology and physiology

The most dramatic morphological differences were observed in homozygous *TSC2* knockout cells. *TSC2*$^{-/-}$ NPCs, neurons, and glia exhibited somatic hypertrophy and neurons displayed increased dendritic arborization [77, 93]. The effects of heterozygous *TSC1* or *2* loss were less clear for these cultures, with either no change in neuronal morphology [93, 97], minor increases in dendritic branching and no change in soma size [96] or increases in both [95]. One note is that the study by Li and colleagues was based on a single cell line from one TSC patient compared to an iPSC line from an unrelated individual. It therefore remains to be determined whether phenotypic differences between these cell lines are due to the *TSC2* mutation or a result of cell line variability or genetic background.

Electrophysiological phenotypes were probed in a subset of studies with either whole cell electrophysiology, multi-electrode arrays (MEA), or calcium imaging [93, 96]. Whole cell recordings showed a strong decrease in the frequency of spontaneous (sEPSCs) and miniature (mEPSCs) excitatory post-synaptic currents in both *TSC2*$^{+/-}$ and *TSC2*$^{-/-}$ neurons in a gene dose-dependent manner [93]. However, mEPSC amplitude was increased in *TSC2*$^{-/-}$ neurons, suggestive of increased synaptic strength. *TSC2*$^{-/-}$, but not *TSC2*$^{+/-}$ neurons also had significantly reduced intrinsic excitability, consistent with their morphological alterations and changes in passive membrane properties [93]. This decreased intrinsic and synaptic excitability in developing *TSC2*$^{-/-}$ neurons suggests that other circuit components, e.g. inhibitory neurons, may be required to generate hyperexcitability at the network level following loss of TSC1/2 function [102, 103]. By contrast, MEA recordings of heterozygous cultures from patient

TSC iPSCs did show increased spontaneous network activity, which was also reflected by the increased frequency, but not amplitude, of calcium transients in these cultures [96]. Discrepancies between these findings may reflect gene dose-dependent effects, cell line and culture variability (which could have significant effects on network activity levels and development), or inhibitory and excitatory neuron composition of the cultures, which was not explored in these studies.

Treatment with rapalogues and other mTOR inhibitors such as AZD-8055 reversed many of the phenotypes of TSC1 or 2 loss in forebrain neural cultures including altered electrophysiology [93, 96], aberrant morphology [93, 96], hyperactive mTORC1 signaling [93, 95, 97] and altered mRNA translation [94].

Cerebellar Purkinje cells

While forebrain excitatory cultures deficient in *TSC1* or *2* have been the primary focus of most studies thus far because of their potential to develop into cortical tuber-like cells, cerebellar tubers can also form in some TSC patients [104, 105]. In addition, mouse studies have demonstrated the importance of Tsc1/2 function in cerebellar Purkinje cells for autism-related behaviors [74, 86, 87]. To generate a cerebellar model for TSC, a human Purkinje cell differentiation protocol was developed and hiPSC lines from three individuals with TSC were generated, using cells from the parents or unaffected individuals as controls [88]. In addition, this study made use of an established *TSC2* heterozygous patient iPSC line, which had been further genetically engineered to create a $TSC2^{-/-}$ cell line together with a repaired $TSC2^{+/+}$ control cell line [98]. This strategy has significant advantages over the use of control iPSC lines from unrelated individuals as it provides an isogenic system in which cells have the same genetic background and differ only in the disease gene.

In this model, many of the same phenotypes as in forebrain cultures were observed including increased rates of NPC proliferation, upregulated expression of astroglial markers, increased cell death, increased cell size, hyperactivation of mTORC1 activity and decreased excitability of differentiated neurons [88]. These properties were observed in both heterozygous and homozygous cultures with more severe deficiencies in $TSC2^{-/-}$ cells. Transcriptomic analysis again revealed more differential gene expression between homozygotes and controls than heterozygotes and controls, with similar differentially expressed transcripts as in forebrain cultures including altered mitochondria and autophagy genes [88, 94]. Interestingly, in cerebellar cultures there was also decreased expression of mRNA processing genes, including many genes which are targets of FMRP, the protein disrupted in the neurodevelopmental disorder Fragile X Syndrome. Finally, treatment with mTOR inhibitors reversed all the observed phenotypic effects of complete *TSC2* loss [88].

3-D brain organoid models of TSC

Recent developments in 3-D differentiation techniques to generate human stem cell-derived brain organoids provide a new platform to investigate neurodevelopmental disorders in a physiologically relevant setting that can be maintained for long periods of time [1, 89-91]. Specifically, these models demonstrate basic cortical patterning, including the presence of human specific cellular niches [106] and neuronal migration

[107]. These features may be particularly relevant for TSC, as cortical tubers are developmental malformations that reflect not only altered differentiation but also defective migration and patterning.

Each 3-D differentiation method has advantages and disadvantages. The earliest method relied upon the tendency of cultured hPSCs to differentiate towards a neuroectodermal fate upon the removal of pluripotency maintaining growth factors [89]. To undergo differentiation, aggregates of hPSCs were implanted into Matrigel (as a scaffold) and placed into spinning culture flasks (bioreactors). This resulted in brain organoids with recognizable brain structures including forebrain, hippocampus, cerebellum and retina, however the number and presence of each of these features varied from culture to culture. A disadvantage of this method is that it's low-throughput, as the number of bioreactors that can be simultaneously cultured is limited. For many researchers, the presence of different brain structures was a confounding factor, rather than a feature. Consistent differentiation towards forebrain and increased throughput were achieved by using small molecule inhibitors to push the hPSCs towards a cortical fate and eliminating the bioreactors to allow for hundreds of concurrent differentiations and experiments [1, 91]. Despite their improvements, these methods have been criticized for being less representative of human neurodevelopment [106, 108]. Another method combining small molecule directed differentiation and 3-D printed plate tops with electric motor-driven paddles (mimicking bioreactors) has also been introduced however it is not widely used [90]. Modifications of these methods to improve consistency [109] or to induce a higher abundance of specific cell types [110, 111] have also been developed.

3-D neural differentiation techniques have already provided insights not only into basic human neuronal development, but also human specific evolutionary adaptations [106] and several neurological disorders including lissencephaly [107], ZIKA-virus induced microcephaly [90, 111, 112], and Timothy syndrome [110]. In Chapter 2, I will describe the results of my thesis project, which combined 3-D neuronal differentiation with CRISPR/Cas9 genome-editing to investigate the "second-hit" hypothesis of cortical tuber development in human brain spheroids [77].

Single-cell RNA sequencing to understand human neural development

The technological advancement of human neuronal models of disease occurred concordantly with technological advancements to analyze these models. One such technology is single cell RNA sequencing (scRNA-Seq) which is well-matched for highlighting individual cellular properties in models with heterogeneous cell types. Currently, the most accessible method of high-throughput scRNA-seq employs a microfluidic lipid-droplet platform (Fig. 3) [113]. Individual cells dissociated from tissue or spheroids are injected into an oil emulsion that contains DNA tagged microbeads in water-based buffer droplets. These bead droplets combine with individual cells, also in a water-based buffer, creating what is analogous to thousands of microscopic test tubes within the oil. Within the droplets, the cells are lysed and their transcripts captured at the 3' end by their poly-A tails and tagged with DNA barcodes (unique molecular identifiers; UMIs) that identify both the cell and the individual transcript. The UMI-attached transcripts then go through cDNA synthesis, PCR amplification and sequencing library

preparation before being loaded onto the sequencer. If desired, tens of thousands of cells can be captured at once, with the only consideration for increased cell number being the cost from using more reagents and the necessary increased sequencing depth. Computational methods to analyze the sequencing data have advanced along with the biochemical technology and now permit the inference of things such as cellular state and developmental trajectory from the basic gene expression data [114-116]. Already, scRNA-Seq has been applied extensively in wildtype brain organoid models [106, 108-110, 117-119] and in human fetal brain tissue [106, 108, 120] providing key insights into the transcriptional landscape of early human neurodevelopment and a reference work to help identify and corroborate cell types in future studies.

Dissertation Research Questions

Recent discoveries regarding the differences between primate cortical development and other mammals underscore the need for human neuronal models to study human neuronal diseases. In the case of TSC, the observation that rodents do not robustly capture the primary neuropathology in TSC, cortical tubers, highlights this need. Advances in genetic engineering and the refinement of neuronal differentiation from hPSCs has created an opportunity to establish human neuronal models of TSC. The primary goal for my dissertation was to establish human neuronal models of TSC and apply them to answer fundamental questions regarding the development of cortical tubers and treatment of TSC. Specifically, I sought to address 1) what are the cortical developmental effects of loss of TSC1/2 and is a “second-hit” mutation necessary for the development of cortical tubers? 2) what are the biological processes that are perturbed by TSC1/2 loss in developing cortical cells that underlie cortical tuber development and can they be reversed or prevented? These questions and others will be addressed in the following chapters. In chapter 2, I will describe the development of a neuronal model of TSC through gene editing of hPSCs and subsequent differentiation into 2-D and 3-D cortical cultures. In chapter 3, I will describe the application of this model towards the discovery of developmental programs and novel genetic markers for TSC. Finally, I will provide concluding remarks on the relevance of this research in the TSC field and future directions for this research.

Figures
Figure 1.1

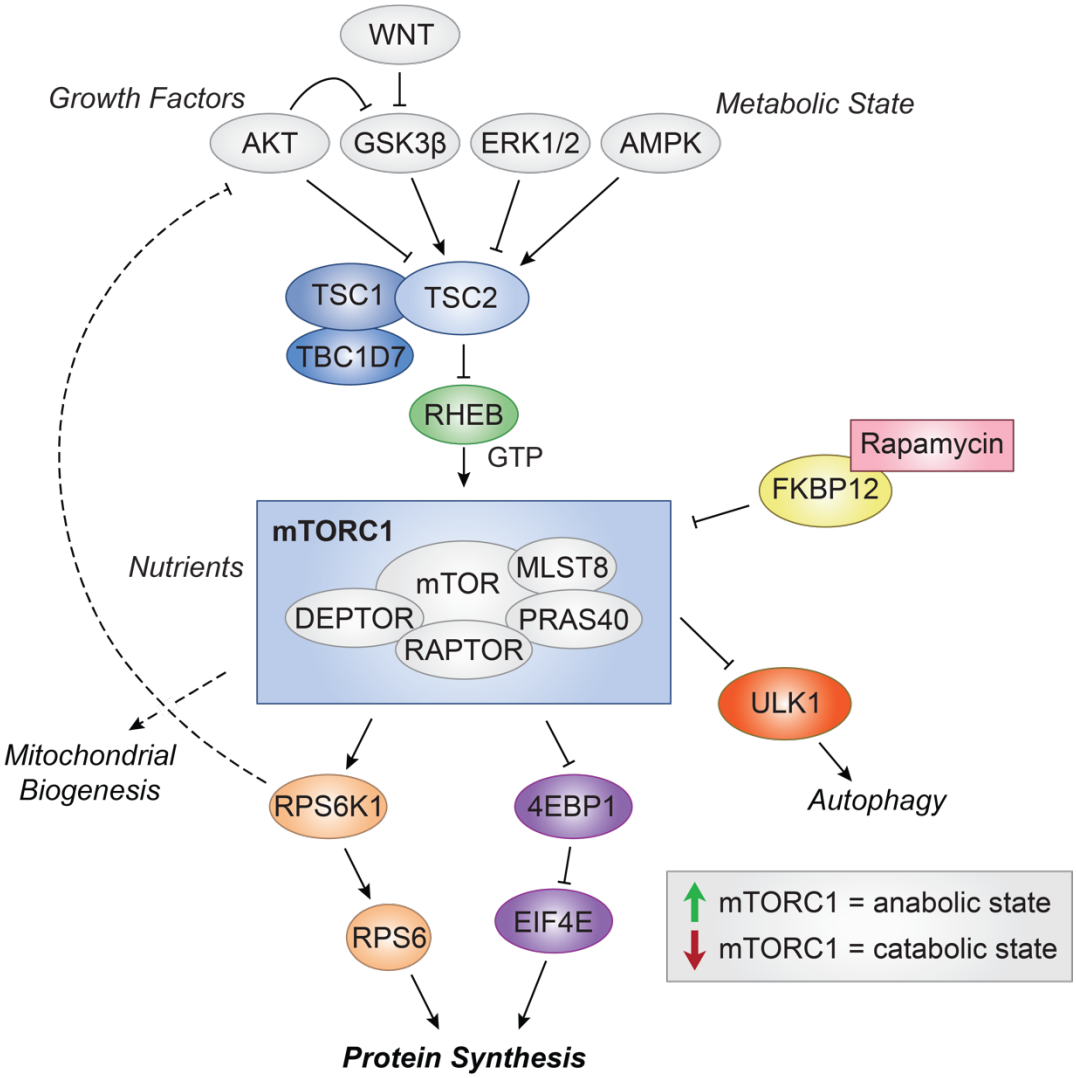

Fig. 1.1:The mTORC1 signaling pathway. Schematic illustrating the primary components and directions of mTORC1 signaling. Arrows indicate activating signals, flat heads indicate repressive signals. Dotted lines indicate speculative connections.

Figure 1.2

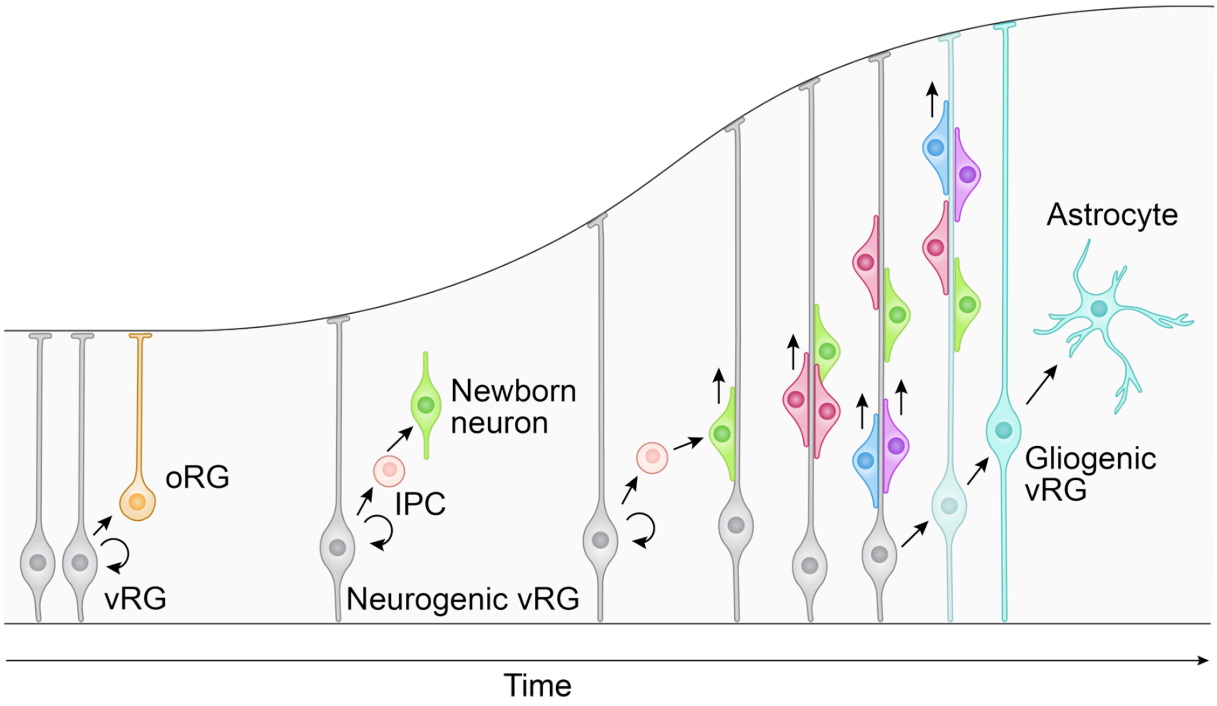

Fig. 1.2: Human Corticogenesis. Schematic illustrating a simplified corticogenesis timeline in humans. RG = Radial Glia, vRG = Ventral Radial Glia, oRG = Outer Radial Glia, IPC = Intermediate Precursor.

Figure 1.3

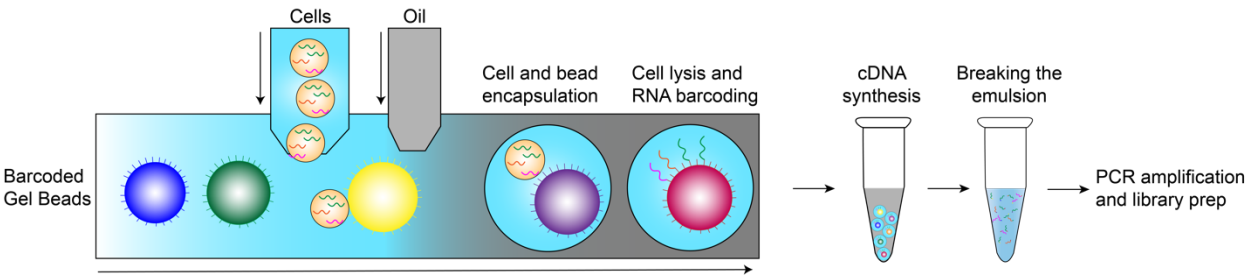

Fig. 1.3: Workflow of Single Cell RNA-sequencing. Schematic illustrating a simplified process of the 10x Genomics droplet based 3' single-cell RNA sequencing process. Gel beads with DNA based unique molecular identifiers (barcodes) are loaded into a microfluidic device where they then become encapsulated with single cells in a water-based droplet within oil. The single cells are then lysed and the poly-A mRNA is captured, tagged with UMIs and reverse transcribed. Following this, the droplets are broken, the tagged cDNA is amplified, then sequenced.

Chapter 2: **Genetically engineered human cortical spheroid models of tuberous sclerosis**

This chapter was previously published in its entirety as “Genetically engineered human cortical spheroid models of tuberous sclerosis” in *Nature Medicine*, 2018 Oct;24(10):1568-78, by John D. Blair, Dirk Hockemeyer and Helen S. Bateup [77]. It has been reproduced in here with full permission of the authors.

Introduction

Tuberous Sclerosis Complex (TSC) is a developmental disorder caused by mutations in the *TSC1* or *TSC2* genes [121, 122]. TSC affects multiple systems causing non-malignant hamartomas that can affect the skin, heart, kidney, lung, and brain [123]. Among the most debilitating aspects of TSC are the neurological symptoms. Approximately 90% of TSC patients have epilepsy that begins in infancy and early childhood and in many cases becomes intractable [124]. Intellectual disability and autism spectrum disorder occur in about half of TSC patients, with other psychiatric conditions prevalent [125]. The origins of the neurological aspects of TSC are not well understood; however, patients present with characteristic pathologies, called cortical tubers, which are macroscopic regions of disorganized and dysmorphic cells in the cortex [70]. Tubers and perituberal cortex often become epileptic foci [45, 126] and increased tuber load is correlated with more severe epilepsy and cognitive impairment [127].

Work from mouse models indicates that loss of *Tsc1* or *Tsc2* from cortical progenitor cells results in altered neuronal differentiation, morphology, and migration [128-133], consistent with histological observations in patient tissue [70]. However, bona fide tubers are not found in rodent models [70, 129, 130, 134, 135]. This may be a result of differences between mouse and human cortical development. Human cortical neurogenesis occurs over a much longer time period (about 140 days in humans [136] compared with 8 days in mice [137]), requires many more cell divisions, and exhibits unique proliferative zones and progenitor cell types [33, 136, 138]. Therefore, an experimental system that recapitulates early human cortical development is needed to understand the molecular and cellular origins of tubers.

At the biochemical level, the protein products of *TSC1* and *2* form a heterodimeric protein complex that is an essential negative regulator of mTOR complex 1 signaling (mTORC1) [13]. mTORC1 is a kinase that controls key cellular processes including nutrient sensing, mRNA translation, cellular metabolism, and autophagy [16]. Two primary effectors of mTORC1 signaling are p70S6 kinase, which phosphorylates the ribosomal protein S6, and 4E-BP1 that controls formation of the translation initiation complex [139]. TSC2 is a GTPase-activating protein (GAP) for the small GTPase Rheb, which is a direct activator of mTORC1 [140]. TSC1 is required to stabilize TSC2 [15] and loss of either protein disrupts TSC1/2 complex function. In the absence of the TSC1/2 complex, mTORC1 signaling is constitutively active, leading to alterations in cell growth, metabolism, and proliferation [141, 142].

The proposed model of cortical tuber formation is that somatic "second-hit" mutations in patients with heterozygous germline mutations result in loss of function of the TSC1/2 complex and hyperactivation of mTORC1 signaling in a subset of cortical progenitor cells [30, 69]. In line with this, there is clear evidence that loss of heterozygosity of *TSC1* or *2* causes TSC-associated hamartomas including those in the brain, lung, and kidney [143-147]. However, second-hit mutations have only been observed in a minority of surgically resected cortical tubers from TSC patients [28, 31, 144, 148], giving rise to the idea that haploinsufficiency may contribute to the neurological and cognitive aspects of TSC [149]. Consistent with this, mice heterozygous for *Tsc1* or *Tsc2* show alterations in social behavior[73] and have cognitive deficits [150, 151]. However, heterozygous mice do not display spontaneous seizures or cytomegalic neurons and glia [43, 131, 150], suggesting that complete loss of *Tsc1* or *2* may be necessary for these core features of TSC.

Here we established novel human cellular models for TSC based on genome editing in human pluripotent stem cells (hPSCs) to investigate the developmental origins and genetic requirements for tuber cell formation. We differentiated these hPSCs into two- and three-dimensional cortical cultures and found that complete loss of *TSC1* or *2* interfered with the normal developmental regulation of mTORC1 signaling resulting in impaired neurogenesis and increased gliogenesis. In addition, we found that biallelic *TSC2* inactivation in a subset of neural progenitor cells was necessary and sufficient to generate dysplastic cells resembling those found in tubers, consistent with the second-hit hypothesis. Together, our findings provide new insight into mTORC1's role in early human cortical development and how its dysregulation leads to focal cortical malformations.

Results

Gene editing TSC1 and TSC2 in hESCs

To establish a genetically controlled platform for assessing the impact of loss-of-function mutations in *TSC1* and *TSC2* on human neural development, we used CRISPR/Cas9 to delete either exon 17 of *TSC1* (Fig. 2.1a) or exon 5 of *TSC2* (Fig. 2.1b) in human embryonic stem cells (hESCs). TSC patient mutations are heterogeneous and can occur in any part of the *TSC1* or *TSC2* gene[152-154]. We chose exons 17 and 5 for targeted deletion based on their small size and expected introduction of a frameshift and premature stop codon. Mutations were engineered in the same WIBR3 hESC line [155], and cell lines were generated with heterozygous or homozygous mutations for each gene (Supplementary Fig. 2.1a,b). All hESC lines expressed the pluripotency markers OCT4 and NANOG, exhibited normal morphology, and had no major chromosomal abnormalities as assessed by array comparative genomic hybridization analysis (Supplementary Fig. 2.1c-g and Supplementary Table 2.1).

We verified by western blotting that homozygous mutant hESCs exhibited complete loss of TSC1 or TSC2 protein and heterozygous cells exhibited partial loss (Fig. 2.1c-e). We observed a significant reduction in TSC2 protein in $TSC1^{-/-}$ cells and TSC1 protein in $TSC2^{-/-}$ cells, consistent with prior data showing that the TSC1 and 2 proteins stabilize each other and that in the absence of one protein, the other is degraded [15]. We examined the phosphorylation state of the mTORC1 pathway targets

ribosomal protein S6 and 4E-BP1 and found significant elevations in p-S6 in *TSC2*$^{-/-}$ cells and p-4E-BP1 in *TSC1*$^{-/-}$ and *TSC2*$^{-/-}$ hESCs (Fig. 2.1c,f,h). Total levels of S6 protein were also significantly increased in *TSC1*$^{-/-}$ cells (Fig. 2.1c & g), consistent with mTORC1's role in promoting the synthesis of ribosomal proteins [18, 101]. Notably, hESCs with heterozygous mutations in *TSC1* or *2* did not display activation of mTORC1 signaling (Fig. 2.1c,f-i).

AKT is an upstream activator of mTORC1 that controls its activity through phosphorylation and inhibition of TSC2 [156]. AKT and other upstream regulators of mTORC1 are subject to negative feedback regulation [157]. Consistent with engagement of a negative feedback pathway, we observed significantly reduced phosphorylation of AKT at serine 473 in both *TSC1*$^{-/-}$ and *TSC2*$^{-/-}$ hESCs, and a small but significant decrease in *TSC1*$^{+/-}$ hESCs (Fig. 2.1c, j). Interestingly, we also observed increased total AKT protein in *TSC1*$^{+/-}$ and *TSC1*$^{-/-}$ hESCs, which was not observed in hESCs with *TSC2* mutations (Fig. 2.1c,k).

Taken together, these results demonstrate that homozygous, but not heterozygous, disruption of *TSC1* or *TSC2* causes increased mTORC1 signaling and decreased AKT phosphorylation in hESCs.

Phenotypes of neural progenitor cells lacking TSC1 or TSC2

To investigate how mutations in *TSC1* or *2* affect early human neural development, we differentiated our panel of hESC lines into forebrain neural progenitor cells (NPCs) using the two-dimensional (2D) dual-SMAD inhibition protocol [84]. We found that nestin-positive NPCs could be generated from hESCs of all genotypes (Supplementary Fig. 2.2a). However, *TSC1*$^{-/-}$ and *TSC2*$^{-/-}$ NPCs were hypertrophic, exhibiting significantly increased cell size (Supplementary Fig. 2a-b), consistent with observations in other cell types exhibiting high mTORC1 signaling [16]. We observed a large increase in p-S6 in both *TSC1*$^{-/-}$ and *TSC2*$^{-/-}$ NPCs, with *TSC2*$^{-/-}$ NPCs exhibiting significantly higher p-S6 levels than *TSC1*$^{-/-}$ cells (Supplementary Fig. 2.2c,f). *TSC1*$^{-/-}$ NPCs displayed increased 4E-BP1 phosphorylation as well as total levels of S6 and 4E-BP1 (Supplementary Fig. 2.2c,g,h,i). We observed strongly reduced S473 AKT phosphorylation in *TSC2*$^{-/-}$ NPCs, and to a more variable extent in *TSC1*$^{-/-}$ NPCs (Supplementary Fig. 2.2c,j). In contrast to hESCs, total levels of AKT were reduced in *TSC1*$^{-/-}$ and *TSC2*$^{-/-}$ NPCs (Supplementary Fig. 2.2c,k). This finding is consistent with TSC1's role as a co-chaperone for Hsp90, which prevents the degradation of AKT [158].

3D cortical spheroid differentiation

The human cortex develops from neuroepithelial cell precursors that generate radial glia progenitors. Radial glia divide asymmetrically to produce excitatory neurons followed by astrocytes, a type of glia [136, 138]. To investigate how mutations in *TSC1* or *2* affect neural development in a three-dimensional (3D) tissue context that recapitulates this progression, we differentiated our panel of hESCs into cortical spheroids using an established protocol [1] (Fig. 2.2a). At 20 days post-differentiation, rosette structures resembling cortical ventricular zones could be observed in spheroids of all genotypes (Fig. 2.2b,c). These structures contained cells that expressed the neural progenitor markers PAX6 and SOX2 (Fig. 2.2b,c). We found no significant differences in the percentage of PAX6 or SOX2-positive cells in spheroids derived from

hESCs with mutations in *TSC1* or *TSC2* (Fig. 2.2d,e), indicating that TSC mutations do not strongly affect differentiation into forebrain progenitors. We also performed staining for the cell proliferation marker Ki-67 and found that 49.7% +/- 5.5% of cells in WT spheroids were proliferating at day 20 (Fig. 2.2c,f). We did not find significant differences in the proportion of Ki-67-positive cells in spheroids with mutations in *TSC1* or *TSC2* at this time point (Fig. 2.2f).

In wild-type spheroids, expression of neuronal markers including NeuN and MAP2 began around day 30-50 post-differentiation and increased through day 150 (Fig. 2.2g,h,j,l,m and Supplementary Fig. 2.3a). Markers of glial-lineage cells, which include astrocytes, emerged later with expression of GFAP, S100B, and CD44 beginning around day 100 and increasing through day 150, consistent with *in vivo* human cortical development [136] (Fig. 2.2g,l,k,l and Supplementary Fig. 2.3b,e,f). While spheroids with heterozygous mutations in *TSC1* or *TSC2* showed a normal profile of neuron and glia development (Fig. 2.2g-m and Supplementary Fig. 3a-f), *TSC1*$^{-/-}$ and *TSC2*$^{-/-}$ spheroids exhibited reduced or delayed expression of neuronal markers and increased expression of glial-lineage markers. This was demonstrated by significantly increased GFAP protein at day 150, and reduced MAP2 protein at day 100, which remained below wild-type levels in *TSC2*$^{-/-}$ spheroids at day 150 (Fig. 2.2g-i). mRNA levels showed a similar pattern with decreased NeuN and increased S100B expression in *TSC2*$^{-/-}$ spheroids at day 100 (Fig. 2.2j,k and Supplementary Fig. 2.3a,b). *TSC2*$^{-/-}$ spheroids also exhibited reduced neuron:glia ratios at day 100, assessed by immunostaining for NeuN and S100B, although this did not reach statistical significance (Fig. 2.2l and Supplementary Fig. 2.3c). This may reflect biased differentiation into glial-lineage cells as opposed to enhanced proliferation as we did not find significantly increased numbers of Ki-67-positive glial cells in *TSC1*$^{-/-}$ or *TSC2*$^{-/-}$ spheroids (Supplementary Fig. 2.3d,e). The neurons and glia that were generated in *TSC1*$^{-/-}$ and *TSC2*$^{-/-}$ spheroids were enlarged, dysmorphic and had high levels of p-S6 (Fig. 2.2l,m and Supplementary Fig. 2.3e,f).

We verified that these phenotypes were not specific to the hESC line used for gene editing by using CRISPR/Cas9 to generate a homozygous deletion of *TSC2* in an independent human induced pluripotent stem cell (hiPSC) line that we reprogrammed from BJ fibroblasts (Supplementary Fig. 1i,j and Supplementary Table 2.1). BJ;*TSC2*$^{-/-}$ spheroids exhibited highly enlarged, dysplastic neurons and glia that had high levels of p-S6, similar to tuber cells (Supplementary Fig. 2.3g,h).

TSC1$^{-/-}$ *and TSC2*$^{-/-}$ *spheroids fail to suppress mTORC1 during neurogenesis*

To determine how TSC2 loss might alter neuron and glia development, we monitored mTORC1 signaling in wild-type and *TSC2*$^{-/-}$ cortical spheroids over time (Fig. 2.3a,c-h). We found that both the total levels and phosphorylation of S6 were strongly reduced in wild-type spheroids as they transitioned from proliferating to differentiating, with the highest levels at day 0, when cells were still pluripotent (Fig. 2.3a,c,d). A similar pattern was observed for 4E-BP1 (Fig. 2.3a,e,f) suggesting that two primary downstream targets of mTORC1 signaling involved in translational control are strongly suppressed during human neural differentiation. Notably, although total levels of 4E-BP1 and S6 decreased between days 20 and 100 in *TSC2*$^{-/-}$ spheroids, likely reflecting changes in cell type composition of the spheroids, the ratio of phosphorylated to total

protein remained as high as in stem cells throughout spheroid development (Fig. 2.3a,c-f). This indicates that *TSC2*$^{-/-}$ cells were unable to suppress mTORC1 signaling during neuronal differentiation. The hyperphosphorylation of mTORC1 pathway targets in *TSC2* mutant spheroids was in contrast to AKT phosphorylation, which was strongly reduced throughout development in *TSC2*$^{-/-}$ spheroids (Fig. 2.3a,g).

Given the dynamic regulation of mTORC1 signaling we observed during cortical spheroid development, we quantitatively compared mTORC1 signaling across all genotypes at multiple developmental time points (Supplementary Fig. 2.4a-g). Homozygous loss of *TSC1* or *TSC2* produced overall similar changes in mTORC1 signaling. However, *TSC2* loss increased S6 phosphorylation to a greater extent than *TSC1* deletion on days 20-100 (Supplementary Fig. 2.4a,b). The phosphorylation of 4E-BP1 was significantly increased over wild-type levels in *TSC2*$^{-/-}$ spheroids on days 20-100 and in *TSC1*$^{-/-}$ spheroids on days 30 and 50 (Supplementary Fig. 2.4a,d). By contrast, AKT phosphorylation was strongly reduced in *TSC2*$^{-/-}$ spheroids at all time points and on days 20-100 in *TSC1*$^{-/-}$ spheroids (Supplementary Fig. 2.4a,f). Heterozygous spheroids exhibited a normal developmental pattern of mTORC1 signaling, with no significant differences in S6, 4E-BP1, or AKT phosphorylation compared to wild-type spheroids (Supplementary Fig. 2.4a-g).

In addition to TSC1 and TSC2, the TSC complex contains a third requisite protein, TBC1D7, which binds to TSC1 and is required for complex stability[12]. Mutations in TBC1D7 have been linked to intellectual disability and megalencephaly [159]. We therefore investigated protein levels of TBC1D7 in *TSC1*$^{-/-}$ and *TSC2*$^{-/-}$ spheroids over time. We found that TBC1D7 levels were strongly reduced in *TSC1*$^{-/-}$ spheroids from day 20 onwards, likely due to degradation in the absence of TSC1 protein (Supplementary Fig. 2.4h,i). We also observed smaller but significant reductions in TBC1D7 in *TSC2*$^{-/-}$ spheroids compared to wild-type at days 20, 50 and 150 (Supplementary Fig. 2.4h,i), which may reflect the approximately 60% loss of TSC1 protein in these cells.

Taken together, these data demonstrate that mTORC1 signaling is strongly suppressed during human neuronal differentiation and that homozygous mutations in *TSC1* or *TSC2* prevent this developmental regulation.

STAT3 phosphorylation is activated in TSC1$^{-/-}$ *and TSC2*$^{-/-}$ *spheroids*

Excitatory neurons and astrocytes are generated from the cortical radial glial lineage in a time-dependent manner with neurons produced first, followed by astrocytes. The molecular mechanisms controlling the neuron-astrocyte cell fate decisions in the human cortex are not well understood. However, studies in rodent models have shown that the gene expression programs that drive neuron and astrocyte differentiation are regulated by competitive cell intrinsic and extrinsic signals [160]. Since the strong developmental suppression of mTORC1 signaling that we observed in wild-type spheroids coincided with the time when neurogenesis begins, we hypothesized that mTORC1 signaling may promote gliogenic signals, which are normally suppressed to allow neurogenesis.

In rodent models, the JAK-STAT signaling pathway induces astrocyte differentiation from cortical precursor cells [161]. Specifically, when activated, the transcription factor STAT3 promotes the transcription of genes involved in astrocyte

differentiation including *Gfap* [161]. We investigated the phosphorylation of STAT3 at two key residues, S727 and Y705, in wild-type, *TSC1*$^{-/-}$, and *TSC2*$^{-/-}$ cortical spheroids over time. We found that S727 was high in hESCs and suppressed in all genotypes during neural differentiation (Fig. 2.3b,i). By contrast, Y705 was low in hESCs and increased in wild-type spheroids from days 100 to 150 when astrocytes begin to appear (Fig. 3b,j). Notably, *TSC1*$^{-/-}$ and *TSC2*$^{-/-}$ spheroids exhibited increased p-STAT3-Y705, an effect that was most pronounced in *TSC2*$^{-/-}$ spheroids (Fig. 2.3b,j). Total STAT3 levels did not change significantly with development or TSC1 or 2 loss (Fig. 2.3b,k).

The increased p-STAT3-Y705 was mTOR-dependent as it was strongly reduced in day 100 *TSC2*$^{-/-}$ spheroids treated chronically with the mTOR inhibitor rapamycin (20nM, treatment started on day 12 of differentiation, 49.9% +/- 23.7% of vehicle control, Supplementary Fig. 2.4j). Rapamycin also strongly reduced the expression of GFAP (4.4% +/- 1.6% of vehicle control) and increased the expression of neuronal proteins including doublecortin (348.1% +/- 15.9% of vehicle control), CAMK2A (193.8% +/- 48.3% of vehicle control) and GluR1 (153.1% +/- 22.1% of vehicle control) in *TSC2*$^{-/-}$ spheroids (Supplementary Fig. 2.4j). These data are consistent with the idea that mTORC1 signaling is gliogenic and that inhibition of mTORC1 signaling suppresses gliogenesis and promotes neurogenesis.

Engineering a conditional TSC2 allele to model a second-hit mutation

Our results in 2D and 3D human neural cultures indicated that homozygous loss of *TSC1* or *TSC2* profoundly affects the developmental regulation of mTORC1 signaling, cell morphology, and neuron-glia differentiation. Notably, we found minimal to no alterations in heterozygous cells. These results are consistent with the idea that tuber cells arise from a somatic second-hit mutation that causes biallelic inactivation of *TSC1* or *TSC2* in a sub-population of neural progenitor cells. To test this idea, we generated a model that recapitulates a second-hit mutation by engineering hESCs with a conditional allele of *TSC2* (Supplementary Fig. 2.1b). This cell line had a constitutive loss-of-function mutation in one allele and a Cre-inducible conditional mutation in the second allele (*TSC2*$^{-/c}$; Fig. 2.4a). We chose to target *TSC2* since the majority of patient mutations are in *TSC2* [152, 162] and homozygous loss of *TSC2* generally caused more severe phenotypes compared to *TSC1* (see Fig. 2.2, 2.3 and Supplementary Fig. 2.3). We confirmed that viral delivery of Cre recombinase to neurons differentiated in 2D from *TSC2*$^{-/c}$ hESCs resulted in loss of TSC2 protein and upregulation of mTORC1 signaling (Fig. 2.4b). To allow for the visualization and fate mapping of Cre-expressing cells, we generated a tdTomato Cre-reporter allele in the *TSC2*$^{-/c}$ hESCs by targeting the AAVS1 safe harbor locus[83, 163] with CRISPR/Cas9 (we refer to this cell line as *TSC2*$^{-/c;LSL\text{-}tdTom}$, Fig. 2.4c). We validated the pluripotency of *TSC2*$^{-/c;LSL\text{-}tdTom}$ hESCs with OCT4 and NANOG staining and teratoma formation assays (Supplementary Fig. 2.1h,m-r).

To test how biallelic inactivation of *TSC2* cell autonomously affects neuronal development, we differentiated *TSC2*$^{c/-;tdTom}$ hESCs, treated with Cre just prior to differentiation, into 2D cultures of NPCs and neurons using dual-SMAD inhibition[84] (Fig. 2.4d,e). We found that Cre-expressing tdTomato-positive cells, which were homozygous mutant for *TSC2*, exhibited significantly increased mTORC1 signaling assessed by phosphorylation of S6 (Fig. 2.4f,g and Supplementary Fig. 2.5a,b). tdTomato-positive cells were also enlarged compared to neighboring GFP-expressing

TSC2 heterozygous cells (Fig. 2.4h,i). In addition to cell soma enlargement, neurons with a second-hit *TSC2* mutation exhibited significant dendritic hypertrophy measured by Sholl analysis (Fig. 2.4j). We also observed highly enlarged, multinucleated tdTomato-positive *TSC2* mutant cells that resembled "giant cells"; a unique cell type found in TSC patient tubers [70] (Supplementary Fig. 2.5c). Multiple nuclei were not observed in *TSC2* heterozygous cells. These results demonstrate that cell autonomous changes in mTORC1 signaling are sufficient to cause enlarged and dysmorphic cells.

Biallelic inactivation of TSC2 in cortical spheroids

To test whether biallelic inactivation of *TSC2* in developing cortical spheroids causes the formation of dysplastic cells, we differentiated *TSC2*$^{-/c;LSL\text{-}tdTom}$ hESCs into cortical spheroids and treated them with a sub-saturating amount of Cre lentivirus on day 12 post-differentiation, during the neural progenitor expansion phase. We confirmed that tdTomato-positive NPCs in cortical spheroids were enlarged (Supplementary Fig. 2.5d,e), consistent with complete loss of TSC2 and activation of mTORC1. We found that Cre-expressing *TSC2*$^{-/c}$ cells gave rise to highly dysmorphic neurons, glial-lineage cells, and giant cells that became larger over time (Fig. 2.4k-o and Supplementary Fig. 2.5f-h). These cells were phenotypically similar to those observed in cortical tubers from TSC patients [9, 70]. Specifically, the cells were hypertrophic and dysplastic with high levels of p-S6 and diffuse cytoplasmic expression of the filament proteins nestin, vimentin, and SMI-311 (Fig. 2.4k-o and Supplementary Fig. 2.5f,g). In addition, some tdTomato-positive *TSC2*$^{-/c}$ cells co-expressed both neuronal (MAP2) and glial (S100B) proteins (Supplementary Fig. 2.5h), which has also been observed in patient tuber cells [9]. Co-expression of these markers was not seen in neighboring heterozygous cells. Importantly, cytomegalic cells did not develop in Cre-treated *TSC2*$^{+/c}$ spheroids (Supplementary Fig. 2.5i), indicating that biallelic inactivation of *TSC2* is required for the formation of dysplastic cells.

We next tested whether a second-hit mutation is required for dysplastic cells to form in the context of TSC patient cells. To do this we reprogrammed fibroblasts from a TSC patient (Coriell cell line #GM04520) into iPSCs (Supplementary Fig. 2.1k and Supplementary Table 1). This patient has a heterozygous deletion of exons 1-14 of *TSC2* (Supplementary Fig. 2.6a) and a history of childhood seizures and mild intellectual disability. To generate a conditional second-hit allele, we first deleted exon 5 of the patient's wild-type *TSC2* allele using CRISPR/Cas9 and then introduced a conditional exon 5 allele using the same strategy as for *TSC2*$^{-/c}$ hESCs (Supplementary Fig. 2.6b,c). The resulting hiPSC line has the patient mutation in one *TSC2* allele and a conditional loss of function mutation in the second allele (referred to as 4520$^{c/-}$, Supplementary Fig. 2.1l and Supplementary Table 2.1).

4520$^{c/-}$ hiPSCs were differentiated into cortical spheroids and Cre-GFP lentivirus was added 12 days post-differentiation. On day 100, we found that Cre-expressing cells were dysmorphic, had high levels of p-S6, and were positive for vimentin (Supplementary Fig. 6d). Neighboring uninfected cells did not exhibit characteristics of tuber cells, indicating that biallelic inactivation is necessary for dysplastic cell formation in TSC patient-derived cortical spheroids.

Rescue of neuronal differentiation and morphology with rapamycin treatment

To test whether the formation of dysplastic cells in *TSC2*$^{-/c;LSL\text{-}tdTom}$ cortical spheroids could be prevented or rescued by blocking mTORC1 signaling, we treated spheroids with the mTOR inhibitor rapamycin at different time points during development (Supplementary Fig. 2.7a). For all conditions, sub-saturating amounts of Cre and GFP lentivirus were added on day 12 and spheroids were harvested on day 110. We found that chronic rapamycin starting on day 12 profoundly rescued mTORC1 hyperactivity and neuronal development in Cre-expressing *TSC2*$^{-/c}$ cells. Specifically, rapamycin at day 12 strongly reduced mTORC1 signaling in both heterozygous and homozygous *TSC2* mutant cells and prevented cellular hypertrophy induced by biallelic *TSC2* inactivation (Fig. 5a-e and Supplementary Fig. 2.7b,c). To assess neuronal differentiation, we calculated the percentage of tdTomato or GFP-positive *TSC2*$^{-/c}$ cells that expressed the neuronal marker HuC/D or the glial protein S100B on day 110 (Fig. 2.5d-g). In GFP-labeled *TSC2* heterozygous cells, 18.7% of cells expressed HuC/D, 36.3% expressed S100B, 0.5% were double labeled, and 44.5% were not labeled by either marker (Fig. 2.5h). The unlabeled cells likely represent neural progenitors or immature neurons and glia. Consistent with findings in the constitutive *TSC2*$^{-/-}$ spheroids, we found that tdTomato-positive *TSC2* homozygous mutant cells preferentially generated glial-lineage cells over neurons at a ratio of 7.3 to 1 (72.6% S100B positive vs. 9.9% HuC/D positive, Fig. 2.5i). We confirmed that the majority of tdTomato-positive cells were likely astrocytes by immunostaining with additional astrocyte markers including EAAT1 and CD44 (Supplementary Fig. 2.7f,g). Chronic rapamycin starting on day 12 completely reversed the glial differentiation bias, causing tdTomato-positive *TSC2*$^{-/c}$ cells to preferentially generate neurons (0.14 to 1 glia to neuron ratio, Fig. 2.5i). A doubling in the percentage of neurons was also observed in GFP-positive cells treated with rapamycin on day 12 (18.7% to 46.5% HuC/D positive, Fig. 2.5h). This is consistent with our western blot results with rapamycin-treated *TSC2*$^{-/-}$ spheroids (see Supplementary Fig. 2.4j), indicating that suppression of mTOR signaling acts downstream of the TSC1/2 complex to promote neuronal differentiation and inhibit or delay glial-lineage cell production.

To test whether rapamycin treatment could reverse the phenotypes of *TSC2* loss, spheroids were treated with rapamycin starting on day 80. Chronic rapamycin starting on day 80 strongly reduced mTORC1 signaling and reversed cellular hypertrophy to a similar extent as day 12 rapamycin treatment (Fig. 2.5a-c,d,f and Supplementary Fig. 2.7b-d). However, rapamycin at day 80 had a more modest effect on the neuronal differentiation of tdTomato-positive *TSC2*$^{-/c}$ cells compared to day 12 rapamycin (Rap d80=22.3% HuC/D positive vs. Rap d12=70.4% HuC/D positive, Fig. 2.5i). Rapamycin at day 80 had little effect on neuronal differentiation in GFP-positive heterozygous cells (Vehicle=18.7% HuC/D positive vs. Rap d80=22.1% HuC/D positive, Fig. 2.5h). These results suggest that 1) the majority of neuronal cell fate decisions are made prior to day 80 in the cortical spheroid model and 2) rapamycin treatment cannot reverse this decision.

Based on these findings, we tested whether rapamycin treatment during the primary period of neuronal differentiation (from day 12 to 80) could prevent phenotypes due to homozygous loss of *TSC2*. We found that rapamycin treatment from day 12-80 improved neuronal differentiation in tdTomato-positive *TSC2*$^{-/c}$ cells (from 9.9% to 30.3% HuC/D positive) and increased the percentage of neurons differentiated from

heterozygous cells (from 18.7% to 30.7%), albeit to a lesser degree than in spheroids continuously treated with rapamycin (Fig. 2.5h,i). Despite improvements in neuronal differentiation, upon rapamycin withdrawal, tdTomato-positive *TSC2*$^{-/c}$ cells reactivated mTORC1 signaling to a similar level as vehicle treated mutant cells (Fig. 2.5a and Supplementary Fig. 2.7e).

Taken together, these results suggest that there is a developmental window for pharmacologic mTORC1 suppression to prevent neuronal differentiation defects caused by loss of *TSC2*. Later rapamycin treatment cannot reverse cell fate decisions but can rescue mTORC1 hyperactivation and reduce neuron and glia hypertrophy. Sustained mTORC1 inhibition is required to prevent the reemergence of mTORC1 hyperactivity in differentiated cells.

Discussion

In this study, we generated a panel of human pluripotent stem cell lines with targeted loss-of-function mutations in the *TSC1* and *TSC2* genes. We used this genetically controlled platform to investigate the contributions of TSC-mTOR signaling to human cortical development and address outstanding questions concerning the neuropathophysiology of TSC. We found that mTORC1 signaling is strongly suppressed during human neuronal differentiation and that this is required for normal neuro- and gliogenesis. Homozygous, but not heterozygous, loss of *TSC1* or *TSC2* disrupts the developmental suppression of mTORC1 signaling resulting in abnormal differentiation and hypertrophy of human neurons and glia. We provide direct support for the second-hit hypothesis of tuber formation, as biallelic inactivation of *TSC2* in neural precursor cells was necessary and sufficient to cause the formation of dysplastic cells in human cortical spheroids. Lastly, we demonstrate that mTOR inhibition during a critical developmental period can rescue the formation of dysplastic cells by promoting neuronal differentiation and preventing cellular hypertrophy.

The biochemical consequences of loss of function of the TSC1/2 complex on mTORC1 signaling are well known; however, this has not been investigated in a 3D model of human cortical development. Here we found that two targets of the mTORC1 pathway involved in translational control, S6 and 4E-BP1, were highly phosphorylated in human pluripotent stem cells and neural precursor cells; cell types that are highly proliferative. Consistent with a recent study in 2D neural cultures [101], we found that mTORC1 signaling was strongly suppressed as neural precursor cells transitioned from self-renewing to differentiating. This effect was seen at the level of total protein and in the phosphorylation state of S6 and 4E-BP1. Homozygous loss-of-function of *TSC1* or *TSC2* prevented the developmental suppression of mTORC1 signaling resulting in sustained mTORC1 activity during neurogenesis and gliogenesis. This constitutive activation of the translational machinery may result in deregulated, ectopic protein expression that interferes with normal differentiation programs.

By direct comparison in an isogenic setting, we did not observe major changes in mTORC1 signaling in hESCs, NPCs, or cortical spheroids with heterozygous mutations in *TSC1* or *TSC2*. The lack of a change in mTORC1 signaling was in line with the normal NPC, neuron, and glia development observed in spheroids with heterozygous mutations. These findings are consistent with a study using 2D differentiation of hESCs

with *TSC2* mutations, which found that complete loss of TSC2 was required for alterations in neuronal differentiation, cell size, and morphology[93]. This study did, however, observe synaptic alterations in *TSC2*$^{+/-}$ neurons, suggesting that while cortical development is generally normal in the context heterozygous mutations, haploinsufficiency may cause functional changes in mature neurons or glia. Our lack of strong phenotypes in heterozygous cells is in contrast to a recent study showing mTORC1 activation, enhanced proliferation, and altered cell morphology in 2D neural cultures derived from TSC patient hiPSCs with a heterozygous mutation in *TSC2* [95]. In this study, the TSC patient cells were compared to a non-isogenic control cell line. It is therefore unclear whether the observed differences were due to the *TSC2* mutation or were a result of other genetic differences or cell line variability.

A major finding of our study is that bidirectional changes in mTORC1 signaling profoundly affect the balance of neuron and glia differentiation in developing human cortical spheroids. Specifically, mTORC1 hyperactivation, resulted in greater production of glial-lineage cells, which include astrocytes, at the expense of neurons. By contrast, mTORC1 suppression promoted neurogenesis. These effects were observed both in cortical spheroids with constitutive mutations in *TSC2* and in cells with a second-hit mutation in *TSC2*, which generated seven times more glia than neurons. The latter result suggests a cell autonomous change in cell fate decision, as neighboring *TSC2* heterozygous cells produced higher neuron to glia ratios. These findings are consistent with histological observations of large numbers of astrocytes in cortical tubers [70, 164], mouse studies demonstrating increased GFAP expression following loss of *Tsc1* or *Tsc2* [128, 131, 132], and a recent study showing reduced neuronal and increased glial markers in 2D human *TSC2*$^{-/-}$ neural cultures [94].

Notably, we found that mTOR blockade with rapamycin during neural precursor expansion strongly promoted neuronal differentiation and inhibited glia production independent of *TSC2* genotype. This is consistent with a study in mice in which the gene encoding the obligate mTORC1 protein Raptor was deleted in cortical progenitor cells, resulting in impaired gliogenesis *in vivo* [165]. However, our findings contrast with a previous report in 2D cultures of mouse neural stem cells, which reported reduced neuron production in response to chronic rapamycin treatment [128]. This may reflect differences in mouse versus human cortical progenitors or in 2D versus 3D culture conditions.

In the developing human cortex, early neuroepithelial progenitors give rise to radial glia, which can divide symmetrically to produce more radial glia, or asymmetrically to produce either a neuron or an astrocyte [33, 136]. The mechanisms underlying neuron-astrocyte cell fate decisions in human cortex are not well understood, however studies in mice have identified a cascade of intrinsic and extrinsic signaling events that govern time-dependent shifts from progenitor self-renewal to neurogenesis to gliogenesis [160]. Our findings demonstrate that suppression of mTORC1 signaling during the transition from proliferation to neuronal differentiation (between day 25 and 43 in the cortical spheroid model) is required for normal neurogenesis. Mechanistically, mTORC1 could be inhibiting neurogenic gene expression programs, activating gliogenic signaling pathways, or increasing glial proliferation. We did not find significant increases in the proportion of Ki-67-positive glia in cortical spheroids with TSC mutations suggesting that increased proliferation is unlikely to account for the large numbers of

glial-lineage cells observed. Instead, we found that Y705 phosphorylation of the gliogenic transcription factor STAT3 was significantly elevated in *TSC1*$^{-/-}$ and *TSC2*$^{-/-}$ cortical spheroids in a rapamycin-sensitive manner, consistent with observations in 2D mouse and human neural cultures [94, 128, 131]. Importantly, we found that p-STAT3 levels were increased prior to the onset of neurogenesis in TSC mutant spheroids. Since neurogenic and gliogenic signals suppress one another, the activation of STAT3 may directly promote gliogenesis, while at the same time interfering with or delaying neurogenesis. In addition to increased glial cell production, it is also possible that high mTORC1 signaling may impair the survival of newborn neurons [128], further contributing to altered neuron:glia ratios.

Our finding that rapamycin treatment early in cortical spheroid development alters cell fate decisions, even in *TSC2*$^{+/-}$ cells, has important clinical implications. Rapamycin derivatives called rapalogues are used clinically to treat TSC and related disorders[30], and it has been suggested that prenatal rapalogue treatment could be beneficial to prevent developmental abnormalities in TSC. Using our model, which allows us to test the impact of drug treatments directly in developing human cortical tissue, we find that strong mTORC1 suppression alters the normal pattern of cortical differentiation. These results suggest that prenatal rapamycin treatment may be detrimental to the developing brain, consistent with behavioral studies in mice exposed to rapamycin *in utero* [166]. Our model will facilitate further testing of therapeutics for TSC and allow the definition of critical windows for treatments to have the most impact without causing detrimental outcomes.

Our findings provide causal evidence that second-hit mutations are necessary and sufficient to generate dysplastic cells in developing human cortical tissue. While this has been proposed to occur [30, 69], second-hit mutations have only been detected in a subset of cortical tubers examined [28, 31, 144, 148]. This is in contrast to TSC-related hamartomas including subependymal giant cell astrocytomas, in which second-hit events are frequently observed [143-147]. Using novel conditional *TSC2* knock-out hESCs and patient-derived hiPSCs, we show that a mosaic second-hit mutation in *TSC2*$^{-/c}$ neural precursor cells causes the formation of dysplastic cells in human cortical spheroids. These cells are strikingly similar to those observed in TSC patient tubers. Specifically, we find cell types resembling dysmorphic neurons, dysplastic glia, and giant cells that are hypertrophic and have high levels of mTORC1 signaling [9]. These cells express many of the same markers that have been observed in patient tubers [70]. Importantly, we did not observe tuber cell features in neighboring *TSC2* heterozygous cells, or in *TSC2*$^{+/c}$ cells treated with Cre, demonstrating that biallelic inactivation is necessary. These findings are consistent with a recent study that identified germline and somatic mutations in *TSC1* and *TSC2* in brain tissue from patients with focal cortical dysplasia (FCD) and hemimegalencephaly, which have histological features similar to tubers [167].

One possible reason that second-hit mutations have not been consistently identified in patient brain tissue is that tubers comprise a mixture of cell types of different origin. Tubers contain dysmorphic cells with high mTORC1 activity as well as normal-appearing neurons and glia. In addition, inflammatory cells from surrounding areas infiltrate the tubers [99, 168], further diluting the numbers of cells with biallelic inactivation. Thus, low allelic frequency may have hindered the identification of somatic

mutations. Indeed, in a FCD case with a second-hit mutation in *TSC2*, the mutation was present in only ~7% of brain cells [167]. Alternatively, mutations may occur in introns [169], promoters, or other regulatory regions, or could be large copy number variants, which are not detectable by exome sequencing.

Taken together, our findings support the model that second-hit somatic mutations in small populations of neural precursor cells give rise to the dysplastic cells that comprise cortical tubers. Such a stochastic mechanism can explain the large heterogeneity in tuber number and size among TSC patients. Since higher tuber load is linked to increased severity of epilepsy and intellectual disability, somatic mosaicism may be a key factor underlying the significant heterogeneity in the presentation of neurological phenotypes in TSC patients. Our findings support the growing body of literature that somatic mutations play a significant role in brain development in both normal and disease states [170].

Methods

hESC cell culture

WIBR3 hESCs (NIH stem cell registry # 0079) were obtained from Dr. Rudolf Jaenisch's lab and authenticated as reported in Lengner et al, 2010 [155]. Human embryonic stem cell culture was carried out as previously described [171]. Briefly, all hESC lines were maintained on a layer of inactivated mouse embryonic fibroblasts (MEFs) in hESC medium composed of DMEM/F12 (Lifetech: 11320-033) supplemented with 20% KnockOut Serum Replacement (KSR) (Lifetech: 10828028), 2 mM glutamine (Lifetech: 25030-081), 1% non-essential amino acids (Lifetech: 11140-050), 0.1 mM β-mercaptoethanol (Lifetech: 21985-023), 1000 U/ml penicillin/streptomycin (Lifetech: 15140-122), and 4 ng/ml FGF2 (Lifetech: PHG0261). Cultures were passaged every 7 days with collagenase type IV (Lifetech: 17104019, 1.5 mg/ml) and gravitational sedimentation by washing 3 times in wash media composed of DMEM/F12 supplemented with 5% fetal bovine serum (Lifetech: 10082-147) and 1000 U/ml penicillin/streptomycin. All hESC lines were tested monthly for mycoplasma contamination.

hiPSC reprogramming

TSC patient (Coriell cell line #GM04520, referred to here as "4520") and control BJ fibroblasts (ATCC: CRL-2522) were reprogrammed into induced pluripotent stem cells using a commercial kit that delivers the reprogramming factors via an mRNA-based system [172] (Stemgent: 00-071). After reprogramming, cell lines were validated by expression of pluripotency markers and aCGH analysis. The patient *TSC2* genotype was confirmed by qPCR (Supplementary Fig. 6a). All hiPSC lines were tested monthly for mycoplasma contamination.

CRISPR/Cas9 genome editing

Single guide RNAs (Supplementary Table 3) targeting the genomic region of interest were inserted into the CRISPR/Cas9-encoding px330 plasmid [173]. Following trypsinization of hESCs, 15 μg of each px330 plasmid and 7.5 μg of a GFP-encoding plasmid were electroporated into approximately $1x10^7$ hESCs and re-plated onto MEFs as previously described [171]. After 72 hours, cells underwent fluorescence activated

cell sorting (FACS) to obtain $1x10^5$ GFP-positive single cells and were then re-plated. After 12 days, 48-72 single-cell derived hESC colonies were manually picked and re-plated onto individual wells. After 7 days, colonies were picked and re-plated, with the remaining cells genotyped using PCR. Genotyping primers are listed in Supplementary Table 2.3. The same guide RNAs and genotyping strategy used to create *TSC2*$^{-/-}$ WIBR3 hESCs were used create homozygous deletion of *TSC2* exon 5 in the BJ hiPSC line.

To generate a conditional allele of *TSC2*, we inserted an exon 5 cassette that was flanked by loxP sites into *TSC2*$^{-/-}$ hESCs. To do this we cloned a new guide RNA targeting the NHEJ junction into px330. A repair plasmid consisting of 500 bp long homology arms, exon 5 surrounded by loxP sites, and a puromycin resistance cassette flanked by FRT sites was created. 15 μg of the px330 and 35 μg of the repair plasmid were electroporated into the desired cells and re-plated onto DR4 MEFs. After 72 hours, puromycin (0.5 μg/mL, Lifetech: A11138-02) was added to hESC medium for the next 7 days. Surviving single cell-derived colonies were manually picked and re-plated. Genotyping was repeated as above to confirm the insertion of the puromycin cassette and the re-insertion of the exon through homology directed repair (HDR). The puromycin resistance cassette was then removed through transfection of Flp recombinase mRNA (Miltenyi Biotec: 130-106-769) with a Stemfect RNA transfection kit (Stemgent: 00-0069) and subsequent single-cell derived colony isolation and genotyping. 4520$^{c/-}$ hiPSCs were generated using the same approach.

The tdTomato Cre-reporter cassette was based on the Ai9 construct generated by Dr. Hongkui Zeng [174] (Addgene plasmid #22799). The reporter cassette was inserted into the AAVS1 safe-harbor locus [76], after exon 1 of the PPP1R12C gene, using the same HDR genome editing methods described above. The STOP cassette (3x STOP-SV40 PA) is excised in the presence of Cre recombinase allowing expression of tdTomato from the CAGGS promoter. tdTomato is expressed in all of the progeny of cells initially infected with Cre lentivirus. All gene-edited hPSC lines were validated by expression of pluripotency markers and aCGH analysis.

Teratoma Formation

TSC2$^{-/c;LSL\text{-}tdTom}$ hESCs were collected by collagenase treatment (1 mg/ml) and separated from feeder cells by sedimentation. Cells were resuspended in 250ul of DMEM + 5% FBS and injected subcutaneously into NOD-SCID mice (Taconic). All animal protocols were approved by UC Berkeley's Animal Care and Use Committee. Teratomas formed within 4-8 weeks, at which time teratomas were isolated, fixed in formalin and embedded in paraffin followed by sectioning and hematoxylin and eosin (H&E) staining. Whole teratoma images were collected at on a Zeiss Axio Scan.Z1 slidescanning microscope (Plan-Apo 20X/0.8 NA).

Array Comparative Genomic Hybridization (aCGH)

hPSC samples were collected by collagenase treatment (1.5 mg/ml) and separated from feeder cells by sedimentation and subsequently pelleted by centrifugation. Samples were frozen and sent to Cell Line Genetics (Madison, WI) for aCGH analysis. For aCGH, >1 μg of DNA was extracted from samples and run on an

Agilent SurePrint G3 Human CGH Microarray covering 60,000 probes evenly spaced across the genome.

Two-dimensional neuronal culture

Neural induction was performed as described previously [175], with minor alterations. Single hESCs were initially plated at a density of 50,000/cm^2 (1.9x10^5 cells/well of a 12 well plate) and maintained in complete conditioned hESC media until >90% confluent. hESCs were transferred to induction media supplemented with 100 ng/ul Noggin (R&D Systems: 6057-NG) and 10 µM SB431542 (Selleck Chemicals: S1067) with daily media changes for 10 days. The composition of induction media changed throughout induction with 100% induction media A (A) from days 1-4, 75% A and 25% induction media B (B) on days 5-6, 50% A and 50% B on days 7-8 and 25% A and 75% B on days 9-10. Induction media A is composed of Knockout DMEM (Lifetech: 10829018) with 15% KSR, 2 mM l-glutamine, 1% non-essential amino acids, 1000 U/ml penicillin/streptomycin) and 55 µM β-mercaptoethanol. Induction media B is composed of 50% DMEM/F12 media (Lifetech: 11320-033), 50% Neurobasal media (Lifetech: 21103049), 1x N-2 Supplement (Lifetech: 17502048), 1x Glutamax (Lifetech: 35050061), 1000 U/ml penicillin/streptomycin (Lifetech: 15070063), 0.2% human Insulin (Sigma: I9278) and 0.075% BSA (Sigma: A4503) w/v) as previously described[175]. After neural induction was complete, cells were dissociated with Accutase (Lifetech: A1110501), spun down for 4 minutes at 800 rpm, resuspended in N2 media supplemented with 25 ng/ml FGF and 40 ng/ml EGF (R&D Systems: 236-EG) and replated at 1:2. Cells were passaged as such every 5 days until passage 4, when they were split at 1:3.

Neuronal differentiation from NPCs was commenced at passage 8. NPCs were plated at low density: 80,000/cm^2 (8x10^5 cells/well of a 6 well plate) in 4 ml of growth media. Growth media (N2B27 media) is composed of 50% DMEM/F12, 50% Neurobasal Media, 1x N-2 Supplement, 1x B-27 Supplement (Lifetech: 17504044), 1x Glutamax, 1000 U/ml penicillin/streptomycin and 0.075% BSA w/v. For the first 12 days, growth media was supplemented with 20 ng/ml BDNF (Sigma: SRP3014) and 20 ng/ml NT-3 (Sigma: SRP3128), with half volume media changes every 4 days. On day 30, cells in 6-well plates were dissociated with Accutase and replated onto poly-D-lysine (Sigma: P6407) and laminin-coated (Lifetech: 23017015) 12 mm glass cover slips in 24-well plates for immunocytochemistry or PDL-coated BioCoat plates (Corning: 62405-749) for western blotting. Cells were matured until day 50-100 when they were harvested for further processing.

Three-dimensional cortical spheroid differentiation

Three-dimensional differentiation of hESCs and hiPSCs into cortical spheroids was performed as described previously [1]. Briefly, confluent, undifferentiated colonies of hESCs were removed from MEFs using collagenase. Colonies were washed once with media and suspended in hESC media without FGF2, supplemented with 10 µm Y-27632 and plated into 6-well low attachment plates (Corning: 3471). On days 1-5, media was changed to hESC-FGF2 media, supplemented with 10 µm Dorsomorphin (Abcam: ab146597) and 10 µm SB431542. On day 6, developing spheroids were put into neural induction media composed of Neurobasal-A (ThermoFisher: 10888022), B-27

Supplement–A (ThermoFisher: 12587-010), Pen/Strep, and Glutamax, supplemented with 20 ng/ml FGF and 20 ng/ml EGF. Media was changed in this manner every day from days 6-15 and then every other day until day 25. From days 25-43, the developing spheroids were grown in neural induction media supplemented with 20 ng/ml BDNF and 20 ng/ml NT-3, with media changes every 4 days. From day 43 on, spheroids were maintained in neural induction media without BDNF or NT-3, with media changes every 4 days until harvest.

Western blotting

2D cultured cells were harvested in lysis buffer containing 2 mM EDTA, 2 mM EGTA, 1% Triton-X, and 0.5% SDS in 1x PBS with Halt phosphatase inhibitor cocktail (Fisher: PI78420) and Complete mini EDTA-free protease inhibitor cocktail (Roche: 4693159001). Three-dimensional spheroids were harvested in lysis buffer containing 1% SDS, phosphatase inhibitor and protease inhibitor in 1x PBS. Total protein was determined by BCA assay (Fisher: PI23227) and 5-15 µg of protein in Laemmli sample buffer were loaded onto 4–15% Criterion TGX gels (Bio-Rad: 5671084). Proteins were transferred to PVDF membranes, blocked in 5% milk in TBS-Tween for one hour at room temperature (RT), and incubated with primary antibodies diluted in 5% milk in TBS-Tween overnight at 4°C. The following day, membranes were incubated with HRP-conjugated secondary antibodies (Bio-Rad: 170-5046, 1705047) for one hour at RT, washed, incubated with chemiluminesence substrate (Perkin-Elmer: NEL105001EA) and developed on GE Amersham Hyperfilm ECL (VWR: 95017-661). Membranes were stripped with 6M guanidine hydrochloride to re-blot on subsequent days. Bands were quantified by densitometry using Image J software. Phospho-proteins were normalized to their respective total proteins and non-phospho-proteins were normalized to a β-Actin loading control. Antibody vendors, catalog numbers, and dilutions are listed in Supplementary Table 2.4.

Immunocytochemistry on two-dimensional cultured cells

Cells plated onto 12 mm glass coverslips were washed in ice-cold 1x PBS with Ca/Mg followed by fixation for 10 minutes in 4% paraformaldehyde (PFA) and three, five-minute washes in 1x PBS. Coverslips were blocked for one hour at RT in buffer containing 5% normal goat serum (NGS) (Lifetech: PCN5000) and 0.3% Triton-X in 1x PBS and incubated in primary antibodies in antibody dilution buffer (1% BSA (Sigma: A4503) and 0.3% Triton-X in 1x PBS) overnight at 4°C. The following day, coverslips were washed three times for five minutes in 1x PBS, incubated with secondary antibodies in antibody dilution buffer (1:500) for one hour at RT and washed three times for five minutes in 1x PBS. Coverslips were mounted onto slides with ProLong Gold Antifade mountant with or without DAPI (Fisher: P36934 or P36935) and allowed to set for one day before imaging. Antibody vendors, catalog numbers, and dilutions are listed in Supplementary Table 2.4.

Immunohistochemistry on three-dimensional spheroids

Spheroids were removed from growth media and washed once in ice-cold 1x PBS with Ca/Mg before being fixed in 4% PFA overnight at 4°C. After fixation, spheroids were placed into a conical tube containing 30% sucrose solution overnight at 4°C and

allowed to settle. The following day, spheroids were frozen in tissue blocks with OCT compound (Fisher: 23-730-571) and sectioned on a cryostat into 10 or 16 µm sections. Sections were washed once with PBS and blocked in buffer containing 10% NGS, 0.1% BSA and 0.3% Triton-X in 1x PBS for one hour at RT. Sections were then incubated overnight at 4°C in primary antibodies in antibody dilution buffer (2% NGS and 0.1% Triton-X in 1x PBS). The following day, sections were washed three times with 1x PBS, incubated in secondary antibody (1:500 in antibody dilution buffer) for one hour at RT and washed again three times with 1x PBS. Slides were coverslipped with ProLong Gold Antifade mountant with or without DAPI and allowed to set for one day before imaging. Antibody vendors, catalog numbers, and dilutions are listed in Supplementary Table 2.4.

Quantitative PCR

RNA was extracted from whole spheroids using an RNeasy kit (Qiagen: 74104) with an on-column DNAse digestion. RNA levels and purity were assessed with a NanoDrop spectrophotometer. Reverse transcription was performed using random hexamer primers and Superscript III reverse transcriptase (Lifetech: 18080051). Real-time PCR was performed in triplicate on 600 ng of cDNA using an Applied Biosystems QuantStudio 6 Flex Real-Time PCR System with SYBR FAST qPCR Master Mix (Kapa Biosystems: 07959389001). Values for all genes were normalized to β-actin for each sample. qPCR primer sequences are listed in Supplementary Table 2.3.

Lentiviral infection

CMV promoter-driven Cre-GFP, Cre-RFP, and/or GFP lentivirus (Kerafast: FCT073, FCT192, and FCT004, titer >$1.0x10^8$ CFU/ml) were added to cell culture media at the indicated time points. For high efficiency infection for western blot experiments, 2.0 µl per well was used in 24-well plates. For sparse infection, 0.25-0.5 µl per well was used in 6-well plates. This amount of Cre-GFP or Cre-RFP virus resulted in Cre expression in approximately 10-15% of the cells in the spheroid or 2D culture.

Sholl Analysis

Cultured two-dimensional *TSC2*$^{-/c;LSL\text{-}tdtom}$ neurons were treated with Cre lentivirus on day 5 of neural induction and fixed on day 75. Coverslips were stained with MAP2 antibody and subsequently imaged. Multiple cells per coverslip were traced by hand using the MAP2 channel. Cell traces were imported into ImageJ and analyzed using the built-in Sholl analysis feature. Concentric circles of 5 µm up to 160 µm from the center of the soma were used for quantification of dendritic intersections.

Rapamycin treatment

20 mM rapamycin (LC Laboratories: R-5000) stock solution was prepared in ethanol and stored at -20°C. Rapamycin stock was diluted to a final concentration of 20 nM and added to spheroids during every media change for the time periods indicated. Ethanol vehicle was added in the same concentration to control samples.

Confocal microscopy and image analysis

Images were taken on either an FV1000 Olympus Fluoview confocal microscope with 10x or 20x objectives or a Zeiss LSM 719 AxioObserver with 20x or 40x objectives. For experiments where two or more conditions were quantitatively compared, the same exposure and acquisition settings were used for each image. All images were processed using ImageJ. Only healthy regions of the spheroids, defined by intact DAPI nuclei, were used for quantification and analysis. To assess cell body size, regions of interest (ROIs) were drawn around each cell. ROIs were saved and applied to the p-S6 images where mean fluorescence units averaged across the ROI were used as the p-S6 value for that cell. For images analyzed for the presence or absence of cellular markers, a threshold was set based on the background fluorescence level and applied to all ROIs. If the mean fluorescence units averaged across the ROI were above the threshold, the cell was considered positive for the marker.

Statistics summary

Sample sizes were chosen based on previous studies. All samples were included in the analysis. No randomization was used to allocate samples to experimental groups. The investigator was blind to genotype for image analysis of constitutive spheroids. Other quantifications were not performed blindly. Statistical analysis was performed using GraphPad Prism software and the specific test for each experiment is noted in the Figure legend and in Supplementary Table 2.2. To compare the means of two normally distributed groups, an unpaired t-test was used. To compare the distributions between two groups, a Kolmogorov-Smirnov test was used. To compare the means of three or more groups, a one-way ANOVA was used followed by Bonferroni's or Sidak's multiple comparisons tests. For data sets with three or more groups with non-normal distributions or different numbers of samples per condition, a Kruskal-Wallis test was used followed by Dunn's multiple comparisons test. To compare two independent variables (e.g. genotype and day of differentiation) a two-way ANOVA was used with Dunnett's multiple comparisons tests. Reported P-values are adjusted for multiple comparisons for experiments with three or more groups. Supplementary Table 2 lists the sample sizes, sample definition, statistical tests, and exact P-values for all experiments.

Figures

Figure 2.1

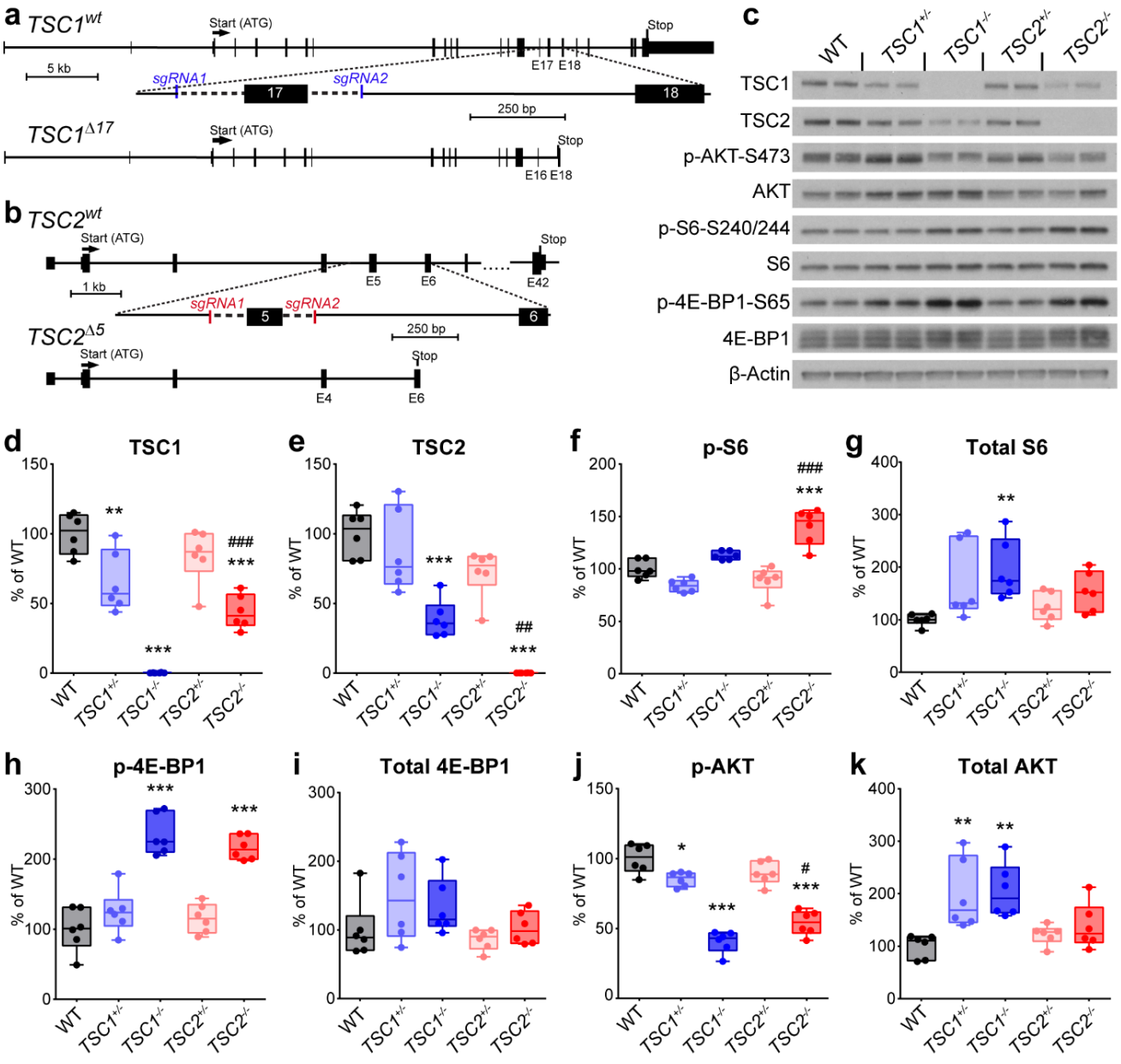

Fig. 2.1: Generation of heterozygous and homozygous knock-out TSC1 and TSC2 hESC lines. (**a**,**b**) CRISPR/Cas9-mediated targeting strategies for TSC1 and TSC2. (**a**) Two single-guide RNAs (sgRNA1 and 2) were designed to target either side of exon 17 of TSC1. The resulting $TSC1^{\Delta 17}$ allele has exon 17 deleted, creating a frameshift and premature stop codon in exon 18. (**b**) Two sgRNAs were designed to target either side of exon 5 of TSC2. The resulting $TSC2^{\Delta 5}$ allele has exon 5 deleted creating a frameshift and premature stop codon in exon 6. (**c**) Representative western blots of hESC lysates from the indicated genotypes. Two biological replicates per genotype are shown. (**d-k**) Box-and-whisker plots displaying western blot quantification for the indicated proteins; center line, median; box limits, 25^{th} to 75^{th} percentile; whiskers, minimum to maximum. Total proteins were normalized to β-Actin loading control, phospho-proteins were normalized to their respective total proteins. This experiment was performed once with six biological replicates. *, $p<0.05$, **, $p<0.01$, ***, $p<0.001$, compared to wild-type (WT); #, $p<0.05$, ##, $p<0.01$, ###, $p<0.001$ compared to $TSC1^{-/-}$; one-way ANOVA with Bonferroni's multiple comparisons tests. See Supplementary Table 2 for sample sizes and P values for all comparisons.

Figure 2.2

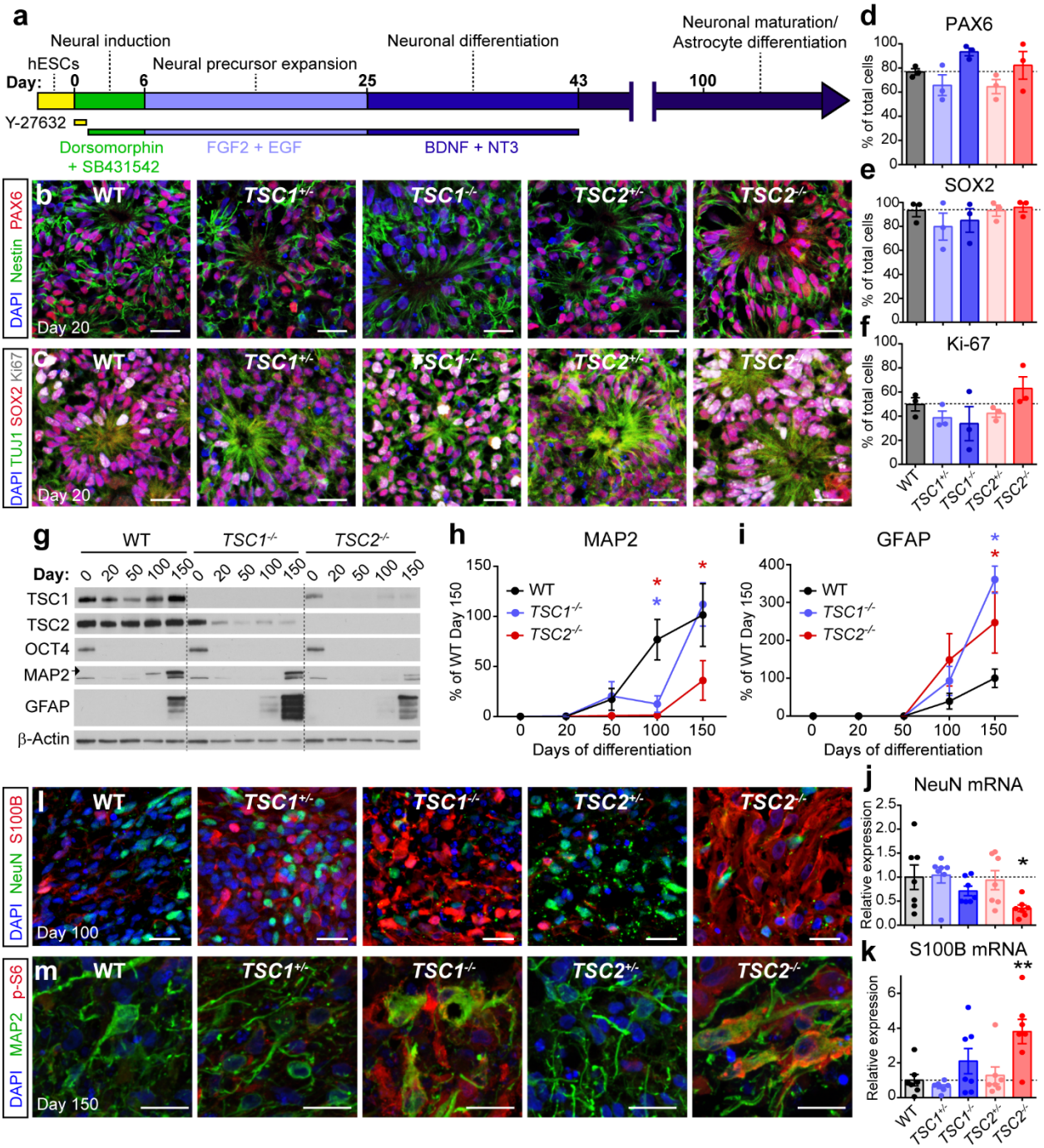
a
Neural induction
hESCs
Neural precursor expansion
Neuronal differentiation
Neuronal maturation/
Astrocyte differentiation
Day: 0 6 25 43 100
Y-27632
Dorsomorphin
+ SB431542
FGF2 + EGF
BDNF + NT3
b
DAPI Nestin PAX6
WT
TSC1+/-
TSC1-/-
TSC2+/-
TSC2-/-
Day 20
c
DAPI TUJ1 SOX2 Ki67
Day 20
d
PAX6
% of total cells
e
SOX2
% of total cells
f
Ki-67
% of total cells
WT
TSC1+/-
TSC1-/-
TSC2+/-
TSC2-/-
g
WT
TSC1-/-
TSC2-/-
Day: 0 20 50 100 150
TSC1
TSC2
OCT4
MAP2
GFAP
β-Actin
h
MAP2
% of WT Day 150
Days of differentiation
i
GFAP
% of WT Day 150
Days of differentiation
l
DAPI NeuN S100B
Day 100
m
DAPI MAP2 p-S6
Day 150
j
NeuN mRNA
Relative expression
k
S100B mRNA
Relative expression

Fig. 2.2: TSC1$^{-/-}$ and TSC2$^{-/-}$ cortical spheroids have impaired neuronal and enhanced glial differentiation. (**a**) Schematic of the 3D cortical differentiation protocol (based on Pasca, A.M. et al, 2015)[1]. (**b,c**) Confocal images of day 20 cortical spheroid sections from the indicated genotypes, stained with antibodies against nestin (green) and PAX6 (red) (**b**) or TUJ1 (green), SOX2 (red), and Ki-67 (grey) (**c**). DAPI staining is in blue. Scale bars represent 25 μm. (**d-f**) Bars graphs (mean +/- s.e.m) displaying quantification of PAX6 (**d**), SOX2 (**e**), or Ki-67 (**f**) positive cells expressed as a percentage of total DAPI-labeled cells in day 20 cortical spheroids. This experiment was replicated three times (three separate differentiations). (**g**) Example western blots of wild-type (WT), TSC1$^{-/-}$, and TSC2$^{-/-}$ cortical spheroids harvested at different time points post-differentiation from hESCs (day 0). (**h,i**) Quantification of western blot results for the neuronal protein MAP2 (**h**) and the glial protein GFAP (**i**) across cortical spheroid development (mean +/- s.e.m.). Two-way ANOVAs revealed significant effects of day ($p<0.001$), genotype ($p<0.05$), and a day x genotype interaction ($p<0.01$) for MAP2 and a significant effect of day ($p<0.001$) for GFAP. Dunnett's multiple comparisons tests revealed significant reductions in MAP2 at day 100 for TSC1$^{-/-}$ ($p<0.01$, blue asterisk) and TSC2$^{-/-}$ ($p<0.001$, red asterisk), and at day 150 and for TSC2$^{-/-}$ ($p<0.01$) compared to WT. GFAP was significantly elevated in TSC1$^{-/-}$ ($p<0.001$, blue asterisk) and TSC2$^{-/-}$ ($p<0.01$, red asterisk) spheroids on day 150 compared to WT. This experiment was replicated three times (three separate differentiations). (**j,k**) Quantitative PCR results (mean +/- s.e.m.) for NeuN (**j**) and S100B (**k**) mRNA in day 100 cortical spheroids. *, $p<0.05$; **, $p<0.001$, one-way ANOVA followed by Dunnett's multiple comparisons test. This experiment was replicated five times (five separate differentiations). (**l**) Confocal images of day 100 cortical spheroid sections stained with antibodies against NeuN (green) and S100B (red). DAPI staining is in blue. Scale bars represent 25 μm. (**m**) Confocal images of day 150 cortical spheroid sections stained with antibodies against MAP2 (green) and phosphorylated S6 (p-S6, ser240/244, red). DAPI staining is in blue. Scale bars represent 20 μm. See Supplementary Table 2 for sample sizes and P values for all comparisons.

Figure 2.3

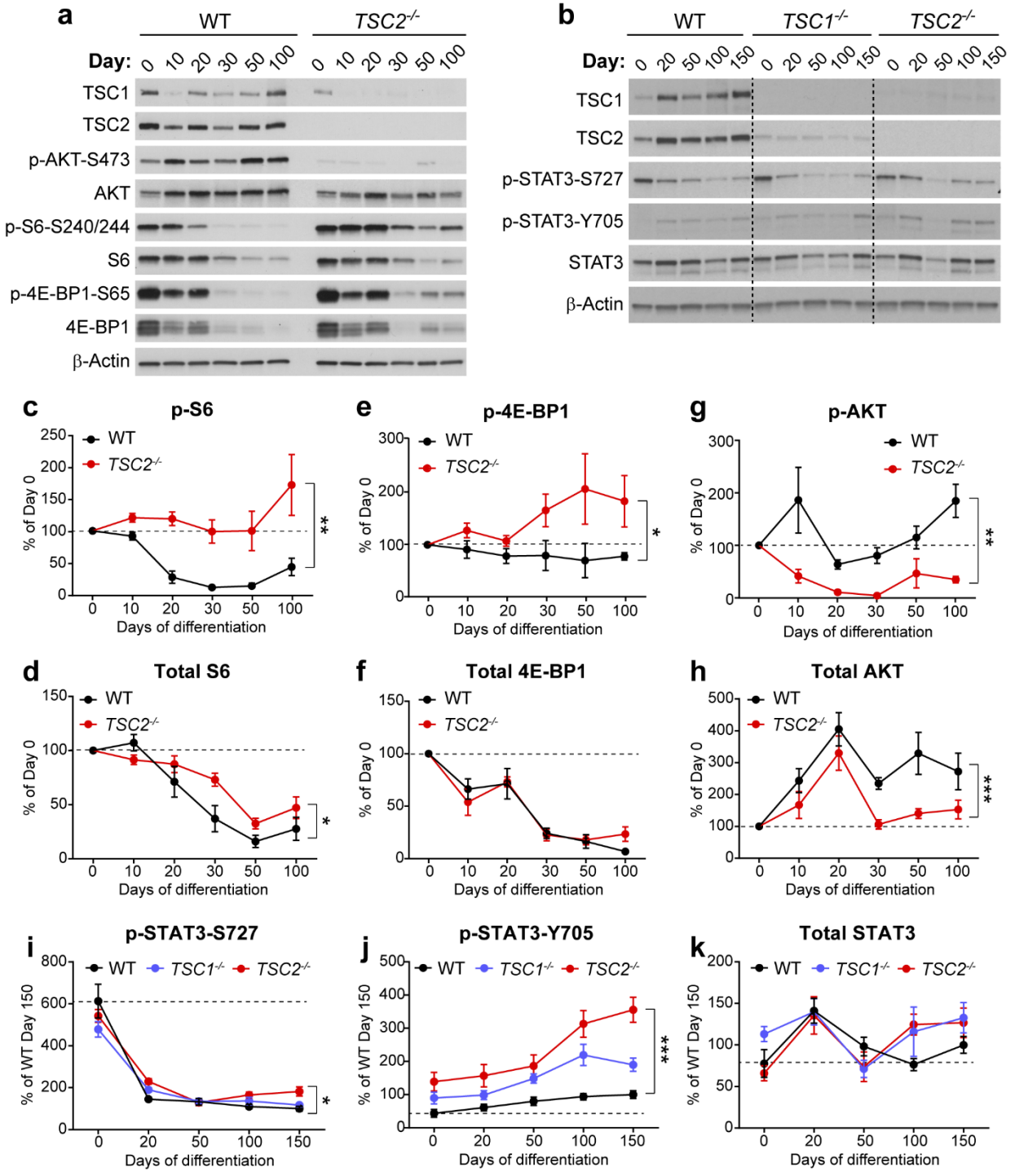
a
WT
TSC2-/-
Day: 0 10 20 30 50 100 0 10 20 30 50 100
TSC1
TSC2
p-AKT-S473
AKT
p-S6-S240/244
S6
p-4E-BP1-S65
4E-BP1
β-Actin
b
WT
TSC1-/-
TSC2-/-
Day: 0 20 50 100 150 0 20 50 100 150 0 20 50 100 150
TSC1
TSC2
p-STAT3-S727
p-STAT3-Y705
STAT3
β-Actin
c
p-S6
e
p-4E-BP1
g
p-AKT
d
Total S6
f
Total 4E-BP1
h
Total AKT
i
p-STAT3-S727
j
p-STAT3-Y705
k
Total STAT3
WT
TSC2-/-
TSC1-/-
% of Day 0
% of WT Day 150
Days of differentiation
*
**
***

Fig. 2.3: TSC1$^{-/-}$ and TSC2$^{-/-}$ cortical spheroids fail to suppress mTORC1 signaling during neuronal differentiation. (**a**) Representative westerns blots of mTORC1 signaling pathway proteins from wild-type (WT) or TSC2$^{-/-}$ cortical spheroids collected on different days post-differentiation. Day 0 is the hESC stage. (**b**) Representative western blots of phosphorylated and total STAT3 protein from WT, TSC1$^{-/-}$ or TSC2$^{-/-}$ cortical spheroids collected on different days post-differentiation. (**c-h**) Quantification of western blot data for WT and TSC2$^{-/-}$ cortical spheroids across development for the indicated phosphorylated and total proteins. Total proteins were normalized to β-Actin loading control and phospho-proteins were normalized to their respective total proteins. Data are represented as mean +/- s.e.m. and expressed as percent of day 0 within each genotype. The dashed lines at 100% represent the day 0 values. *, $p<0.05$, **, $p<0.01$, ***, $p<0.001$, two-way ANOVA, significant effect of genotype. This experiment was replicated three times (three separate differentiations). (**i-k**) Quantification of western blot data for WT, TSC1$^{-/-}$, and TSC2$^{-/-}$ cortical spheroids across development for phosphorylated and total STAT3. S727 and Y705 phosphorylated STAT3 were normalized to total STAT3. Total STAT3 was normalized to β-Actin loading control. Data are represented as mean +/- s.e.m. and expressed as percent of the WT value on day 150. The dashed lines at 100% represent the WT day 0 values. *, $p<0.05$, ***,$p<0.001$, two-way ANOVA, significant effect of genotype. This experiment was replicated three times (three separate differentiations). See Supplementary Table 2 for sample sizes and P values for all comparisons.

Figure 2.4

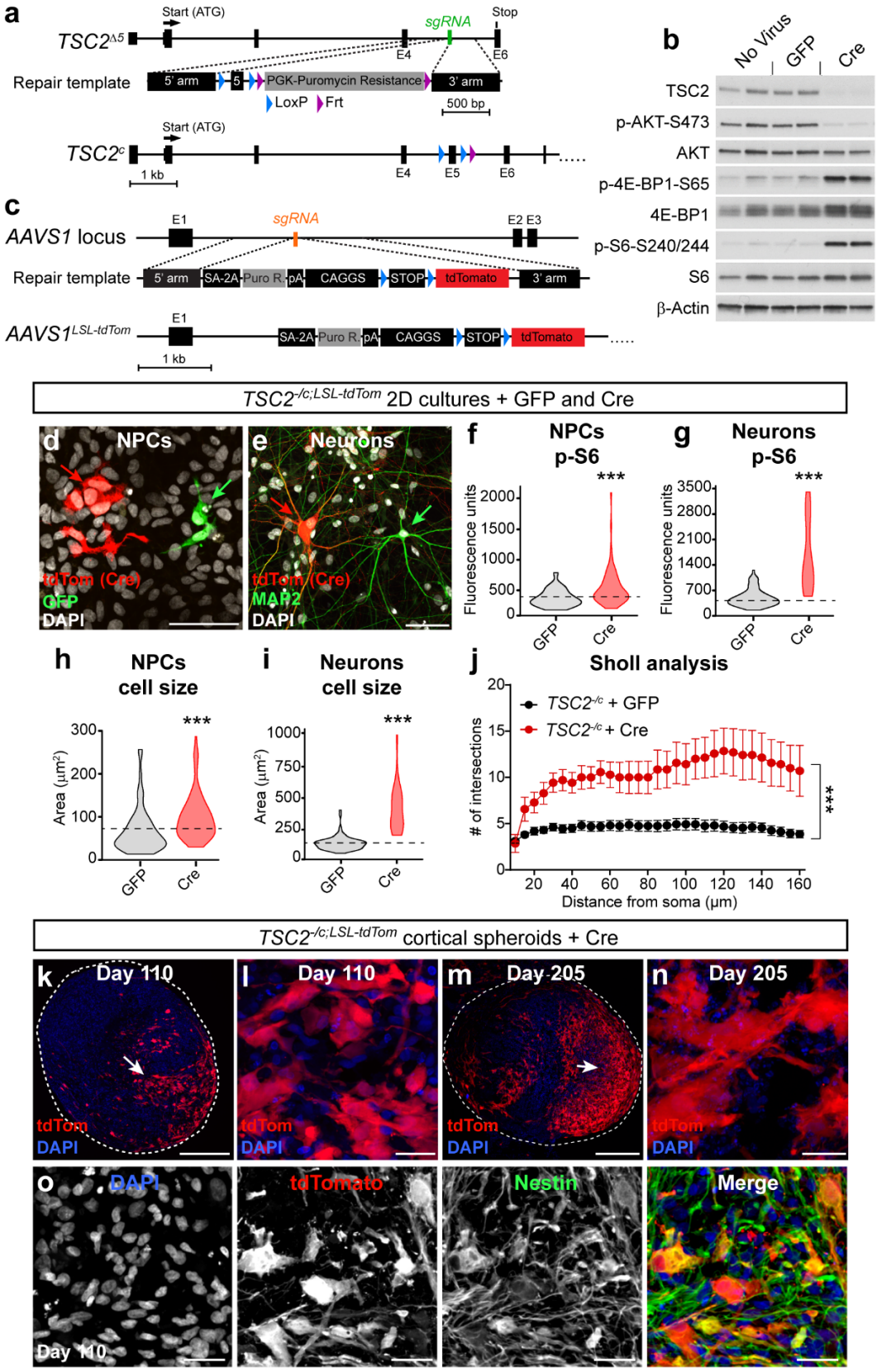
a
Start (ATG)
sgRNA
Stop
TSC2Δ5
E4
E6
Repair template
5' arm
5
PGK-Puromycin Resistance
3' arm
LoxP
Frt
500 bp
Start (ATG)
TSC2c
1 kb
E4
E5
E6
b
No Virus
GFP
Cre
TSC2
p-AKT-S473
AKT
p-4E-BP1-S65
4E-BP1
p-S6-S240/244
S6
β-Actin
c
AAVS1 locus
E1
sgRNA
E2 E3
Repair template
5' arm
SA-2A
Puro R
pA
CAGGS
STOP
tdTomato
3' arm
AAVS1LSL-tdTom
1 kb
TSC2-/c;LSL-tdTom 2D cultures + GFP and Cre
d NPCs
tdTom (Cre)
GFP
DAPI
e Neurons
tdTom (Cre)
MAP2
DAPI
f NPCs p-S6
Fluorescence units
***
GFP
Cre
g Neurons p-S6
Fluorescence units
***
GFP
Cre
h NPCs cell size
Area (μm²)
***
GFP
Cre
i Neurons cell size
Area (μm²)
***
GFP
Cre
j Sholl analysis
TSC2-/c + GFP
TSC2-/c + Cre
# of intersections
***
Distance from soma (μm)
TSC2-/c;LSL-tdTom cortical spheroids + Cre
k Day 110
tdTom
DAPI
l Day 110
tdTom
DAPI
m Day 205
tdTom
DAPI
n Day 205
tdTom
DAPI
o DAPI
Day 110
tdTomato
Nestin
Merge

Fig. 2.4: Conditional inactivation of TSC2 models a second-hit mutation and causes the formation of dysplastic cells. (**a**) CRISPR/Cas9-based gene editing strategy to create a conditional allele of TSC2. (**b**) Western blots of lysates from $TSC2^{-/c}$ neurons in 2D culture treated with either GFP or Cre lentivirus on day 2 of differentiation and harvested on day 21. This experiment was replicated two times (only one experiment with two biological replicates is shown). (**c**) To generate a Cre-reporter allele, a gene trap approach was used to insert a CAGGS promoter-floxed STOP-tdTomato cassette into the AAVS1 locus of $TSC2^{-/c}$ hESCs ($TSC2^{-/c;LSL\text{-}tdTom}$). (**d**) $TSC2^{-/c;LSL\text{-}tdTom}$ hESCs were differentiated into 2D cultures of NPCs. Sub-saturating amounts of Cre-GFP and GFP lentivirus were added to NPCs on day 10 post-neural induction (passage 3) and cells were harvested on day 25 (passage 6). Scale bar represents 50 μm. (**e**) Cre-GFP and GFP viruses were added to neurons on day 5 post-neuronal differentiation and neurons were harvested on day 75. Cre-expressing cells are marked by tdTomato expression (red). Scale bar represents 50 μm. (**f-i**) Violin plots displaying p-S6 levels (**f,g**) and cell size (**h,i**) for GFP and Cre treated NPCs or neurons. ***, $p<0.001$, Kolmogorov-Smirnov test. Dashed lines indicate the mean of GFP-positive cells. These data were obtained from one differentiation. (**j**) Sholl analysis (as mean +/- s.e.m.) of dendritic arborization of day 75 neurons in 2D culture expressing either GFP or Cre. ***, $p<0.001$, two-way ANOVA, significant effect of genotype. These data were obtained from one differentiation. (**k-n**) $TSC2^{c/-;tdTom}$ hESCs were differentiated into three-dimensional cortical spheroids and treated with sub-saturating amounts of Cre lentivirus on day 12. (**k**) Confocal image of a section from a day 110 cortical spheroid showing a region of tdTomato-positive TSC2 homozygous mutant cells. Scale bar represents 250 μm. (**l**) Higher magnification image showing enlarged and dysmorphic tdTomato-positive cells. Scale bar represents 25 μm. (**m**) Confocal image of a section from a day 205 cortical spheroid. Scale bar represents 250 μm. (**n**) Higher magnification image of day 205 tdTomato-positive cells. Scale bar represents 25 μm. (**o**) Confocal images of a day 110 cortical spheroid section stained with an antibody against Nestin (green). DAPI staining is in blue. Scale bar represents 25 μm. See Supplementary Table 2 for sample sizes and P values for all comparisons.

Figure 2.5

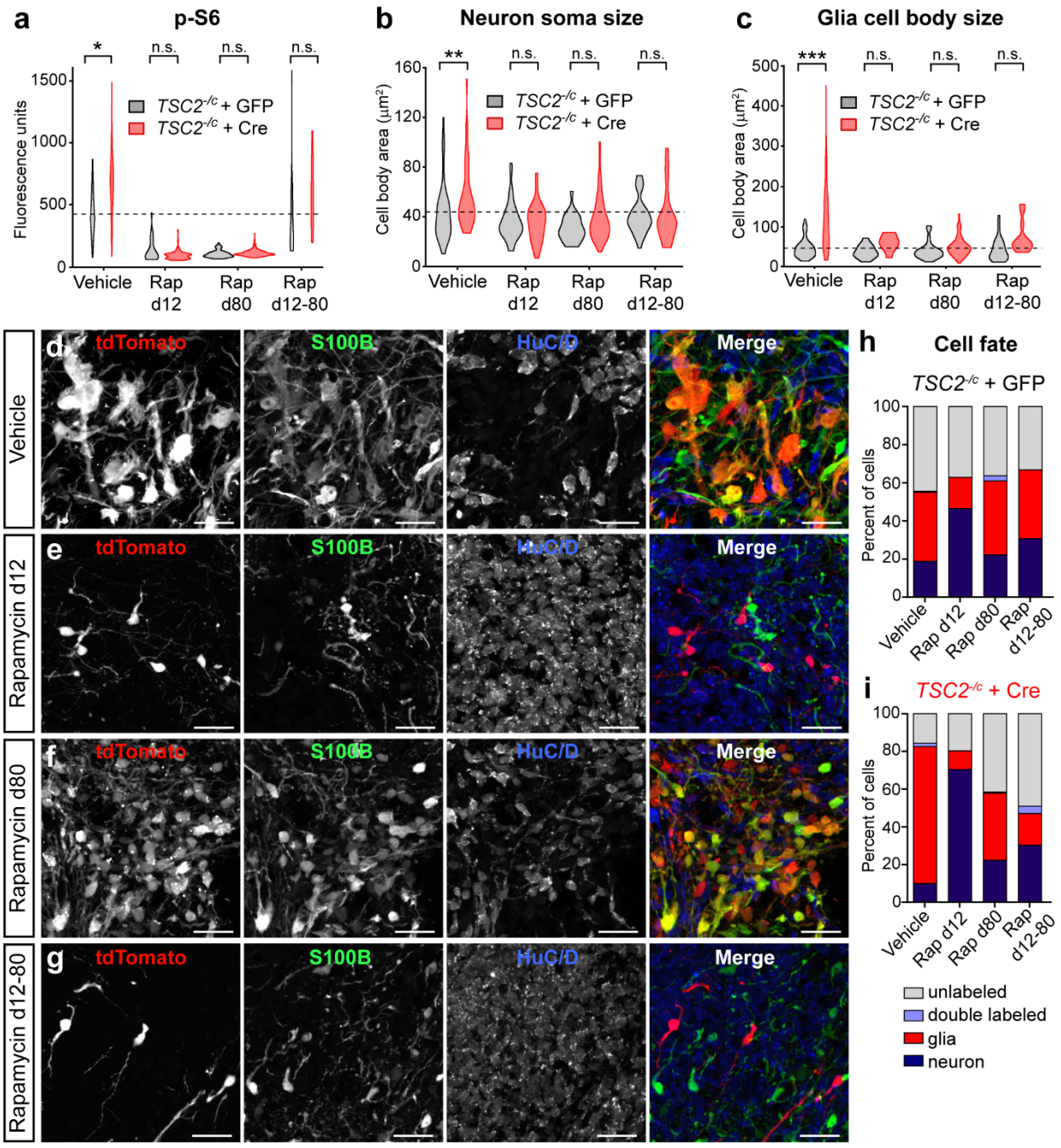
a
p-S6
Fluorescence units
1500
1000
500
0
*
n.s.
n.s.
n.s.
TSC2-/c + GFP
TSC2-/c + Cre
Vehicle
Rap d12
Rap d80
Rap d12-80
b
Neuron soma size
Cell body area (µm²)
160
120
80
40
0
**
n.s.
n.s.
n.s.
c
Glia cell body size
500
400
300
200
100
0
***
n.s.
n.s.
n.s.
Vehicle
Rapamycin d12
Rapamycin d80
Rapamycin d12-80
d
e
f
g
tdTomato
S100B
HuC/D
Merge
h
Cell fate
TSC2-/c + GFP
Percent of cells
100
80
60
40
20
0
Vehicle
Rap d12
Rap d80
Rap d12-80
i
TSC2-/c + Cre
unlabeled
double labeled
glia
neuron

Fig. 2.5: Cellular hypertrophy and neuronal differentiation defects in TSC2 mutant cells can be prevented by early rapamycin treatment. (**a**) Day 110 $TSC2^{-/c;LSL\text{-}tdTom}$ spheroids were sectioned and stained with antibodies against phosphorylated S6 (p-S6, Ser240/244). Violin plots display the distribution of mean p-S6 fluorescence per cell calculated for GFP-expressing TSC2 heterozygous cells ($TSC2^{-/c}$ + GFP, grey) and tdTomato-expressing TSC2 homozygous mutant cells ($TSC2^{-/c}$ + Cre, red) for each treatment condition. Spheroids were treated with vehicle, chronic rapamycin from day 12 to 110 (Rap d12), chronic rapamycin from day 80 to 110 (Rap d80), or chronic rapamycin from day 12 to 80 (Rap d12-80). The dashed line indicates the mean of GFP+ vehicle-treated cells. n.s.=not significant, *, $p<0.05$ Kruskal-Wallis test with Dunn's multiple comparisons test. (**b,c**) Sections from $TSC2^{-/c;LSL\text{-}tdTom}$ spheroids were stained with antibodies against the neuronal marker HuC/D and the glial marker S100B. Neuron soma (**b**) and glial cell body (**c**) cross-sectional area were calculated for each genotype and rapamycin condition. The dashed lines indicate the means of GFP+ vehicle-treated cells. n.s.=not significant, **, $p<0.01$, ***, $p<0.001$, Kruskal-Wallis test with Dunn's multiple comparisons test. (**d-g**) Example confocal images of HuC/D and S100B immunostained sections from day 110 $TSC2^{-/c;LSL\text{-}tdTom}$ spheroids with the indicated treatments. Scale bars represent 25 μm. (**h,i**) Graphs display the percentage of GFP (**h**) or tdTomato (**i**) positive cells expressing HuC/D (neuron, dark blue) or S100B (glia, red) for each rapamycin condition. For all panels, data were obtained from one differentiation, 2-4 spheroids per treatment. See Supplementary Table 2 for sample sizes and P values for all comparisons.

Supplementary Figures

Supplementary Figure 2.1

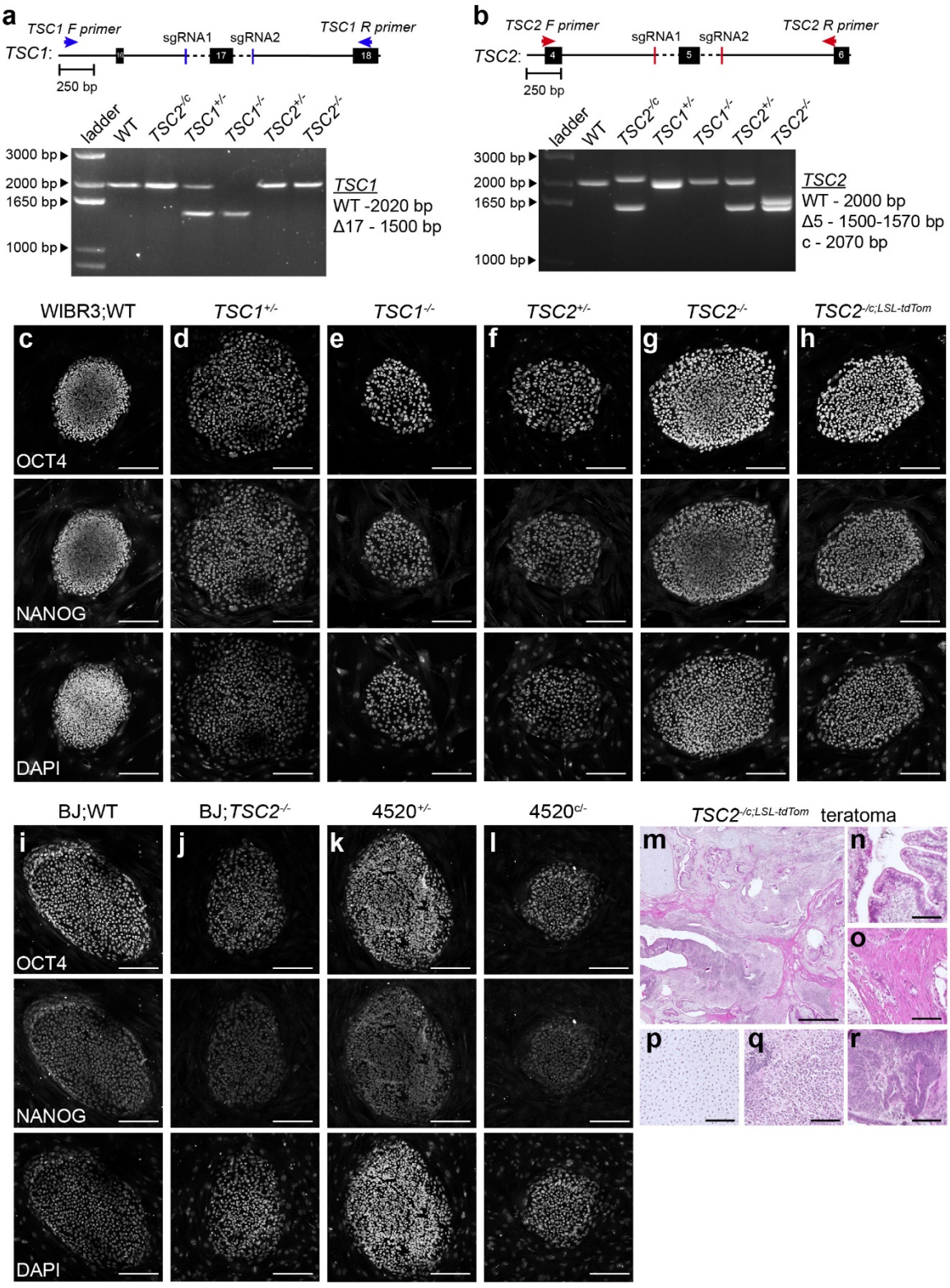

Supplementary Fig. 2.1. Validation of human pluripotent stem cell lines. (**a**) Top, genotyping strategy for the exon 17 *TSC1* mutation. Bottom, PCR genotyping for *TSC1*. The wild-type (WT) allele produces a 2020 bp product and the exon 17 deleted allele produces a 1500 bp product. (**b**) Top, genotyping strategy for the exon 5 *TSC2* mutation. Bottom, PCR genotyping for *TSC2*. The WT allele produces a 2000 bp product, the floxed exon 5 allele produces a 2070 bp product, the exon 5 deleted allele produces a 1500 bp product, and Cre-mediated deletion of floxed exon 5 produces a 1570 bp product. Note that the $TSC2^{-/-}$ hESC line was generated by Cre-mediated deletion of exon 5 from $TSC2^{-/c}$ hESCs. (**c-l**) Images of hESC (**c-h**) and hiPSC (**i-l**) colonies of the indicated genotypes stained for the pluripotency markers OCT4 (top row) and NANOG (middle row). Nuclear DAPI staining is in the bottom row. The scale bars in panels **c-l** represent 200 μm. (**m-r**) Images of a hematoxylin and eosin (H&E) stained teratoma derived from $TSC2^{-/c;LSL\text{-}tdTom}$ hESCs showing all three germ layers: endoderm (**n**), mesoderm (**o,p**), and ectoderm (**q,r**). The scale bar for panel **m** represents 1 mm, the scale bars for panels **n-r** represent 100 μm.

Supplementary Figure 2.2

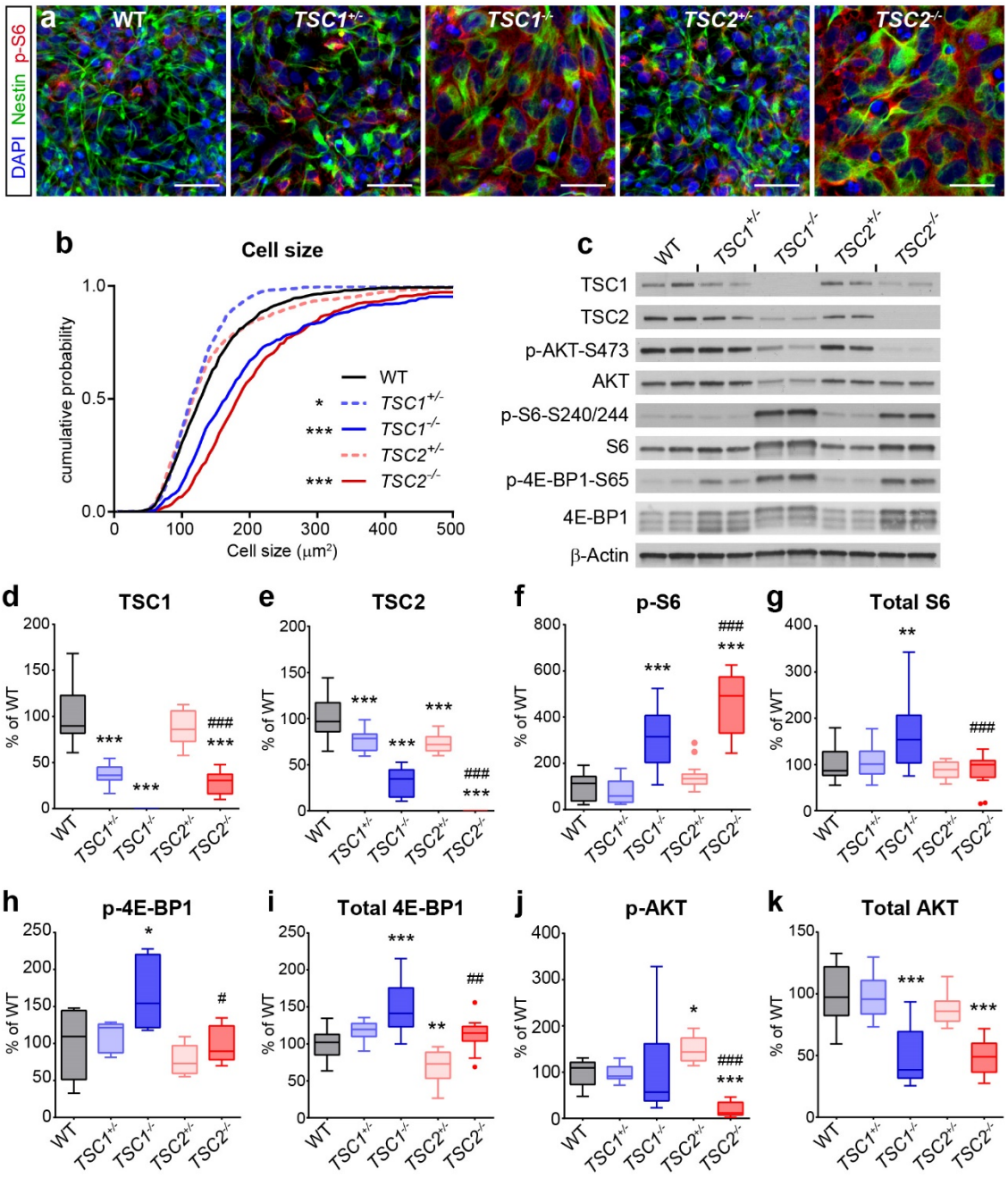

Supplementary Fig. 2.2. Homozygous loss of *TSC1* or *TSC2* in human neural precursor cells (NPCs) causes increased mTORC1 signaling and cellular hypertrophy. (**a**) Confocal images of immunostained human NPCs in two-dimensional culture. The intermediate filament protein and NPC marker nestin is in green, phosphorylated S6 (Ser240/244) is in red, and nuclei are labeled with DAPI in blue. Scale bars represent 25 μm. (**b**) Cumulative probability plot of cross-sectional cell area for NPCs of the indicated genotypes. *, $p<0.05$; ***, $p<0.001$ compared to WT, Kruskal-Wallis test with Dunn's multiple comparisons test. This experiment was replicated three times (three separate differentiations). (**c**) Representative western blots of NPC lysates from the indicated genotypes (two independent biological replicates per genotype are shown). (**d-k**) Box-and-whisker plots of western blot results for the indicated proteins; center line, median; box limits, 25th to 75th percentile, whiskers, Tukey (1.5x interquartile range). TSC1, TSC2, and total proteins were normalized to β-Actin loading control, phospho-proteins were normalized to their respective total protein. Results are displayed as a percentage of wild-type (WT) values. This experiment was replicated four times (four separate differentiations). *, $p<0.05$; **, $p<0.01$; ***, $p<0.001$ compared to WT; ##, $p<0.01$, ###, $p<0.001$ compared to *TSC1*$^{-/-}$; one-way ANOVA with Bonferroni's multiple comparisons test. See Supplementary Table 2 for sample sizes and P values for all comparisons.

Supplementary Figure 2.3

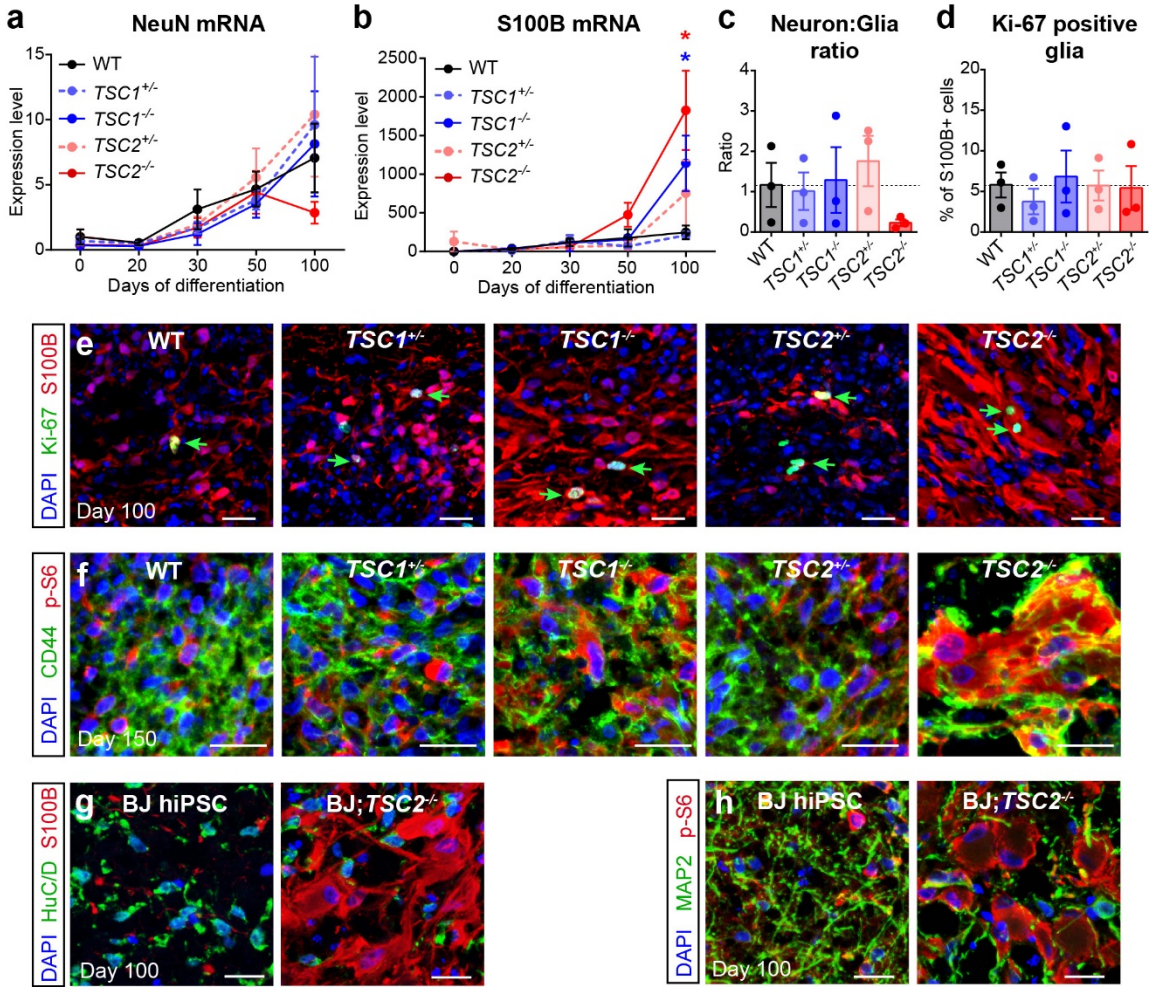

Supplementary Fig. 2.3. Expression of neuron and glia markers in cortical spheroids with mutations in *TSC1* or *TSC2*. (**a**) Quantitative PCR results for NeuN (**a**) and S100B (**b**) mRNA over time in cortical spheroids of the indicated genotypes displayed as mean +/- s.e.m. Day 0 represents the hESC stage. n=4 spheroids per genotype per time point. Two-way ANOVAs revealed significant effects of time for both NeuN ($p<0.001$) and S100B ($p<0.001$). S100B also showed a significant effect of genotype ($p<0.05$) and a time x genotype interaction ($p<0.001$). Dunnet's multiple comparisons tests revealed significant differences in S100B between wild-type (WT) and *TSC1*$^{-/-}$ spheroids (blue, *, $p<0.001$) and WT and *TSC2*$^{-/-}$ (red, *, $p<0.001$) on day 100. (**c**) Bar graphs display mean +/- s.e.m. neuron to glia ratio quantified as the proportion of NeuN-positive cells to S100B-positive cells in day 100 spheroids. n=3 spheroids per genotype. (**d**) Bar graphs display mean +/- s.e.m. Ki67-positive glia quantified as the proportion of S100B-positive cells that were Ki67-positive in day 100 spheroids. n=3 spheroids per genotype. (**e**) Confocal images of cortical spheroids of the indicated genotypes harvested on day 100 and immunostained with antibodies against the cell proliferation marker Ki-67 (green) and the glial protein S100B (red). DAPI staining is in blue. (**f**) Confocal images of cortical spheroids of the indicated genotypes harvested on day 150 and immunostained with antibodies against the glial protein CD44 (green) and phosphorylated S6 (p-S6, Ser240/244, red). DAPI staining is in blue. (**g,h**) Confocal images of day 100 cortical spheroids differentiated from control (BJ) hiPSCs or hiPSCs with homozygous deletion of exon 5 of *TSC2* (BJ;*TSC2*$^{-/-}$). Spheroids were stained with antibodies against the neuronal protein HuC/D (green) and glial protein S100B (red) (**g**) or the dendritic protein MAP2 (green) and phosphorylated S6 (red) (**h**). DAPI staining is in blue. Scale bars in all panels represent 25 μm. See Supplementary Table 2 for sample sizes and P values for all comparisons.

Supplementary Figure 2.4

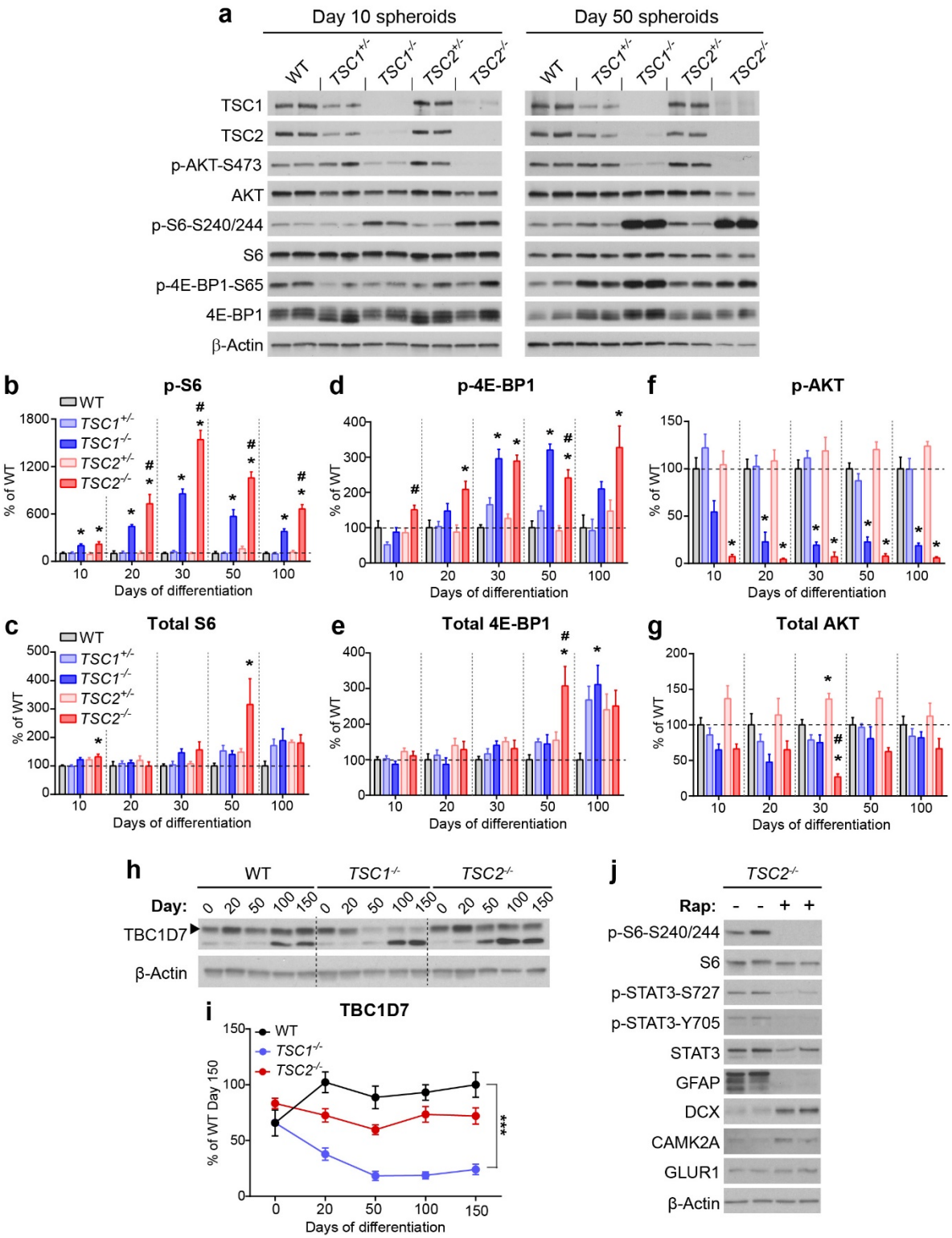

Supplementary Fig. 2.4. mTORC1 signaling is elevated in *TSC1*$^{-/-}$ and *TSC2*$^{-/-}$ cortical spheroids during neuronal differentiation. (**a**) Representative western blots from cortical spheroids of the five genotypes (WT, *TSC1*$^{+/-}$, *TSC1*$^{-/-}$, *TSC2*$^{+/-}$, *TSC2*$^{-/-}$) collected on day 10 (left panels) or day 50 (right panels) post-differentiation. Data from two independent spheroids per genotype are shown. This experiment was replicated three times (three separate differentiations). (**b-g**) Quantification of western blot data for cortical spheroids of the five genotypes on day 10, 20, 30, 50 and 100 post-differentiation from stem cells. Total proteins were normalized to β-Actin loading control and phospho-proteins were normalized to their respective total proteins. Data are represented as mean +/- s.e.m. and expressed as a percentage of wild-type (WT) on each day. The dashed lines at 100% represent the wild-type values. *, $p<0.05$ compared to WT; #, $p<0.05$ compared to *TSC1*$^{-/-}$, one-way ANOVA with Sidak's multiple comparisons test. For display purposes, only one star is used to denote significance. Please see Supplementary Table 2 for exact P values for all comparisons. (**h**) Representative western blots for TBC1D7 and β-Actin loading control for WT, *TSC1*$^{-/-}$, and *TSC2*$^{-/-}$ spheroids harvested on different days post-differentiation. Day 0 is from hESCs. The arrowhead indicates the TBC1D7 protein band. (**i**) Quantification of TBC1D7 in spheroids from the indicated genotypes over time, displayed as mean +/- s.e.m. A two-way ANOVA revealed significant effects of time ($p<0.05$), genotype (***, $p<0.001$), and a time x genotype interaction ($p<0.001$). (**j**) Western blots from day 100 *TSC2*$^{-/-}$ cortical spheroids treated chronically with vehicle or 20 nM rapamycin (Rap) beginning on day 12. Rapamycin treatment reduced the phosphorylation of S6 and STAT3 and expression of the glial protein GFAP. Rapamycin increased expression of the neuronal proteins doublecortin (DCX), CAM2KA, and GLUR1 in *TSC2*$^{-/-}$ spheroids. Data from two spheroids per treatment are shown. See Supplementary Table 2 for sample sizes and P values for all comparisons.

Supplementary Figure 2.5

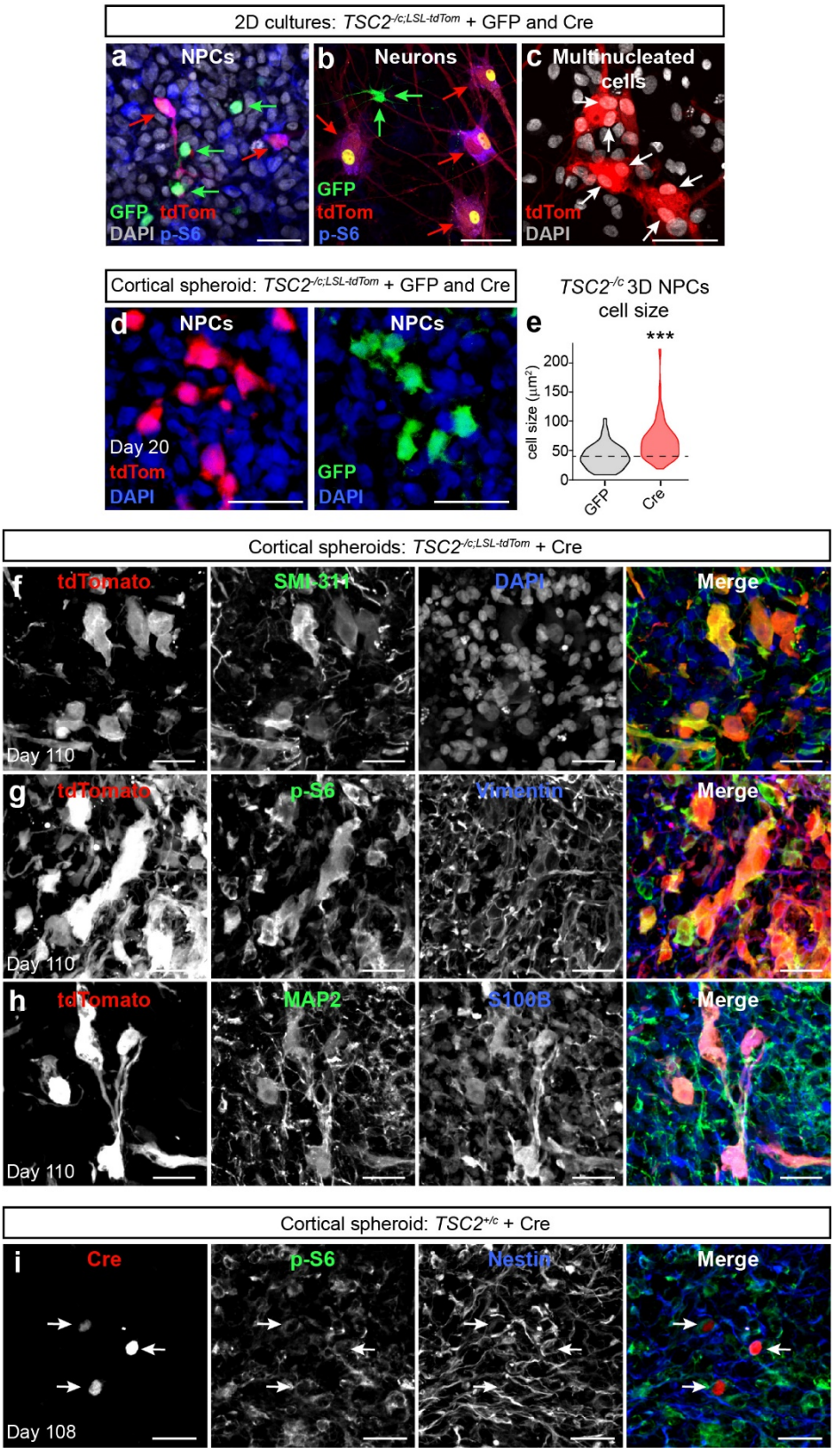

Supplementary Fig. 2.5. A second-hit mutation in *TSC2* results in hypertrophic, dysplastic cells. (**a**) *TSC2*$^{-/c;LSL\text{-}tdTom}$ hESCs were differentiated into neural precursor cells (NPCs) in two-dimensional (2D) cultures. Lentiviruses expressing Cre or GFP were added on day 10 and NPCs were fixed on day 25. NPCs were stained with antibodies against GFP (green) and phosphorylated S6 (p-S6, Ser240/244, blue). DAPI staining is in grey. Scale bar represents 25 μm. (**b**) NPCs were differentiated into neurons in 2D by addition of BDNF and NT3. Neurons were fixed on day 75 and stained with antibodies against GFP (green) and p-S6 (blue). Green arrows show GFP-expressing *TSC2*$^{+/-}$ neurons and red arrows show highly enlarged tdTomato-expressing *TSC2*$^{-/-}$ neurons. Scale bar represents 50 μm. (**c**) Large, tdTomato-positive cells with multiple nuclei were observed in 2D neuronal cultures. DAPI staining is in grey. Scale bar represents 50 μm. (**d**) Cortical spheroids were differentiated from *TSC2*$^{-/c;LSL\text{-}tdTom}$ hESCs, infected with Cre-RFP and GFP lentivirus on day 6, and harvested on day 20. DAPI staining is in blue. Scale bars represent 25 μm. (**e**) Violin plots display cross-sectional cell area for GFP-positive (GFP) *TSC2*$^{+/-}$ NPCs and neighboring tdTomato-positive (Cre) *TSC2*$^{-/-}$ NPCs (n=49 cells for GFP and 144 cells for Cre; ***, p<0.001 Kolmogorov-Smirnov test). (**f-h**) Cortical spheroids were differentiated from *TSC2*$^{-/c;LSL\text{-}tdTom}$ hESCs and infected with Cre lentivirus on day 12. Spheroids were fixed on day 110 and sections were stained with antibodies against SMI-311 (green) (**f**), p-S6 (green, Ser240/244) and vimentin (blue) (**g**), or MAP2 (green) and S100B (blue) (**h**). In panel **f**, DAPI staining is in blue. Scale bars represent 25 μm. (**i**) Images of a section of a cortical spheroid differentiated from *TSC2*$^{+/c}$ hESCs infected with subsaturating amounts of Cre-GFP lentivirus on day 12 (note that the Cre-GFP fusion protein is nuclear localized and is pseudo-colored red in this image). The spheroid was fixed on day 108 and sections were stained with antibodies against p-S6 (green, Ser240/244) and nestin (blue). Cre-expressing cells (arrows) do not show upregulated p-S6 or high nestin expression. Scale bars represent 25 μm. See Supplementary Table 2 for sample sizes and P values for all comparisons.

Supplementary Figure 2.6

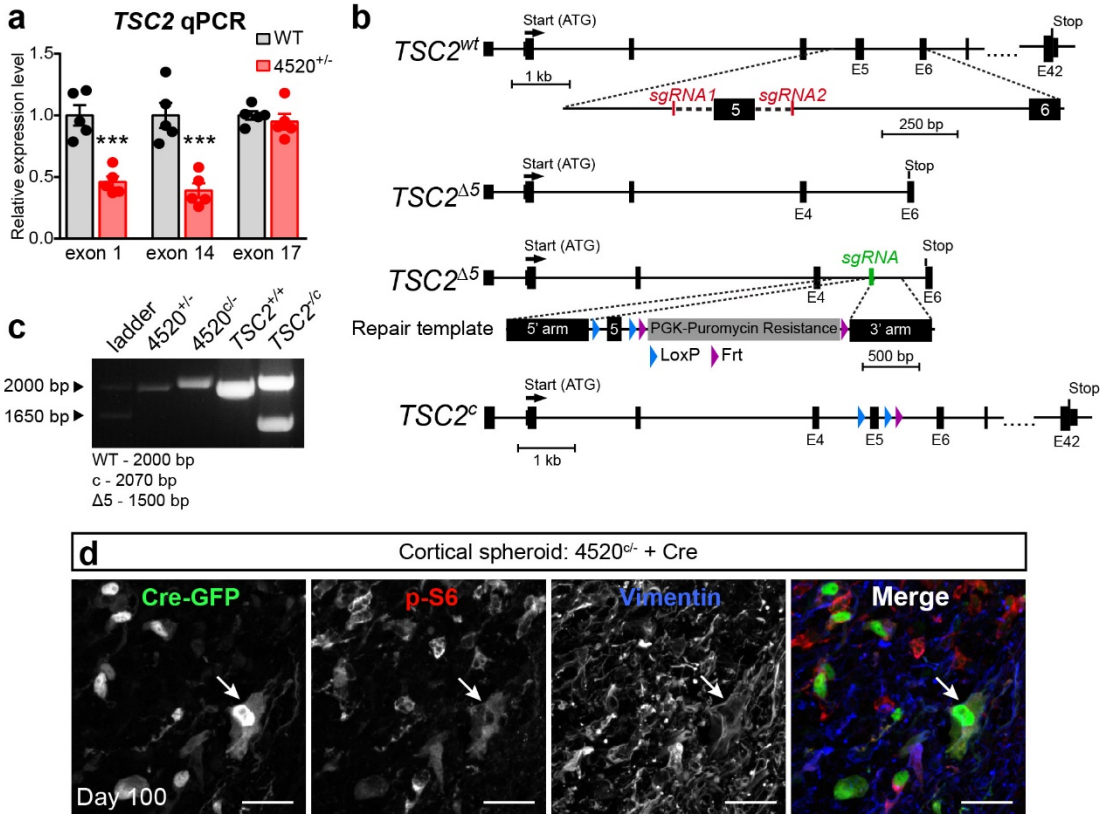

Supplementary Fig. 2.6. A second-hit mutation in *TSC2* causes dysplastic cells in cortical spheroids from TSC patient-derived hiPSCs. (**a**) Bar graphs displaying quantitative PCR using primers surrounding exons 1, 14, or 17 of the *TSC2* gene. $4520^{+/-}$ hiPSCs show ~50% loss of exons 1 and 14 (**, p<0.001, t-test), confirming a heterozygous *TSC2* exon 1-14 deletion. Bars represent mean +/- s.e.m. (**b**) Targeting strategy to generate a conditional *TSC2* allele in $4520^{+/-}$ hiPSCs. Exon 5 of the patient's wild-type *TSC2* allele was deleted and the hiPSCs were retargeted with a repair template containing exon 5 flanked by loxP sites. The puromycin resistance selection cassette was excised using Flp recombinase. (**c**) PCR confirmation of *TSC2* gene editing in 4520 hiPSCs. The $4520^{c/-}$ cells do not have a Δ5 band at 1500 bp since exons 1-14 are deleted. (**d**) $4520^{c/-}$ hiPSCs were differentiated into cortical spheroids and treated with sub-saturating amounts of Cre-GFP lentivirus on day 12 post-differentiation. Spheroids were fixed on day 100 and sections were stained with antibodies against phosphorylated S6 (p-S6, Ser240/244, red) and the filament protein vimentin (blue). Scale bars represent 25 μm. See Supplementary Table 2 for sample sizes and P values for all comparisons.

Supplementary Figure 2.7

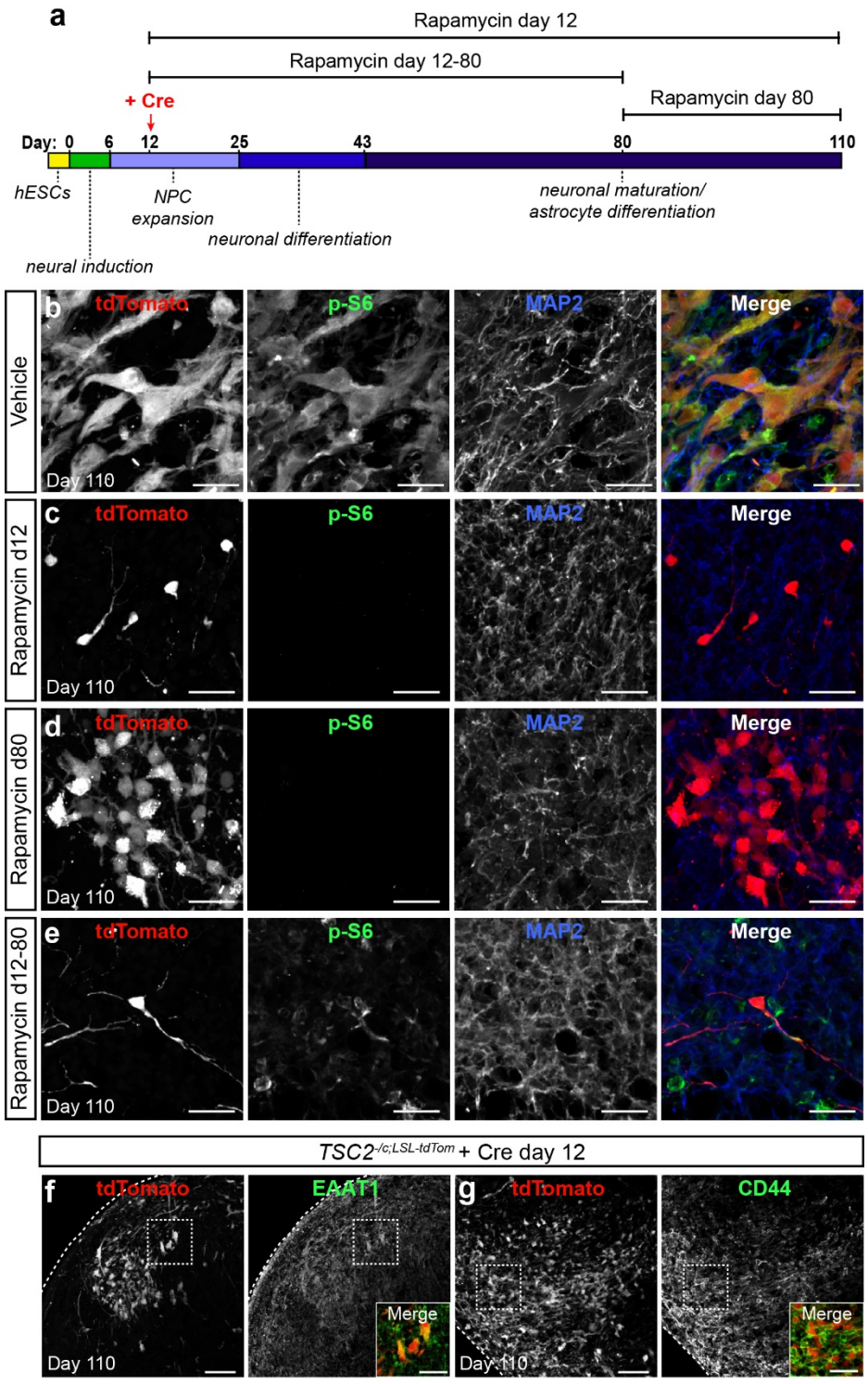

Supplementary Fig. 2.7. Rapamycin treatment decreases mTORC1 signaling and cellular hypertrophy in cortical spheroids. (**a**) Schematic of experimental design. *TSC2*$^{-/c;LSL\text{-}tdTom}$ cortical spheroids were treated with subsaturating amounts of Cre and GFP-expressing lentiviruses on day 12. Spheroids were randomly divided into four treatment groups: rapamycin (20 nm) from day 12 to 110, rapamycin from day 12 to 80, rapamycin from day 80 to 110, or vehicle from day 12 to 110. All spheroids were fixed at day 110. (**b-e**) Example images from sections of *TSC2*$^{-/c;LSL\text{-}tdTom}$ cortical spheroids from the indicated treatment groups. Sections were stained with antibodies against the phosphorylated S6 (p-S6, Ser240/244, green) and MAP2 (blue). The tdTomato Cre-reporter (red) is expressed in cells with a second-hit *TSC2* mutation. Scale bars represent 25 μm. (**f,g**) Cortical spheroids were differentiated from *TSC2*$^{-/c;LSL\text{-}tdTom}$ hESCs and infected with sub-saturating amounts of Cre-expressing lentivirus on day 12. Spheroids were fixed on day 110 and sections were stained with antibodies against the glial proteins EAAT1 (**f**) or CD44 (**g**). Scale bars represent 100 μm. Insets show higher magnification merged images of the boxed regions. Scale bars in the inset panels represent 50 μm.

Supplementary Table 2.1: Array Comparative Genomic Hybridization (aCGH) analysis

Cell line	Chromosome	Amp/Del	Start	Stop	Size (kb)	Chr Band	Log2 Ratio
WIBR3 hESC (WT)	20	Amp	29,888,477	31,184,566	1,296	p11.1-q11.21	0.533546
	X	Del	298,292	2,362,192	2,064	p22.33	-0.25415
TSC1+/- hESC	20	Amp	29,888,477	31,121,463	1,233	q11.21	0.509756
TSC1-/- hESC	20	Amp	29,888,477	31,121,463	1,233	q11.21	0.578807
	8	Amp	109,462,648	109,567,917	105	q23.1	0.66984
	16	Amp	2,291,184	2,807,527	516	p13.3	0.289215
TSC2+/- hESC	20	Amp	29,888,477	31,121,463	1,233	q11.21	0.508089
	4	Amp	47,788,813	47,880,747	92	p12	1.089298
TSC2-/- hESC	20	Amp	29,888,477	31,121,463	1,233	q11.21	0.540013
	16	Amp	2,291,184	2,807,527	516	p13.3	0.287484
TSC2-/c;LSL-tdTom hESC	20	Amp	29,888,477	31,121,463	1,233	q11.21	0.538177
	4	Amp	47,788,813	47,880,747	92	p12	1.232229
4520 hiPSC	10	Amp	28,570,980	28,861,837	291	p12.1	0.526755
	10	Amp	47,011,584	47,655,146	644	q11.22	0.93809
	15	Del	56,688,324	56,792,398	104	q21.3	-0.8952
	16	Del	2,021,652	2,100,490	79	p13.3	-0.51941
4520c/- hiPSC	10	Amp	28,570,980	28,861,837	291	p12.1	0.548874
	10	Amp	47,011,584	47,655,146	644	q11.22	0.911855
	15	Del	56,688,324	56,792,398	104	q21.3	-0.85206
	16	Del	2,034,897	2,100,490	66	p13.3	-0.59314
BJ hiPSC	7	Amp	5,390,677	7,137,580	1,747	p22.1	0.528635
	11	Del	9,594,314	13,034,698	3,440	p15.4-p15.2	-0.72857
	11	Del	63,742,981	64,672,800	930	q13.1	-0.76727
	X	Amp	112,776,336	115,098,133	2,322	q23	0.271009
BJ;TSC2-/- hiPSC	6	Del	32,523,337	32,604,038	81	p21.32	-0.62057
	7	Amp	5,520,557	7,137,580	1,617	p22.1	0.590032
	X	Del	169,064	2,656,392	2,487	p22.33	-0.25095
	Y	Del	119,064	2,606,392	2,487	p11.32-p11.31	-0.25095

Supplementary Table 2.2: Comprehensive Statistical Summary for each Fig.

p<0.001	p<0.01	p<0.05	not significant

Fig. 2.1

				Bonferroni's multiple comparisons tests P values				
Panel	**Protein**	**one-way ANOVA P value**	**F**	**WT vs TSC1+/-**	**WT vs TSC1-/-**	**WT vs TSC2+/-**	**WT vs TSC2-/-**	**TSC1-/- vs TSC2-/-**
d	**TSC1**	<0.0001	37.45	0.0036	<0.0001	0.4447	<0.0001	0.0003
e	**TSC2**	<0.0001	29.79	>0.9999	<0.0001	0.0637	<0.0001	0.0053
f	**p-S6**	<0.0001	26.1	0.0798	0.254	0.4739	<0.0001	0.0009
g	**Total S6**	0.0133	3.914	0.0763	0.0075	>0.9999	0.2763	0.6662
h	**p-4E-BP1**	<0.0001	33.48	0.5388	<0.0001	>0.9999	<0.0001	>0.9999
i	**Total 4E-BP1**	0.0772	2.396	0.2478	0.8573	>0.9999	>0.9999	>0.9999
j	**p-AKT**	<0.0001	56.27	0.024	<0.0001	0.1956	<0.0001	0.0458
k	**Total AKT**	0.0009	6.642	0.004	0.0019	>0.9999	0.7686	0.0702

Fig. 2.2

				Sidak's multiple comparisons test P values			
Panel	**Protein**	**one-way ANOVA P value**	**F**	**WT vs TSC1+/-**	**WT vs TSC1-/-**	**WT vs TSC2+/-**	**WT vs TSC2-/-**
d	**PAX6**	0.0842	2.812	0.7576	0.4353	0.6906	0.9752
e	**SOX2**	0.5525	0.7992	0.6614	0.9108	>0.9999	0.9998
f	**Ki-67**	0.2086	1.784	0.8515	0.6215	0.9585	0.7558

		two-way ANOVA P values			Dunnett's multiple comparisons test P values		
Panel	**Protein**	**Day**	**Genotype**	**Interaction**	**Day**	**WT vs TSC1-/-**	**WT vs TSC2-/-**
h	**MAP2**	<0.0001	0.0148	0.0032	**0**	>0.9999	>0.9999
h	**MAP2**				**20**	0.9997	>0.9999
h	**MAP2**				**50**	0.9782	0.5904
h	**MAP2**				**100**	0.0019	0.0003
h	**MAP2**				**150**	0.7956	0.0016
i	**GFAP**	<0.0001	0.0854	0.536	**0**	>0.9999	>0.9999
i	**GFAP**				**20**	>0.9999	>0.9999
i	**GFAP**				**50**	>0.9999	>0.9999
i	**GFAP**				**100**	0.4479	0.0536
i	**GFAP**				**150**	0.0002	0.0074

				Sidak's multiple comparisons test P values			
Panel	**mRNA**	**one-way ANOVA P value**	**F**	**WT vs TSC1+/-**	**WT vs TSC1-/-**	**WT vs TSC2+/-**	**WT vs TSC2-/-**
j	**NeuN**	0.0442	2.789	0.9996	0.6765	0.9983	0.0461
k	**S100B**	0.0015	5.745	0.9801	0.4818	0.9936	0.0029

Fig. 2.3

		two-way ANOVA P values			Dunnett's multiple comparisons test P values		
Panel	Protein	Day	Genotype	Interaction	Day comparison	WT	TSC2-/-
c	p-S6	0.0005	0.0047	0.0008	0 vs 10	0.9972	0.8522
c	p-S6				0 vs 20	0.0051	0.8882
c	p-S6				0 vs 30	0.0005	>0.9999
c	p-S6				0 vs 50	0.0007	>0.9999
c	p-S6				0 vs 100	0.0426	0.0054
d	Total S6	<0.0001	0.0129	0.0498	0 vs 10	0.9772	0.9546
d	Total S6				0 vs 20	0.0738	0.8048
d	Total S6				0 vs 30	<0.0001	0.1087
d	Total S6				0 vs 50	<0.0001	<0.0001
d	Total S6				0 vs 100	<0.0001	0.0002
e	p-4E-BP1	0.4428	0.0368	0.0875	0 vs 10	0.9997	0.9492
e	p-4E-BP1				0 vs 20	0.9828	0.9999
e	p-4E-BP1				0 vs 30	0.9859	0.3233
e	p-4E-BP1				0 vs 50	0.9295	0.0255
e	p-4E-BP1				0 vs 100	0.9806	0.1239
f	Total 4E-BP1	<0.0001	0.8186	0.5605	0 vs 10	0.01	0.0003
f	Total 4E-BP1				0 vs 20	0.0357	0.0545
f	Total 4E-BP1				0 vs 30	<0.0001	<0.0001
f	Total 4E-BP1				0 vs 50	<0.0001	<0.0001
f	Total 4E-BP1				0 vs 100	<0.0001	<0.0001
g	p-AKT	0.0014	0.0021	0.01	0 vs 10	0.0355	0.2754
g	p-AKT				0 vs 20	0.753	0.028
g	p-AKT				0 vs 30	0.9764	0.0156
g	p-AKT				0 vs 50	0.9925	0.3683
g	p-AKT				0 vs 100	0.0402	0.1802
h	Total AKT	<0.0001	<0.0001	0.2635	0 vs 10	0.0487	0.6164
h	Total AKT				0 vs 20	<0.0001	0.0006
h	Total AKT				0 vs 30	0.0706	0.9999
h	Total AKT				0 vs 50	0.0006	0.9172
h	Total AKT				0 vs 100	0.0127	0.7973

		two-way ANOVA P values			Dunnett's multiple comparisons test P values		
Panel	**Protein**	**Day**	**Genotype**	**Interaction**	**Day**	**WT vs TSC1-/-**	**WT vs TSC2-/-**
i	**p-STAT3-S727**	<0.0001	0.0389	0.0413	**0**	0.0015	0.1251
i	**p-STAT3-S727**				**20**	0.4009	0.0562
i	**p-STAT3-S727**				**50**	0.9982	0.9916
i	**p-STAT3-S727**				**100**	0.7146	0.2623
i	**p-STAT3-S727**				**150**	0.8713	0.0654
j	**p-STAT3-Y705**	<0.0001	<0.0001	0.0101	**0**	0.3033	0.0126
j	**p-STAT3-Y705**				**20**	0.4432	0.0188
j	**p-STAT3-Y705**				**50**	0.0868	0.0048
j	**p-STAT3-Y705**				**100**	0.0009	<0.0001
j	**p-STAT3-Y705**				**150**	0.0194	<0.0001
k	**STAT3**	<0.0001	0.4518	0.1274	**0**	0.207	0.8264
k	**STAT3**				**20**	0.9982	0.9575
k	**STAT3**				**50**	0.3849	0.4552
k	**STAT3**				**100**	0.1475	0.0662
k	**STAT3**				**150**	0.2554	0.3927

Fig. 2.4

Panel	**Cell type**	**Variable**	**Kolmogorov-Smirnov test P value**
f	**NPCs**	p-S6	0.0003
g	**Neurons**	p-S6	<0.0001
h	**NPCs**	cell size	0.0001
i	**Neurons**	cell size	<0.0001

		two-way ANOVA P values		
Panel	**Analysis**	**Distance from soma**	**Genotype**	**Interaction**
j	**Sholl**	<0.0001	<0.0001	<0.0001

Fig. 2.5

	Panel b p-S6	**Panel c Neuron Size**	**Panel d Astrocyte Size**
Kruskal-Wallis test P value	< 0.0001	< 0.0001	< 0.0001
Comparison	**Dunn's multiple comparisons test P value**		
Vehicle GFP vs. Vehicle Cre	0.0191	0.0055	< 0.0001
Rap d12 GFP vs. Rap d12 Cre	0.5489	> 0.9999	0.9468
Rap d80 GFP vs. Rap d80 Cre	> 0.9999	0.5091	0.3144
Rap d12-80 GFP vs. Rap d12-80 Cre	> 0.9999	> 0.9999	0.1082
Vehicle GFP vs. Rap d12 GFP	< 0.0001	> 0.9999	> 0.9999
Vehicle GFP vs. Rap d80 GFP	< 0.0001	0.0355	> 0.9999
Vehicle GFP vs. Rap d12-80 GFP	> 0.9999	> 0.9999	> 0.9999
Vehicle Cre vs. Rap d12 Cre	< 0.0001	< 0.0001	0.594
Vehicle Cre vs. Rap d80 Cre	< 0.0001	< 0.0001	< 0.0001
Vehicle Cre vs. Rap d12-80 Cre	> 0.9999	0.0294	0.902

Rap = rapamycin

Supplementary Fig. 2.2

			Dunn's multiple comparisons test P values				
Panel	Variable	Kruskal-Wallis test P value	WT vs TSC1+/-	WT vs TSC1-/-	WT vs TSC2+/-	WT vs TSC2-/-	TSC1-/- vs TSC2-/-
b	2D NPC size	<0.0001	0.0372	0.0002	>0.9999	0.0008	>0.9999

				Bonferroni's multiple comparisons tests P values				
Panel	Protein	one-way ANOVA P value	F	WT vs TSC1+/-	WT vs TSC1-/-	WT vs TSC2+/-	WT vs TSC2-/-	TSC1-/- vs TSC2-/-
d	TSC1	<0.0001	74.29	<0.0001	<0.0001	0.421	<0.0001	0.0004
e	TSC2	<0.0001	123.6	<0.0001	<0.0001	<0.0001	<0.0001	<0.0001
f	p-S6	<0.0001	42.24	>0.9999	<0.0001	0.9565	<0.0001	0.0007
g	Total S6	<0.0001	7.521	>0.9999	0.001	>0.9999	>0.9999	<0.0001
h	p-4E-BP1	0.0024	5.582	>0.9999	0.0145	>0.9999	>0.9999	0.0105
i	Total 4E-BP1	<0.0001	17.68	0.3838	<0.0001	0.0071	>0.9999	0.0036
j	p-AKT	<0.0001	16.32	>0.9999	>0.9999	0.0188	<0.0001	<0.0001
k	Total AKT	<0.0001	26.94	>0.9999	<0.0001	0.369	<0.0001	>0.9999

Supplementary Fig. 2.3

		two-way ANOVA P values			Dunnett's multiple comparisons test P values				
Panel	mRNA	Day	Genotype	Interaction	Day	WT vs TSC1+-	WT vs TSC1-/-	WT vs TSC2+-	WT vs TSC2-/-
a	NeuN	<0.0001	0.8074	0.8336	0	0.9998	0.9975	>0.9999	0.998
a	NeuN				20	>0.9999	0.9999	>0.9999	0.9999
a	NeuN				30	0.9571	0.8894	0.9779	0.9577
a	NeuN				50	0.9939	0.9797	0.9916	0.9999
a	NeuN				100	0.749	0.9841	0.5439	0.3382
b	S100B	<0.0001	0.032	<0.0001	0	>0.9999	>0.9999	0.9469	>0.9999
b	S100B				20	0.9999	>0.9999	>0.9999	>0.9999
b	S100B				30	>0.9999	>0.9999	0.9968	0.9957
b	S100B				50	0.9723	0.9999	0.9797	0.4965
b	S100B				100	0.9997	0.0008	0.971	<0.0001

				Sidak's multiple comparisons test P values			
Panel	Variable	one-way ANOVA P value	F	WT vs TSC1+/-	WT vs TSC1-/-	WT vs TSC2+/-	WT vs TSC2-/-
c	Neuron:Astrocyte ratio	0.4581	0.9857	0.9995	0.9998	0.9227	0.7066
d	Ki-67 positive astrocytes	0.909	0.2405	0.9539	0.9966	>0.9999	>0.9999

Supplementary Fig. 2.4

					Sidak's multiple comparisons test P values				
Panel	**Protein**	**Day**	**one-way ANOVA P value**	**F**	**WT vs TSC1+/-**	**WT vs TSC1-/-**	**WT vs TSC2+/-**	**WT vs TSC2-/-**	**TSC1-/- vs TSC2-/-**
b	**p-S6**	**10**	0.0005	7.278	>0.9999	0.0253	0.9988	0.0064	0.9872
b	**p-S6**	**20**	<0.0001	24.33	>0.9999	0.0015	>0.9999	<0.0001	0.0082
b	**p-S6**	**30**	<0.0001	127.9	0.9996	<0.0001	>0.9999	<0.0001	<0.0001
b	**p-S6**	**50**	<0.0001	67.74	>0.9999	<0.0001	0.9362	<0.0001	<0.0001
b	**p-S6**	**100**	<0.0001	59.63	>0.9999	<0.0001	0.9981	<0.0001	<0.0001

					Sidak's multiple comparisons test P values				
Panel	**Protein**	**Day**	**one-way ANOVA P value**	**F**	**WT vs TSC1+/-**	**WT vs TSC1-/-**	**WT vs TSC2+/-**	**WT vs TSC2-/-**	**TSC1-/- vs TSC2-/-**
c	**Total S6**	**10**	0.0062	4.635	> 0.9999	0.1427	0.1658	0.0155	0.8742
c	**Total S6**	**20**	0.808	0.3982	0.9948	0.9822	0.832	> 0.9999	0.9819
c	**Total S6**	**30**	0.0332	3.128	> 0.9999	0.1534	0.9986	0.0698	0.9937
c	**Total S6**	**50**	0.0169	3.729	0.9174	0.9774	0.9389	0.0081	0.0547
c	**Total S6**	**100**	0.1662	1.771	0.3448	0.1283	0.2034	0.271	0.9999

					Sidak's multiple comparisons test P values				
Panel	**Protein**	**Day**	**one-way ANOVA P value**	**F**	**WT vs TSC1+/-**	**WT vs TSC1-/-**	**WT vs TSC2+/-**	**WT vs TSC2-/-**	**TSC1-/- vs TSC2-/-**
d	**p-4E-BP1**	**10**	0.0007	6.932	0.0936	0.976	0.9562	0.0684	0.015
d	**p-4E-BP1**	**20**	0.0016	5.966	> 0.9999	0.4489	0.9966	0.0044	0.1977
d	**p-4E-BP1**	**30**	<0.0001	25.68	0.0739	< 0.0001	0.8387	< 0.0001	0.9996
d	**p-4E-BP1**	**50**	<0.0001	29.35	0.2763	< 0.0001	0.9983	< 0.0001	0.0259
d	**p-4E-BP1**	**100**	0.0009	6.64	> 0.9999	0.1559	0.8962	0.0012	0.1448

					Sidak's multiple comparisons test P values				
Panel	**Protein**	**Day**	**one-way ANOVA P value**	**F**	**WT vs TSC1+/-**	**WT vs TSC1-/-**	**WT vs TSC2+/-**	**WT vs TSC2-/-**	**TSC1-/- vs TSC2-/-**
e	**Total 4E-BP1**	**10**	0.1296	1.973	0.9999	0.8885	0.3947	0.9341	0.3764
e	**Total 4E-BP1**	**20**	0.3034	1.282	0.9938	0.9933	0.5412	0.8224	0.505
e	**Total 4E-BP1**	**30**	0.1155	2.076	0.929	0.2219	0.0797	0.5328	0.9949
e	**Total 4E-BP1**	**50**	0.0007	7.042	0.7642	0.8603	0.6846	0.0003	0.0057
e	**Total 4E-BP1**	**100**	0.019	3.593	0.05	0.0065	0.1356	0.1202	0.8719

					Sidak's multiple comparisons test P values				
Panel	Protein	Day	one-way ANOVA P value	F	WT vs TSC1+/-	WT vs TSC1-/-	WT vs TSC2+/-	WT vs TSC2-/-	TSC1-/- vs TSC2-/-
f	p-AKT	10	<0.0001	15.47	0.6686	0.0568	0.9997	< 0.0001	0.0462
f	p-AKT	20	<0.0001	25.97	> 0.9999	< 0.0001	0.9825	< 0.0001	0.6643
f	p-AKT	30	<0.0001	34	0.9041	< 0.0001	0.5476	< 0.0001	0.8982
f	p-AKT	50	<0.0001	62.04	0.5801	< 0.0001	0.1364	< 0.0001	0.4457
f	p-AKT	100	<0.0001	44.54	> 0.9999	< 0.0001	0.1932	< 0.0001	0.7868

					Sidak's multiple comparisons test P values				
Panel	Protein	Day	one-way ANOVA P value	F	WT vs TSC1+/-	WT vs TSC1-/-	WT vs TSC2+/-	WT vs TSC2-/-	TSC1-/- vs TSC2-/-
g	Total AKT	10	0.0007	6.881	0.9108	0.1748	0.1381	0.2034	> 0.9999
g	Total AKT	20	0.0371	3.011	0.821	0.1111	0.9767	0.4692	0.9398
g	Total AKT	30	< 0.0001	23.4	0.2951	0.1644	0.0166	< 0.0001	0.0019
g	Total AKT	50	0.0002	8.291	0.9996	0.6407	0.054	0.0522	0.7006
g	Total AKT	100	0.164	1.782	0.9124	0.8414	0.9694	0.3774	0.9302

		two-way ANOVA P values			Dunnett's multiple comparisons test P values		
Panel	Protein	Day	Genotype	Interaction	Day	WT vs TSC1-/-	WT vs TSC2-/-
h	TBC1D7	0.0234	< 0.0001	< 0.0001	0	0.9999	0.1505
h	TBC1D7				20	< 0.0001	0.0078
h	TBC1D7				50	< 0.0001	0.0094
h	TBC1D7				100	< 0.0001	0.0955
h	TBC1D7				150	< 0.0001	0.0128

Supplementary Fig. 2.5

Panel	Cell type	Variable	Kolmogorov-Smirnov test P value
e	NPCs	cell size	<0.0001

Supplementary Fig. 2.6

Panel	Exon	unpaired t-test P value	t
a	1	0.0004	5.747
	14	0.0008	5.176
	27	0.495	0.7149

Supplementary Table 2.3: Sequences for sgRNAs, PCR primers, and qPCR primers

sgRNA name	sgRNA sequence	Reference
TSC2_exon5_L1	CTGCAGCATCAGCATTGTAC	
TSC2_exon5_R1	TGCACCTGGGCTCACCTGCG	
TSC2_exon5_L2	TGCAGCATCAGCATTGTACA	
TSC2_exon5_R2	CCCACCCTGCTTCATGCACC	
TSC1_ exon17_L1	ACTATGTGTCTCCCCCGTGA	
TSC1_ exon17_R1	AGACATGAATGGTGACACCT	
TSC2_Δ5_Junction	GGCCCCCTGCCCTGTATGCG	
AAVS1_T2	GGGCCACTAGGGACAGGAT	Mali, P. et al, Science, 2013 (PMID: 23287722)

PCR Primer Name	Sequence	PCR Conditions
TSC2_exon5_GT_F	AGTGGAAGCACTCTGGAAGG	Tm= 59^{o} C, 39 cycles
TSC2_exon5_GT_R	GACGCCGAATCTACATCTCC	WT band: 2000 bp
		Targeted band:1500 bp
		Conditional band:2070 bp
TSC1_exon17_GT_F	GTGTATGCAGTGCAGCTCCAG	Tm= 57^{o} C, 39 cycles
TSC1_exon17_GT_R	TTCTGCAGACTAACCTTCCACA	WT band: 2000 bp
		Targeted band:1500 bp
AAVS1-F primer	CTCTAACGCTGCCGTCTCTC	Tm= 57^{o} C, 35 cycles
AAVS1-WT-R primer	GCTTCTCCTCTTGGGAAGTG	WT band: 1273 bp
AAVS1-Targeted-R primer	CGTCACCGCATGTTAGAAGA	Targeted band: 992 bp

qPCR Primer Name	Sequence	Conditions
S100_F	GGAGACGGCGAATGTGACTT	All qPCRs performed with Tm= 60^{o}C for 40 cycles
S100_R	GAACTCGTGGCAGGCAGTAGTAA	
NeuN_F	GTAGAGGGACGGAAAATTGAGG	
NeuN_R	CATAGAATTCAGGCCCGTAGAC	
B-actin_F	ATAGCACAGCCTGGATAGCAACGTAC	
B-actin_R	CACCTTCTACAATGAGCTGCGTGTG	
TSC2_exon1_F	AGCTCCGAGCATCCCTTAGT	
TSC2_exon1_R	CATGTGAAGCAGGAGCTGTC	
TSC2_exon14_F	GAGCAGGTGCTAGCTTGCTT	
TSC2_exon14_R	GGAGCATCTCTCCAGACGAC	
TSC2_exon17_F	TTTTCTGAGTGCCTGTGGTG	
TSC2_exon17_R	CAAAGGCCTGTCAGGAAGAG	

Supplementary Table 2.4: List of antibodies used

Antibody	Host species	Company	Catalog #	Western blot dilution	ICC/IHC dilution
4E-BP1	rabbit	Cell Signaling	9644	1:1000	
phospho-4E-BP1 (Ser65)	rabbit	Cell Signaling	9451	1:1000	
AKT	rabbit	Cell Signaling	4691	1:1000	
phospho-AKT (Ser473)	rabbit	Cell Signaling	4060	1:1000	
B-Actin	mouse	Sigma	a1972	1:15000	
CAMK2A	mouse	Cell Signaling	50049		1:300
CD44	mouse	Cell Signaling	3570		1:400
Doublecortin (DCX)	rabbit	Cell Signaling	4604		1:2000
EAAT1	rabbit	Cell Signaling	5684		1:100
GFAP	rabbit	Fisher	180063	1:100	1:100
GFP	chicken	AbCam	ab13970		1:5000
GLUR1	rabbit	Millipore	AB1504	1:800	
HuC/D	mouse	Fisher	A21271		1:500
Ki-67	mouse	Cell Signaling	9449T		1:500
MAP2	chicken	AbCam	ab5392		1:5000
MAP2	mouse	AbCam	ab11267	1:2000	
NANOG	goat	R & D Systems	AF1997		1:40
Nestin	mouse	Covance	MMS-570P-100		1:1000
NeuN	mouse	Millipore	MAB377		1:1000
OCT4	rabbit	AbCam	ab19857	1:1000	1:500
PAX6	rabbit	Anaspec	PRB-278P-100		1:300
RFP	rabbit	Rockland	RL600-401-379		1:2000
S100B	rabbit	Abcam	ab868	1:200	1:300
S6	rabbit	Cell Signaling	2317S	1:1000	
phospho-S6 (Ser240/244)	rabbit	Cell Signaling	5364S	1:2000	1:1000
SMI-311	mouse	Biolegend	837301		1:1000
SOX2	rabbit	ThermoFisher	48-1400		1:150
phospho-STAT3 (Ser727)	rabbit	Cell Signaling	94994	1:1000	
phospho-STAT3 (Tyr705)	rabbit	Cell Signaling	9145	1:800	
STAT3	mouse	Cell Signaling	9139	1:1000	
TBC1D7	rabbit	Cell Signaling	14949	1:1000	
Tuj1	chicken	Millipore	AB9354		1:2000
TSC1	rabbit	Cell Signaling	6935S	1:1000	
TSC2	rabbit	Cell Signaling	4308	1:1000	
Vimentin	mouse	EMD Millipore	MAB3400		1:1000

Chapter 3: **Single Cell Transcriptomics of Human Models of Tuberous Sclerosis**

This chapter was undertaken as a collaborative study by John D. Blair, Dirk Hockemeyer, Helen S. Bateup, Gerald Grant and Brenda Porter.

Introduction

Tuberous Sclerosis (TSC) is a multisystem developmental disorder associated with early-onset epilepsy and varying degrees of intellectual disability [6]. Neuropathologically, TSC is defined by the presence of “cortical tubers”, which are focal cortical malformations composed of dysplastic neurons and astrocytes that can become seizure foci [44]. Several studies have characterized cortical tuber cells through immunostaining of resected tissue from patients; however the transcriptional profile of these cells has been mostly inaccessible [44-46]. We recently established a model of TSC [77] using human pluripotent stem cell based genome engineering [76] and 3-D cortical differentiation [1]. Here we applied single-cell sequencing at multiple development time-points to these models understand the developmental trajectories and molecular identity of human cortical cells with mutations in *TSC2*.

TSC is caused by mutations in either *TSC1* or *TSC2* [10, 11], which encode for proteins forming a complex that acts as a negative regulator of mTORC1 [13], a key cellular signaling node controlling anabolic processes such as mRNA translation and catabolic processes such as autophagy [176]. A leading hypothesis for how *TSC1/*2 mutations lead to cortical tubers is through a “second-hit” mechanism whereby patients first have a germline heterozygous mutation followed by a somatic mutation of the functional allele in a subset of precursor cells causing loss of heterozygosity [30]. These cells are thought to subsequently clonally divide and develop into cortical tubers. We generated a model of TSC that recapitulated this two-hit mechanism by engineering one *TSC2* conditional knock-out (KO) allele that is disrupted by Cre-recombinase and one constitutive loss-of-function allele ($TSC2^{c/-}$). We also engineered constitutive isogenic heterozygous and homozygous *TSC2* mutations in pluripotent stem cells ($TSC2^{+/-}$ and $TSC2^{-/-}$) as well as a “single-hit” model with the same conditional KO allele, but complemented by a functional wild-type allele ($TSC2^{c/+}$) [77]. The conditional cell lines were further engineered to express a Cre-inducible TdTomato, ensuring the simple identification of Cre-exposed cells.

Our previous study demonstrated the necessity of *TSC2* loss of heterozygosity to cause aberrant differentiation towards an astro-glial lineage, which is consistent with observations from patient tissue that show large numbers of GFAP-positive cells in some tubers [164]. However, the differentiation phenotypes of our model of TSC were based on a relatively small number of astrocyte proteins and transcripts, and in some cases were inferred from spheroids processed in bulk, which is suboptimal for a tissue model with a diversity of cell types. Recent advances in single cell transcriptional profiling technology have made possible the simultaneous measurement of mRNA transcripts from a diverse pool of cells that have been cultured together in a controlled

system. In this study, we apply single-cell transcriptomics to our models of TSC, demonstrating aberrant differentiation trajectories resulting from loss of *TSC2* and revealing previously unknown differentially expressed genes.

Results

Cellular origin and diversity of cortical tubers from patients with Tuberous Sclerosis

Normally during human cortical development, neuroepithelial cells proliferate at the ventricular zone and differentiate into radial glia, providing a pool of progenitor cells that will further differentiate into excitatory neurons and eventually astrocytes while migrating towards the pial surface [33]. In TSC, it has been hypothesized that cortical tubers arise from stochastic somatic *TSC1* or *TSC2* mutations in progenitor cells during early stages of forebrain cortical development, resulting in focal regions of dysmorphic cells that comprise the cortical tuber [30]. It is also plausible that the dysmorphic cells in cortical tubers may come from an inhibitory neuron lineage which develop away from the forebrain and migrate into the cortex later in development [37]. We aimed to confirm the origin of cortical tuber cells by immunofluorescent staining for canonical forebrain layer markers in cortical tuber samples from patients.

We identified cortical tuber cells in patient samples as those that were high in phosphorylated ribosomal protein S6 (p-S6), a robustly detectable downstream target of mTORC1 signaling. Staining with cortical layer-specific excitatory neuronal markers, including TBR1 and CTIP2, revealed that cells high in p-S6 with neuronal-like morphology were often positive for these markers, indicating that a large portion of cortical tuber cells come from an excitatory lineage (Fig 3.1a).

Other cell types within cortical tubers include multi-nucleated giant or balloon cells and dysplastic astro-glia. Both of these cell types were observed in resected tuber samples. These cells were high in p-S6 and expressed the radial glial marker Vimentin (Fig 3.1a).

Cellular diversity of a human cortical model of TSC

In order to better understand the developmental process of cortical tubers and to differentially expressed genes that might provide insight into tuber cell biology, we utilized our previously established cortical spheroid model of TSC [77]**.** We used $TSC2^{c/-;lsl\text{-}TdTom}$ hESCs, which have a constitutive loss of function mutation in *TSC2* on one allele and a Cre-inducible mutation on the second allele. In the presence of Cre recombinase, *TSC2* is deleted and tdTomato is expressed from a safe-harbor locus to enable the identification of cells with a “second-hit” mutation and their progeny. $TSC2^{c/-;lsl\text{-}TdTom}$ brain spheroids were grown as previously described [109] and infected on day 8 of differentiation with a sub-saturating amount of lentivirus expressing Cre-recombinase, creating a subset of tdTomato+ $TSC2^{-/-}$ cells. Spheroids from three separate differentiations were harvested at days 50 (~1.7 months), 120 (~4 months) and 220 (~7.3 months) of differentiation, with each spheroid containing both heterozygous ($TSC2^{c/-}$) and homozygous ($TSC2^{-/-}$) cells. Cells were sorted by tdTomato expression using FACS and processed using the using the 10X Genomics platform (Fig 3.1b). We applied a bioinformatics pipeline using on Seurat v3 to analyze the sequencing data and

establish cell clusters defined by their transcriptional signature (see methods). As previously reported for wild-type cortical spheroids [109, 110, 117], we identified several distinct cell types present in the spheroids. It was immediately apparent that there was a population of cells that had initiated an apoptotic program, as indicated by increased expression of *DDIT3* (CHOP), PPP1R15A, GADD45A and GDF15 [177], potentially due to the stress of the processing pipeline. We applied an expression filter to remove them (Supplementary Fig. 3.1a-d; Methods) and found that the filtered out cells were similarly distributed between genotypes and timepoints (Supplementary Fig.3.1e,f). The distribution of general cell types (i.e. neural precursor cell, glia, and neurons) filtered out also reflected the overall cellular composition of the spheroids. Post-filtering, the number of cells expressing apoptotic stress markers was reduced (Supplementary Fig. 3.1g).

Clustering analysis on the final set of cells (n=28,440 cells from 9 batches of spheroids) resulted in 23 clusters (Fig. 3.1c). Cluster identities were assigned using previously established canonical markers from developing human fetal cortex [108, 120] and human brain spheroid studies [106, 110, 117] (Supplementary Table 3.1; Fig. 3.1d). Identifiable clusters included: Excitatory Neurons (Cluster 3: *SATB2*+, *NEUROD6*+, -*SYN1*+, *RELN*+), Mature Inhibitory Neurons (Cluster 12: *GAD1*+, *GAD2*+, *RBFOX3*+), and Astrocytes (Cluster 19: *S100B*+, *AQP4*+, *GFAP*+,*SLC1A3*+). Many canonical cell markers were expressed broadly across multiple clusters including *MKI67* (M-Phase Cells), *SOX2* (Radial Glia and Astrocytes), *STMN2* (Pan-neuronal), *S100B* (Radial Glia and Astrocytes), *GFAP* (Radial Glia and Reactive Astrocytes), *NEUROD6* (Mature/Maturing Neurons), *SATB2* (Upper Layer excitatory neurons) and *GAD1* (Inhibitory neurons) (Fig. 3.1e). There are also cells within these clusters that express endothelial cell (*ITM2A*, *CLDN5*), pericyte (multifunctional mural cells; *RGS5*) and oligodendrocyte precursor cell (*OLIG1*,*OLIG2*) markers. Identifying cells by differentiation batch did not reveal any major batch effects (Supplementary Fig. 3.1h). Data normalization and batch correction using an alternate method, scVI [116], gave similar results for clustering and grouped canonical gene expression, indicating that the clustering observations were robust (Supplementary Fig. 3.2a-d).

When the cells were separated out by time-point (Supplementary Fig. 3.3a), we found that later time-points (Day 120 and Day 220) had a greater proportion of their total cells in more mature excitatory neuron clusters and less represented in more mature inhibitory clusters compared to Day 50 (Supplementary Fig. 3.3b). Neuronal cluster maturity is relative to other cells in the dataset and is defined by burgeoning expression of *SYN1* (Synapsin 1) and *DLG4* (PSD-95) in neurons, indicating the presence of synapses, and strong expression of *MAPT* [178] and *MAP2* indicating the presence of elaborated axons and dendrites (Supplementary Fig. 3.3c). Maturity is more difficult to determine in astrocytes and endothelial cells as they retain stem cell and radial glia markers. Differential gene expression between time-points shows a decrease in ribosomal protein gene transcription and an increase in mitochondrial gene transcription (Supplementary Fig. 3.3d,e; Supplementary Table 3.2) highlighting the terminal differentiation of cells towards divergent mature cell types that use oxidative phosphorylation for energy production [179] and have relatively low levels of translation overall [101], most likely because of a reduced need for cell division and growth.

Previous studies have indicated that human brain spheroids do not reflect the true processes of human cortical development, citing glycolytic stress and ER stress as the primary reasons for this [106, 108]. In our dataset, we find that the glycolysis genes *PGK1* and *BNIP3* are highly expressed at all timepoints, although higher in some specific clusters (Fig. 3.1d; Supplementary Fig. 3.3f). The ER stress markers *GORASP2* and *ARCN1* were not highly expressed in our post-filtered dataset.

Given the presence of these previously reported stress markers, we combined our dataset with two separate single cell datasets from primary fetal tissue [108, 120], to assess the degree of cell type overlap between the two. (Supplementary Fig. 3.4a-f). We found many clusters overlapped, although different between the datasets, and many clusters that were unique to spheroids or fetal tissue. Fetal tissue specific clusters included microglia and red-blood cells, which spheroids would not develop as they come from a different lineage, while astrocytes, which are not present in one of the primary datasets [120] as it was taken before the astrogenic phase of cortical development, seemed to be more unique to spheroids. Among other clusters that were specific to the cortical spheroids, some were represented by high expression of glycolytic genes (Supplementary Table 3.3), confirming that high glycolysis rates are a hallmark of human brain spheroid culture. The middling degree of overlap may reflect the overall immaturity of spheroid cultures, as the more mature neuronal clusters of the primary tissue were the most poorly aligned clusters in each dataset.

Differential gene expression in TSC2$^{-/-}$ cells

When observing the dimensionality reduction of cells classified by genotype (Fig. 3.2a), we observed an uneven distribution across the clusters. There were large discrepancies in the proportion of *TSC2$^{-/-}$* cells in clusters defined as radial glia, astrocytes and endothelial cells compared to *TSC2$^{c/-}$* cells (Fig. 3.2b). Complimentary to this, *TSC2$^{c/-}$* cells tended to reside in neuronal clusters, both mature and immature. When further breaking down neurogenic and neuronal clusters by genotype, we observe that *TSC2$^{-/-}$* cells were less represented in mature excitatory neuronal clusters but were relatively well represented in neurogenic radial glia (*HES6*+, *ASCL1*+). This reflects previous observations that early neuronal development is largely normal in *TSC1/2* KO cell cultures, but that maturation may compromised by increased death of newly-born excitatory neurons [93]. Correspondingly, *TSC2$^{-/-}$* cells did not appear to be deficient in the formation of inhibitory neurons (Fig. 3.2b), which are mostly thought to be mostly born elsewhere in the developing brain, only later migrating into the cortex [37].

Overall differential gene expression between the two genotypes expectedly showed an increase the expression of many genes that are found in radial glia and astrocytes (*CLU*, *PTGDS*, *SPARCL1*, *S100B*) (Fig. 3.2c; Supplementary Table 3.4). We submitted the 243 genes with an adjusted p-value of <0.05 and a Log2 Fold-change of <-0.25 (significantly overexpressed in *TSC2$^{-/-}$* cells) for gene ontology (GO) analysis. The most significant gene ontology category outputs were related to the immune response which, given that there are no immune cells in our spheroid system, may be due to incomplete annotation (Fig. 3.2d). Many of the genes leading to this annotation (*CTSD,LAMP1,CTSB,CD63,LAMP2)* are indicated in lysosomal function, which likely reflects a compensatory increase to combat that repression of autophagy by increased

mTORC1 signaling. Other significant GO categories included “negative regulation of neuron differentiation” and interestingly “cellular protein metabolic process” and “protein stabilization”. With the increase in mTORC1 signaling following the loss of *TSC2*, it is highly likely there is an increase in protein synthesis, which in turn may lead to an increase in transcripts involved in protein stabilization and metabolism.

Given that *TSC2*$^{-/-}$ cells cluster more in radial glia and astrocyte clusters, it is not surprising that the top differentially expressed genes are primarily those expressed in those clusters. However, if we take three of those genes and look at the gene expression by cluster (Fig. 3.2e), it becomes clear that *CLU*, *B2M* and *PTGDS* are not only overexpressed in glial clusters, but also in *TSC2*$^{-/-}$ cells in clusters with other identities. In contrast, *APOE* expression is mostly restricted to astrocyte and radial glia clusters. *CLU*, *B2M* and *APOE* are of significant interest because of their roles in neurodegenerative disorders. *CLU* has multiple isoforms with opposing functions; one is a nuclear protein that promotes apoptosis, while the others are cytosolic and secretory molecular chaperones that inhibit apoptosis and assist with protein folding [180]. Genetic variants of *CLU* are associated with Alzheimer’s Disease and Clusterin protein has been shown to bind Amyloid-β and assist with its clearance in some contexts while increasing Amyloid-β’s neurotoxicity in others [180]. Like *CLU*, genetic variants in *APOE* are associated with Alzheimer’s disease. *APOE* is primarily a cholesterol carrier and is expressed by astrocytes in the central nervous system [181]. One of its functions is to bind and clear Amyloid-β. It is unclear if the upregulation of *CLU* and *APOE* are a result of *TSC2*$^{-/-}$ cells being more astrocytic in nature or if this is an aberrant response to an increase in protein aggregates, perhaps caused by an increase in overall translation. Several other astrocyte and astrocyte development-promoting genes are more highly expressed in *TSC2*$^{-/-}$ cells, like *PTGDS*. *PTGDS* encodes for Prostoglandin D2 synthase, the enzyme that produces Prostoglandin D2, a neurotrophic factor that is known to help promote the development of *GFAP*+ astrocytes [182] and may be expressed in specific subsets of astrocytes in the central nervous system [183]. *B2M*, a ubiquitous component of MHC Class I molecules expressed in all cells, is induced in reactive astrocytes following injury [184], indicating that the *TSC2*$^{-/-}$ cells may be developing into reactive astrocytes, rather than quiescent homeostatic astrocytes.

Further analysis of differential gene expression on a cluster level reveals likely compensatory transcriptional responses to increases in mTORC1 signaling (Table S4). For example, we observed decreased expression of ribosomal protein genes (RPs) and increased expression of autophagy-related genes (*MAP1LC3*, *SQSTM1*, *GABARAP*) in *TSC2*$^{-/-}$ cells. This highlights the role of mTORC1 as a kinase and translational effector, as opposed to a transcriptional response activator (Supplementary Fig. 3.5a,b) as it can be presumed that the changes in the expression of these classes of genes are feedback response to combat the effects of increased mTORC1 signaling. Interestingly, these differences are only apparent in immature or non-neuronal clusters, likely reflecting the general decrease in translation [101] and corresponding increase in autophagy that occurs during neuronal development [185], diminishing the differences between *TSC2*$^{c/-}$ and *TSC2*$^{-/-}$ cells.

Additionally, in some more mature neuronal clusters, a small subset (10-25%) of *TSC2*$^{-/-}$ cells expressed *HOX* cluster genes that are normally expressed in caudal regions of the spinal cord (*HOX* groups 6-13, but also *HOXB2*) [186]. It is unclear

whether this is ectopic expression in otherwise normally developing cortical neurons or if this reflects an altered developmental program that is specifically affecting a small percentage of *TSC2*$^{-/-}$ cells.

TSC2$^{-/-}$ *cells preferentially differentiate along an astro-glial lineage*

Our scRNA-seq results and previous work using immunostaining and western blotting to asses protein expression, suggests that loss of the TSC1/2 complex during human cortical development alters astrocyte development and biology [77]. Together with prior work analyzing resected tuber samples and mouse models of TSC [164], which revealed altered astrocyte numbers and astrocyte function, this suggests that astrocytes may play a key role in TSC pathophysiology. Knowing that *TSC2*$^{-/-}$ cells in our model are overrepresented in astrocyte and radial glia clusters, we used trajectory analysis [115] to illuminate the differentiation differences between *TSC2*$^{c/-}$ and *TSC2*$^{-/-}$ cells. Upon isolating the cells from each genotype and redoing the dimensionality reduction, trajectories for *TSC2*$^{c/-}$ and *TSC2*$^{-/-}$ cells were mapped separately (Fig. 3.3a,b). In the *TSC2*$^{c/-}$ trajectory, there are two main branches, one moving towards astrocyte/endothelial cell differentiation and the other towards neuronal differentiation. In contrast to this, there appears to be three primary branches for the *TSC2*$^{-/-}$ cells, one that is sparsely populated and goes towards neurons, one towards astrocyte/endothelial cells, and the other towards more reactive astrocytes. To understand the differences between the development of these populations and to identify any further subtypes of cells, we isolated and re-clustered the cells in original clusters 4, 8, 14, 13, 19 and 22 (Fig. 3.1), which include non-neurogenic radial glia, astro-glia and endothelial cells. This sorted the cells into three relatively distinct large “domains” and several small outgroups while preserving some of the initial cluster identity (Fig. 3.3c). Interestingly, in this analysis, the cells also separated strongly by timepoint, likely reflecting the maturity of the cells (Fig. 3.3d) as the three primary regions roughly correspond to uncommitted radial glia, glial precursors/reactive astrocytes and then a collection of astrocyte/endothelial/pericytes (Fig. 3.3e). The astrocyte/endothelial/pericyte domain expresses *S100B*, *CLU*, *IGFBP7* and *WIF1* – all markers of mature astrocytes [117, 187], but lacks many other canonical astrocyte markers such as *AQP4*, *AGT*, and *SLC4A4*. Additionally, these three clusters express unique markers of endothelial cells (*CLDN5* and *IT2MA*) or pericytes (*RGS5*) found in fetal human brain [120] (Fig. 3.3f). The presence of endothelial cells amongst radial glia and astrocyte populations is unsurprising as it is known that endothelial cells are also born from radial glia late in cortical development [35].

The domain corresponding to glial precursors/reactive astrocytes expresses canonical astrocyte markers (*GFAP*, *AQP4*, *SLC4A4*, *ALDH1L1*, *CD44*, *AGT* and *S100B*) at variable levels in each cluster, likely reflecting their level of maturity, but also potentially their reactivity (Fig. 3.3f). Additionally, a population of oligodendrocyte precursor cells can now be identified within this domain (*OLIG1* and *OLIG2* expressing cells) [120]. The distribution of genotypes within each cluster shows *TSC2*$^{-/-}$ cells being more represented in glial precursor and reactive astrocyte clusters and correspondingly less represented in the uncommitted radial glia (Fig. 3.3g). Interestingly, in the cluster that resembles pericytes, the representation of *TSC2*$^{c/-}$ cells is greater than *TSC2*$^{-/-}$ cells. Together, this is evidence that *TSC2*$^{c/-}$ cells either take much longer to develop

mature astrocytes or they are biased towards different differentiation pathways. Differential gene expression analysis of the astrocyte precursor/reactive astrocyte clusters shows that even within these clusters, *CLU*, *PTGDS*, *APOE* and *B2M* are more highly expressed (Fig. 3.3h; Supplementary Table 3.5), although it is still unresolved whether this simply means that these cells are more mature than their *TSC2*$^{-/-}$ counterparts, or if this overexpression could be pathological.

TSC2$^{+/-}$ *spheroids show similar transcriptional profiles as wild-type spheroids*

To compare the effects of heterozygous versus homozygous loss of *TSC2* against wildtype on neurodevelopment, further demonstrating the requirement for a second hit mutation to develop cortical tubers, we compared genetically engineered constitutive *TSC2*$^{+/+}$, *TSC2*$^{+/-}$, and *TSC2*$^{-/-}$ spheroids at day 120 (Fig. 3.4a). Dimensionality reduction and clustering from the combined genotypes resulted in domains of clusters corresponding to broad cell type – e.g. mitotic cells, neurons, radial glia/astrocytes and endothelial cells/pericytes (Fig. 3.4B,C), without strong batch effects (Supplementary Fig. 3.6a). As before, *TSC2*$^{-/-}$ cells were well represented in mature inhibitory neuronal subtypes and less represented in mature excitatory neurons clusters (Fig. 3.4d). Interestingly, *TSC2*$^{+/-}$ were more represented in the mature excitatory neuron clusters than *TSC2*$^{+/+}$ cells. Even more surprisingly, *TSC2*$^{-/-}$ cells were underrepresented in astrocyte/astrocyte precursor clusters, while *TSC2*$^{+/+}$ and *TSC2*$^{+/-}$ were about equally represented. This underrepresentation may be due to a technical problem, as at day 120 many presumed *TSC2*$^{-/-}$ astrocytes/giant cells (*S100B*+/*GFAP*+) are so large, that they may be eliminated by size exclusion before the FACS step. Previous work [77] has shown that there are significantly more *S100B*+ cells at day 100 in *TSC2*$^{-/-}$ spheroids compared to both *TSC2*$^{+/-}$ and *TSC2*$^{+/+}$ spheroids and that levels of *S100B* transcript at day 100 and GFAP protein at days 100 and 150 are significantly higher in *TSC2*$^{-/-}$ spheroids than in *TSC2*$^{+/+}$ spheroids. This indicates that there may be a loss of *S100B*+ glial-lineage cells during the processing of our single cell sequencing pipeline.

Differential expression analysis between each set of genotypes across all clusters expectedly showed changes that were primarily driven by cell type distribution (Table S6). Notable strong exceptions included *NNAT* – an early neural development promoting gene up in *TSC2*$^{+/-}$ and *TSC2*$^{+/+}$ spheroids, [188] and *CRYAB* – a molecular chaperone that binds misfolded proteins and is overexpressed in TSC lesions [189] and *TSC2*$^{-/-}$ mouse embryonic fibroblasts [190], in addition to *TSC2*$^{-/-}$ spheroids (Fig. 3.4e,f). Notably, *CRYAB* expression is present in all clusters of *TSC2*$^{-/-}$ cells, with the highest expression being in astrocyte/glial precursor clusters, while in *TSC2*$^{+/+}$ and *TSC2*$^{+/-}$ cells, *CRYAB* expression is limited astrocyte/glial precursor clusters, in which it is expressed at relatively low levels (Fig. 3.4f). Analyzing some of the differentially expressed genes that we identified in the conditional spheroid model reveals that *CLU*, *PTGDS* and *APOE* are overexpressed in *TSC2*$^{-/-}$ cells in many clusters, including neuronal ones, indicating that homozygous loss of *TSC2* can drive transcription of these astrocyte associated genes regardless of cellular context (Fig. 3.4e). Compared to Homozygous loss of *TSC2*, heterozygous loss of *TSC2* drives many fewer transcriptional changes (Supplementary Table 3.6), however these changes may lead to

minor differences in cell fate, as seen by the differential presence of *TSC2*$^{+/-}$ and *TSC2*$^{+/+}$ cells in many clusters (Fig. 3.6d).

To assess how the second-hit spheroid model and constitutive spheroid model fit together, we combined all day 120 samples of each of the five genotypes into one analysis. As before, dimensionality reduction and clustering resulted in large domains separated by broad cell type with genotypes sorted into each in expected proportions based on previous results (Supplementary Fig. 3.6b-e). *CRYAB* gene expression per genotype per cluster again showed very high expression in the constitutive *TSC2*$^{-/-}$ cells but also increased expression in the conditional *TSC2*$^{-/-}$ cells in several clusters, although to a lesser extent (Supplementary Fig. 3.6e). Concordantly, *PTGDS* expression per cluster was highly enriched in both constitutive and conditional *TSC2*$^{-/-}$ cells, again to varying degrees based on cluster.

Single-hit heterozygous cells show similar transcriptional differences as two-hit homozygous cells

To further demonstrate the limited effects of heterozygous TSC2 loss on cortical development, we sequenced single cells from day 50 and day 120 *TSC2*$^{c/+}$ spheroids [77], engineered to express a Cre-dependent tdTomato reporter. Lentivirus expressing Cre recombinase was added on day 8 of spheroid development and the same scRNA-seq processing paradigm was followed as with the *TSC2*$^{c/-}$ spheroids (Fig. 3.5a). In this model, Cre recombinase induces a single-hit loss-of-function mutation in *TSC2*, while the surrounding cells express wild-type levels of *TSC2*. Dimensionality reduction and clustering revealed similar domains of clusters as previous Day 50 and Day 120 analyses (see Supplementary Fig. 3.3), however there were less well-defined differences between excitatory and inhibitory neurons, with clusters expressing excitatory markers (*RELN*) also expressing inhibitory markers (*GAD1*,*GAD2*) (Fig. 3.5b,c). As before, there were also limited batch effects within time-points (Supplementary Fig. 3.7a). *TSC2*$^{c/+}$ cells were over-represented in one cluster of maturing inhibitory neurons (cluster 0) and one cluster of granin (*SCG2*+,*SCG5*+,*CHGA*+,*CHGB*+) expressing neurons, while *TSC2*$^{-/+}$ cells were overrepresented in one of the astrocyte precursor clusters (cluster 5) and the endothelial cells/pericyte clusters (clusters 17 and 20). This is a similar distribution to the *TSC2*$^{c/-}$ cells at these ages although the differences were not as large (Supplementary Fig. 3.7b-d). This indicates that the loss of one copy of *TSC2* during development may lead to differences in cell fate, however the consequences of those cell fate decisions may not be the same. For instance, immunofluorescence from sections of day 120 *TSC2*$^{c/+}$ spheroids infected with Cre lentivirus shows a lack of gross morphological changes or increases in mTORC1 signaling in the TdTomato positive cells as seen in the *TSC2*$^{c/-}$ spheroids at similar ages [77]. Considering that the differences between astrocytes and endothelial cells/pericytes does not become strongly apparent until later timepoints (Fig. 3.3e), it's unclear whether heterozygous cells will still generate astrocytes like the homozygous knockouts.

To determine whether conditional heterozygous TSC2 cells showed any differences (i.e. *TSC2*$^{c/+}$ with Cre and *TSC2*$^{c/-}$ without Cre), we combined all the samples from the conditional models at day 50 and day 120 to look for gene level differences within clusters. Dimensionality reduction and clustering gave similar cell

types as all other analyses (Supplementary Fig. 3.8a, b). The distribution of genotypes between each cluster was as expected given previous results with *TSC2*$^{c/-}$ with cre (TSC2 KO) and *TSC2*$^{c/+}$ with Cre (TSC2 Het) cells being more represented in astrocyte/astrocyte precursor/endothelial cell clusters (clusters 1 and 12) and *TSC2*$^{c/+}$ without cre (TSC2 WT) and *TSC2*$^{c/-}$ without cre (TSC2 Het) cells more represented in the maturing excitatory neuron cluster (cluster 10) (Supplementary Fig. 3.8c). The only clusters where TSC2 KO cells appear to be specifically up or down compared to all other genotypes are the mitotic cell clusters (cluster 16 and 19) and three immature neuron clusters (Cluster 0, 5 and 9).

Examining previously identified differentially expressed genes (*CLU*, *PTGDS* and *APOE* and *CRYAB*) in *TSC2*$^{c/+}$ with and without Cre cells alone, we observed that they are significantly overexpressed in many clusters, following a similar pattern as the *TSC2*$^{c/-}$ spheroid model (Fig. 3.5f; Supplementary Table 3.7) and additionally overexpressed in *TSC2*$^{c/+}$ with Cre. The combined datasets show that *TSC2*$^{c/-}$ cells with cre have higher expression of *CLU*, *PTGDS* and *APOE* in many clusters compared to all genotypes, but for some clusters *TSC2*$^{c/+}$ cells with Cre also have higher expression than the *TSC2*$^{c/+}$ and *TSC2*$^{c/-}$ controls, particularly neuronal clusters where expression may be ectopic (Supplementary Fig. 3.8d). Taken together, this analysis suggests that early perturbations in TSC2 genotype may affect gene expression and cellular differentiation in similar ways, albeit with different magnitudes, regardless of whether cells are going from wildtype to heterozygous loss or heterozygous to homozygous loss.

Discussion

In this study, we performed single cell sequencing of human cortical spheroids derived from genetically engineered hPSC lines that model the developmental disorder TSC. We find that up until approximately day 220 (~7.3 months post-differentiation), cortical spheroids primarily produce cell types represented in early neurodevelopment including radial glia, immature neurons and immature astrocytes. At day 220 we begin to see increased expression of genes that define more mature neurons and astrocytes, including the synaptic proteins *SYN1* and *DLG4*, and the astrocyte genes *AQP4* and *GFAP*. We find that homozygous loss of *TSC2* during early development leads to high expression of glial cell markers and a shift in differentiation towards reactive astrocyte and endothelial cell fates. Heterozygous loss of *TSC2* during development also leads to a shift in cell fate, however it is not as pronounced.

The transcriptional signatures observed within our dataset primarily corresponded to cell state (M-phase, glycolytic) and cell identity (neuron, astrocyte, etc.). Notably, we were not able to discover a unified transcriptional signature of $TSC2^{-/-}$ cells, highlighting the necessity of a single cell approach to uncover the complete spectrum of how loss of TSC2 affects transcriptional programs. This was not surprising, as changes in mTORC1 signaling most strongly affect non-transcriptional cell processes through kinase activity and differential phosphorylation of downstream targets [16]. The transcriptional changes we did find, likely reflect changes in cell differentiation programs or a response to altered cellular metabolism induced by changes in mTORC1 activity. For example, we observed some clusters that had notable transcriptional differences in genes associated with translation and autophagy, with ribosomal protein gene expression downregulated in $TSC2^{-/-}$ cells and autophagy gene expression concordantly upregulated. Since high levels of mTORC1 signaling are expected to increase protein synthesis and suppress autophagy, these results support the idea that transcriptional changes between $TSC2^{c/-}$ and $TSC2^{-/-}$ cells of the same identity or cell state (in this case, cells of the same cluster) are likely compensatory. This also highlights the challenges with inferring the status of biological processes from transcriptional information alone.

Many of the genes that we observed with increased transcription in $TSC2^{-/-}$ cells are normally expressed in radial glia and astrocytes [106, 108, 117]. We find both increased numbers of glial-lineage cells and increased expression of glial genes (i.e. *CLU*, *PTGDS*, *APOE*) within these cells. Taken together with the data presented in Chapter 2, this reflects an overall shift away from the creation or maintenance of neurons when mTORC1 signaling is deregulated during early cortical development. At an individual cluster level, the noted increases in genes such as *CLU* and *APOE*, which are both involved in responses to protein aggregate stress [180, 181], may be due to a response to a biological insult like protein aggregation or may represent a stronger commitment to, or maturity within, the glial lineage as these genes are highly expressed within glia. As these genes were strongly expressed in many $TSC2^{-/-}$ cell types, this may reflect a maintenance of radial glia markers, as observed in $TSC2^{-/-}$ cells in neurogenic and neuronal clusters, an increased number of radial glia or as an earlier differentiation towards mature *GFAP* and *AQP4* expressing astrocytes. The commitment to the glial lineage results not only in a greater proportion of radial glia and earlier differentiation

towards astrocytes, but also an increased number of endothelial cells, which are normally born from radial glia late in cortical development [35] . One caveat in assessing the true distribution of glial cells is their transcriptional similarity, at least at early timepoints. Defining features may be the relative levels of gene expression rather than the specific genes expressed. For instance, both radial glia and astrocytes express *CLU* and *SOX2*; however they are higher expressed in astrocytes. In contrast, expression of a small number of genes may determine a specific glial cell type, such as in oligodendrocyte precursor cells (*OLIG1*, *OLIG2*, *PDGFRA*), making it difficult to computationally distinguish them from radial glia, as the vast majority of transcribed genes remains unchanged [108, 120].

One of the key outstanding questions regarding the genesis of cortical tubers is whether they are formed by somatic "second-hit" mutations in sporadic pools of progenitor cells or if they develop from the same heterozygous cells that also produce the normal, adjacent brain tissue [30]. Our previous work indicated that homozygous loss of *TSC1* or *TSC2* was necessary for cortical tuber formation, as heterozygous spheroids had unperturbed mTORC1 signaling, normal cell morphology and the same distribution of neurons and glia as wild-type spheroids [77]. We aimed to expand on this result more comprehensively, with both constitutive and conditional models, and with a higher resolution through scRNA-seq. Firstly, we investigated whether there were differences between constitutive $TSC2^{+/+}$and $TSC2^{+/-}$ cells in developing spheroids. We found that gene expression and cellular differentiation between these two groups was very similar, and that the gene expression differences between either $TSC2^{+/-}$ or $TSC2^{+/+}$ compared individually to constitutive-$TSC2^{-/-}$ cells were almost identical. What was surprising however, was a decrease in the proportion of $TSC2^{-/-}$ cells that expressed early astrocyte markers and a corresponding increase in cells expressing early neuronal markers. Through extensive western blotting, immunofluorescence and bulk qPCR in our previous study [77], we found that $TSC2^{-/-}$ cells at around four months overwhelmingly express glial markers, indicating that the lack of a glial bias by scRNA-seq analysis may reflect a technical artifact. A logical reason for this is that mTORC1 controls cell size [23], and $TSC2^{-/-}$ cells, especially those that express glial markers, are abnormally large [44, 46]. Our methods for obtaining scRNA-Seq data involves two processes (FACS and droplet generation using the 10X Genomics pipeline) that require each cell to pass through a size exclusionary step. For FACS, before loading the dissociated sample, the single cell suspension is passed through a 70 μm cell strainer to match the 70 μm pore of the FACS machine. For droplet generation, the cells must travel through a 35 μm channel. It is therefore plausible that the consistently larger size of glial cells from $TSC2^{-/-}$ spheroids made it difficult for them to fit into the droplet generating device, leading to their exclusion from analysis. We did not observe any plugging or obstruction of the FACS tube or the droplet generating channel during sample processing, indicating that perhaps the cells were lost during the cell strainer step or perished during processing. This artifact would also be likely to affect our $TSC2^{c/-}$ cells with Cre, however it may not be as pronounced due to their slightly smaller size [77].

To further investigate the role of heterozygous loss of *TSC2* during development, we used a conditional cell line that induces a single-hit mutation in the presence of Cre recombinase ($TSC2^{c/+}$). In this model, we found a small, yet significant shift away from

neuronal differentiation and an increase in glial gene expression in *TSC2*$^{c/+}$ cells with Cre compared to the surrounding wild-type cells. However, when combining the two datasets, changes in the *TSC2* Het cells were not as pronounced as those observed with complete loss of *TSC2*. This suggests that there could be a graded effect of early developmental *TSC2* loss on differentiation and gene expression, somewhat contrasting the results obtained from constitutive spheroids. Interestingly, in several clusters, the proportions and gene expression of *TSC2*$^{c/+}$ with Cre cells was more similar to *TSC2*$^{c/-}$ with Cre cells than to *TSC2*$^{c/-}$ cells without Cre. This result leads to speculation about the effects of lentiviral infection on these outcomes. However, based on previous work with control lentiviruses, and similar outcomes with immunofluorescence and western blots of constitutive *TSC2*$^{-/-}$ spheroids, we believe this is unlikely. As an alternative explanation, this data implies that mTORC1 signaling must be tightly controlled during development, and perturbations away from a steady state may lead to differential differentiation decisions. Additionally, non-cell autonomous effects could influence differentiation i.e. the presence of WT cells further promotes the differentiation of *TSC2*$^{c/+}$ cells with Cre into astrocytes if they are already slightly more poised to do so. Further research using spheroids derived from combined aggregates of *TSC2*$^{c/+}$ and *TSC2*$^{c/-}$ cell lines, further edited to non-conditionally express another fluorophore in one cell line, could be effective in dissecting this observation.

In this study we present results from spheroids derived using a single differentiation protocol intended to reproduce cortical forebrain development [1]. Several recent single cell sequencing studies indicate that different differentiation protocols produce cells from regions of the cortex or even the whole brain in different proportions [191]. While we believe that cortical tubers are derived from second-hit mutations in forebrain neural progenitor cells, alternate differentiation protocols should be tested to further confirm this and model the effects of *TSC2* loss on other cell types. Additionally, although experimentally challenging, spheroids could be assessed at even later timepoints. Recent studies [117] and comparisons to primary tissue in this study, indicate that even at day 220, the spheroids are still relatively immature. Differentiation to 500 days or even 2 years maybe be necessary to describe the full effects of *TSC2* loss across cortical development.

Taken together, our study further confirms the glial-lineage bias of cells with homozygous loss of *TSC2*, and provides a new, in-depth understanding of the transcriptional progression of differentiation of these cells. This resource and the identification of a number of previously uninvestigated candidate genes provide a platform for further studies to understand the pathophysiology of TSC and potential treatments.

Methods

Human cortical tuber staining

After surgical resection at the Stanford Pediatric Epilepsy Center, human cortical samples were flash frozen in liquid nitrogen and stored at -80 °C until cryosectioning. Samples were removed from -80, split using a razor blade and one half was placed into OCT compound and frozen while the other half was returned to the freezer for later processing. OCT sample blocks were cryosectioned to create 16 µm sections. Following sectioning, samples were fixed with 4% PFA in PBS for 10 minutes and then washed three times in 1x PBS. Blocking occurred in buffer containing 10% Normal Goat Serum (NGS), 0.1% BSA, and 0.3% Triton X-100 in 1x PBS for 1 hour at room temperature. Sections were then incubated overnight at 4 °C in primary antibodies in antibody dilution buffer (2% NGS and 0.1% Triton X-100 in 1x PBS). The following day, sections were washed three times with 1× PBS, incubated in secondary antibody (1:500 in antibody dilution buffer) and Hoescht stain if applicable (1:1000) for 1 hour at room temperature. Sections were washed again three times with 1x PBS. Slides were coverslipped with ProLong Glass Anti-fade Mountant and allowed to set for at least 1 day before imaging. Antibody vendors, catalog numbers, and dilutions are listed in Supplementary Table 3.8.

Human pluripotent stem cell culture

WIBR3 hESCs (NIH stem cell registry 0079) were initially obtained from Dr. Rudolf Jaenisch's laboratory and authenticated as reported in Lengner et al [155]. Further cell lines were engineered to contain *TSC2* mutations in our lab as described in Blair et al [77]. For this paper, a tdTomato Cre reporter was further engineered into the $TSC2^{c/+}$ cell line exactly as previously described [77]. hESC culture was carried out as previously described [79]. Briefly, all hESC lines were maintained on a layer of inactivated mouse embryonic fibroblasts (MEFs, CD-1 strain, Charles River) in hESC medium composed of DMEM/F12 (Thermo Fisher Scientific) supplemented with 20% KnockOut Serum Replacement (KSR) (Thermo Fisher Scientific), 2 mM L-glutamine (Thermo Fisher Scientific), 1% nonessential amino acids (Thermo Fisher Scientific), 0.1 mM 2-mercaptoethanol (Thermo Fisher Scientific), 1,000 U ml−1 penicillin-streptomycin (Thermo Fisher Scientific), and 4 ng ml−1 fibroblast growth factor (FGF)-Basic (AA 1-155) recombinant human protein (Thermo Fisher Scientific). Cultures were passaged every 7 days with collagenase type IV (1.5 mg ml−1; Thermo Fisher Scientific) and gravitational sedimentation by washing 3 times in wash media composed of DMEM/F12 supplemented with 5% fetal bovine serum (FBS, Thermo Fisher Scientific) and 100 U ml−1 penicillin/streptomycin. Thawed cell lines were not passaged more than five times before discarding and going back to an earlier stock in order to reduce the likelihood of large chromosomal abnormalities. All hESC lines were tested monthly for *Mycoplasma* contamination.

Human cortical spheroid differentiation

3-D differentiation of hESCs and hiPSCs into cortical spheroids was performed as described previously [1, 109]. Briefly, confluent, undifferentiated colonies of hESCs were removed from MEFs and dissociated from each other using Accutase for 20 minutes. The cell suspension was collected and strained through a 40 µm strainer in

hESC wash media. This cell suspension was spun down for 5 minutes at 1000 rpm. The supernatant was removed and resuspended in 5 ml of hESC media without fibroblast growth factor 2 (FGF2), supplemented with 10 μm Y-27632 dihydrochloride. Cells were counted and diluted to a concentration of 2.7 $x10^6$ cells/ml and 6 ml of this suspension was deposited into one well of a 6-well Aggrewell plate. After the aggregation of single cells into EBs, the EBs were removed and put into 10 cm ultra-low attachment dishes. On days 1–5, media was changed to hESC-FGF2 media, supplemented with 10 μM Dorsomorphin (ab146597, Abcam) and 10 μM SB431542. On day 6, developing spheroids were put into neural induction media composed of Neurobasal-A (Thermo Fisher Scientific), B-27 Supplement minus vitamin A (Thermo Fisher Scientific), penicillin-streptomycin, and GlutaMAX, supplemented with 20 ng ml−1 FGF and 20ng ml−1 EGF. Media was changed in this manner every day from days 6–15 and then every other day until day 25. From days 25–43, the developing spheroids were grown in neural induction media supplemented with 20 ng ml−1 BDNF and 20 ng ml−1 NT-3, with media changes every 4 days. From day 43 onward, spheroids were maintained in neural induction media without BDNF or NT-3, with media changes every 4 days until harvest.

Spheroid dissociation for FACS and scRNA-Seq

Dissociation of spheroids for FACS followed a protocol for dissociation of post-natal day 0 mouse cortex for primary culture [192]. First, dissociation media (DM) was made consisting of 488.9 ml Ca and Mg free HBSS (Invitrogen), 5 ml of 100 mM Sodium Pyruvate (Lifetech), 1.1 ml 45% stock D-glucose (Sigma) and 5 ml pH 7.3 HEPES (Invitrogen). Next, the dissociation solution was made consisting of 5 ml DM, 172 ul Papain Solution (Worthington), and 5-7 crystals of L-Cysteine (Sigma). This solution was warmed at 37 °C for 15 minutes and then filter-sterilized through a 0.22 μm filter. The spheroid was then removed from culture media, placed into this solution and left in a 37 °C bath for 30 minutes. During this time, trypsin inhibitor (TI) solution was made consisting of 10 mg of Trypsin Inhibitor (Sigma) in 10 ml DM, placed in 37 °C for >15 minutes, removed and filter sterilized. After 30 minutes of incubation, the dissociation solution was removed from the tube with the spheroid, leaving the spheroid intact, and replaced with 3 ml of TI. The TI was immediately removed, and the spheroid was washed again in 3 ml of TI, which again, was immediately removed, replacing again with 4 ml of TI and put into the 37 °C water bath for 4 minutes. During this time, the sorting buffer (SB) of 1x PBS with Ca and Mg with 10 μM Y-27632 (Calbio Chem) was made and placed on ice. After the 4 minutes at 37 °C, the TI was removed from the tube with the spheroid and 2 ml of SB was added. The spheroid was then mechanically dissociated by triturating 5-10 times through a 5 ml pipette within this solution. The whole solution including the dissociated cells was then taken up into the pipette and passed through a 70 μm cell strainer into a 50 ml conical tube. This strained solution was then placed into a polypropylene FACS tube (BD Biosciences) and placed on ice.

FACS and Single Cell Sequencing

Dissociated cells were sorted on a BD Aria Fusion cell sorter with an attached 70 μm bore. When sorting for fluorophores, a negative control of a dissociated non-fluorophore tagged spheroid was sorted first to ensure proper gating. For all sorting, a

target number of 10,000 cells was implemented, with a maximum time of one hour sorting, so as to limit the amount of time single cells were sitting on ice. For experiments with a tdTomato fluorophore, both tdTomato-negative and tdTomato-positive cells were collected from the same sample into separate tubes. After sorting, the cells were immediately centrifuged at 300 x g for 5 minutes at 4 °C and then counted on a hemocytometer to estimate concentration. Cells were then processed through the 10x Genomics pipeline, following the protocol exactly, with a targeted loading of 2000 cells per sample. All samples were run with the 10x Single Cell 3' v2 kit with the exception of the Day 220 timepoint in *TSC2*$^{-/-}$ spheroids which was run with the 10x Single Cell 3' v3 kit. cDNA recovered following the 10x protocol was assessed for quality using a fragment analyzer, and library prepped. All 10x work was done in the Functional Genomics Lab at UC Berkeley. Libraries were sequenced at two samples per lane, pooling if doing more than two samples (i.e. four samples across two lanes) on a HiSeq 4000 (Illumina) in the Vincent J. Coates Genomics Sequencing Lab at UC Berkeley.

Single Cell Sequencing Processing

FASTQ files were aligned to a modified version of the human genome (GRCh38) with added dsRed-WPRE (TdTomato construct) gene using Cell Ranger 3.0.2 (10x Genomics). Cell Ranger gene expression matrix outputs were then loaded into Seurat 3.0 [114] using R-Studio v1.2 and R v3.6. Data from each individual sample was turned into a Seurat object and metadata regarding timepoint, genotype and batch was added to each object. Each object was subset, extracting cells where > 500 RNA features were expressed and where <20% of the genes expressed were mitochondrial. Raw RNA counts from each object were normalized using the default parameters from Seurat (Log normalization with a scale factor of 10,000). The top 2000 variable features from each object were also determined using the default parameters in Seurat (selection.method = vst). Objects were then integrated by first finding the integration anchors using control samples as the reference and otherwise default parameters (dims = 1:20) and then integrating the anchor set. Following this integration, cells were further subset by selecting for all cells expressing the cellular stress marker DDIT3 at one standard deviation from the mean or lower. Principal Component Analysis (PCA) dimensionality reduction was then run on this population of cells, followed by UMAP dimensionality reduction using the first 20 PCs. Shared nearest neighbors for each cell and clusters were identified using the default parameters from Seurat except with resolution = 1. Marker genes for each cluster were determined using the FindAllMarkers function as well as looking at gene expression of known canonical genes. Differential gene expression for all comparisons was determined using the FindMarkers function. All plots were created using ggplot2, including ggplot2 calls in Seurat. Proportional bar graphs were created using GraphPad Prism 8.

For benchmarking analysis with scVI [116], cell datasets were initially filtered and combined using the Seurat pipeline above. Integration and batch correction of the combined dataset was done using scVI v0.2.2, using the top 2000 variable features as identified in the Seurat pipeline, and 400 iterations of the autoencoder. The integrated and corrected gene expression matrices were then reloaded into Seurat in R and the subsequent UMAP dimensionality reduction and analyses was doing using the same parameters as above.

Developmental trajectory analysis
Datapoints were isolated by genotype and normalized gene expression matrices were extracted from the Seurat objects and imported into Monocle 3 [115] as a CDS object. Graphs were learned using default parameters. Cells were ordered for both datasets using both M-phase NPCs and immature neurons as a starting point, based on the known maturity of the endpoints presented.

Figures

Figure 3.1

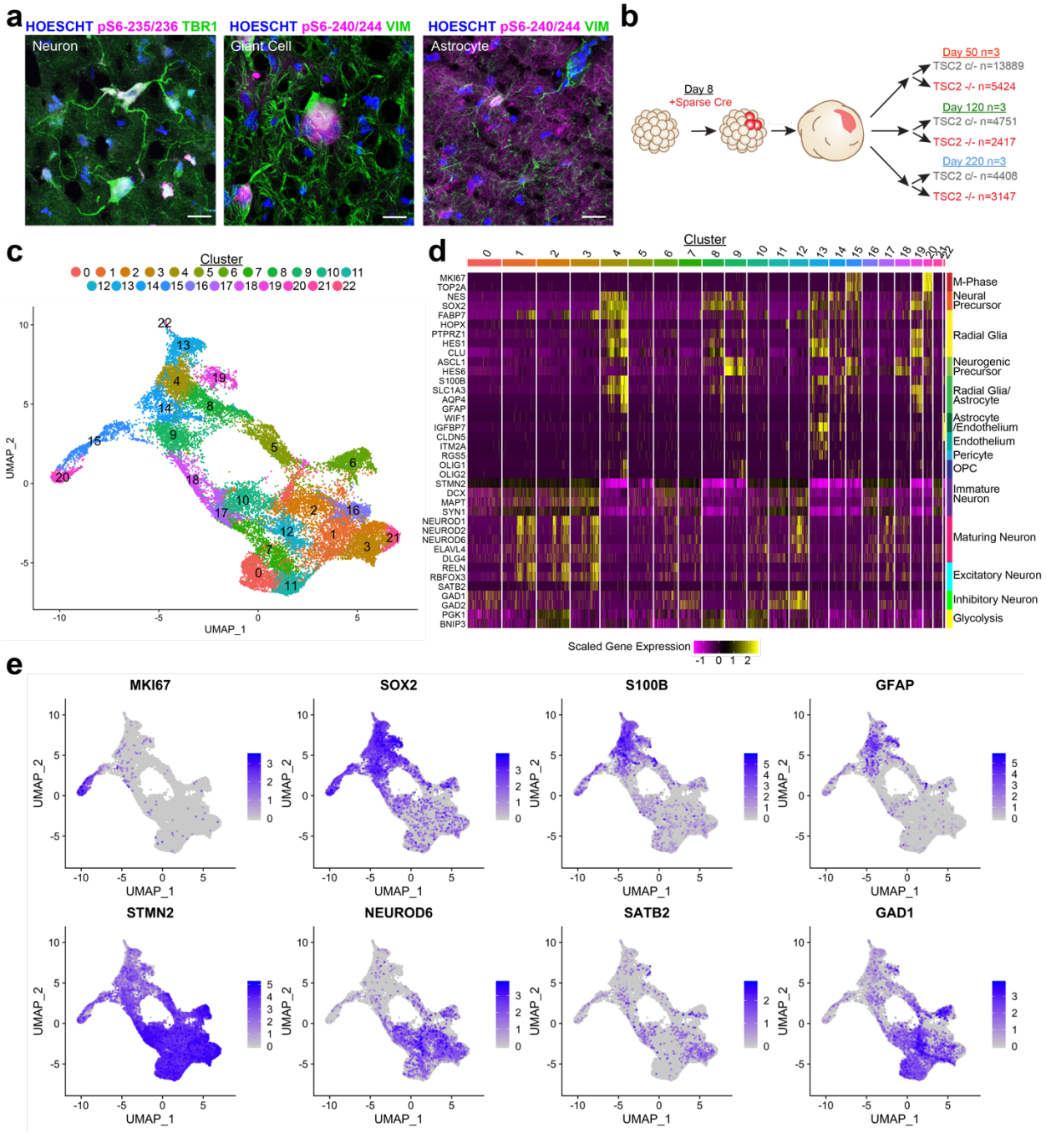

Fig. 3.1: Molecular identities of patient cortical tuber cells and cortical spheroid cells. (**a**) Immunofluorescent images of cells from a resected cortical tuber from one TSC patient. Scale bar represents 20 μm. (**b**) Schematic showing the number of batches and cells for each genotype and time-point for *TSC2*$^{-/-}$ single cell sequencing experiments (**c**) UMAP dimensionality reduction plot showing cluster assignments for cells from *TSC2*$^{-/-}$ single cell sequencing experiments. Each point represents one cell. (**d**) Heatmap showing scaled gene expression in each cell sorted by cluster. Displayed genes were selected based on canonical genes representing known cell types from the literature. (**e**) UMAP plots showing normalized gene expression in each cell of a selection of canonical genes from the literature. MKI67 (M-phase), SOX2 (Radial glia/Neural Precursors), S100B (Glia), GFAP (radial glia/reactive astrocytes), STMN2 (Early neuron/Pan-neuronal), NEUROD6 (maturing neuron), SATB2 (More mature excitatory neuron), GAD1 (Inhibitory neuron).

Figure 3.2

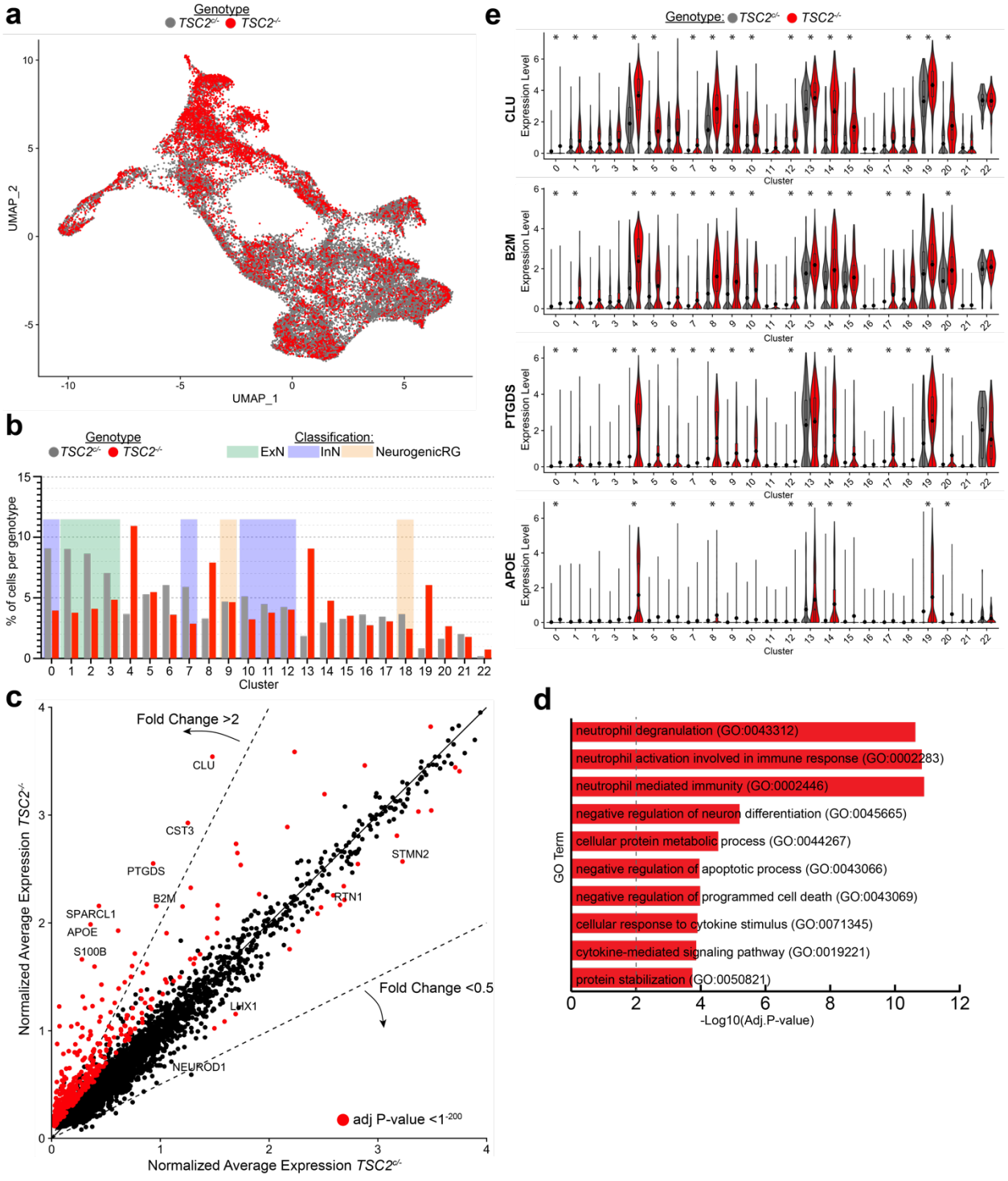
a
Genotype
TSC2-/-
TSC2-/-
UMAP_2
UMAP_1
b
Genotype
TSC2-/-
TSC2-/-
Classification:
ExN
InN
NeurogenicRG
% of cells per genotype
Cluster
c
Fold Change >2
Fold Change <0.5
CLU
CST3
PTGDS
B2M
SPARCL1
APOE
S100B
STMN2
RTN1
LHX1
NEUROD1
adj P-value <1-200
Normalized Average Expression TSC2-/-
Normalized Average Expression TSC2-/-
d
neutrophil degranulation (GO:0043312)
neutrophil activation involved in immune response (GO:0002283)
neutrophil mediated immunity (GO:0002446)
negative regulation of neuron differentiation (GO:0045665)
cellular protein metabolic process (GO:0044267)
negative regulation of apoptotic process (GO:0043066)
negative regulation of programmed cell death (GO:0043069)
cellular response to cytokine stimulus (GO:0071345)
cytokine-mediated signaling pathway (GO:0019221)
protein stabilization (GO:0050821)
GO Term
-Log10(Adj.P-value)
e
Genotype:
TSC2-/-
TSC2-/-
CLU
B2M
PTGDS
APOE
Expression Level
Cluster

Fig. 3.2: Differential clustering and gene expression between *TSC2*$^{c/-}$ and *TSC2*$^{-/-}$ cells (**a**) UMAP plot showing distribution differences between *TSC2*$^{c/-}$ and *TSC2*$^{-/-}$ cells. (**b**) Bar graph displaying the proportions of cells from each genotype in each cluster. Specific clusters of excitatory neurons (ExN), Inhibitory neurons (InN) and Neurogenic Radial Glia (Neurogenic RG) are specifically highlighted. (**c**) Scatter plot displaying the normalized average gene expression of each genotype. Each point represents a gene. Genes that have statistically significant gene expression differences between each genotype of adjusted $p<1^{-200}$ are highlighted in red. Specific genes of interest are labeled. (**d**) Bar graph displaying the top ten gene ontology terms for biological process from a list of the 243 genes with adjusted p-value of <0.05 and a Log2 Fold-change of <-0.25 between each genotype submitted to Enrichr. Statistical significance of each term is indicated by the –Log10 of the adjusted p-value. (**e**) Combined violin and box-and-whisker plots displaying the gene expression differences between each genotype per cluster for the indicated genes. * = adjusted p-value <0.05. Circular points indicate the mean expression for each genotype per cluster, boxes indicate the 25th to 75th percentile and the center line indicates the median, shape of the violin plot indicates the distribution of cells.

Figure 3.3

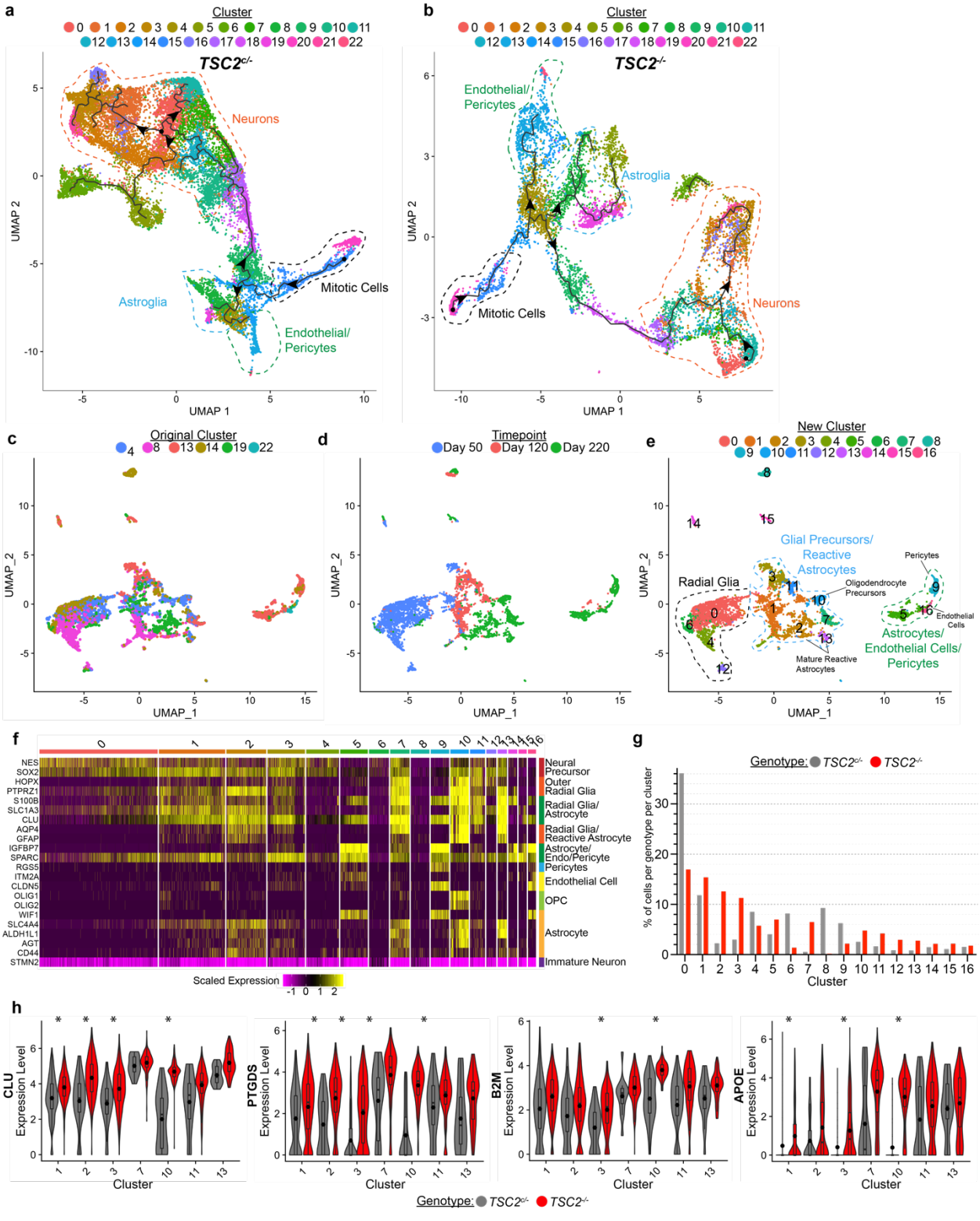
a
Cluster
TSC2-/-
Neurons
Astroglia
Mitotic Cells
Endothelial/
Pericytes
UMAP 1
UMAP 2
b
Cluster
TSC2-/-
Endothelial/
Pericytes
Astroglia
Mitotic Cells
Neurons
UMAP 1
UMAP 2
c
Original Cluster
UMAP_1
UMAP_2
d
Timepoint
Day 50
Day 120
Day 220
UMAP_1
UMAP_2
e
New Cluster
Glial Precursors/
Reactive
Astrocytes
Radial Glia
Oligodendrocyte
Precursors
Pericytes
Endothelial
Cells
Mature Reactive
Astrocytes
Astrocytes/
Endothelial Cells/
Pericytes
UMAP_1
UMAP_2
f
NES
SOX2
HOPX
PTPRZ1
S100B
SLC1A3
CLU
AQP4
GFAP
IGFBP7
SPARC
RGS5
ITM2A
CLDN5
OLIG1
OLIG2
WIF1
SLC4A4
ALDH1L1
AGT
CD44
STMN2
Neural
Precursor
Outer
Radial Glia
Radial Glia/
Astrocyte
Radial Glia/
Reactive Astrocyte
Astrocyte/
Endo/Pericyte
Pericytes
Endothelial Cell
OPC
Astrocyte
Immature Neuron
Scaled Expression
g
Genotype: TSC2-/- TSC2-/-
% of cells per genotype per cluster
Cluster
h
CLU
PTGDS
B2M
APOE
Expression Level
Cluster
Genotype: TSC2-/- TSC2-/-

Fig. 3.3: Developmental trajectories of *TSC2*$^{c/-}$ and *TSC2*$^{-/-}$ cells and glial-subtype analysis. (**a**) UMAP plot displaying subset *TSC2*$^{c/}$ cells with linear developmental trajectory from Monocle overlaid. Cells are colored by original cluster assignments and cell types are indicated from previous canonical gene analysis. Arrowheads indicate direction of developmental pseudotime. (**b**) same as in (**a**) but for *TSC2*$^{-/-}$ cells. (**c**) UMAP plot displaying isolated glial cells from both genotypes colored by original cluster assignment. (**d**) same UMAP as (**c**) colored by timepoint. (**e**) same UMAP as (**c**) colored by new cluster assignment. (**f**) Heatmap displaying scaled gene expression from a subset of radial glia, astrocyte, endothelial cell, pericyte and oligodendrocyte genes for clustered glial cells as displayed in (**e**). (**g**) Proportion of cells from each genotype represented in each cluster. (**h**) Combined violin and box-and-whisker plots displaying the gene expression differences between each genotype per cluster for the indicated genes. Only clusters identified as glial precursors/astrocytes are shown. * = adjusted p-value <0.05. Circular points indicate the mean expression for each genotype per cluster, boxes indicate the 25th to 75th percentile and the center line indicates the median, shape of the violin plot indicates the distribution of cells.

Figure 3.4

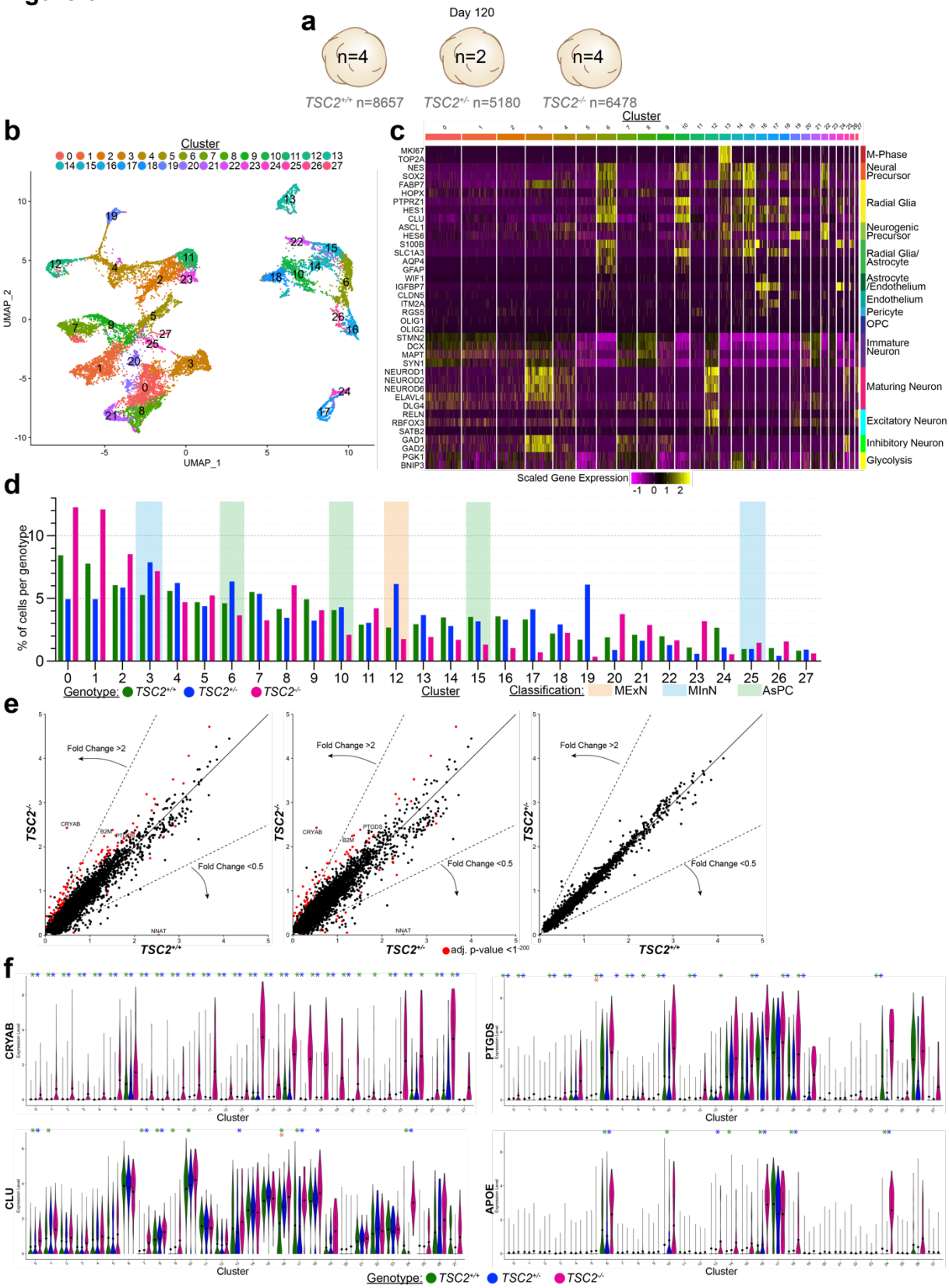
a
Day 120
n=4
n=2
n=4
TSC2+/+ n=8657
TSC2+/- n=5180
TSC2-/- n=6478
b
Cluster
UMAP_1
UMAP_2
c
Cluster
M-Phase
Neural Precursor
Radial Glia
Neurogenic Precursor
Radial Glia/ Astrocyte
Astrocyte /Endothelium
Endothelium
Pericyte
OPC
Immature Neuron
Maturing Neuron
Excitatory Neuron
Inhibitory Neuron
Glycolysis
Scaled Gene Expression
d
% of cells per genotype
Genotype: TSC2+/+ TSC2+/- TSC2-/-
Cluster
Classification: MExN MInN AsPC
e
Fold Change >2
Fold Change <0.5
TSC2-/-
TSC2+/-
TSC2+/+
adj. p-value <1-200
f
CRYAB
PTGDS
CLU
APOE
Cluster
Genotype: TSC2+/+ TSC2+/- TSC2-/-

Fig. 3.4: Molecular identity, differential clustering and gene expression in cells from constitutive TSC2 knockout spheroids. (**a**) Schematic showing number of cells and batches for each genotype. (**b**) UMAP dimensionality reduction plot showing cluster assignments for all cells, with each point representing one cell. (**c**) Heatmap showing scaled gene expression in each cell sorted by cluster. Displayed genes were selected based on canonical genes representing known cell types from the literature. (**d**) Bar graph displaying the proportions of cells from each genotype in each cluster. Specific clusters of maturing excitatory neurons (MExN), maturing inhibitory neurons (MInN) and Astro-like precursor (AsPC) are specifically highlighted. (**e**) Scatter plot displaying the normalized average gene expression of each genotype, compared in each permutation. Each point represents a gene. Genes that have statistically significant gene expression differences between each genotype of adjusted $p<1^{-200}$ are highlighted in red. Specific genes of interest are labeled. (**f**) Combined violin and box-and-whisker plots displaying the gene expression differences between each genotype per cluster for the indicated genes. * = adjusted p-value <0.05. Blue stars indicate *TSC2*$^{-/-}$ vs *TSC2*$^{+/-}$. Green stars indicate *TSC2*$^{-/-}$ vs *TSC2*$^{+/+}$. Orange stars indicate *TSC2*$^{+/-}$ vs *TSC2*$^{+/+}$. Circular points indicate the mean expression for each genotype per cluster, boxes indicate the 25th to 75th percentile and the center line indicates the median, shape of the violin plot indicates the distribution of cells.

Figure 3.5

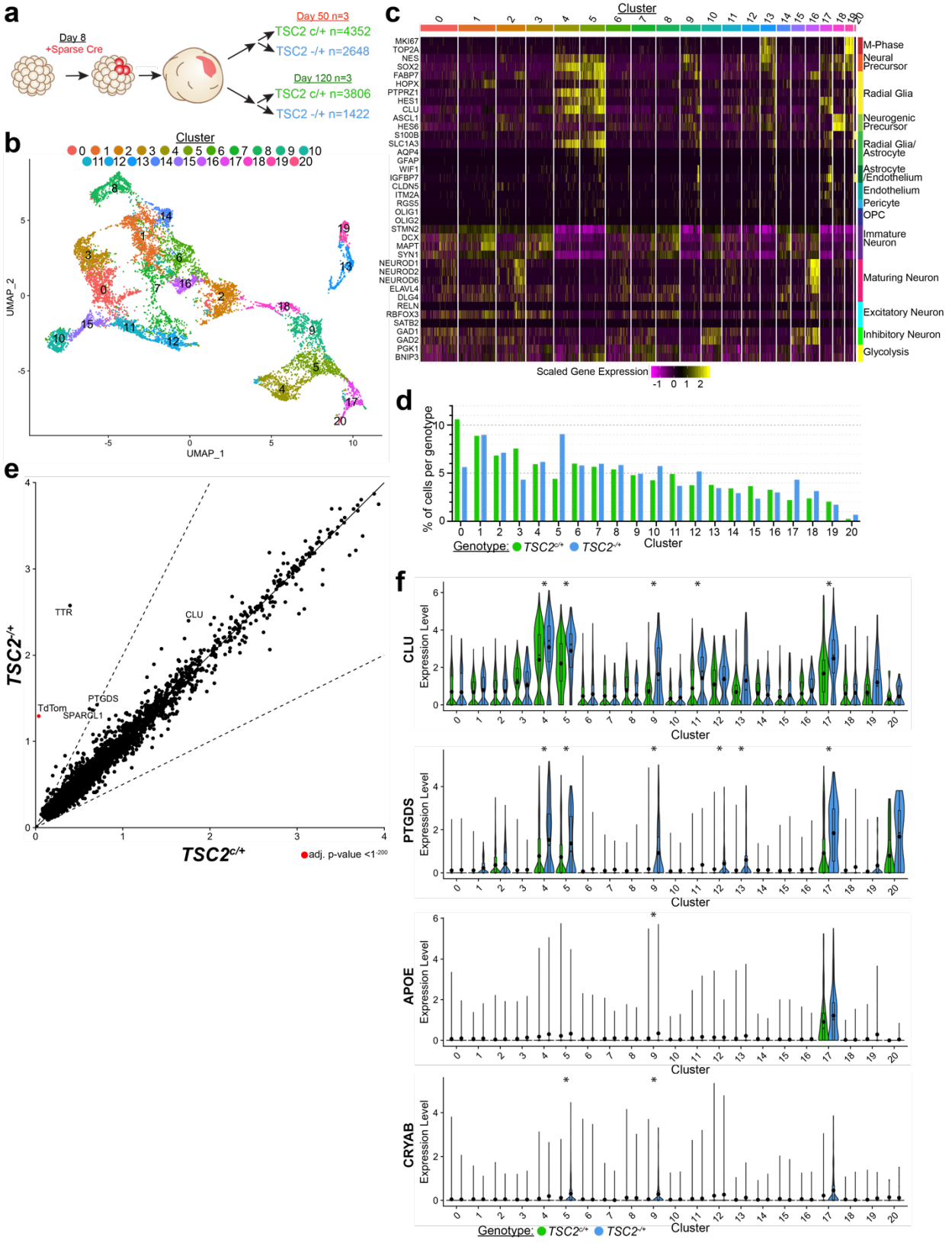
a
Day 8
+Sparse Cre
Day 50 n=3
TSC2 c/+ n=4352
TSC2 -/+ n=2648
Day 120 n=3
TSC2 c/+ n=3806
TSC2 -/+ n=1422
b
Cluster
UMAP_1
UMAP_2
c
Cluster
M-Phase
Neural Precursor
Radial Glia
Neurogenic Precursor
Radial Glia/ Astrocyte
Astrocyte /Endothelium
Endothelium
Pericyte
OPC
Immature Neuron
Maturing Neuron
Excitatory Neuron
Inhibitory Neuron
Glycolysis
Scaled Gene Expression
d
% of cells per genotype
Genotype: TSC2c/+ TSC2-/+
Cluster
e
TSC2c/+
TSC2-/+
TTR
CLU
PTGDS
TdTom
SPARCL1
adj. p-value <1-200
f
CLU
PTGDS
APOE
CRYAB
Expression Level
Cluster
Genotype: TSC2c/+ TSC2-/+

Fig. 3.5: Molecular identity, differential clustering and gene expression in cells from *TSC2*$^{c/+}$ spheroids. (**a**) Schematic showing number of cells and batches for each genotype and timepoint. "*TSC2*$^{-/+}$" indicates *TSC2*$^{c/+}$ cells treated with Cre (**b**) UMAP dimensionality reduction plot showing cluster assignments for all cells, with each point representing one cell. (**c**) Heatmap showing scaled gene expression in each cell sorted by cluster. Displayed genes were selected based on canonical genes representing known cell types from the literature. (**d**) Bar graph displaying the proportions of cells from each genotype in each cluster. (**e**) Scatter plot displaying the normalized average gene expression of each genotype. Each point represents a gene. Genes that have statistically significant gene expression differences between each genotype of adjusted $p<1^{-200}$ are highlighted in red. Specific genes of interest are labeled. (**f**) Combined violin and box-and-whisker plots displaying the gene expression differences between each genotype per cluster for the indicated genes. * = adjusted p-value <0.05. Circular points indicate the mean expression for each genotype per cluster, boxes indicate the 25th to 75th percentile and the center line indicates the median, shape of the violin plot indicates the distribution of cells.

Supplementary Figure 3.1

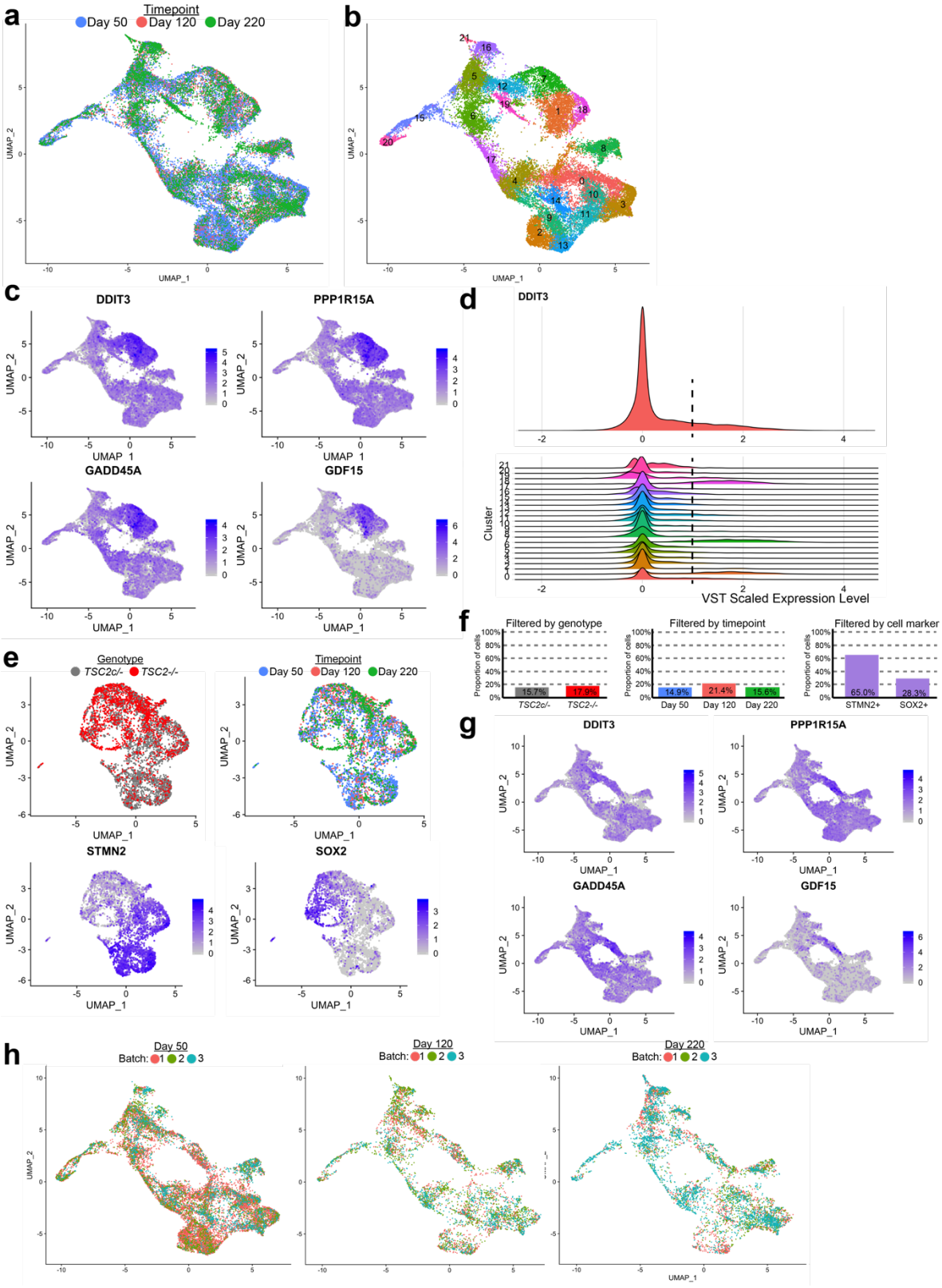

Supplementary Fig. 3.1: Filtering of highly stressed cells from analysis dataset. (**a**) UMAP plot showing cells from *TSC2*$^{-/-}$ single cell sequencing experiments colored by timepoint before filtering. Each point represents one cell. (**b**) UMAP plot showing cells from *TSC2*$^{-/-}$ single cell sequencing experiments colored by cluster assignment. Each point represents one cell. (**c**) UMAP plots showing normalized gene expression of four stress marker genes in the prefiltered dataset. Scales represent normalized expression values (**d**) Ridge plot displaying VST scaled DDIT3 expression for the whole prefiltered dataset and then per cluster. Dashed line indicates cut-off (1 Standard Deviation from the mean) at which cells above that level were filtered out. (**e**) UMAP plots of dimensionality reduced filtered cells colored by genotype, timepoint, STMN2 (neuronal marker) expression and SOX2 (glial marker) expression. Scale represents normalized gene expression values. (**f**) Corresponding bar graphs showing the percentage of total cells for each genotype and timepoint filtered out, as well as the proportion of filtered cells expressing STMN2 or SOX2. (**g**) UMAP plots showing normalized gene expression of four stress marker genes in all cells post-filtering. Scales represent normalized expression values. (**h**) UMAP plots split by timepoint and colored by batch

Supplementary Figure 3.2

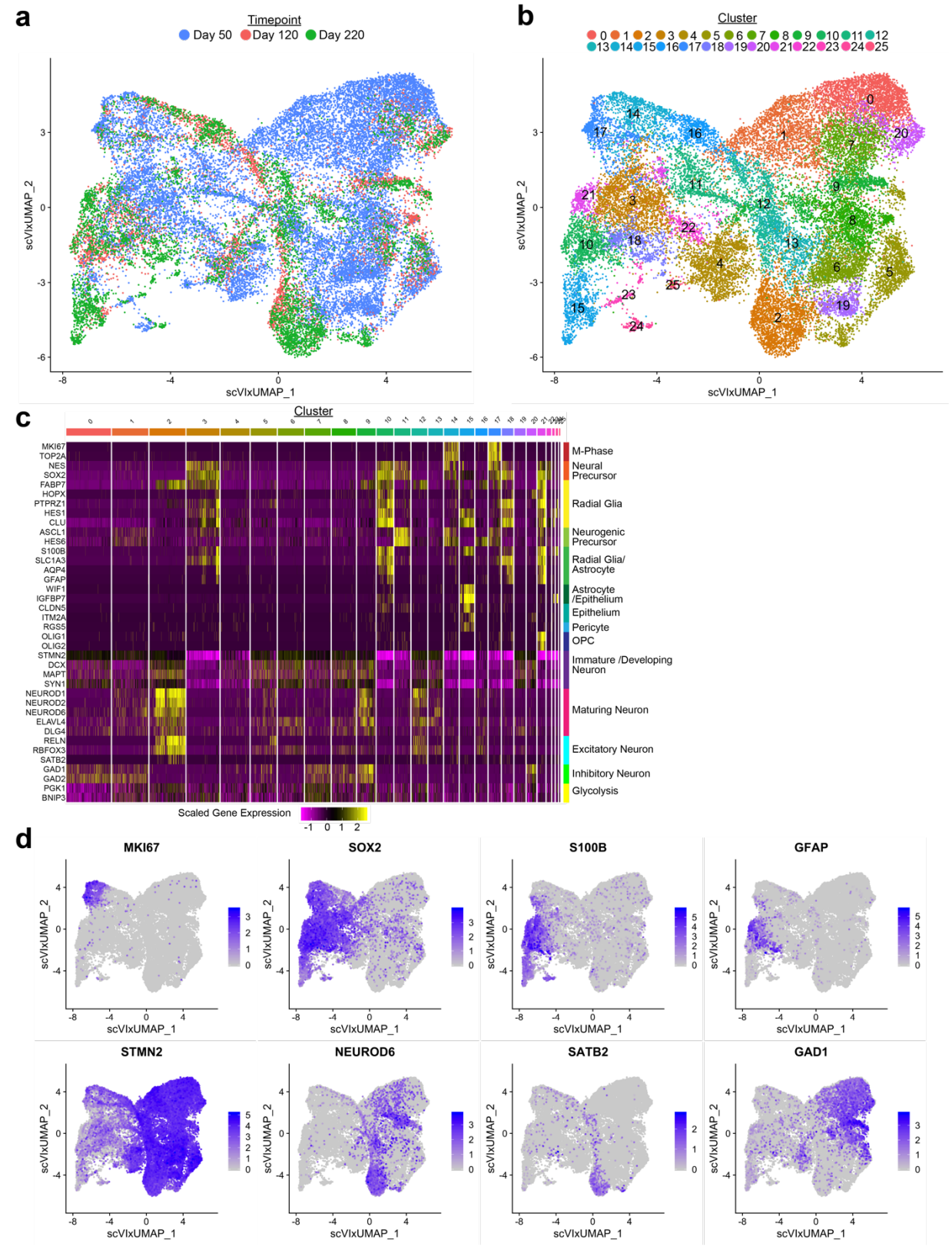

Supplementary Fig. 3.2: Batch integration and data preprocessing using scVI. (**a**) UMAP plot colored by timepoint following data pre-processing and batch integration using scVI (**b**) UMAP plot as (**a**) colored by cluster assignment. (**c**) Heatmap showing scaled gene expression in each cell sorted by cluster. Displayed genes were selected based on canonical genes representing known cell types from the literature. (**d**) UMAP plots showing normalized gene expression in each cell of a selection of canonical genes from the literature. MKI67 (M-phase), SOX2 (Radial glia/Neural Precursors), S100B (Glia), GFAP (radial glia/reactive astrocytes), STMN2 (Early neuron/Pan-neuronal), NEUROD6 (maturing neuron), SATB2 (More mature excitatory neuron), GAD1 (Inhibitory neuron).

Supplementary Figure 3.3

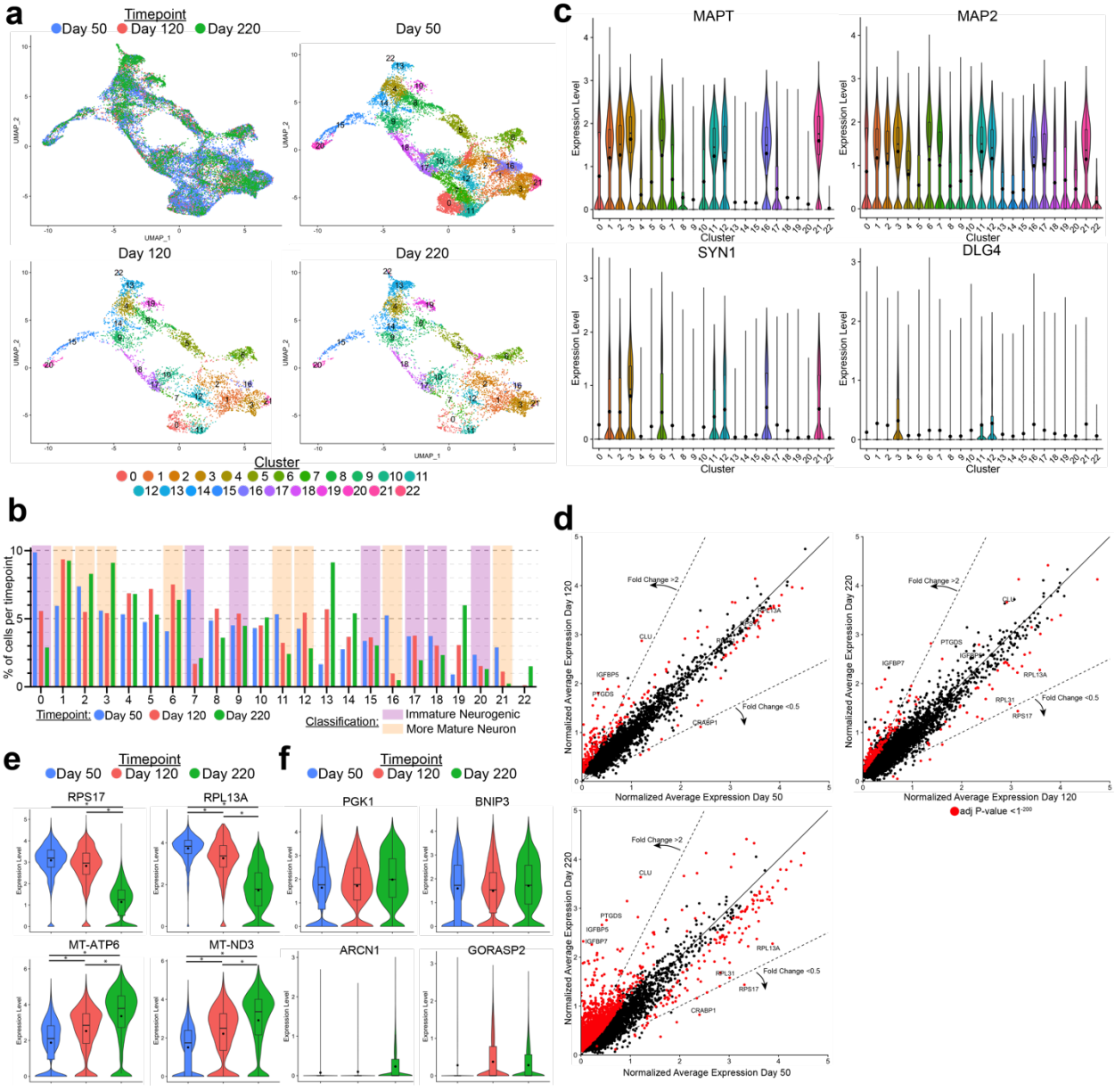

Supplementary Fig. 3.3: Evaluation of clustering and gene expression differences by timepoint (**a**) UMAP plots split by timepoint and colored by cluster assignment. (**b**) bar graph displaying the proportional number of cells from each timepoint in each cluster. Specific clusters representing immature neurogenic cells and more mature neurons are specifically highlighted. (**c**) Combined Box and Violin plots displaying the normalized gene expression levels in each cluster for four genes representing neuronal maturation: MAPT (axonal marker), MAP2 (dendritic marker), SYN1 (presynaptic protein), DLG4 (also known as PSD-95; Postsynaptic marker). Circular points indicate the mean expression for each genotype per cluster, boxes indicate the 25^{th} to 75^{th} percentile and the center line indicates the median, shape of the violin plot indicates the distribution of cells. (**d**) Scatter plots displaying the normalized average gene expression of each timepoint compared in each permutation. Each point represents a gene. Genes that have statistically significant gene expression differences between each genotype of adjusted $p<1^{-200}$ are highlighted in red. Specific genes of interest are labeled. (**e**) Combined Box and Violin plots displaying the normalized gene expression levels in each timepoint for four genes that are highly significantly changed throughout development. (**f**) Combined Box and Violin plots displaying the normalized gene expression levels in each timepoint for four genes that represent glycolysis (PGK1 and BNIP3), and ER stress (ARCN1 and GORASP2).

Supplementary Figure 3.4

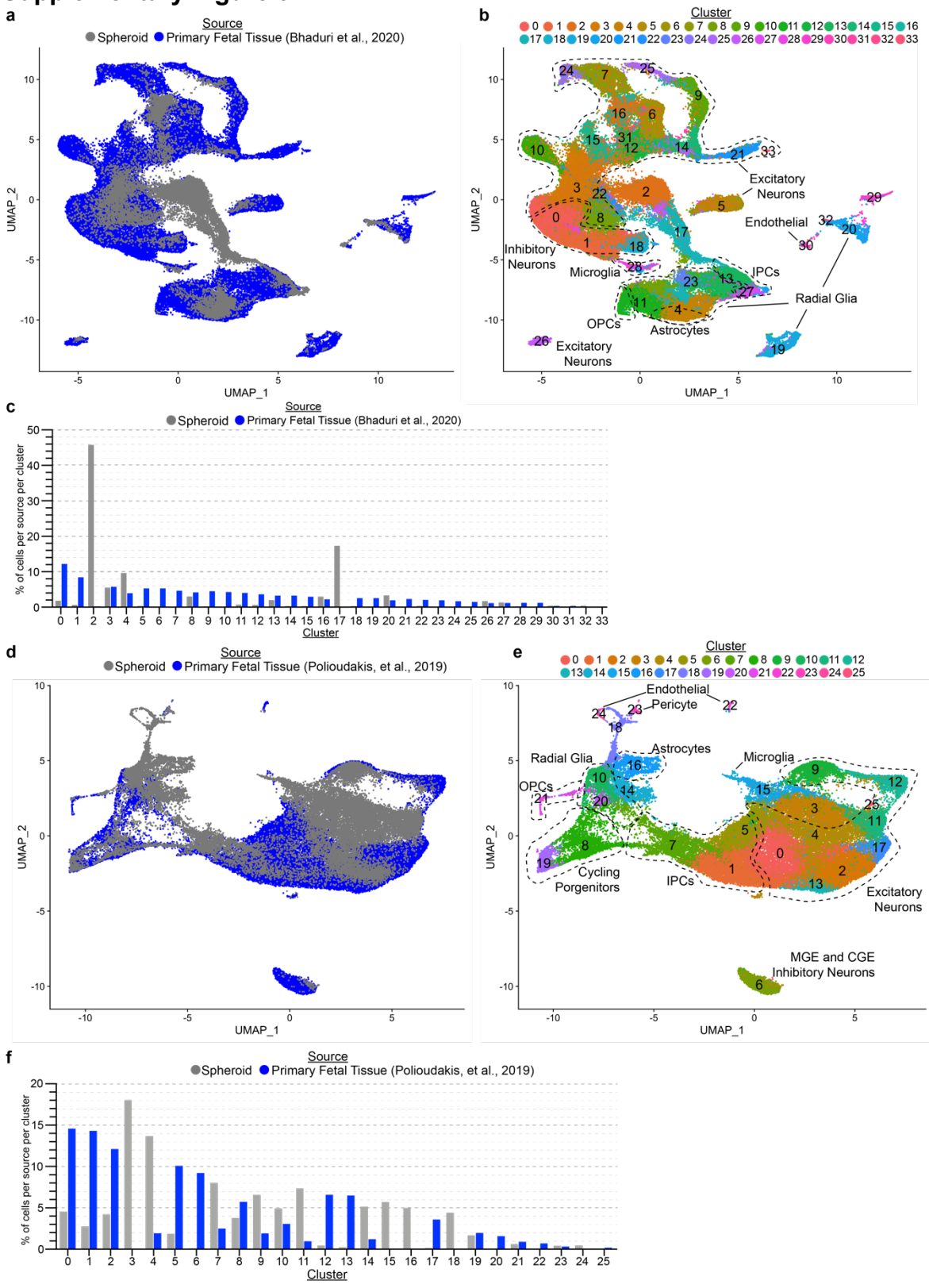

Supplementary Fig. 3.4: Comparison of TSC2c/- dataset to published primary fetal brain datasets (**a**) UMAP plot of combined datasets from this paper (*TSC2*$^{c/-}$ experiments only) and primary fetal tissue from Bhaduri et al (2020). (**b**) UMAP plot with combined clusters indicated by color and labeled identity. Where possible, identity is assigned according to the original paper's definitions. Unlabeled clusters are spheroid specific. OPCs – oligodendrocyte precursors, IPCs – intermediate precursor cells (**c**) - Bar graph displaying the proportions of cells from each source in each cluster. (**d**) UMAP dimensionality reduction plot of combined datasets from this paper (*TSC2*$^{c/-}$ experiments only) and primary fetal tissue from Polioudakis et al (2019). (**e**) UMAP plot with combined clusters indicated by color and labeled identity. Where possible, identity is assigned according to the original paper's definitions. Unlabeled clusters are spheroid specific, with the exception of astrocytes which are also spheroid specific in this analysis. OPCs – oligodendrocyte precursors, IPCs – intermediate precursor cells (**f**) - Bar graph displaying the proportions of cells from each source in each cluster.

Supplementary Figure 3.5

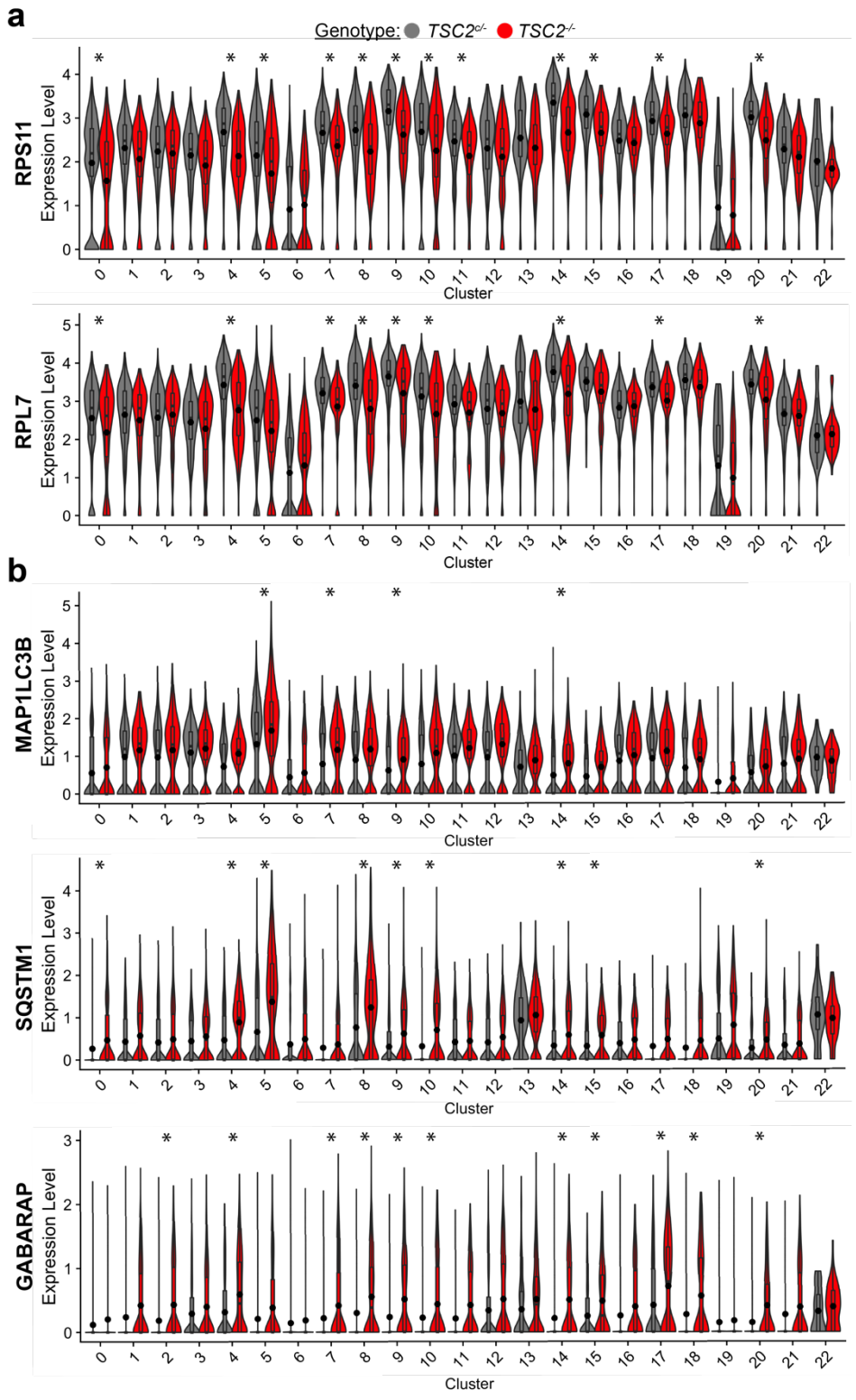

Supplementary Fig. 3.5: Differentially expressed genes involved in known mTORC1 controlled processes. (**a**) Combined violin and box-and-whisker plots displaying the gene expression differences between each genotype per cluster for the indicated translation related genes. * = adjusted p-value <0.05. Circular points indicate the mean expression for each genotype per cluster, boxes indicate the 25^{th} to 75^{th} percentile and the center line indicates the median, shape of the violin plot indicates the distribution of cells. (**b**) Combined violin and box-and-whisker plots displaying the gene expression differences between each genotype per cluster for the indicated autophagy related genes.

Supplementary Figure 3.6

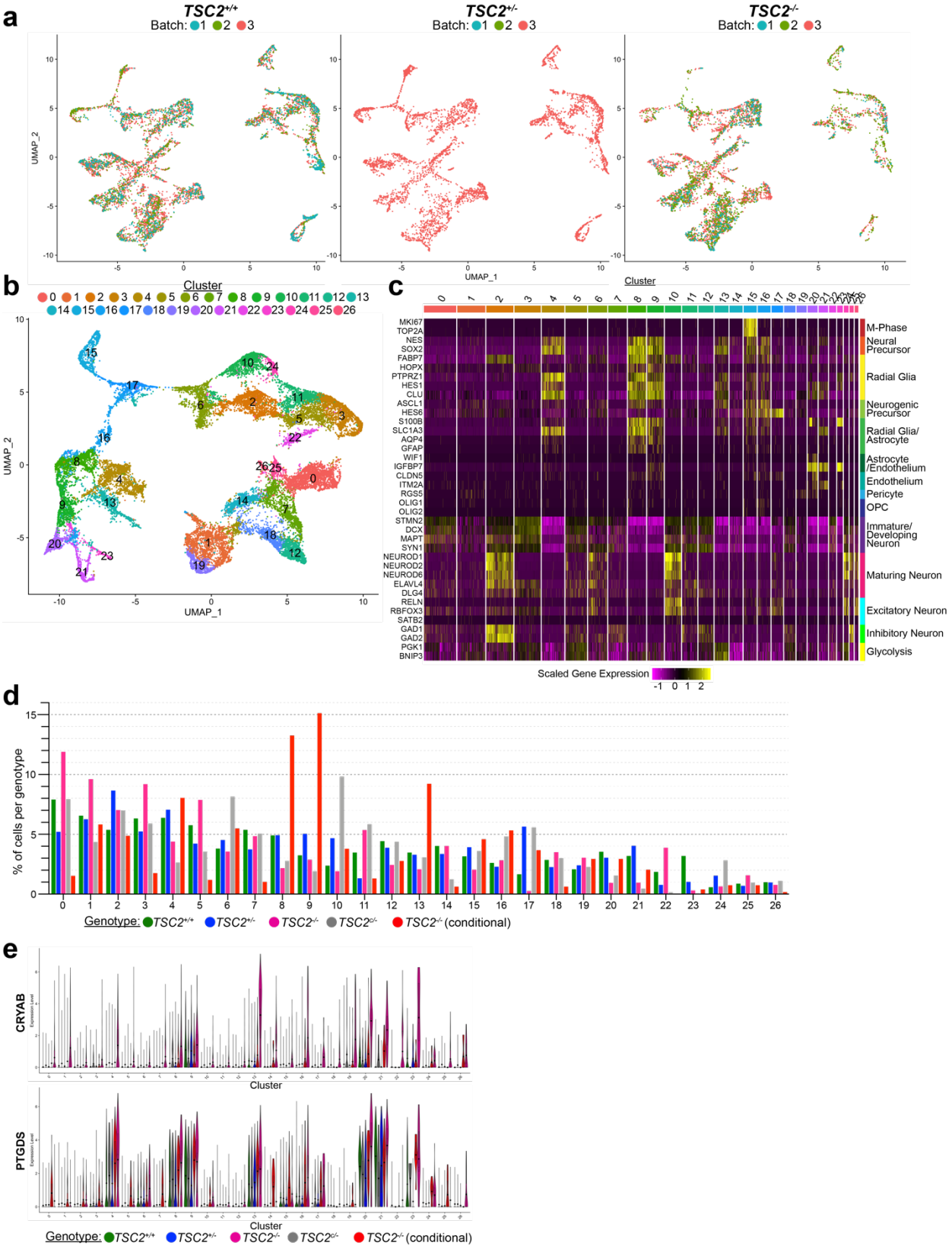

Supplementary Fig. 3.6: Further analysis of Constitutive TSC2 knockout spheroids. (**a**) UMAP plots of constitutive *TSC2* spheroid dataset split by genotype and colored by batch. (**b**) UMAP plots of clusters from integrated datasets from Day 120 in the *TSC2*$^{-/-}$ dataset and the constitutive dataset, (**c**) Heatmap showing scaled gene expression in each cell sorted by cluster. Displayed genes were selected based on canonical genes representing known cell types from the literature. (**d**) Bar graph displaying the proportions of cells from each genotype in each cluster. (**e**) Combined violin and box-and-whisker plots displaying the gene expression differences between each genotype per cluster for the indicated genes. * = adjusted p-value <0.05. Circular points indicate the mean expression for each genotype per cluster, boxes indicate the 25th to 75th percentile and the center line indicates the median, shape of the violin plot indicates the distribution of cells.

Supplementary Figure 3.7

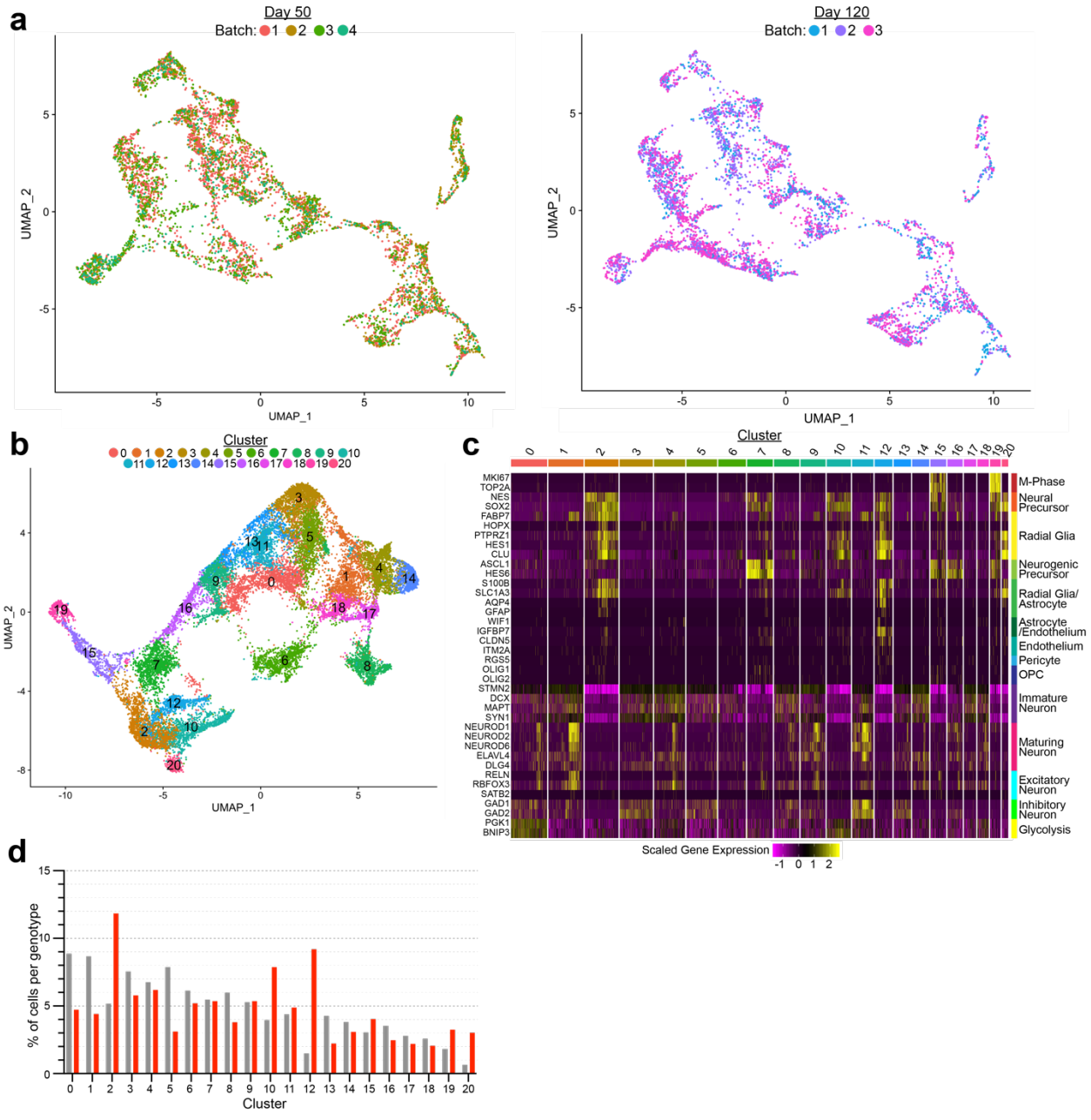

Supplementary Fig. 3.7: Individual analysis of Day 120 TSC2 knockout spheroids. (**a**) UMAP plots of *TSC2*$^{c/+}$ spheroid dataset split by timepoint and colored by batch. (**b**) UMAP plot of subset and reprocessed Day 50 and Day 120 cells from the *TSC2*$^{c/-}$ analysis, colored by cluster. (**c**) Heatmap showing scaled gene expression in each cell sorted by cluster. (**d**) Bar graph displaying the proportions of cells from each genotype in each cluster.

Supplementary Figure 3.8

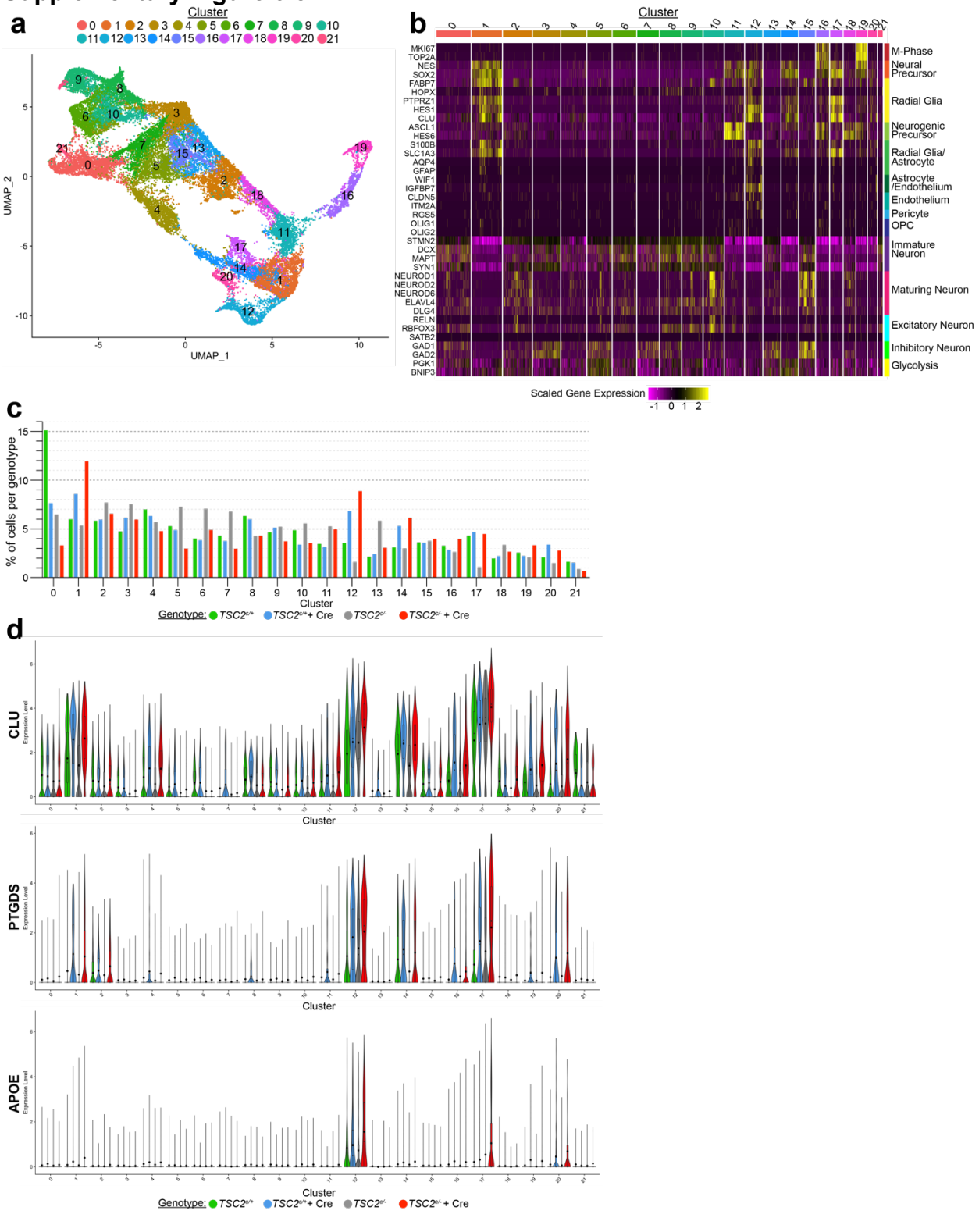

Supplementary Fig. 3.8: Combined analysis of Conditional TSC2 spheroids. (**a**) UMAP plot of integrated and reprocessed Day 50 and Day 120 cells from both *TSC2*$^{c/-}$ and *TSC2*$^{c/+}$ experiments colored by cluster. (**b**) Heatmap showing scaled gene expression in each cell sorted by cluster. (**c**) Bar graph displaying the proportions of cells from each genotype in each cluster. (**d**) Combined violin and box-and-whisker plots displaying the gene expression differences between each genotype per cluster for the indicated genes. * = adjusted p-value <0.05. Circular points indicate the mean expression for each genotype per cluster, boxes indicate the 25th to 75th percentile and the center line indicates the median, shape of the violin plot indicates the distribution of cells.

Supplementary Tables

Supplementary Table 3.1: Top 10 Genes enriched in each cluster from *TSC2*$^{c/-}$ experiments

Gene	logFC	pct.1	pct.2	p.adj	cluster
NTM	1.61	0.95	0.80	0.00	0
RALYL	1.22	0.76	0.63	0.00	0
LHX1	1.11	0.92	0.82	0.00	0
SOX4	0.50	1.00	0.99	0.00	0
TFAP2A	0.92	0.84	0.83	0.00	0
RP11-445F12.1	0.97	0.79	0.76	0.00	0
RTN1	0.54	0.93	0.93	0.00	0
FOXP1	1.12	0.72	0.70	0.00	0
CHMP2B	0.98	0.71	0.65	0.00	0
FOXP2	0.98	0.69	0.68	0.00	0
BASP1	0.46	0.99	0.96	0.00	1
STMN2	0.52	1.00	0.93	0.00	1
MLLT11	0.45	1.00	0.96	0.00	1
SIX2	0.25	0.74	0.59	0.00	1
GAP43	0.53	0.97	0.83	0.00	1
STMN1	0.39	1.00	0.98	0.00	1
CD24	0.39	0.99	0.97	0.00	1
UCHL1	0.41	0.97	0.89	0.00	1
DCX	0.43	0.94	0.86	0.00	1
BEX1	0.37	0.99	0.95	0.00	1
PGK1	0.79	0.98	0.86	0.00	2
BNIP3	0.71	0.96	0.85	0.00	2
ALDOA	0.61	0.98	0.90	0.00	2
VAMP2	0.50	0.99	0.95	0.00	2
ENO1	0.54	0.99	0.93	0.00	2
HILPDA	0.75	0.87	0.69	0.00	2
IGFBP2	0.69	0.96	0.81	0.00	2
DDIT4	0.64	0.95	0.83	0.00	2
FAM162A	0.65	0.88	0.69	0.00	2
SEC61G	0.40	0.93	0.85	0.00	2
GAP43	0.91	0.99	0.83	0.00	3
NRN1	0.89	0.91	0.56	0.00	3
RPRM	0.78	0.81	0.53	0.00	3
MAB21L1	0.74	0.87	0.52	0.00	3
CELF4	0.73	0.95	0.72	0.00	3
UCHL1	0.73	1.00	0.89	0.00	3
ZFHX3	0.73	0.90	0.56	0.00	3
POU2F2	0.72	0.89	0.64	0.00	3
BEX5	0.72	0.90	0.66	0.00	3
BASP1	0.70	1.00	0.96	0.00	3
PTN	2.12	0.99	0.73	0.00	4
TTYH1	1.79	0.99	0.63	0.00	4
FABP7	1.71	0.91	0.41	0.00	4
VIM	1.50	1.00	0.81	0.00	4
GPM6B	1.49	0.99	0.74	0.00	4
C1orf61	1.44	0.99	0.78	0.00	4

Gene	logFC	pct.1	pct.2	p.adj	cluster
FGFBP3	1.26	0.93	0.59	0.00	4
HES4	1.14	0.97	0.63	0.00	4
NTRK2	1.11	0.94	0.50	0.00	4
SOX2	1.06	0.94	0.54	0.00	4
NEAT1	1.48	0.91	0.76	0.00	5
FTL	0.81	0.98	0.97	0.00	5
CDKN1A	1.04	0.71	0.53	0.00	5
EIF1	0.48	0.99	0.99	0.00	5
BBC3	0.92	0.73	0.55	0.00	5
ARF4	0.99	0.82	0.72	0.00	5
HERPUD1	0.88	0.76	0.61	0.00	5
SLC3A2	0.78	0.72	0.55	0.00	5
RPS27L	0.53	0.86	0.76	0.00	5
GDF15	1.05	0.51	0.30	0.00	5
MT-ND4	0.99	0.97	0.94	0.00	6
MT-ND2	0.97	0.95	0.85	0.00	6
SEZ6L2	0.94	0.91	0.72	0.00	6
MT-CO2	0.91	0.98	0.94	0.00	6
RTN1	0.86	0.97	0.93	0.00	6
MAP1B	0.77	0.98	0.94	0.00	6
CELF4	1.04	0.94	0.72	0.00	6
TAC1	1.25	0.80	0.45	0.00	6
MT-CO1	0.67	0.98	0.95	0.00	6
MAB21L2	0.62	0.81	0.47	0.00	6
LHX1	0.99	0.96	0.82	0.00	7
CRABP1	0.92	0.91	0.79	0.00	7
MLLT11	0.64	1.00	0.96	0.00	7
CD24	0.63	1.00	0.97	0.00	7
TMSB10	0.53	1.00	1.00	0.00	7
TFAP2A	0.85	0.90	0.82	0.00	7
NETO2	1.00	0.81	0.68	0.00	7
STMN1	0.50	1.00	0.98	0.00	7
RP11-445F12.1	0.77	0.85	0.76	0.00	7
GAP43	0.50	0.95	0.83	0.00	7
VIM	1.31	1.00	0.82	0.00	8
TTYH1	1.00	0.95	0.64	0.00	8
FGFBP3	0.97	0.90	0.60	0.00	8
SOX2	0.87	0.89	0.55	0.00	8
ZFP36L1	0.80	0.86	0.52	0.00	8
RPS27L	0.81	0.95	0.76	0.00	8
RPL36	0.56	1.00	0.97	0.00	8
ENO1	0.72	0.99	0.93	0.00	8
PLP1	0.98	0.79	0.47	0.00	8
ALDOA	0.66	0.98	0.90	0.00	8
HES6	2.55	1.00	0.71	0.00	9
ASCL1	1.79	0.96	0.63	0.00	9
RGS16	1.42	0.92	0.56	0.00	9
DLL1	1.21	0.87	0.49	0.00	9
BTG1	1.13	1.00	0.94	0.00	9
CKB	1.11	0.99	0.90	0.00	9
VIM	1.04	0.99	0.82	0.00	9
MIAT	1.03	0.99	0.93	0.00	9

Gene	logFC	pct.1	pct.2	p.adj	cluster
GADD45G	0.93	0.81	0.48	0.00	9
RPS27L	0.92	0.96	0.76	0.00	9
BNIP3	1.02	0.98	0.85	0.00	10
ENO1	0.93	0.99	0.93	0.00	10
MIAT	0.91	0.99	0.93	0.00	10
ALDOA	0.84	0.98	0.90	0.00	10
PGK1	0.91	0.97	0.86	0.00	10
CRABP1	1.07	0.93	0.79	0.00	10
NHLH1	1.12	0.80	0.57	0.00	10
GAPDH	0.54	1.00	1.00	0.00	10
TAGLN3	0.88	0.94	0.85	0.00	10
LHX5-AS1	0.90	0.85	0.67	0.00	10
LYPD1	1.37	0.90	0.62	0.00	11
FOXP1	1.35	0.94	0.69	0.00	11
CHMP2B	1.26	0.94	0.64	0.00	11
NTM	1.26	0.99	0.80	0.00	11
RALYL	1.21	0.95	0.63	0.00	11
TFAP2A	1.17	0.98	0.82	0.00	11
LHX1	1.13	1.00	0.82	0.00	11
FOXP2	1.11	0.92	0.67	0.00	11
CA8	0.99	0.78	0.52	0.00	11
RP11-445F12.1	0.87	0.94	0.75	0.00	11
LAMP5	1.35	0.84	0.37	0.00	12
PAX2	1.26	0.84	0.41	0.00	12
ASIC4	0.84	0.82	0.56	0.00	12
NEUROD6	0.95	0.79	0.39	0.00	12
DNER	0.85	0.95	0.70	0.00	12
SERTAD4	0.68	0.89	0.69	0.00	12
GAD2	0.92	0.84	0.62	0.00	12
NEUROD1	0.98	0.79	0.51	0.00	12
GAD1	0.68	0.80	0.52	0.00	12
LRTM1	0.43	0.76	0.55	0.00	12
TRH	1.72	0.87	0.40	0.00	13
SPARC	1.17	0.94	0.32	0.00	13
TPBG	1.04	0.89	0.50	0.00	13
ANXA2	1.00	0.88	0.38	0.00	13
CLU	0.97	0.96	0.51	0.00	13
ZFP36L1	0.96	0.97	0.52	0.00	13
TIMP1	0.92	0.91	0.43	0.00	13
TTYH1	0.89	0.99	0.64	0.00	13
EMX2	0.88	0.87	0.37	0.00	13
VIM	0.85	1.00	0.82	0.00	13
RPL12	0.86	1.00	0.96	0.00	14
RPS6	0.85	1.00	0.97	0.00	14
RPL41	0.74	1.00	0.99	0.00	14
RPS2	0.72	1.00	0.99	0.00	14
RPL36	0.70	1.00	0.97	0.00	14
RPS17	0.70	1.00	0.99	0.00	14
RPS18	0.67	1.00	1.00	0.00	14
RPS12	0.61	1.00	0.98	0.00	14
RPS27	0.57	1.00	0.99	0.00	14
CYP26A1	0.71	0.86	0.48	0.00	14

Gene	logFC	pct.1	pct.2	p.adj	cluster
KIAA0101	1.96	0.95	0.43	0.00	15
TUBA1B	1.86	1.00	0.89	0.00	15
HMGN2	1.80	1.00	0.88	0.00	15
HMGB2	1.60	0.94	0.57	0.00	15
TOP2A	1.47	0.88	0.56	0.00	15
TYMS	1.46	0.93	0.49	0.00	15
H2AFZ	1.40	1.00	0.91	0.00	15
DEK	1.38	0.98	0.68	0.00	15
NUSAP1	1.26	0.89	0.43	0.00	15
MCM7	1.25	0.91	0.53	0.00	15
PEG10	2.53	0.99	0.80	0.00	16
CALB2	2.02	0.92	0.54	0.00	16
RP11-395G23.3	1.06	0.81	0.51	0.00	16
NRN1	1.08	0.86	0.57	0.00	16
PBX3	0.89	0.90	0.74	0.00	16
TMEFF2	0.96	0.76	0.52	0.00	16
VAMP2	0.49	0.99	0.95	0.00	16
UCHL1	0.54	0.98	0.90	0.00	16
BASP1	0.51	0.99	0.96	0.00	16
EN1	0.98	0.66	0.46	0.00	16
CRABP1	1.36	0.96	0.79	0.00	17
NHLH1	1.21	0.92	0.57	0.00	17
ROBO3	1.14	0.87	0.54	0.00	17
TAGLN3	1.08	0.99	0.85	0.00	17
CNTN2	1.02	0.84	0.44	0.00	17
RGMB	1.02	0.89	0.54	0.00	17
TMSB4X	0.62	1.00	1.00	0.00	17
STMN2	0.79	1.00	0.94	0.00	17
KLHL35	1.10	0.87	0.59	0.00	17
THSD7A	0.88	0.91	0.66	0.00	17
NHLH1	1.71	0.93	0.57	0.00	18
TAGLN3	1.48	0.99	0.85	0.00	18
GNG5	1.25	0.93	0.68	0.00	18
HES6	1.29	0.93	0.72	0.00	18
MIAT	0.96	0.99	0.93	0.00	18
RGS16	1.51	0.84	0.57	0.00	18
LMO1	1.06	0.82	0.58	0.00	18
TMSB4X	0.56	1.00	1.00	0.00	18
TCF4	1.00	0.82	0.54	0.00	18
SLC25A6	0.72	0.96	0.90	0.00	18
CYP26B1	0.58	0.95	0.50	0.00	19
CLU	1.40	0.92	0.52	0.00	19
WNT7B	0.78	0.89	0.42	0.00	19
SOX3	0.39	0.97	0.59	0.00	19
FGFBP3	1.16	0.96	0.60	0.00	19
GPM6B	1.22	0.96	0.75	0.00	19
TTYH1	1.39	0.93	0.64	0.00	19
RP3-395M20.12	0.28	0.92	0.50	0.00	19
PTN	1.51	0.93	0.74	0.00	19
NTRK2	1.21	0.85	0.52	0.00	19
UBE2C	3.10	0.98	0.46	0.00	20
PTTG1	2.68	0.99	0.49	0.00	20

Gene	logFC	pct.1	pct.2	p.adj	cluster
HMGB2	2.62	0.99	0.58	0.00	20
CENPF	2.47	0.97	0.50	0.00	20
CDC20	2.16	0.97	0.42	0.00	20
NUSAP1	2.10	0.97	0.44	0.00	20
BIRC5	2.10	0.97	0.46	0.00	20
KIF20A	0.63	0.71	0.04	0.00	20
HMGN2	1.91	1.00	0.88	0.00	20
CCNB2	1.99	0.95	0.53	0.00	20
NRN1	1.71	0.96	0.58	0.00	21
POU2F2	1.54	0.95	0.65	0.00	21
MAB21L1	1.46	0.90	0.54	0.00	21
RPRM	1.99	0.88	0.54	0.00	21
GAP43	1.05	1.00	0.83	0.00	21
KCNIP4	1.27	0.82	0.39	0.00	21
BASP1	0.82	1.00	0.96	0.00	21
ZFHX3	1.21	0.90	0.58	0.00	21
DOK5	1.23	0.83	0.46	0.00	21
STMN2	0.81	1.00	0.94	0.00	21
EFCAB1	0.99	0.94	0.27	0.00	22
CAPS	1.76	1.00	0.36	0.00	22
PIFO	1.18	1.00	0.32	0.00	22
C9orf116	1.42	1.00	0.38	0.00	22
C5orf49	1.10	1.00	0.47	0.00	22
RSPH1	1.34	0.98	0.33	0.00	22
C1orf194	1.16	0.99	0.41	0.00	22
FAM183A	1.15	0.98	0.44	0.00	22
DYNLRB2	0.99	0.97	0.38	0.00	22
ZMYND10	1.04	0.97	0.40	0.00	22

Supplementary Table 3.2: Top 10 DE Genes in each direction from each timepoint in *TSC2*$^{c/-}$ experiments

Day 50 vs Day 120

Gene	logFC	pct.1	pct.2	p.adj
IGFBP5	-1.67	0.08	0.40	0.00
CLU	-1.66	0.27	0.69	0.00
NEUROD1	-1.48	0.07	0.34	0.00
NFIB	-1.41	0.10	0.54	0.00
PTGDS	-1.37	0.07	0.39	0.00
SPARCL1	-1.33	0.03	0.25	0.00
B2M	-1.20	0.22	0.58	0.00
CST3	-1.18	0.39	0.58	0.00
MGP	-1.13	0.00	0.22	0.00
PTN	-1.10	0.52	0.71	0.00
PEG10	0.67	0.50	0.52	0.00
CD24	0.70	0.91	0.75	0.00
FDFT1	0.70	0.54	0.33	0.00
LHX1	0.73	0.44	0.31	0.00
TFAP2A	0.75	0.47	0.21	0.00
SOX11	0.78	0.74	0.63	0.00
MIAT	0.79	0.81	0.57	0.00
TMSB15A	0.79	0.74	0.49	0.00
HES6	0.81	0.40	0.37	0.00
CRABP1	1.29	0.54	0.28	0.00

Day 120 vs Day 220

Gene	logFC	pct.1	pct.2	p.adj
IGFBP7	-1.80	0.09	0.23	0.00
JUND	-1.64	0.25	0.90	0.00
MTRNR2L12	-1.61	0.15	0.75	0.00
CD81	-1.55	0.19	0.86	0.00
GNAS	-1.44	0.69	0.94	0.00
CP	-1.16	0.02	0.13	0.00
S100B	-1.07	0.18	0.32	0.00
VEGFA	-1.07	0.23	0.62	0.00
FOS	-1.06	0.20	0.52	0.00
CST3	-1.04	0.58	0.60	0.04
MLLT11	0.80	0.86	0.70	0.00
RPL17	0.86	0.70	0.53	0.00
RPLP2	0.87	0.96	0.88	0.00
RPL7	0.91	0.94	0.84	0.00
AC090498.1	0.92	0.61	0.36	0.00
RPL36A	1.00	0.85	0.71	0.00
RPS20	1.14	0.86	0.65	0.00
RPL13A	1.31	0.97	0.83	0.00
RPL31	1.40	0.93	0.76	0.00
RPS17	1.70	0.96	0.76	0.00

Day 50 vs Day 220

Gene	logFC	pct.1	pct.2	p.adj
CLU	-2.43	0.27	0.71	0.00
IGFBP7	-2.28	0.01	0.23	0.00
PTGDS	-2.24	0.07	0.49	0.00
IGFBP5	-2.24	0.08	0.54	0.00
CST3	-2.21	0.39	0.60	0.00
SPARCL1	-2.04	0.03	0.34	0.00
TTR	-1.84	0.01	0.12	0.00
MTRNR2L12	-1.82	0.03	0.75	0.00
CD81	-1.78	0.07	0.86	0.00
JUND	-1.76	0.14	0.90	0.00
MIAT	1.19	0.81	0.48	0.00
TUBB	1.19	0.98	0.88	0.00
TFAP2A	1.24	0.47	0.13	0.00
TMSB15A	1.27	0.74	0.36	0.00
RPS20	1.27	0.90	0.65	0.00
CD24	1.40	0.91	0.60	0.00
RPL31	1.43	0.95	0.76	0.00
CRABP1	1.58	0.54	0.13	0.00
RPL13A	1.60	0.99	0.83	0.00
RPS17	1.87	0.97	0.76	0.00

Supplementary Table 3.3: Cluster Markers of combined Primary Tissue and Spheroids

Cluster markers when combined with Bhaduri et al, 2020

gene	logFC	pct.1	pct.2	p.adj	cluster
MT-ND3	0.77	0.95	0.96	0.00	0
RPS27	0.66	1.00	1.00	0.00	0
RPL36	0.66	0.97	0.98	0.00	0
SOX11	0.65	0.72	0.82	0.00	0
TMSB10	0.65	1.00	0.99	0.00	0
RPL41	0.62	0.97	0.99	0.00	0
MT-CO3	0.61	0.99	0.99	0.00	0
MT-CO2	0.58	0.97	0.97	0.00	0
MT-CO1	0.57	0.98	0.98	0.00	0
TMSB4X	0.56	1.00	1.00	0.00	0
PLS3	1.41	0.31	0.17	0.00	1
RBP1	1.25	0.58	0.38	0.00	1
SOX4	0.56	0.97	0.92	0.00	1
DCX	0.54	0.67	0.66	0.00	1
TCF4	0.47	0.61	0.68	0.00	1
SOX11	0.45	0.79	0.81	0.00	1
H3F3B	0.40	0.95	0.94	0.00	1
TMSB10	0.35	1.00	0.99	0.00	1
TMSB4X	0.34	1.00	1.00	0.00	1
FTL	0.34	0.96	0.97	0.00	1
BCYRN1	0.65	0.28	0.09	0.00	2
PGK1	0.42	0.77	0.33	0.00	2
LHX1	0.42	0.41	0.02	0.00	2
FAM162A	0.40	0.43	0.12	0.00	2
RP11-445F12.1	0.36	0.36	0.02	0.00	2
BNIP3	0.33	0.68	0.21	0.00	2
CALB2	0.32	0.32	0.08	0.00	2
CALY	0.31	0.25	0.02	0.00	2
PLCG2	0.30	0.29	0.07	0.00	2
LYPD1	0.27	0.32	0.06	0.00	2
ZBTB18	0.62	0.72	0.54	0.00	3
MEF2C	0.54	0.83	0.63	0.00	3
CSRP2	0.44	0.79	0.65	0.00	3
FABP7	0.42	0.96	0.83	0.00	3
STMN4	0.41	0.72	0.62	0.00	3
UCHL1	0.38	0.76	0.66	0.00	3
STMN2	0.38	1.00	0.87	0.00	3
GAP43	0.37	0.76	0.63	0.00	3
RTN1	0.30	0.80	0.70	0.00	3

Cluster markers when combined with Polioudakis al, 2019

gene	logFC	pct.1	pct.2	p.adj	cluster
SLA	0.85	0.79	0.73	0.00	0
NEUROD6	0.70	0.83	0.78	0.00	0
SOX11	0.52	0.92	0.87	0.00	0
STMN2	0.43	0.97	0.81	0.00	0
NEUROD2	0.66	0.72	0.73	0.00	0
ZBTB18	0.69	0.69	0.72	0.00	0
CD24	0.41	0.66	0.69	0.00	0
NFIB	0.39	0.74	0.82	0.00	0
GAP43	0.40	0.57	0.60	0.00	0
EPHA5	0.25	0.40	0.61	0.00	0
ENC1	1.10	0.93	0.73	0.00	1
EZR	0.90	0.83	0.71	0.00	1
RASGEF1B	0.79	0.33	0.26	0.00	1
NHLH1	0.75	0.28	0.15	0.00	1
SOX4	0.75	0.99	0.86	0.00	1
SDCBP	0.73	0.55	0.44	0.00	1
HES6	0.69	0.62	0.41	0.00	1
PRDX1	0.66	0.54	0.43	0.00	1
MEIS2	0.62	0.81	0.72	0.00	1
NEUROD6	0.60	0.85	0.77	0.00	1
SYT4	1.12	0.77	0.45	0.00	2
NEFM	0.90	0.64	0.37	0.00	2
DOK5	0.87	0.61	0.43	0.00	2
ARPP21	0.73	0.77	0.58	0.00	2
ZBTB18	0.72	0.87	0.70	0.00	2
GAP43	0.71	0.87	0.57	0.00	2
NEUROD2	0.71	0.90	0.71	0.00	2
STMN2	0.70	1.00	0.81	0.00	2
MEF2C	0.66	0.80	0.58	0.00	2
UCHL1	0.64	0.89	0.65	0.00	2
BNIP3	0.92	0.91	0.34	0.00	3
DDIT4	0.89	0.73	0.21	0.00	3
PGK1	0.84	0.93	0.38	0.00	3
IGFBP2	0.83	0.82	0.34	0.00	3
ENO1	0.68	0.96	0.46	0.00	3
ALDOA	0.55	0.93	0.39	0.00	3
FAM162A	0.74	0.67	0.19	0.00	3
ATF5	0.26	0.29	0.14	0.00	3
LHX5	0.32	0.26	0.06	0.00	3

BEX1	0.28	0.76	0.71	0.00	3	NXPH4	0.28	0.33	0.13	0.00	3
CLU	1.74	0.96	0.18	0.00	4	STMN2	0.38	1.00	0.81	0.00	4
GPX3	1.37	0.70	0.10	0.00	4	SYT1	0.26	0.92	0.55	0.00	4
ZFP36L1	1.33	0.83	0.17	0.00	4	BEX1	0.26	0.92	0.66	0.00	4
BCAN	1.32	0.68	0.11	0.00	4	HS6ST3	0.34	0.59	0.23	0.00	4
PON2	1.31	0.72	0.12	0.00	4	NTM	0.35	0.70	0.44	0.00	4
SLC1A3	1.31	0.74	0.15	0.00	4	CELF4	0.43	0.59	0.25	0.00	4
HES1	1.30	0.87	0.19	0.00	4	RALYL	0.48	0.50	0.20	0.00	4
HOPX	1.27	0.68	0.15	0.00	4	LHX1	0.40	0.47	0.13	0.00	4
PSAT1	1.24	0.73	0.11	0.00	4	BEX5	0.25	0.40	0.22	0.00	4
PEA15	1.24	0.86	0.22	0.00	4	TFAP2A	0.28	0.45	0.11	0.00	4
CRYM	1.38	0.42	0.24	0.00	5	EPHA5	0.32	0.23	0.61	0.00	5
RPL36A	1.10	0.89	0.61	0.00	5	SOX4	0.61	0.81	0.88	0.00	5
NEUROD6	1.04	0.85	0.57	0.00	5	BHLHE22	0.27	0.23	0.56	0.00	5
ID2	0.97	0.64	0.46	0.00	5	SEMA3C	0.42	0.25	0.59	0.00	5
NFIB	0.92	0.84	0.63	0.00	5	CLMP	0.44	0.28	0.62	0.00	5
SNAP25	0.89	0.42	0.33	0.00	5	ELAVL4	0.29	0.26	0.61	0.00	5
RAB3A	0.85	0.38	0.31	0.00	5	PENK	0.27	0.18	0.48	0.00	5
NTM	0.83	0.51	0.41	0.00	5	THBS1	0.38	0.15	0.42	0.00	5
ARL6IP1	0.71	0.55	0.49	0.00	5	CASC15	0.44	0.19	0.48	0.00	5
SLIRP	0.64	0.50	0.48	0.00	5	GOLIM4	0.36	0.22	0.51	0.00	5
DOK5	1.11	0.98	0.39	0.00	6	DCX	1.14	0.82	0.77	0.00	6
NEFM	1.08	0.83	0.26	0.00	6	TCF4	0.89	0.81	0.83	0.00	6
NEFL	1.04	0.58	0.14	0.00	6	SOX4	0.76	0.91	0.87	0.00	6
ARPP21	0.86	0.89	0.38	0.00	6	GAD2	1.39	0.30	0.19	0.00	6
TENM2	0.86	0.43	0.12	0.00	6	KIF20B	0.30	0.10	0.51	0.00	6
RUNX1T1	0.86	0.89	0.35	0.00	6	NREP	0.59	0.75	0.79	0.00	6
ADCY1	0.79	0.76	0.31	0.00	6	TMSB10	0.34	0.95	0.95	0.00	6
BHLHE22	0.78	0.59	0.24	0.00	6	PLS3	1.73	0.41	0.37	0.00	6
RPS2	0.77	0.97	0.54	0.00	6	PLPP5	0.34	0.16	0.52	0.00	6
LPL	0.75	0.44	0.18	0.00	6	H3F3B	0.48	0.78	0.86	0.00	6
CRYM	1.56	0.85	0.22	0.00	7	HES6	1.62	0.91	0.40	0.00	7
KCTD12	1.14	0.62	0.17	0.00	7	PPP1R17	1.23	0.92	0.40	0.00	7
SYT6	1.11	0.47	0.15	0.00	7	SSTR2	0.99	0.82	0.42	0.00	7
ZNF385D	1.07	0.45	0.10	0.00	7	CCND2	0.88	0.96	0.73	0.00	7
TRPM3	1.05	0.41	0.07	0.00	7	PRDX1	0.75	0.76	0.42	0.00	7
LMO3	1.01	0.78	0.34	0.00	7	GADD45G	0.70	0.78	0.39	0.00	7
MGLL	0.99	0.55	0.21	0.00	7	HES5	0.68	0.70	0.16	0.00	7
ARPP21	0.90	0.85	0.38	0.00	7	NEUROD4	0.66	0.68	0.18	0.00	7
SSTR2	0.88	0.53	0.22	0.00	7	TMEM158	0.61	0.81	0.40	0.00	7
PCP4	0.84	0.26	0.09	0.00	7	SOX4	0.59	0.99	0.87	0.00	7
PPP1R17	0.98	0.29	0.17	0.00	8	HIST1H4C	2.38	0.89	0.71	0.00	8
MDK	0.73	0.55	0.38	0.00	8	HIST1H1D	2.30	0.77	0.50	0.00	8
FOS	0.69	0.71	0.48	0.00	8	HMGB2	2.12	0.93	0.31	0.00	8
PRDX1	0.57	0.70	0.62	0.00	8	TOP2A	1.82	0.81	0.44	0.00	8
MEIS2	0.50	0.64	0.55	0.00	8	MKI67	1.80	0.77	0.37	0.00	8
SOX4	0.36	0.97	0.92	0.00	8	KIAA0101	1.76	0.73	0.12	0.00	8

SOX11	0.32	0.83	0.81	0.00	8	HMGN2	1.72	0.92	0.49	0.00	8
MT-CO3	0.29	1.00	0.99	0.00	8	SMC4	1.70	0.88	0.55	0.00	8
MT-CO1	0.29	1.00	0.98	0.00	8	CENPU	1.69	0.75	0.39	0.00	8
MT-ND3	0.29	0.97	0.95	0.00	8	HELLS	1.61	0.78	0.36	0.00	8
LY6H	1.30	0.77	0.16	0.00	9	PCLO	0.90	0.83	0.54	0.00	9
RPRM	1.23	0.81	0.21	0.00	9	ARPP21	0.89	0.88	0.59	0.00	9
RAC3	1.09	0.72	0.18	0.00	9	GRIN2B	0.83	0.75	0.37	0.00	9
TTC9B	1.07	0.53	0.10	0.00	9	MEF2C	0.82	0.91	0.58	0.00	9
HES6	1.06	0.65	0.14	0.00	9	FLRT2	0.68	0.80	0.38	0.00	9
GADD45GIP1	1.04	0.69	0.20	0.00	9	LPL	0.57	0.75	0.39	0.00	9
MAP1LC3A	1.04	0.62	0.14	0.00	9	RSPO3	0.28	0.68	0.21	0.00	9
RSPO3	1.03	0.51	0.16	0.00	9	NECAB1	0.27	0.73	0.25	0.00	9
PRELID1	1.01	0.57	0.15	0.00	9	NBEA	0.80	0.86	0.60	0.00	9
VSTM2L	1.00	0.57	0.14	0.00	9	RUNX1T1	0.75	0.83	0.46	0.00	9
NEFM	1.08	0.76	0.26	0.00	10	PTN	2.51	1.00	0.48	0.00	10
LRRN3	1.01	0.52	0.15	0.00	10	PEA15	2.03	0.98	0.43	0.00	10
INHBA	0.90	0.32	0.16	0.00	10	VIM	1.89	0.99	0.38	0.00	10
GRIN2B	0.86	0.60	0.28	0.00	10	PTPRZ1	1.87	0.99	0.69	0.00	10
INA	0.85	0.59	0.24	0.00	10	SLC1A3	1.86	0.95	0.38	0.00	10
NR4A2	0.84	0.34	0.15	0.00	10	SFRP1	1.84	0.99	0.51	0.00	10
RORB	0.80	0.40	0.21	0.00	10	FABP7	1.83	1.00	0.75	0.00	10
NBEA	0.79	0.70	0.35	0.00	10	ID4	1.74	0.94	0.27	0.00	10
NEUROD6	0.78	0.98	0.57	0.00	10	HES1	1.70	0.94	0.33	0.00	10
KCNQ1OT1	0.77	0.60	0.27	0.00	10	NRG1	1.68	0.92	0.33	0.00	10
PDGFRA	1.74	0.36	0.06	0.00	11	NEFL	1.01	0.75	0.15	0.00	11
S100B	1.67	0.40	0.07	0.00	11	MEF2C	0.89	0.99	0.58	0.00	11
SCRG1	1.66	0.52	0.12	0.00	11	NEFM	0.88	0.94	0.37	0.00	11
BCAN	1.56	0.45	0.12	0.00	11	GAP43	0.68	0.98	0.58	0.00	11
MT3	1.54	0.44	0.12	0.00	11	ARPP21	0.67	0.98	0.58	0.00	11
MT2A	1.35	0.42	0.19	0.00	11	VSNL1	0.64	0.75	0.23	0.00	11
PTN	1.33	0.83	0.41	0.00	11	UCHL1	0.64	0.99	0.66	0.00	11
PTPRZ1	1.32	0.94	0.56	0.00	11	SCN2A	0.63	0.89	0.39	0.00	11
HOPX	1.30	0.34	0.17	0.00	11	SERPINI1	0.60	0.79	0.27	0.00	11
DBI	1.29	0.92	0.53	0.00	11	STMN2	0.58	1.00	0.82	0.00	11
CTTNBP2	0.98	0.56	0.30	0.00	12	LMO3	2.73	0.86	0.49	0.00	12
ENC1	0.94	0.89	0.49	0.00	12	CRYM	2.20	0.68	0.34	0.00	12
ARPP21	0.84	0.69	0.39	0.00	12	KCTD12	1.50	0.51	0.30	0.00	12
RBFOX1	0.82	0.47	0.28	0.00	12	CELF4	1.35	0.56	0.27	0.00	12
VCAN	0.81	0.75	0.43	0.00	12	ATP1B1	1.27	0.64	0.36	0.00	12
SLA	0.77	0.78	0.46	0.00	12	ZNF385D	1.27	0.41	0.19	0.00	12
SYT4	0.75	0.57	0.33	0.00	12	MEF2C	1.26	0.88	0.59	0.00	12
NEUROD2	0.75	0.69	0.42	0.00	12	TMEM178A	1.18	0.41	0.20	0.00	12
TUBB2A	0.72	0.98	0.61	0.00	12	VCAN	1.10	0.78	0.71	0.00	12
ACAT2	0.64	0.61	0.41	0.00	12	SYT1	1.09	0.78	0.57	0.00	12
KIAA0101	1.78	0.76	0.17	0.00	13	VCAN	1.11	0.94	0.70	0.00	13
HMGB2	1.66	0.89	0.24	0.00	13	CSRP2	1.06	0.86	0.58	0.00	13
NUSAP1	1.58	0.66	0.16	0.00	13	CTTNBP2	1.02	0.74	0.60	0.00	13

CENPF	1.46	0.67	0.23	0.00	13	CLMP	0.97	0.75	0.59	0.00	13
TOP2A	1.46	0.61	0.18	0.00	13	SLA	0.96	0.95	0.73	0.00	13
PTTG1	1.32	0.57	0.16	0.00	13	GAP43	0.94	0.90	0.58	0.00	13
PCNA	1.30	0.62	0.20	0.00	13	BCL11A	0.88	0.81	0.64	0.00	13
UBE2C	1.24	0.48	0.14	0.00	13	ZBTB18	0.86	0.90	0.71	0.00	13
CDK1	1.18	0.47	0.12	0.00	13	STMN2	0.85	1.00	0.82	0.00	13
BIRC5	1.16	0.45	0.11	0.00	13	MAPT	0.77	0.86	0.61	0.00	13
PPP1R17	1.21	0.42	0.16	0.00	14	VIM	1.39	0.93	0.39	0.00	14
NRN1	1.07	0.48	0.14	0.00	14	FABP5	1.33	0.87	0.49	0.00	14
SSTR2	0.98	0.47	0.23	0.00	14	HES1	1.21	0.89	0.34	0.00	14
HES6	0.80	0.34	0.15	0.00	14	PEA15	1.20	0.83	0.44	0.00	14
RPS2	0.79	0.98	0.55	0.00	14	ID4	1.17	0.81	0.28	0.00	14
ENC1	0.79	0.90	0.49	0.00	14	SFRP1	1.15	0.91	0.51	0.00	14
EZR	0.79	0.66	0.36	0.00	14	TTYH1	1.02	0.70	0.20	0.00	14
CASC15	0.74	0.41	0.23	0.00	14	SLC1A3	1.01	0.85	0.39	0.00	14
FTH1	0.69	0.98	0.61	0.00	14	FOS	0.97	0.93	0.58	0.00	14
CNR1	0.68	0.37	0.18	0.00	14	SOX2	0.96	0.84	0.49	0.00	14
VSTM2L	0.94	0.50	0.15	0.00	15	TRIB3	0.30	0.26	0.07	0.00	15
SCG2	0.86	0.38	0.12	0.00	15	SNHG21	0.33	0.28	0.09	0.00	15
FGF12	0.81	0.63	0.28	0.00	15	VGF	0.29	0.27	0.07	0.00	15
SNCA	0.73	0.55	0.25	0.00	15	RGS16	0.30	0.29	0.17	0.00	15
SYT4	0.71	0.71	0.33	0.00	15	PIM3	0.28	0.30	0.14	0.00	15
FABP3	0.71	0.34	0.16	0.00	15	ATF3	0.38	0.30	0.13	0.00	15
LDB2	0.63	0.48	0.27	0.00	15	EGLN3	0.36	0.26	0.12	0.00	15
GNAL	0.63	0.34	0.14	0.00	15	HSPA1A	0.52	0.34	0.35	0.00	15
CACNA2D1	0.62	0.39	0.18	0.00	15	SRPRA	0.28	0.30	0.21	0.00	15
GNAI1	0.61	0.49	0.25	0.00	15	HSPA1B	0.47	0.82	0.36	0.00	15
RPRM	1.40	0.87	0.21	0.00	16	VIM	1.55	0.89	0.40	0.00	16
ARPP21	1.06	0.95	0.39	0.00	16	VEGFA	1.44	0.80	0.21	0.00	16
PCLO	0.96	0.82	0.33	0.00	16	PTPRZ1	1.39	0.98	0.69	0.00	16
INHBA	0.90	0.45	0.15	0.00	16	SLC1A3	1.22	0.88	0.40	0.00	16
DOK5	0.90	0.93	0.40	0.00	16	CLU	1.09	0.89	0.24	0.00	16
NEFL	0.89	0.49	0.16	0.00	16	TNC	1.07	0.80	0.12	0.00	16
LRRC4C	0.89	0.54	0.15	0.00	16	SFRP1	1.02	0.98	0.51	0.00	16
NEFM	0.88	0.71	0.27	0.00	16	NRG1	1.01	0.98	0.34	0.00	16
PRKCB	0.84	0.46	0.12	0.00	16	AKAP12	0.87	0.98	0.53	0.00	16
LSAMP	0.84	0.60	0.19	0.00	16	PEA15	0.86	0.93	0.44	0.00	16
NEAT1	0.89	0.64	0.11	0.00	17	MEF2C	2.08	0.99	0.59	0.00	17
VIM	0.85	0.81	0.26	0.00	17	NEFM	1.94	0.92	0.39	0.00	17
DDIT4	0.78	0.71	0.16	0.00	17	NEFL	1.92	0.74	0.16	0.00	17
CRYAB	0.76	0.67	0.12	0.00	17	FABP7	1.26	0.99	0.76	0.00	17
RGS16	0.72	0.71	0.08	0.00	17	GAP43	1.14	0.92	0.59	0.00	17
HSPB1	0.67	0.69	0.14	0.00	17	NEUROD6	1.02	0.96	0.78	0.00	17
DLK1	0.65	0.27	0.04	0.00	17	UCHL1	0.95	0.91	0.66	0.00	17
HSPA1A	0.59	0.95	0.32	0.00	17	STMN2	0.90	1.00	0.82	0.00	17
GADD45B	0.52	0.92	0.10	0.00	17	MAP1B	0.78	1.00	0.96	0.00	17
ADM	0.51	0.33	0.03	0.00	17	STMN1	0.62	1.00	0.96	0.00	17

SST	1.41	0.40	0.17	0.00	18	IGFBP7	2.51	0.83	0.23	0.00	18
DLX2	1.18	0.35	0.14	0.00	18	SPARC	1.56	0.96	0.26	0.00	18
CXCR4	1.14	0.44	0.15	0.00	18	FOS	1.47	1.00	0.59	0.00	18
PLS3	1.11	0.46	0.17	0.00	18	COL4A1	1.21	0.86	0.19	0.00	18
GAD2	1.06	0.29	0.05	0.00	18	VIM	1.15	0.99	0.40	0.00	18
NXPH1	1.02	0.27	0.06	0.00	18	ZFP36L1	1.09	0.95	0.23	0.00	18
CALB2	1.01	0.26	0.09	0.00	18	IFITM3	1.07	0.78	0.16	0.00	18
GAD1	0.98	0.31	0.06	0.00	18	PTN	1.03	0.99	0.49	0.00	18
CELF4	0.88	0.48	0.21	0.00	18	ANXA2	1.03	0.84	0.12	0.00	18
FTH1	0.74	0.92	0.61	0.00	18	HES1	1.02	0.99	0.34	0.00	18
HSPB1	1.79	0.90	0.14	0.00	19	CENPF	3.47	1.00	0.52	0.00	19
HES1	1.66	0.93	0.21	0.00	19	TOP2A	3.43	0.99	0.45	0.00	19
VIM	1.64	0.98	0.26	0.00	19	MKI67	3.13	0.99	0.38	0.00	19
SOX2	1.58	0.93	0.21	0.00	19	HMGB2	3.02	1.00	0.33	0.00	19
TTYH1	1.52	0.84	0.12	0.00	19	ASPM	2.99	0.97	0.32	0.00	19
EMX2	1.52	0.93	0.23	0.00	19	NUSAP1	2.85	0.98	0.30	0.00	19
SOX3	1.50	0.71	0.06	0.00	19	UBE2C	2.70	0.92	0.16	0.00	19
HSPA1B	1.48	0.88	0.20	0.00	19	PTTG1	2.69	0.96	0.16	0.00	19
HES4	1.47	0.68	0.07	0.00	19	TPX2	2.68	0.96	0.26	0.00	19
ID4	1.47	0.79	0.09	0.00	19	CENPE	2.65	0.94	0.38	0.00	19
DLK1	1.82	0.87	0.03	0.00	20	EGR1	2.66	0.96	0.50	0.00	20
CRABP2	1.58	0.88	0.05	0.00	20	FOS	2.62	0.98	0.59	0.00	20
ID3	1.58	0.77	0.06	0.00	20	CYR61	2.59	0.83	0.20	0.00	20
CTGF	1.47	0.78	0.07	0.00	20	HES1	2.52	0.94	0.35	0.00	20
CYR61	1.46	0.88	0.13	0.00	20	VIM	2.10	0.98	0.40	0.00	20
HMGA1	1.46	0.96	0.16	0.00	20	ID4	2.19	0.85	0.29	0.00	20
MEST	1.44	0.90	0.13	0.00	20	JUN	2.03	0.93	0.55	0.00	20
MGST1	1.35	0.69	0.06	0.00	20	PTN	1.19	0.94	0.50	0.00	20
GPC3	1.31	0.74	0.04	0.00	20	SFRP1	1.55	0.86	0.52	0.00	20
HSPB1	1.24	0.91	0.14	0.00	20	SPARC	1.79	0.72	0.27	0.00	20
NTS	1.52	0.52	0.08	0.00	21	OLIG1	2.29	0.83	0.08	0.00	21
HPCA	1.01	0.62	0.18	0.00	21	OLIG2	1.46	0.61	0.06	0.00	21
NEUROD1	0.88	0.45	0.11	0.00	21	BCAN	2.09	0.86	0.21	0.00	21
CLSTN2	0.87	0.37	0.08	0.00	21	PDGFRA	2.28	0.75	0.08	0.00	21
DCC	0.86	0.44	0.10	0.00	21	PTPRZ1	1.64	0.99	0.70	0.00	21
EPHA4	0.84	0.49	0.16	0.00	21	PMP2	2.25	0.74	0.19	0.00	21
CRYAB	0.80	0.48	0.13	0.00	21	DBI	1.57	0.90	0.36	0.00	21
NTF3	0.74	0.27	0.07	0.00	21	EGR1	1.62	0.84	0.50	0.00	21
SNCA	0.71	0.65	0.25	0.00	21	SCRG1	2.03	0.73	0.12	0.00	21
SSTR2	0.69	0.56	0.23	0.00	21	SOX2	1.25	0.85	0.50	0.00	21
NR2F1	0.89	0.55	0.30	0.00	22	IGFBP7	3.16	0.82	0.24	0.00	22
MEIS2	0.81	0.87	0.55	0.00	22	CLDN5	3.32	0.81	0.22	0.00	22
SLA	0.72	0.66	0.47	0.00	22	ITM2A	3.54	0.83	0.34	0.00	22
NEUROD6	0.61	0.82	0.58	0.00	22	ADGRL4	1.80	0.37	0.06	0.00	22
NFIB	0.59	0.88	0.64	0.00	22	GNG11	2.62	0.60	0.17	0.00	22
PRDX1	0.58	0.80	0.62	0.00	22	PTRF	1.94	0.43	0.08	0.00	22
MT-ND1	0.34	0.99	0.88	0.00	22	APCDD1	2.22	0.49	0.11	0.00	22

SOX11	0.34	0.97	0.81	0.00	22
TPT1	0.33	0.97	0.84	0.00	22
MLLT11	0.33	0.96	0.82	0.00	22
HES1	1.83	0.71	0.22	0.00	23
EMX2	1.72	0.68	0.24	0.00	23
KIAA0101	1.44	0.44	0.18	0.00	23
PTN	1.42	0.89	0.42	0.00	23
RPS27L	1.07	0.67	0.38	0.00	23
SDCBP	0.99	0.65	0.42	0.00	23
HMGB2	0.97	0.46	0.25	0.00	23
CNN3	0.91	0.60	0.40	0.00	23
MDK	0.86	0.60	0.38	0.00	23
HMGN3	0.86	0.74	0.54	0.00	23
CRYM	1.61	0.84	0.24	0.00	24
PAPPA2	1.28	0.36	0.10	0.00	24
SEMA3E	1.17	0.38	0.12	0.00	24
TRPM3	1.13	0.38	0.08	0.00	24
MGLL	1.08	0.51	0.22	0.00	24
AC004158.3	1.03	0.64	0.30	0.00	24
B3GALT2	1.00	0.48	0.20	0.00	24
KCTD12	1.00	0.46	0.18	0.00	24
LMO3	1.00	0.68	0.35	0.00	24
GRIN2B	0.97	0.62	0.29	0.00	24
PPP1R1B	1.51	0.68	0.13	0.00	25
TTC9B	1.28	0.67	0.11	0.00	25
CRYM	1.16	0.78	0.24	0.00	25
LY6H	1.07	0.71	0.18	0.00	25
CYP26A1	1.05	0.37	0.09	0.00	25
SYT6	1.03	0.48	0.16	0.00	25
KCTD12	1.00	0.63	0.18	0.00	25
LMO3	1.00	0.94	0.35	0.00	25
IGFBP5	0.98	0.51	0.15	0.00	25
ARPP21	0.93	0.93	0.40	0.00	25
CNTNAP2	1.28	0.77	0.13	0.00	26
NHLH1	1.27	0.57	0.04	0.00	26
NEUROD1	1.12	0.66	0.11	0.00	26
THSD7A	0.98	0.60	0.12	0.00	26
ODC1	0.95	0.73	0.18	0.00	26
NRN1	0.94	0.68	0.14	0.00	26
HEY1	0.89	0.55	0.13	0.00	26
HSPA1B	0.88	0.78	0.21	0.00	26
HSPB1	0.88	0.67	0.15	0.00	26
PHLDA1	0.87	0.60	0.14	0.00	26
UBE2C	2.17	0.94	0.14	0.00	27
TOP2A	2.16	0.95	0.19	0.00	27
PTTG1	2.14	0.98	0.17	0.00	27
NUSAP1	2.12	0.96	0.16	0.00	27
SPARC	2.33	0.64	0.28	0.00	22
ARHGAP29	2.43	0.49	0.12	0.00	22
SLC2A1	2.03	0.46	0.12	0.00	22
ITIH5	2.70	0.94	0.05	0.00	23
FOXS1	1.19	0.75	0.03	0.00	23
CLDN7	0.52	0.59	0.02	0.00	23
BGN	2.06	0.85	0.07	0.00	23
OLFML3	1.74	0.83	0.05	0.00	23
EDNRA	1.99	0.88	0.07	0.00	23
PRELP	1.36	0.78	0.02	0.00	23
TFPI	2.39	0.97	0.19	0.00	23
PLXDC1	2.18	0.91	0.09	0.00	23
RGS5	3.26	0.99	0.16	0.00	23
TCTEX1D1	0.76	0.94	0.01	0.00	24
SPAG6	1.03	0.95	0.01	0.00	24
OLFML3	0.28	1.00	0.05	0.00	24
GRAMD3	1.13	0.90	0.06	0.00	24
EFCAB1	1.14	0.96	0.11	0.00	24
MORN5	0.89	0.95	0.01	0.00	24
DYNLRB2	1.28	0.98	0.04	0.00	24
PIFO	1.30	1.00	0.04	0.00	24
ZMYND10	1.10	0.97	0.05	0.00	24
PMAIP1	0.41	1.00	0.04	0.00	24
GAD1	1.96	0.77	0.15	0.00	25
CELF4	1.89	0.77	0.28	0.00	25
RTN1	0.82	0.99	0.76	0.00	25
NRXN3	1.13	0.52	0.12	0.00	25
SYT1	1.11	0.91	0.57	0.00	25
SCN9A	1.77	0.68	0.32	0.00	25
VSTM2A	1.35	0.51	0.13	0.00	25
ATP1B1	1.20	0.74	0.37	0.00	25
CHGB	1.26	0.74	0.41	0.00	25
XKR4	1.22	0.49	0.15	0.00	25

CENPF	2.04	0.95	0.23	0.00	27
CCNB2	2.00	0.86	0.12	0.00	27
CCNB1	1.98	0.81	0.10	0.00	27
BIRC5	1.91	0.89	0.11	0.00	27
CDK1	1.89	0.83	0.12	0.00	27
ASPM	1.87	0.77	0.12	0.00	27
SPP1	2.85	0.85	0.14	0.00	28
APOC1	2.49	0.68	0.14	0.00	28
S100A11	2.31	0.61	0.07	0.00	28
RGS10	2.28	0.58	0.10	0.00	28
CD68	1.91	0.43	0.10	0.00	28
FCGRT	1.86	0.42	0.08	0.00	28
B2M	1.70	0.74	0.27	0.00	28
ARPC1B	1.69	0.38	0.10	0.00	28
SAT1	1.56	0.68	0.29	0.00	28
NPC2	1.50	0.42	0.15	0.00	28
LUM	2.32	0.99	0.03	0.00	29
CRABP2	2.10	0.99	0.05	0.00	29
CTGF	2.01	0.97	0.08	0.00	29
CYR61	1.76	0.97	0.14	0.00	29
CRABP1	1.75	0.92	0.06	0.00	29
ID3	1.60	0.88	0.07	0.00	29
GPC3	1.57	0.87	0.04	0.00	29
HMGA1	1.53	0.99	0.17	0.00	29
FRZB	1.49	0.87	0.09	0.00	29
TPM1	1.46	0.99	0.21	0.00	29
FN1	2.47	0.89	0.07	0.00	30
NDUFA4L2	2.32	0.72	0.07	0.00	30
IFITM3	2.08	0.90	0.11	0.00	30
SPARC	2.05	0.88	0.11	0.00	30
COL4A2	1.94	0.80	0.08	0.00	30
ITM2A	1.93	0.66	0.13	0.00	30
GNG11	1.90	0.80	0.06	0.00	30
S100A11	1.77	0.76	0.07	0.00	30
IGFBP7	1.77	0.58	0.01	0.00	30
BGN	1.75	0.64	0.02	0.00	30
CXCR4	0.68	0.48	0.16	0.00	31
CALB2	0.80	0.35	0.09	0.00	31
PLS3	0.64	0.46	0.18	0.00	31
ENC1	0.50	0.88	0.50	0.00	31
MIAT	0.48	0.77	0.40	0.00	31
NRXN3	0.59	0.30	0.08	0.00	31
EIF5	0.49	0.76	0.40	0.00	31
GAD1	0.52	0.27	0.07	0.00	31
VCAN	0.46	0.79	0.44	0.00	31
ARL4C	0.54	0.54	0.25	0.00	31
FAM183A	1.37	0.97	0.02	0.00	32

GRAMD3	1.17	0.92	0.03	0.00	32
ROPN1L	1.17	0.88	0.03	0.00	32
PIFO	1.14	1.00	0.01	0.00	32
MORN5	0.79	0.96	0.03	0.00	32
SPAG6	0.75	0.84	0.01	0.00	32
CCDC170	0.73	0.92	0.01	0.00	32
FAM92B	0.65	0.81	0.00	0.00	32
TCTEX1D1	0.63	0.92	0.01	0.00	32
SIX3	0.61	0.98	0.04	0.00	32
NUPR1	1.27	0.76	0.03	0.00	33
CBLN1	1.28	0.81	0.03	0.00	33
TRH	1.37	0.83	0.02	0.00	33
ADAM12	1.00	0.68	0.01	0.00	33
CALB2	1.60	0.97	0.09	0.00	33
PCP4	1.95	0.92	0.10	0.00	33
TAGLN2	1.56	0.97	0.16	0.00	33
CD9	1.20	0.81	0.07	0.00	33
RBMS1	1.10	0.78	0.03	0.00	33
KLHL13	1.21	0.81	0.05	0.00	33

Supplementary Table 3.4: Top 10 DE genes in each direction between genotypes in *TSC2*$^{c/-}$ experiments

All Clusters

Gene	logFC	pct.1	pct.2	p.adj
CLU	-2.06	0.35	0.68	0.00
SPARCL1	-1.72	0.05	0.34	0.00
CST3	-1.67	0.39	0.66	0.00
APOE	-1.63	0.05	0.27	0.00
PTGDS	-1.62	0.13	0.44	0.00
S100B	-1.38	0.05	0.30	0.00
PTN	-1.35	0.48	0.78	0.00
MT3	-1.32	0.19	0.42	0.00
TTR	-1.20	0.03	0.12	0.00
B2M	-1.19	0.29	0.61	0.00
LINC00599	0.45	0.35	0.22	0.00
CELF4	0.47	0.45	0.31	0.00
SYP	0.47	0.56	0.43	0.00
BASP1	0.48	0.90	0.83	0.00
RTN1	0.48	0.87	0.74	0.00
HMP19	0.50	0.58	0.38	0.00
NTM	0.51	0.48	0.42	0.00
LHX1	0.54	0.46	0.25	0.00
STMN2	0.66	0.86	0.56	0.00
NEUROD1	0.69	0.23	0.10	0.00

Cluster 0

Gene	logFC	pct.1	pct.2	p.adj
DsRed-WPRE	-1.34	0.01	0.18	0.00
CLU	-1.10	0.08	0.24	0.00
MTRNR2L12	-0.77	0.05	0.14	0.00
PTGDS	-0.74	0.02	0.12	0.00
VEGFA	-0.69	0.12	0.23	0.00
GOLGA8A	-0.63	0.10	0.21	0.00
MT-ND3	-0.60	0.52	0.67	0.00
IGFBP2	-0.53	0.47	0.65	0.00
CALB1	-0.49	0.13	0.24	0.00
MT-ND4L	-0.47	0.11	0.21	0.03
RPL7	0.25	0.90	0.82	0.00
RPL10	0.26	0.97	0.92	0.00
RPS29	0.26	0.92	0.87	0.00
RPL13A	0.27	0.95	0.84	0.00
STMN2	0.27	0.96	0.92	0.00
RPLP0	0.27	0.84	0.79	0.00
RPS11	0.36	0.81	0.71	0.00
NTM	0.40	0.83	0.77	0.00

Cluster 1

Gene	logFC	pct.1	pct.2	p.adj
DsRed-WPRE	-1.13	0.04	0.21	0.00
CLU	-0.94	0.31	0.47	0.00
CRYAB	-0.84	0.05	0.11	0.04
PTGDS	-0.80	0.08	0.26	0.00
PTN	-0.62	0.39	0.61	0.00
FTH1	-0.55	1.00	0.99	0.00
HOXA10	-0.55	0.01	0.13	0.00
HOXA9	-0.52	0.01	0.11	0.00
HOXB8	-0.45	0.01	0.11	0.00
B2M	-0.44	0.24	0.39	0.00

Cluster 2

Gene	logFC	pct.1	pct.2	p.adj
DsRed-WPRE	-0.96	0.04	0.21	0.00
CLU	-0.61	0.27	0.41	0.00
IGFBP2	-0.56	0.80	0.94	0.00
PTN	-0.46	0.38	0.59	0.00
DDIT3	-0.44	0.26	0.42	0.00
LAMP5	-0.42	0.05	0.15	0.00
FTL	-0.41	0.98	1.00	0.00
VIM	-0.39	0.57	0.72	0.00
MEST	-0.39	0.32	0.54	0.00
FTH1	-0.39	1.00	1.00	0.00
ZBTB18	0.60	0.25	0.09	0.00
PRDM8	0.65	0.35	0.17	0.00
C11orf96	0.67	0.21	0.07	0.00
CBLN1	0.67	0.37	0.16	0.00
SSTR2	0.68	0.31	0.14	0.00
NFIB	0.70	0.36	0.17	0.00
MT-ATP6	0.74	0.68	0.68	0.03
ZIC2	0.81	0.33	0.12	0.00
ZIC1	0.93	0.37	0.16	0.00
NEUROD1	1.07	0.37	0.14	0.00

Cluster 3

Gene	logFC	pct.1	pct.2	p.adj
DsRed-WPRE	-0.45	0.06	0.18	0.00
PTN	-0.37	0.46	0.66	0.00
ITM2C	-0.33	0.39	0.54	0.00
CST3	-0.32	0.46	0.61	0.00
DDIT3	-0.28	0.30	0.45	0.00
PTGDS	-0.27	0.13	0.25	0.00
RELN	0.30	0.30	0.19	0.05
KCNK1	0.32	0.31	0.18	0.00
MT-CO3	0.34	0.99	0.98	0.00
MT-CYB	0.36	0.96	0.97	0.00
NEUROD1	0.38	0.40	0.25	0.00
CBLN1	0.38	0.45	0.31	0.00
ZBTB18	0.38	0.32	0.22	0.04
ZIC2	0.42	0.36	0.25	0.03
MT-ATP6	0.48	0.96	0.96	0.00
ZIC1	0.54	0.39	0.27	0.00

Cluster 4

Gene	logFC	pct.1	pct.2	p.adj
APOE	-1.67	0.12	0.53	0.00
PTGDS	-1.52	0.24	0.71	0.00
CLU	-1.45	0.75	0.98	0.00
CST3	-1.38	0.70	0.92	0.00
S100B	-1.36	0.32	0.72	0.00
AQP4	-1.33	0.10	0.46	0.00
MT3	-1.29	0.48	0.85	0.00
SPARCL1	-1.23	0.24	0.72	0.00
GFAP	-1.13	0.11	0.31	0.00
B2M	-1.12	0.50	0.88	0.00
RPL13A	0.56	1.00	0.99	0.00
TUBB	0.57	0.97	0.97	0.00
RPL7	0.57	0.99	1.00	0.00
PTMA	0.58	0.98	0.99	0.00
BTG1	0.62	0.83	0.81	0.00
SOX4	0.70	0.96	0.93	0.00
TMSB15A	0.72	0.56	0.30	0.00
MIAT	0.73	0.63	0.52	0.00
CD24	0.78	0.62	0.45	0.00
STMN2	1.14	0.45	0.25	0.00

Cluster 5

Gene	logFC	pct.1	pct.2	p.adj
CRYAB	-1.86	0.10	0.27	0.00
DsRed-WPRE	-1.45	0.03	0.28	0.00
PTGDS	-1.41	0.08	0.33	0.00
IGFBP5	-1.39	0.06	0.23	0.00
GADD45B	-1.38	0.09	0.29	0.00
CLU	-1.12	0.36	0.66	0.00
NDUFA4L2	-1.09	0.08	0.24	0.00
FTH1	-1.02	0.97	0.98	0.00
S100B	-0.94	0.01	0.13	0.00
SQSTM1	-0.90	0.39	0.67	0.00
TMEM59L	0.53	0.47	0.32	0.00
HMP19	0.53	0.39	0.19	0.00
NRXN1	0.54	0.24	0.12	0.00
STMN4	0.54	0.66	0.46	0.00
SYP	0.56	0.53	0.33	0.00
TUBB2B	0.56	0.88	0.70	0.00
BASP1	0.60	0.78	0.60	0.00
NREP	0.65	0.63	0.39	0.00
SOX4	0.71	0.87	0.62	0.00
STMN2	0.76	0.81	0.44	0.00

Cluster 6

Gene	logFC	pct.1	pct.2	p.adj
PTGDS	-1.88	0.07	0.27	0.00
SPARCL1	-1.65	0.01	0.15	0.00
APOE	-1.55	0.06	0.16	0.00
DsRed-WPRE	-1.21	0.02	0.28	0.00
BCYRN1	-1.14	0.12	0.25	0.00
CST3	-1.10	0.28	0.41	0.04
PTN	-1.07	0.47	0.63	0.00
B2M	-0.80	0.16	0.29	0.00
PMEL	-0.73	0.02	0.14	0.00
VIM	-0.67	0.31	0.47	0.00
TSPAN7	0.34	0.62	0.52	0.04
LINC00632	0.41	0.87	0.78	0.00

Cluster 7

Gene	logFC	pct.1	pct.2	p.adj
DsRed-WPRE	-1.49	0.02	0.42	0.00
CLU	-0.92	0.13	0.31	0.00
FTH1	-0.61	1.00	1.00	0.00
PTGDS	-0.58	0.03	0.13	0.00
B2M	-0.55	0.10	0.27	0.00
IGFBP2	-0.52	0.51	0.68	0.02
FTL	-0.50	0.97	0.97	0.00
UQCRB	-0.45	0.66	0.87	0.00
TAC1	-0.43	0.04	0.12	0.00
MIF	-0.41	0.65	0.90	0.00
STMN2	0.26	1.00	0.96	0.00
RPL7	0.28	0.99	0.94	0.00
RPS11	0.31	0.96	0.95	0.00
MALAT1	0.32	1.00	0.98	0.00
LHX1	0.38	0.88	0.81	0.00

Cluster 8

Gene	logFC	pct.1	pct.2	p.adj
CLU	-1.50	0.68	0.94	0.00
DsRed-WPRE	-1.29	0.05	0.37	0.00
SPARCL1	-1.27	0.14	0.50	0.00
PTGDS	-1.26	0.22	0.60	0.00
IGFBP5	-1.20	0.43	0.69	0.00
S100B	-1.04	0.08	0.34	0.00
MT-ND3	-1.04	0.36	0.66	0.00
CST3	-1.04	0.46	0.77	0.00
MT3	-1.03	0.35	0.68	0.00
CRYAB	-0.96	0.13	0.36	0.00
BTG1	0.42	0.94	0.94	0.00
RBMX	0.43	0.83	0.85	0.00
MALAT1	0.45	1.00	0.99	0.00
RPS11	0.45	0.96	0.96	0.00
SOX4	0.46	0.85	0.84	0.00
RPL7	0.48	0.99	0.97	0.00
MIAT	0.49	0.60	0.56	0.00
RTN1	0.58	0.67	0.60	0.00
LAMP2	0.74	0.22	0.50	0.00
STMN2	0.84	0.45	0.23	0.00

Cluster 9

Gene	logFC	pct.1	pct.2	p.adj
CLU	-1.86	0.37	0.72	0.00
CST3	-1.41	0.55	0.71	0.00
PTGDS	-1.34	0.16	0.35	0.00
PTN	-1.26	0.46	0.77	0.00
MT3	-1.15	0.12	0.34	0.00
GFAP	-1.14	0.02	0.16	0.00
DsRed-WPRE	-1.14	0.02	0.33	0.00
SPARCL1	-1.10	0.03	0.28	0.00
FABP5	-1.00	0.47	0.70	0.00
PTPRZ1	-0.99	0.20	0.48	0.00
BARHL1	0.51	0.22	0.03	0.00
CHGA	0.53	0.22	0.07	0.00
GAP43	0.54	0.36	0.27	0.03
LHX1	0.56	0.30	0.09	0.00
NFIB	0.57	0.53	0.53	0.03
RAB26	0.70	0.23	0.02	0.00
NRN1	0.78	0.33	0.22	0.00
SFRP1	0.97	0.29	0.12	0.00
STMN2	1.08	0.53	0.30	0.00
MGP	1.42	0.29	0.02	0.00

Cluster 10

Gene	logFC	pct.1	pct.2	p.adj
CLU	-1.36	0.32	0.58	0.00
DsRed-WPRE	-1.27	0.03	0.32	0.00
PTGDS	-1.03	0.22	0.45	0.00
MT3	-0.93	0.05	0.23	0.00
IGFBP5	-0.92	0.19	0.33	0.00
FTH1	-0.88	0.99	0.99	0.00
DDIT3	-0.79	0.11	0.40	0.00
FTL	-0.77	0.95	0.98	0.00
SAT1	-0.74	0.23	0.51	0.00
MAFB	-0.73	0.06	0.16	0.01
TUBB	0.36	0.98	0.92	0.00
LHX1	0.40	0.65	0.50	0.00
RP11-445F12.1	0.47	0.53	0.39	0.00
MT-CO1	0.51	0.84	0.72	0.00
GAP43	0.56	0.75	0.69	0.00
STMN2	0.59	0.97	0.79	0.00
MT-ND4	0.61	0.79	0.68	0.00
MT-CO2	0.81	0.79	0.70	0.00
MT-ATP6	0.93	0.63	0.57	0.02
MT-CO3	0.95	0.74	0.66	0.00

Cluster 11

Gene	logFC	pct.1	pct.2	p.adj
DsRed-WPRE	-0.89	0.04	0.31	0.00
ANK2	-0.30	0.26	0.45	0.00
MIF	-0.27	0.75	0.93	0.00
MT-CO1	-0.26	0.99	0.99	0.00
PKIA	-0.25	0.48	0.71	0.00
RPS11	0.29	0.99	0.96	0.00

Cluster 12

Gene	logFC	pct.1	pct.2	p.adj
DsRed-WPRE	-1.39	0.03	0.45	0.00
HOXB8	-0.66	0.02	0.20	0.00
CLU	-0.62	0.32	0.55	0.00
HOXB7	-0.61	0.02	0.22	0.00
PAX8	-0.58	0.08	0.27	0.00
HOXD9	-0.56	0.03	0.19	0.00
HOXC10	-0.54	0.04	0.22	0.00
PTGDS	-0.53	0.10	0.25	0.00
RP11-369C8.1	-0.52	0.02	0.11	0.00
B2M	-0.52	0.17	0.43	0.00
MARCKS	0.28	0.91	0.92	0.00
TFAP2A	0.35	0.75	0.62	0.00
HMP19	0.38	0.87	0.82	0.00
HIST1H4C	0.42	0.76	0.71	0.00
NTM	0.51	0.72	0.60	0.00

Cluster 13

Gene	logFC	pct.1	pct.2	p.adj
SPARCL1	-1.05	0.72	0.84	0.00
BCYRN1	-1.00	0.12	0.40	0.00
CRYAB	-0.93	0.46	0.64	0.00
TRH	-0.76	0.12	0.26	0.01
AQP4	-0.75	0.05	0.27	0.00
APOE	-0.74	0.45	0.65	0.00
CST3	-0.74	0.92	0.98	0.00
CTSH	-0.70	0.35	0.48	0.00
CLU	-0.68	0.88	0.93	0.00
DsRed-WPRE	-0.65	0.10	0.26	0.00
WIF1	0.42	0.39	0.24	0.00
CPXM2	0.44	0.34	0.21	0.00
PCP4	0.48	0.55	0.43	0.00
C9orf24	0.52	0.30	0.18	0.00
WFIKKN2	0.59	0.27	0.13	0.00
NDUFA4L2	0.61	0.74	0.60	0.00
CYP1B1	0.62	0.47	0.30	0.00
FOLR1	0.66	0.42	0.26	0.00
MT1E	0.67	0.34	0.15	0.00
TRPM3	0.89	0.49	0.32	0.00

Cluster 14

Gene	logFC	pct.1	pct.2	p.adj
APOE	-2.32	0.09	0.41	0.00
S100B	-2.23	0.14	0.52	0.00
CLU	-2.16	0.45	0.82	0.00
MT3	-2.13	0.22	0.61	0.00
CST3	-2.06	0.59	0.83	0.00
SPARCL1	-1.75	0.11	0.49	0.00
SPRY2	-1.60	0.09	0.20	0.03
GFAP	-1.41	0.03	0.17	0.00
ITM2C	-1.37	0.25	0.62	0.00
NR2F1-AS1	-1.36	0.15	0.40	0.00
DCC	0.67	0.34	0.07	0.00
CHGA	0.71	0.24	0.03	0.00
PTMA	0.74	1.00	0.96	0.00
NRN1	0.83	0.39	0.21	0.00
RAB26	0.87	0.32	0.02	0.00
NFIB	0.89	0.55	0.35	0.00
STMN2	0.89	0.47	0.22	0.00
SFRP1	1.21	0.40	0.15	0.00
HES6	1.40	0.60	0.31	0.00
MGP	1.79	0.39	0.10	0.00

Cluster 15

Gene	logFC	pct.1	pct.2	p.adj
CLU	-1.66	0.46	0.76	0.00
DsRed-WPRE	-1.57	0.03	0.37	0.00
CST3	-1.41	0.63	0.84	0.00
S100B	-1.31	0.07	0.31	0.00
SPARCL1	-1.26	0.04	0.25	0.00
MT3	-1.20	0.19	0.43	0.00
APOE	-1.17	0.04	0.23	0.00
PTGDS	-1.06	0.18	0.37	0.00
PTN	-0.94	0.71	0.95	0.00
TTYH1	-0.85	0.37	0.78	0.00
SOX4	0.39	0.95	0.92	0.00
CBX3	0.40	0.91	0.87	0.00
RTN1	0.41	0.77	0.65	0.00
CHGA	0.44	0.25	0.09	0.00
DLL3	0.45	0.53	0.34	0.00
LHX1	0.53	0.40	0.14	0.00
MT-ND1	0.58	0.89	0.93	0.01
SFRP1	0.59	0.37	0.24	0.01
STMN2	0.69	0.54	0.34	0.00
MGP	0.72	0.36	0.16	0.00

Cluster 16

Gene	logFC	pct.1	pct.2	p.adj
IGFBP2	-0.67	0.63	0.76	0.03
EIF4B	-0.30	0.44	0.66	0.00
DsRed-WPRE	-0.27	0.02	0.12	0.00
DCX	-0.27	0.88	0.98	0.00
GTF2I	-0.25	0.57	0.82	0.00
C7orf73	-0.25	0.62	0.83	0.02
HSP90AA1	0.28	0.96	0.97	0.00

Cluster 17

Gene	logFC	pct.1	pct.2	p.adj
DsRed-WPRE	-1.15	0.04	0.31	0.00
HOXA9	-0.78	0.01	0.20	0.00
HOXC10	-0.72	0.02	0.19	0.00
HOXB6	-0.72	0.01	0.23	0.00
MID1	-0.70	0.11	0.40	0.00
HOXB8	-0.62	0.02	0.22	0.00
PMEL	-0.61	0.04	0.20	0.00
HOXA10	-0.59	0.02	0.22	0.00
HOXC9	-0.58	0.02	0.19	0.00
LAMP5	-0.55	0.07	0.17	0.04
RPS29	0.26	1.00	0.99	0.00
RPL10	0.27	1.00	1.00	0.00
RPS11	0.27	0.99	0.98	0.00
RPL7	0.30	0.99	0.97	0.00
STMN2	0.31	1.00	0.99	0.00
GAP43	0.34	0.90	0.90	0.00
LHX1	0.36	0.64	0.49	0.02
MT-CO3	0.48	0.98	0.97	0.00
NEUROD1	0.78	0.40	0.23	0.00

Cluster 18

Gene	logFC	pct.1	pct.2	p.adj
DsRed-WPRE	-1.37	0.01	0.32	0.00
CLU	-0.91	0.30	0.51	0.00
DLK1	-0.88	0.06	0.20	0.00
S100B	-0.87	0.02	0.15	0.00
IGFBP2	-0.81	0.47	0.69	0.00
PTGDS	-0.78	0.09	0.24	0.00
HOXA9	-0.69	0.00	0.17	0.00
HOXA10	-0.62	0.00	0.15	0.00
B2M	-0.58	0.31	0.55	0.00
COTL1	-0.55	0.36	0.59	0.00
ACTG1	0.26	1.00	1.00	0.00
BASP1	0.39	0.92	0.87	0.00
LHX1	0.54	0.64	0.49	0.00
RTN1	0.55	0.72	0.65	0.00
NEUROD1	0.57	0.45	0.27	0.00
STMN2	0.60	0.87	0.79	0.00
LINC00599	0.63	0.55	0.40	0.00

Cluster 19

Gene	logFC	pct.1	pct.2	p.adj
DsRed-WPRE	-1.39	0.03	0.25	0.00
GFAP	-1.39	0.10	0.30	0.00
AQP4	-0.92	0.19	0.43	0.00
PTGDS	-0.92	0.46	0.77	0.00
MT-ATP8	-0.84	0.09	0.38	0.00
HSPA1A	-0.76	0.26	0.56	0.00
CLU	-0.75	0.87	0.98	0.00
IFITM3	-0.73	0.06	0.25	0.01
NEAT1	-0.73	0.82	0.93	0.03
ATP1B2	-0.67	0.33	0.61	0.00
TMSB4X	0.29	0.90	0.80	0.01
RPL15	0.40	0.79	0.70	0.01
RPL37A	0.42	0.79	0.68	0.00
RPL10	0.46	0.84	0.82	0.00
RPL13A	0.54	0.65	0.53	0.02
TMSB10	0.59	0.79	0.65	0.00
SOX4	0.82	0.67	0.57	0.00
RTN1	0.87	0.57	0.43	0.00
STMN2	0.90	0.33	0.16	0.00

Cluster 20

Gene	logFC	pct.1	pct.2	p.adj
APOE	-1.57	0.02	0.23	0.00
CLU	-1.44	0.43	0.85	0.00
SPARCL1	-1.39	0.06	0.33	0.00
DsRed-WPRE	-1.36	0.03	0.40	0.00
MT3	-1.26	0.17	0.45	0.00
CST3	-1.10	0.63	0.82	0.00
PTGDS	-1.05	0.08	0.33	0.00
IGFBP2	-0.98	0.69	0.96	0.00
S100B	-0.85	0.06	0.27	0.00
NPC2	-0.77	0.48	0.84	0.00
IGFBPL1	0.35	0.24	0.08	0.00
HNRNPM	0.36	0.84	0.84	0.01
BASP1	0.41	0.87	0.84	0.00
RTN1	0.41	0.79	0.68	0.00
RPS11	0.43	0.98	0.96	0.00
CBX3	0.43	0.93	0.86	0.00
PTMA	0.43	0.99	0.98	0.00
RBMX	0.44	0.99	0.96	0.00
SSTR2	0.57	0.26	0.10	0.01
STMN2	0.86	0.55	0.36	0.00

Cluster 21

Gene	logFC	pct.1	pct.2	p.adj
C6orf62	-0.35	0.23	0.49	0.00
ATRX	-0.34	0.40	0.72	0.00
TULP4	-0.34	0.24	0.49	0.00
TTC3	-0.31	0.90	0.98	0.00
TROVE2	-0.29	0.34	0.56	0.04
RNF187	-0.29	0.36	0.63	0.01
C19orf25	-0.28	0.22	0.42	0.02

Cluster 22

Gene	logFC	pct.1	pct.2	p.adj
RFX3	0.47	0.78	0.46	0.05

Supplementary Table 3.5: Top 10 DE genes in each direction between genotypes for Fig. 3

All Clusters Combined

Gene	logFC	pct.1	pct.2	p.adj
APOE	-1.41	0.16	0.48	0.00
CLU	-1.37	0.69	0.94	0.00
SPARCL1	-1.32	0.28	0.69	0.00
CST3	-1.26	0.65	0.88	0.00
S100B	-1.22	0.25	0.56	0.00
AQP4	-1.22	0.06	0.31	0.00
MT3	-1.15	0.37	0.68	0.00
GFAP	-1.09	0.05	0.20	0.00
DsRed-WPRE	-1.08	0.06	0.29	0.00
TRH	-1.02	0.03	0.13	0.00
PTMA	0.57	0.96	0.93	0.00
BTG1	0.57	0.84	0.78	0.00
CD24	0.58	0.56	0.41	0.00
RPL7	0.59	0.96	0.91	0.00
TMSB15A	0.59	0.41	0.23	0.00
SOX4	0.61	0.85	0.78	0.00
RPS11	0.62	0.94	0.90	0.00
TPGS1	0.65	0.25	0.40	0.00
HES6	0.87	0.35	0.30	0.00
STMN2	0.91	0.43	0.22	0.00

Cluster 0

Gene	logFC	pct.1	pct.2	p.adj
DsRed-WPRE	-1.63	0.02	0.24	0.00
PTGDS	-0.92	0.04	0.24	0.00
CLU	-0.77	0.57	0.87	0.00
SPARC	-0.56	0.38	0.73	0.00
B2M	-0.56	0.28	0.62	0.00
S100B	-0.54	0.07	0.28	0.00
IGFBP2	-0.54	0.78	0.95	0.00
MT-CO1	-0.53	0.89	0.97	0.00
FTH1	-0.52	0.97	0.99	0.00
IGFBP5	-0.50	0.20	0.43	0.00
SOX4	0.26	0.93	0.94	0.00
GNB2L1	0.26	0.98	0.97	0.00
RPL7	0.29	0.99	0.99	0.00
MALAT1	0.31	1.00	1.00	0.00
PTMA	0.34	0.97	0.98	0.00
RBMX	0.38	0.86	0.89	0.00
CBX3	0.39	0.63	0.67	0.00
BTG1	0.47	0.85	0.88	0.00

Cluster 1

Gene	logFC	pct.1	pct.2	p.adj
DLK1	-1.25	0.12	0.32	0.00
DsRed-WPRE	-1.21	0.10	0.25	0.00
FRZB	-1.15	0.03	0.19	0.00
CNN3	-0.67	0.64	0.90	0.00
IFITM3	-0.65	0.13	0.28	0.01
COL1A2	-0.63	0.07	0.25	0.00
PI15	-0.55	0.15	0.40	0.00
PTGDS	-0.54	0.70	0.82	0.00
ID4	-0.52	0.43	0.71	0.00
BAALC	-0.48	0.22	0.48	0.00
PTMA	0.30	0.89	0.91	0.00
TMSB15A	0.40	0.28	0.15	0.01
OLIG1	0.44	0.14	0.02	0.00
NOVA1	0.56	0.83	0.79	0.00
RTN1	0.65	0.80	0.56	0.00
STMN2	0.73	0.47	0.21	0.00

Cluster 2

Gene	logFC	pct.1	pct.2	p.adj
PTGDS	-1.17	0.64	0.89	0.00
CLU	-1.11	0.89	0.99	0.00
CTSH	-1.06	0.14	0.50	0.03
ATP1B2	-0.80	0.57	0.81	0.00
METRN	-0.79	0.46	0.76	0.02
RTN1	0.82	0.66	0.43	0.02

Cluster 3

Gene	logFC	pct.1	pct.2	p.adj
APOE	-1.35	0.24	0.59	0.00
BCYRN1	-1.35	0.16	0.56	0.00
PTGDS	-1.27	0.32	0.76	0.00
CLU	-0.87	0.93	1.00	0.00
SNHG25	-0.83	0.42	0.77	0.00
B2M	-0.83	0.72	0.91	0.00
SPARCL1	-0.82	0.58	0.89	0.00
S100B	-0.77	0.16	0.49	0.02
CST3	-0.77	0.82	0.98	0.00
ATP1A2	-0.73	0.41	0.76	0.00
STMN2	0.77	0.57	0.36	0.03

Cluster 4

Gene	logFC	pct.1	pct.2	p.adj
DsRed-WPRE	-1.96	0.06	0.49	0.00
S100B	-1.69	0.02	0.18	0.00
PTGDS	-1.36	0.16	0.42	0.00
GGCT	-0.98	0.17	0.42	0.00
S100A10	-0.77	0.16	0.36	0.03
FTH1	-0.69	1.00	1.00	0.01
COX7B	-0.53	0.62	0.82	0.00
NQO1	-0.53	0.13	0.34	0.01
ANXA5	-0.52	0.41	0.64	0.02
ANXA1	-0.52	0.05	0.22	0.02
MALAT1	0.34	1.00	0.98	0.00
STMN2	0.63	0.56	0.28	0.00

Cluster 5

Gene	logFC	pct.1	pct.2	p.adj
RIPPLY1	-1.44	0.06	0.36	0.00
CP	-1.20	0.70	0.95	0.00
HSPA1A	-1.12	0.70	0.96	0.00
CST3	-0.98	0.90	1.00	0.00
NR2F1	-0.95	0.51	0.84	0.00
CFI	-0.94	0.13	0.74	0.00
CLU	-0.93	0.96	1.00	0.00
GNG11	-0.92	0.18	0.65	0.00
SFRP2	-0.88	0.42	0.79	0.00
S100B	-0.85	0.46	0.81	0.00
RPL27A	0.75	0.97	0.98	0.00
RPLP2	0.77	0.97	0.98	0.00
RPL36A	0.86	0.92	0.96	0.00
RPL7	0.90	0.97	0.98	0.00
RPL37A	0.90	0.98	1.00	0.00
RPL17	0.99	0.89	0.78	0.00
RPL31	1.28	0.93	0.95	0.00
RPS17	1.31	0.97	0.94	0.00
RPL13A	1.40	0.95	0.97	0.00
RPS20	1.41	0.87	0.87	0.00

Cluster 6

Gene	logFC	pct.1	pct.2	p.adj
PLCG2	-1.48	0.23	0.63	0.00
NPFFR1	-1.15	0.03	0.25	0.00
HSPA1A	-0.84	0.13	0.51	0.00
HSPA1B	-0.81	0.07	0.41	0.00
HRH4	-0.47	0.00	0.16	0.00
GOLGA8A	-0.41	0.03	0.25	0.01
FRY	-0.39	0.02	0.20	0.01
PSMA7	0.72	0.81	0.51	0.00
ENO1	0.72	0.91	0.67	0.00
TPI1	0.74	0.93	0.69	0.00
VAMP2	0.74	0.84	0.67	0.04
NDN	0.75	0.68	0.29	0.04
H3F3A	0.77	0.92	0.76	0.00
CFL1	0.81	0.85	0.71	0.00
SEC62	0.83	0.66	0.33	0.03
BASP1	0.89	0.75	0.41	0.01
SOX4	1.09	0.81	0.69	0.01

Cluster 7

Gene	logFC	pct.1	pct.2	p.adj
FSIP2-AS1	0.30	0.29	0.02	0.01

Cluster 8

Gene	logFC	pct.1	pct.2	p.adj
TNNC2	-3.04	0.00	0.14	0.00
HES1	-2.71	0.04	0.57	0.00
IGF2	-2.48	0.00	0.14	0.00
TNNT3	-2.26	0.00	0.14	0.00
MT3	-2.08	0.16	0.86	0.04
C1QTNF3	-1.91	0.02	0.57	0.00
GNG11	-1.85	0.10	0.71	0.01
SPARC	-1.79	0.16	1.00	0.00
TNNI2	-1.78	0.00	0.14	0.00
MYL1	-1.75	0.00	0.14	0.00

Cluster 9

Gene	logFC	pct.1	pct.2	p.adj
RSPO3	-1.37	0.10	0.36	0.01
CRYAB	-1.06	0.64	0.91	0.00
WLS	-0.77	0.96	1.00	0.00
MT-ATP8	-0.65	0.87	0.99	0.00
MT-ND3	-0.56	1.00	1.00	0.00
CLU	-0.53	1.00	1.00	0.00
PLCG2	-0.50	0.94	0.95	0.00
MT-CO3	-0.44	1.00	1.00	0.00
MT-ATP6	-0.42	1.00	1.00	0.00
GNG11	-0.41	0.16	0.46	0.00
RPLP1	0.27	1.00	1.00	0.00

Cluster 10

Gene	logFC	pct.1	pct.2	p.adj
APOE	-2.25	0.18	0.93	0.00
CLU	-1.80	0.75	1.00	0.00
PTGDS	-1.69	0.44	0.99	0.00
AQP4	-1.68	0.37	0.99	0.00
SPARCL1	-1.64	0.40	0.91	0.00
CCL2	-1.59	0.05	0.49	0.00
CRYAB	-1.44	0.22	0.94	0.00
HOPX	-1.40	0.46	0.94	0.00
GFAP	-1.25	0.57	0.99	0.00
MT3	-1.20	0.89	0.98	0.00
HES6	1.04	0.73	0.72	0.02
CADM2	1.15	0.67	0.51	0.00
PLPPR1	1.15	0.27	0.01	0.00
PDGFRA	1.18	0.29	0.00	0.00
APOD	1.23	0.25	0.01	0.00
KCNQ1OT1	1.24	0.60	0.30	0.00
OLIG2	1.27	0.79	0.55	0.00
SOX4	1.28	0.97	0.99	0.00
NOVA1	1.33	1.00	0.97	0.00
OLIG1	1.51	0.91	0.84	0.00

Cluster 11

Gene	logFC	pct.1	pct.2	p.adj
BAALC	-1.07	0.22	0.69	0.00
STMN2	0.84	0.42	0.10	0.01

Cluster 12

Gene	logFC	pct.1	pct.2	p.adj
DsRed-WPRE	-2.13	0.05	0.74	0.00
NPC2	-1.39	0.52	0.87	0.04
MOXD1	0.67	0.57	0.12	0.03

Cluster 13

Gene	logFC	pct.1	pct.2	p.adj
MT-ND3	-0.89	0.95	1.00	0.01
MT-CO3	-0.77	0.95	1.00	0.05

Cluster 14

Gene	logFC	pct.1	pct.2	p.adj
RPL36A	-0.80	0.81	0.95	0.02
SLC25A6	-0.78	0.81	0.96	0.01
RPLP2	-0.75	0.97	1.00	0.00
RPL35	-0.72	0.95	1.00	0.00
RPS27	-0.70	1.00	1.00	0.00
NAP1L1	-0.67	0.84	0.96	0.05
RPL38	-0.65	1.00	0.99	0.00
RPS19	-0.64	1.00	1.00	0.00
NBEAL1	-0.63	0.41	0.91	0.01
RPL23	-0.61	0.97	1.00	0.03
CD81	1.05	0.87	0.49	0.00
PCSK2	1.05	0.46	0.09	0.03
MAP2	1.06	0.68	0.22	0.00
GNAS	1.08	0.97	0.90	0.00
COL3A1	1.09	0.62	0.12	0.00
CSRP1	1.09	0.81	0.35	0.00
AQP1	1.16	0.54	0.12	0.01
NDUFA4L2	1.42	0.81	0.48	0.03
IGF1	1.43	0.60	0.16	0.01
FGL2	1.44	0.62	0.12	0.00

Cluster 15

Gene	logFC	pct.1	pct.2	p.adj
ITM2A	0.35	0.44	0.05	0.03

Cluster 16

Gene	logFC	pct.1	pct.2	p.adj
RFX3	0.46	0.84	0.49	0.01

Supplementary Table 3.6: Top 10 DE genes in each direction between genotypes for constitutive *TSC2*$^{+/+}$, *TSC2*$^{+/-}$, *TSC2*$^{-/-}$ Spheroids

WT vs HET

Gene	logFC	pct.1	pct.2	p.adj
TTR	-0.78	0.07	0.12	0.00
MGP	-0.72	0.08	0.17	0.00
SFRP1	-0.59	0.18	0.29	0.00
SPARCL1	-0.52	0.21	0.26	0.00
NEUROD1	-0.40	0.13	0.23	0.00
IGFBP5	-0.40	0.36	0.46	0.00
ZIC1	-0.38	0.28	0.46	0.00
RPS10	-0.38	0.76	0.81	0.00
ZIC2	-0.35	0.25	0.43	0.00
NFIB	-0.33	0.33	0.47	0.00
MT-ND5	0.32	0.70	0.72	0.00
MT-CO2	0.34	0.80	0.81	0.00
MT-ND3	0.35	0.75	0.75	0.00
PRSS23	0.43	0.16	0.08	0.00
MT-CO3	0.48	0.77	0.78	0.00
PLP1	0.49	0.19	0.14	0.00
MT-ATP6	0.50	0.78	0.77	0.00
NR2F2	0.51	0.61	0.46	0.00
MT-ND1	0.54	0.72	0.72	0.00
MT-CYB	0.66	0.75	0.76	0.00

WT vs KO

Gene	logFC	pct.1	pct.2	p.adj
CRYAB	-1.94	0.11	0.50	0.00
FTH1	-1.04	0.96	1.00	0.00
SST	-1.01	0.03	0.12	0.00
B2M	-0.92	0.46	0.77	0.00
NEAT1	-0.92	0.78	0.82	0.00
VGF	-0.89	0.32	0.60	0.00
NEFL	-0.87	0.48	0.79	0.00
LGALS3	-0.85	0.16	0.29	0.00
FTL	-0.84	0.93	0.99	0.00
GARS	-0.83	0.48	0.76	0.00
SLC1A3	0.78	0.23	0.08	0.00
PTPRZ1	0.78	0.39	0.25	0.00
SPARCL1	0.93	0.21	0.11	0.00
TTYH1	0.95	0.44	0.31	0.00
COL1A2	0.98	0.15	0.05	0.00
GPM6B	0.99	0.82	0.74	0.00
LGALS1	1.01	0.24	0.17	0.00
CST3	1.10	0.50	0.54	0.00
PTN	1.26	0.76	0.73	0.00
NNAT	2.55	0.64	0.00	0.00

HET vs KO

Gene	logFC	pct.1	pct.2	p.adj
CRYAB	-1.90	0.11	0.50	0.00
SST	-1.21	0.03	0.12	0.00
VGF	-1.07	0.29	0.60	0.00
FTH1	-1.06	0.96	1.00	0.00
FTL	-0.96	0.92	0.99	0.00
LGALS3	-0.93	0.15	0.29	0.00
B2M	-0.91	0.48	0.77	0.00
NEAT1	-0.89	0.77	0.82	0.00
SCG2	-0.89	0.30	0.68	0.00
SPP1	-0.87	0.07	0.38	0.00
IGFBP7	0.93	0.11	0.05	0.00
LGALS1	0.95	0.27	0.17	0.00
GPM6B	0.97	0.80	0.74	0.00
HIST1H4C	0.97	0.78	0.59	0.00
TRH	1.00	0.11	0.06	0.00
COL1A2	1.13	0.15	0.05	0.00
MGP	1.16	0.17	0.01	0.00
PTN	1.42	0.73	0.73	0.00
SPARCL1	1.45	0.26	0.11	0.00
NNAT	2.48	0.63	0.00	0.00

Supplementary Table 3.7: Top 10 DE genes in each direction between genotypes for conditional *TSC2*$^{c/+}$ cells

All Clusters

Gene	logFC	pct.1	pct.2	p.adj
TTR	-2.18	0.07	0.18	0.00
DsRed-WPRE	-1.26	0.02	0.42	0.00
SPARCL1	-0.76	0.09	0.22	0.00
PTGDS	-0.72	0.15	0.31	0.00
AC090498.1	-0.71	0.34	0.49	0.00
CLU	-0.65	0.53	0.57	0.00
C1orf61	-0.63	0.46	0.62	0.00
RPL17	-0.53	0.61	0.77	0.00
PTN	-0.51	0.70	0.78	0.00
LGALS1	-0.49	0.10	0.23	0.00
LINC00632	0.38	0.82	0.75	0.00
HMP19	0.39	0.71	0.58	0.00
TSPAN7	0.41	0.53	0.43	0.00
CALY	0.41	0.38	0.25	0.00
MT-CO3	0.44	0.91	0.88	0.00
MT-ND4	0.46	0.93	0.91	0.00
MT-ATP6	0.47	0.88	0.83	0.00
MT-CYB	0.54	0.86	0.81	0.00
MT-ND2	0.55	0.87	0.82	0.00
MT-ND1	0.62	0.82	0.75	0.00

Supplementary Table 3.8: Antibodies used for this study

Antibody	Host species	Company	Catalog #	IHC dilution
TBR1	Rabbit	Abcam	31940	1:500
pS6-235/236	Mouse	Cell Signaling	62016	1:1000
pS6-240/244	Rabbit	Cell Signaling	5364	1:1000
Vimentin	Mouse	EMD Millipore	MAB3400	1:500

Chapter 4: **Discussion and future directions**

Thesis summary

Human neurodevelopmental disorders have historically been difficult to study. The inaccessibility of affected human neural tissue combined with fundamental differences between human and rodent cortical development has resulted in the lack of an experimental model that accurately captures the pathophysiology of these disorders. Emerging technologies in genome editing and *in vitro* neural differentiation from human pluripotent stem cells have opened new experimental options that better reproduce the complex genetic and developmental landscape in these disorders. In this dissertation, I have presented my work in creating and applying a human neuronal model of one such developmental disorder, tuberous sclerosis (TSC).

TSC is caused by mutations in the genes *TSC1* or *TSC2*, which act as negative regulators of mTORC1 signaling. I first genetically engineered human pluripotent stem cell lines to generate a panel of heterozygous and homozygous loss of function mutations in *TSC1* or *TSC2*. This resulted in complete loss of protein in the homozygous cell lines and a 50% loss of protein in the heterozygous cell lines. These cell lines were differentiated to cortical spheroids, producing heterogeneous collections of neurons and glia over 150 days. The homozygous knock-out cell lines showed consistent activation of mTORC1 signaling throughout spheroid development, while wild-type and heterozygous cell lines repressed mTORC1 activation as the spheroids became neurogenic. Concordant with this phenomenon, homozygous knock-out cell lines also produced disproportionately more glial-lineage cells compared with wild-type and heterozygous cells, indicating that mTORC1 signaling can have a major impact on cell-fate decisions.

Patients with TSC are born with heterozygous presumed loss-of-function mutations, as biallelic mutations are assumed embryonic lethal. However, homozygous mutations have been commonly identified in both non-neural and neural TSC lesions, indicating that a somatic “second-hit” mutation may lead to the formation of cortical tubers, brain lesions that are associated with epilepsy in TSC patients. To address this question, I further genetically engineered hPSCs to create a conditional *TSC2* heterozygous cell line where the functional allele could be excised with Cre-recombinase. Differentiating these cells into spheroids and treating them with a sub-saturating amount of Cre during the neural precursor phase, revealed a strong bias towards glial differentiation in cells that had a complete loss of *TSC2*. Chronic treatment with the mTOR inhibitor rapamycin counteracted this phenomenon, strongly promoting neurogenesis.

Understanding how complete loss of *TSC2* affects cellular identity and developmental trajectory is essential to understanding how cortical tubers are formed. I applied single cell sequencing to cortical spheroids with a series of conditional and constitutive loss-of-function mutations in *TSC2* over several time-points. Cells generated from *TSC2*$^{-/-}$ precursors overwhelmingly occupied glial clusters - both radial glia and reactive astrocytes. Additionally, *TSC2*$^{-/-}$ cells also clustered more strongly with cells that expressed epithelial cell markers. There was no coordinated transcriptional signature shared by all *TSC2*$^{-/-}$ cells, further evidence that the effects of mTORC1 signaling are primarily non-transcriptional. However, among glial cells there were strong

specific transcriptional increases in some genes that are associated with a protein folding response, but are also involved in glia maturation.

Future directions

The experiments in this dissertation primarily explore the origin and formation of cortical tubers, however there is much to learn about the cell biology of tuber cells. Hypothetically, the affected processes within tuber cells are related to mTORC1 signaling. Given that, it would be logical to investigate how 1) protein synthesis and 2) autophagy is affected by TSC1/2 loss in neurons and human neuronal models.

One avenue to study protein synthesis is through translational profiling. There are numerous methods for translational profiling including ribosome footprinting [193], translating ribosome affinity purification (TRAP) [194], and translating ribosomes in polysomes sequencing (TRIP-seq) [195]. A pilot study using TRAP in primary cultured mouse hippocampal neurons revealed many strong translational changes upon *Tsc1* loss and/or treatment with rapamycin (Fig. 4.1A,B). Interestingly, many of the most differentially translated transcripts were involved in glycolysis. These transcripts changed bi-directionally, increasing in *Tsc1*$^{-/-}$ neurons and decreasing in rapamycin-treated cultures. Functionally, measuring metabolic flux using the Seahorse assay revealed a detectable change in cellular metabolism, with an increase in glycolysis (Fig. 4.1C). Activation of glycolysis has previously been associated with cancer cells with increased mTORC1 signaling [196], indicating that this could be a universal response to mTORC1 hyperactivity, not limited to hippocampal neurons.

The effects of increased glycolysis may be detrimental for neuronal development. One study has shown that failure to repress glycolysis during early neuronal development leads to cell death [179], while another implied that persistent glycolytic stress during *in vitro* human cortical development leads to a lack of neuronal maturation and specification [108]. These results may explain the simultaneous increase in transcription of glycolysis genes and glial markers in a 2-D cultured human model of TSC [93, 94]. In our own 3-D model of TSC, persistent expression of HK2, an enzyme that catalyzes the first step of glycolysis, was seen in *TSC2*$^{-/-}$ spheroids compared to controls (Fig. 4.1D).

In addition to increases in translation of specific mRNAs, we have also observed a universal increase in translation in TSC1/2 knockout neural cultures. The recovery of RNA from bound ribosomes, an indicator of the translation level of RNA at that time, from our TRAP experiment was higher in *Tsc1*$^{-/-}$ cultures than in controls and much higher than in samples treated with rapamycin. In a separate polysome fractionation experiment, peaks representing high ribosome occupancy were bigger in *TSC2*$^{-/-}$ human neural precursor cells compared to controls, again indicating higher overall translation (Fig. 4.2A). As a caveat, it is important to note that increased translation does not always manifest as increased functional protein. Hypothetically, a side-effect of increased translation could be activation of the unfolded protein response (UPR). The UPR features several branches, one of them being activated by phosphorylation of eIF2α [197]. We observed increased levels of p-eIF2α at some developmental time-points in *TSC2*$^{-/-}$ spheroid cultures compared to wild-type, suggesting that the UPR may be activated (Fig. 4.2B, however ATF4, which is downstream of p-eIF2α, levels should

be measured). Additionally, there are other UPR branches, mediated by IRE1-XBP1 and ATF6, that should also be assayed for activity in these cultures. Increases in the UPR and ER-stress may also lead to aberrant differentiation in neural cultures, as neurons, being long lived and post-mitotic, require strict proteostasis control to maintain homeostasis [108]. A hypothetical disruption of protein levels or an increase in stress response could cause premature cell death. This may help explain some of the observations in this dissertation and therefore ways to decrease translation and the UPR either through chemical inhibitors like ISRIB or genetically through expression of a constitutively active 4EBP1 [62] could be explored.

Another way to maintain proteostasis is through autophagy. Hypothetically, increasing autophagy could counteract over-translation, breaking down the excess proteins being synthesized in cells with reduced TSC1/2 function [198]. Phosphorylation of ULK1 by mTORC1 prevents autophagy and in our spheroid models, p-ULK1 is increased throughout development in *TSC2*$^{-/-}$ spheroids (Fig. 4.3A). Concordantly, there is also an increase in another autophagy protein, p62/SQSTM1, likely a compensatory response to the prevention of autophagy by p-ULK1 (Fig. 4.3B). Previous work has highlighted autophagy disruption in TSC model systems through a genetic LC3-GFP-mCherry reporter [199]. This reporter takes advantage of the pH sensitivity of GFP and insensitivity of mCherry to fluorescently label lysosomes and lysosome formation. Genetically encoding this reporter with cell specific promoters would be highly informative in understanding the deficits of autophagy in *TSC2*$^{-/-}$ cells in spheroids.

The time-points chosen for the experiments in this dissertation were based on the major milestones for cortical neurogenesis and astrogenesis, in order to understand disrupted differentiation and formation of cortical tubers. However, it may be useful to investigate even earlier time points to detect what may be driving the divergence from wildtype in *TSC2*$^{-/-}$ cultures. Preliminary single cell sequencing data of constitutive wild-type and *TSC2*$^{-/-}$ spheroids at day 1, day 6 and day 13 suggests that differentiation differences start from the stem cell stage (Fig. 4.4A-D). DLK1, a notch ligand, was consistently overexpressed in *TSC2*$^{-/-}$ spheroids at each time-point (Fig. 4.4E). Recently, DLK1 was found to be overexpressed in a specific subset of human neural progenitors from primary tissue, although it is unclear what the significance of these progenitors is and what cell types they develop into [200]. Other differentially expressed genes are also consistent with those seen in later time-points including IGFBP5, CRYAB and APOE (Fig. 4.4F). Further batches and intermediate time points should be investigated to confirm these results.

In conclusion, this dissertation describes efforts to create and apply a human neuronal model of tuberous sclerosis and in doing so has made key findings on the origin and properties of neural-lineage cells in TSC. There are myriad ways to apply this model, much more than what has been described here, that may lead to further insights and ultimately a reduced burden on patients with this devastating disorder.

Methods

Primary Mouse Hippocampal Cultures

Primary dissociated mouse hippocampal cultures were prepared from p0 *Tsc1*$^{fl/fl}$ mice [42] according to protocols outlined in Beaudoin et al, 2012 [192]. For all experiments, 1.5 x10^5 cells were plated on 24-well plates precoated with Poly-D-Lysine. At days in vitro (DIV) 2, neuronal cultures were infected with GFP-L10 lentivirus and either GFP-Ires-Cre (*Tsc1* KO) or GFP (*Tsc1* WT) lentivirus. Half-media changes happened every four days. At DIV 7, cultures were treated with 50 nM Rapamycin (+ Rap) or vehicle (etOH). Rapamycin was replaced with each subsequent media change. At DIV 14, cultures were harvested for TRAP or western blotting.

Translating Ribosome Affinity Purification (TRAP)

TRAP processing followed established protocol [201] with alterations to adapt for primary cultures outlined here. Firstly, media was removed from cultures and replaced with ice cold lysis buffer containing Cycloheximide (CHX). The plate was then placed on a shaker at 4 C for 5 minutes. Following this step, the lysate was taken from the wells and put into 1.5 ml tubes where it continued processing according to the protocol. For each sample, it was necessary to combine four wells of culture to get enough material. At the final step, RNA was extracted with an Agilent Absolutely RNA Nanoprep kit (Agilent). For this experiment, three batches of primary cultures were made and processed separately. Each batch consisted of *Tsc1* KO, *Tsc1* KO + Rap, *Tsc1* WT (Control) and *Tsc1* WT + Rap samples. Following RNA extraction, RNA was assessed for quality using a Bioanalyzer (Agilent), and loaded onto Affymetrix GeneChip Mouse Gene 1.0 ST arrays (Affymetrix) for expression analysis.

Microarray Analysis

Raw data files from the Affymetrix GeneChip Mouse Gene 1.0 ST array were assessed for quality control, background subtracted and quantile normalized using the aroma.affymetrix package [202] in R 3.1.2. As RNA was extracted from each set of conditions on three different dates, we corrected for batch effects using ComBat [203]. Corrected data was statistically analyzed using the limma package [204] and significant genes were determined using an multiple comparison adjusted p-value of <0.05 for each comparison.

Western Blotting

2D cultured cells were harvested in lysis buffer containing 2 mM EDTA, 2 mM EGTA, 1% Triton-X, and 0.5% SDS in 1x PBS with Halt phosphatase inhibitor cocktail (Fisher: PI78420) and Complete mini EDTA-free protease inhibitor cocktail (Roche: 4693159001). Three-dimensional spheroids were harvested in lysis buffer containing 1% SDS, phosphatase inhibitor and protease inhibitor in 1x PBS. Total protein was determined by BCA assay (Fisher: PI23227) and 5-15 µg of protein in Laemmli sample

buffer were loaded onto 4–15% Criterion TGX gels (Bio-Rad: 5671084). Proteins were transferred to PVDF membranes, blocked in 5% milk in TBS-Tween for one hour at room temperature (RT), and incubated with primary antibodies diluted in 5% milk in TBS-Tween overnight at 4°C. The following day, membranes were incubated with HRP-conjugated secondary antibodies (Bio-Rad: 170-5046, 1705047) for one hour at RT, washed, incubated with chemiluminesence substrate (Perkin-Elmer: NEL105001EA) and developed on GE Amersham Hyperfilm ECL (VWR: 95017-661). Membranes were stripped with 6M guanidine hydrochloride to re-blot on subsequent days. Bands were quantified by densitometry using Image J software. Phospho-proteins were normalized to their respective total proteins and non-phospho-proteins were normalized to a β-Actin loading control. Antibody vendors, catalog numbers, and dilutions are listed in Supplementary Table 4.1.

Seahorse Glycolysis Stress Test

The Seahorse glycolysis stress test was performed according to manufacturer's protocols with the Glycolysis Stress Kit (Agilent) on a Seahorse Xfe96 analyzer (Agilent). Each sample is represented by an average of 16-wells consisting of 2.0-2.5 $x10^4$ primary cultured neurons prepared and maintained as above.

Human NPC cultures

NPC cultures were made from WT WIBR3 hESCs and *TSC2*$^{-/-}$ hESCs from Blair et al., 2018 [77].Neural induction was performed as described previously [175], with minor alterations. Single hESCs were initially plated at a density of 50,000/cm^2 ($1.9x10^5$ cells/well of a 12 well plate) and maintained in complete conditioned hESC media until >90% confluent. hESCs were transferred to induction media supplemented with 100 ng/ul Noggin (R&D Systems: 6057-NG) and 10 μM SB431542 (Selleck Chemicals: S1067) with daily media changes for 10 days. The composition of induction media changed throughout induction with 100% induction media A (A) from days 1-4, 75% A and 25% induction media B (B) on days 5-6, 50% A and 50% B on days 7-8 and 25% A and 75% B on days 9-10. Induction media A is composed of Knockout DMEM (Lifetech: 10829018) with 15% KSR, 2 mM l-glutamine, 1% non-essential amino acids, 1000 U/ml penicillin/streptomycin) and 55 μM β-mercaptoethanol. Induction media B is composed of 50% DMEM/F12 media (Lifetech: 11320-033), 50% Neurobasal media (Lifetech: 21103049), 1x N-2 Supplement (Lifetech: 17502048), 1x Glutamax (Lifetech: 35050061), 1000 U/ml penicillin/streptomycin (Lifetech: 15070063), 0.2% human Insulin (Sigma: I9278) and 0.075% BSA (Sigma: A4503) w/v) as previously described[175]. After neural induction was complete, cells were dissociated with Accutase (Lifetech: A1110501), spun down for 4 minutes at 800 rpm, resuspended in N2 media supplemented with 25 ng/ml FGF and 40 ng/ml EGF (R&D Systems: 236-EG) and replated at 1:2. Cells were passaged as such every 5 days until passage 4, when they were split at 1:3.

Polysome Profiling

Polysome profiling was undertaken using approximate 1.8 x10^7 cells for each experiment as outlined in Blair et al, 2017 [101]. Cells were treated with 100 mg/mL cycloheximide dissolved in pre-warmed media at 37C for 5 min before harvesting, and 100 mg/mL cycloheximide was added to all downstream buffers. Cells were dissociated with Accutase and spun down for 4 min at 800 rpm. Cell pellets were washed with PBS, spun down, and resuspended in 500 mL hypotonic lysis buffer on ice (10 mM HEPES [pH 7.9], 1.5 mM MgCl2, 10 mM KCl, 0.5 mM DTT, 1% Triton X-100, and 100 mg/mL cycloheximide). All samples were then incubated on ice for 10 min, triturated ten times through a 26G needle, and spun at 1,500 3 g for 5 min at 4C (to pellet nuclei and cell bodies), and the supernatant was transferred to a new tube. Sucrose gradients from 10-50% were made in 100 mM KCl, 20 mM HEPES pH 7.6 and 5 mM MgCl2 with 100 µg/ml cycloheximide and 0.66 U/µl Superasein (Thermo-Fisher) and pre-chilled in centrifuge buckets for at least 30 minutes before use. 100 µl of lysate was then applied to the top of a 12 ml 10-50% sucrose gradient. Tubes were spun for 2 hours at 36,000 RPM (221,632 g) in a SW-41 rotor. The bottom of the tube was punctured and 2M sucrose pumped in using a peristaltic pump. Absorbance at 260 nm was monitored using a Brandel (Gaithersburg, MD) gradient fractionator and ISCO (Lincoln, NE) UA-6 detector.

Human Spheroid Culture

3-D differentiation of hESCs and hiPSCs into cortical spheroids was performed as described previously [1, 109]. Briefly, confluent, undifferentiated colonies of hESCs were removed from MEFs and dissociated from each other using Accutase for 20 minutes. The cell suspension was collected and strained through a 40 μm strainer in hESC wash media. This cell suspension was spun down for 5 minutes at 1000 rpm. The supernatant was removed and resuspended in 5 ml of hESC media without fibroblast growth factor 2 (FGF2), supplemented with 10 µm Y-27632 dihydrochloride. Cells were counted and diluted to a concentration of 2.7 x10^6 cells/ml and 6 ml of this suspension was deposited into one well of a 6-well Aggrewell plate. After the aggregation of single cells into EBs, the EBs were removed and put into 10 cm ultra-low attachment dishes. On days 1–5, media was changed to hESC-FGF2 media, supplemented with 10 µM Dorsomorphin (ab146597, Abcam) and 10 µM SB431542. On day 6, developing spheroids were put into neural induction media composed of Neurobasal-A (Thermo Fisher Scientific), B-27 Supplement minus vitamin A (Thermo Fisher Scientific), penicillin-streptomycin, and GlutaMAX, supplemented with 20 ng ml−1 FGF and 20ng ml−1 EGF. Media was changed in this manner every day from days 6–15 and then every other day until day 25. From days 25–43, the developing spheroids were grown in neural induction media supplemented with 20 ng ml−1 BDNF and 20 ng ml−1 NT-3, with media changes every 4 days. From day 43 onward, spheroids were maintained in neural induction media without BDNF or NT-3, with media changes every 4 days until harvest.

Single Cell Sequencing

Dissociation of spheroids for FACS followed a protocol for dissociation of post-natal day 0 mouse cortex for primary culture [192]. First, dissociation media (DM) was

made consisting of 488.9 ml Ca and Mg free HBSS (Invitrogen), 5 ml of 100 mM Sodium Pyruvate (Lifetech), 1.1 ml 45% stock D-glucose (Sigma) and 5 ml pH 7.3 HEPES (Invitrogen). Next, the dissociation solution was made consisting of 5 ml DM, 172 ul Papain Solution (Worthington), and 5-7 crystals of L-Cysteine (Sigma). This solution was warmed at 37 °C for 15 minutes and then filter-sterilized through a 0.22 μm filter. The spheroid was then removed from culture media, placed into this solution and left in a 37 °C bath for 30 minutes. During this time, trypsin inhibitor (TI) solution was made consisting of 10 mg of Trypsin Inhibitor (Sigma) in 10 ml DM, placed in 37 °C for >15 minutes, removed and filter sterilized. After 30 minutes of incubation, the dissociation solution was removed from the tube with the spheroid, leaving the spheroid intact, and replaced with 3 ml of TI. The TI was immediately removed, and the spheroid was washed again in 3 ml of TI, which again, was immediately removed, replacing again with 4 ml of TI and put into the 37 °C water bath for 4 minutes. During this time, the sorting buffer (SB) of 1x PBS with Ca and Mg with 10 μM Y-27632 (Calbio Chem) was made and placed on ice. After the 4 minutes at 37 °C, the TI was removed from the tube with the spheroid and 2 ml of SB was added. The spheroid was then mechanically dissociated by triturating 5-10 times through a 5 ml pipette within this solution. The whole solution including the dissociated cells was then taken up into the pipette and passed through a 70 μm cell strainer into a 50 ml conical tube. This strained solution was then placed into a polypropylene FACS tube (BD Biosciences) and placed on ice.

FACS and Single Cell Sequencing

Dissociated cells were sorted on a BD Aria Fusion cell sorter with an attached 70 μm bore. For all sorting, a target number of 10,000 cells was implemented, with a maximum time of one hour sorting, so as to limit the amount of time single cells were sitting on ice. After sorting, the cells were immediately centrifuged at 300 x g for 5 minutes at 4 °C and then counted on a hemocytometer to estimate concentration. Cells were then processed through the 10x Genomics pipeline, following the protocol exactly, with a targeted loading of 2000 cells per sample. All samples were run with the 10x Single Cell 3' v3 kit. cDNA recovered following the 10x protocol was assessed for quality using a fragment analyzer, and library prepped. All 10x work was done in the Functional Genomics Lab at UC Berkeley. Libraries were sequenced across two lanes on a NovaSeq SP chip (Illumina) in the Vincent J. Coates Genomics Sequencing Lab at UC Berkeley.

Single Cell Sequencing Processing

FASTQ files were aligned to the human genome (GRCh38) using Cell Ranger 3.0.2 (10x Genomics). Cell Ranger gene expression matrix outputs were then loaded into Seurat 3.0 [114] using R-Studio v1.2 and R v3.6. Data from each individual sample was turned into a Seurat object and metadata regarding timepoint, genotype and batch was added to each object. Each object was subset, extracting cells where > 500 RNA features were expressed and where <20% of the genes expressed were mitochondrial. Raw RNA counts from each object were normalized using the default parameters from Seurat (Log normalization with a scale factor of 10,000). The top 2000 variable features from each object were also determined using the default parameters in Seurat (selection.method = vst). Objects were then integrated by first finding the integration

anchors using control samples as the reference and otherwise default parameters (dims = 1:20) and then integrating the anchor set. Following this integration, cells were further subset by selecting for all cells expressing the cellular stress marker DDIT3 at one standard deviation from the mean or lower. Principal Component Analysis (PCA) dimensionality reduction was then run on this population of cells, followed by UMAP dimensionality reduction using the first 20 PCs. Shared nearest neighbors for each cell and clusters were identified using the default parameters from Seurat except with resolution = 1. Marker genes for each cluster were determined using the FindAllMarkers function as well as looking at gene expression of known canonical genes. Differential gene expression for all comparisons was determined using the FindMarkers function. All plots were created using ggplot2, including ggplot2 calls in Seurat. Proportional bar graphs were created using GraphPad Prism 8.

Figures
Figure 4.1

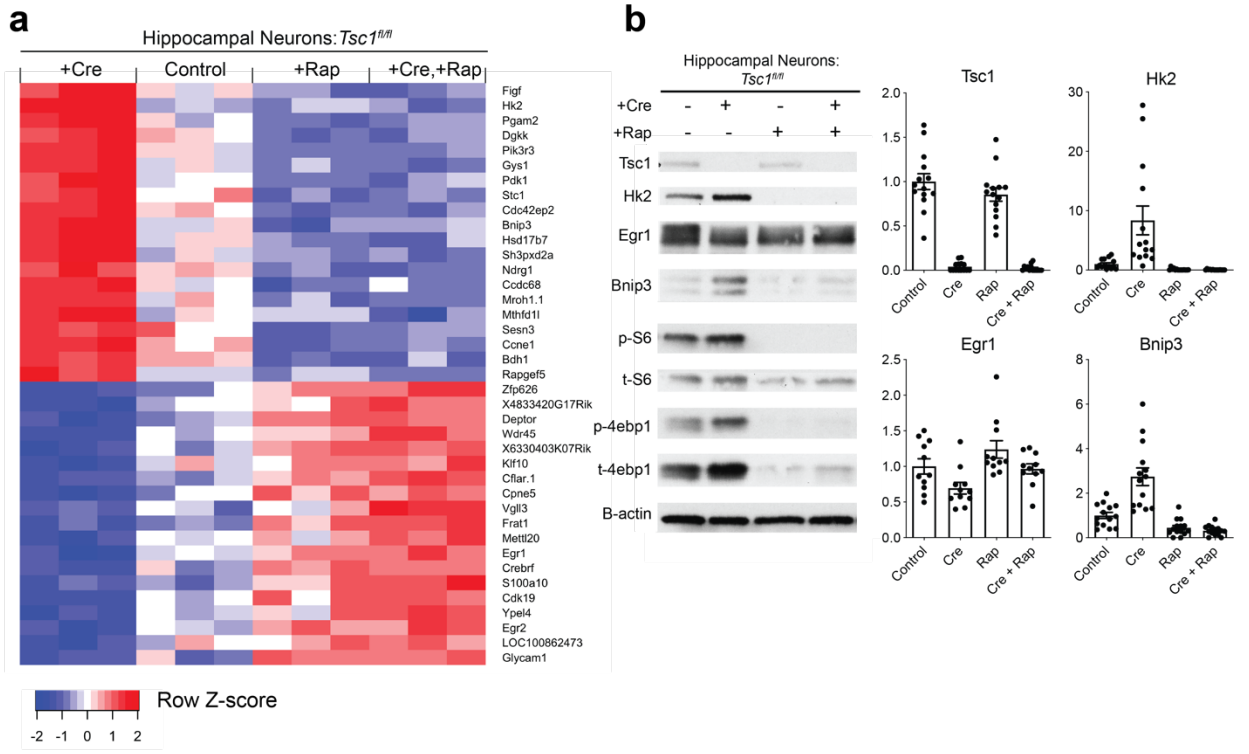

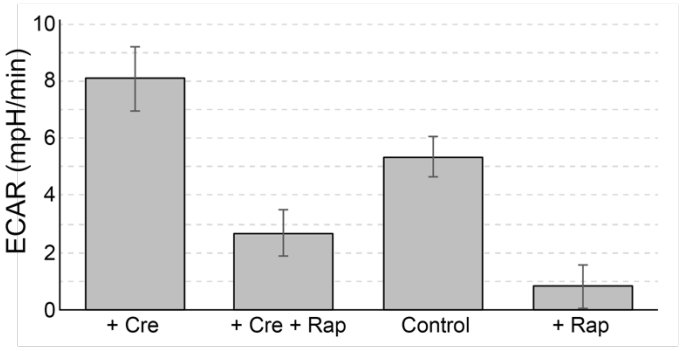

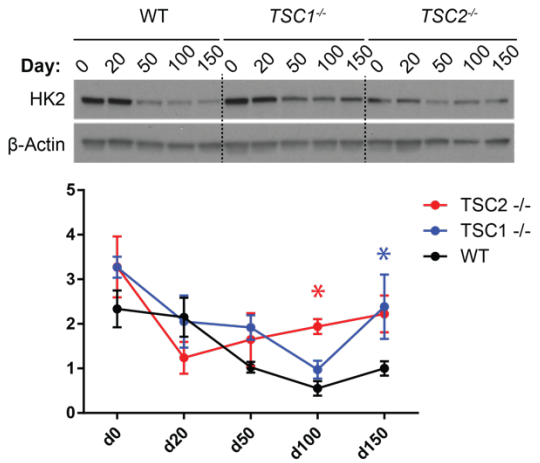

Fig. 4.1: (a) Heatmap showing the top differentially translated genes from TRAP experiment on *Tsc1*$^{fl/fl}$ primary mouse hippocampal neurons treated with Cre-recombinase, rapamycin or both (see methods). **(b)** Example western blots and quantification of protein levels in *Tsc1*$^{fl/fl}$ primary mouse hippocampal neurons for a selection of the top differentially translated mRNAs from TRAP experiments **(c)** quantification of glycolysis in *Tsc1*$^{fl/fl}$ primary mouse hippocampal neurons as indicated by Extracellular Acidification Rate (ECAR). **(d)** Quantification of western blots from hESC spheroid cultures over time (n=5 for each genotype). Error bars indicate standard error of the mean (S.E.M.). Asterisk indicates $p < 0.01$ between indicated sample color and wildtype samples at that timepoint from a two-way ANOVA measuring across time and between genotypes.

Figure 4.2

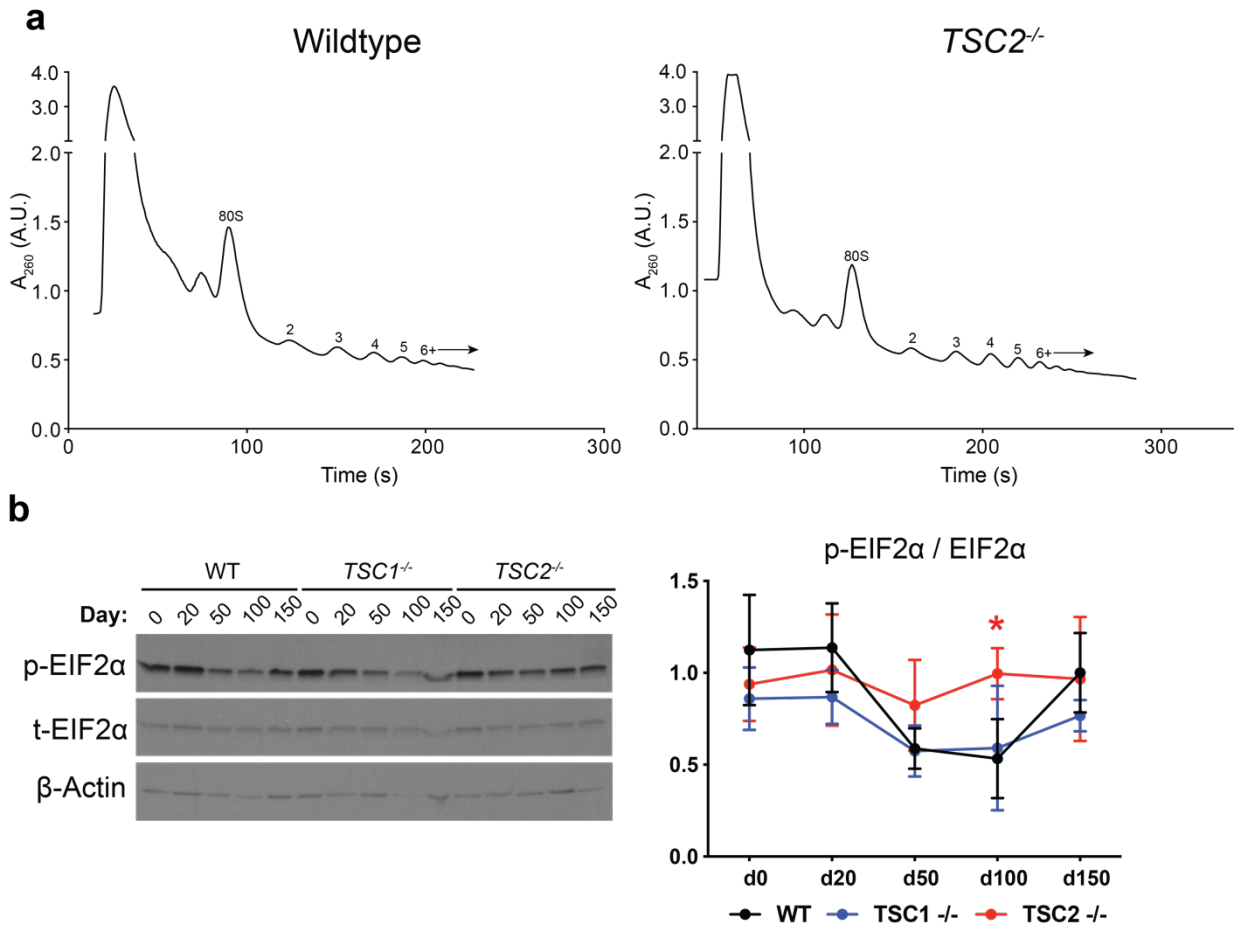

Fig. 4.2: (a) Polysome fraction profiles from WT and *TSC2*$^{-/-}$ human neural precursor cells. Numbers indicate the number of ribosomes bound to the RNA transcripts under the peaks. Larger peaks indicate more transcripts bound. **(b)** Example western blots from hESC spheroid cultures over time (n=5 for each sample). Right, quantification of western blots for phosphorylation (Ser51) levels of EIF2α normalized to total EIF2α protein. Error bars indicate S.E.M.. Asterisk indicates p <0.01 between indicated sample color and wildtype from a two-way ANOVA measuring across time and between genotypes.

Figure 4.3

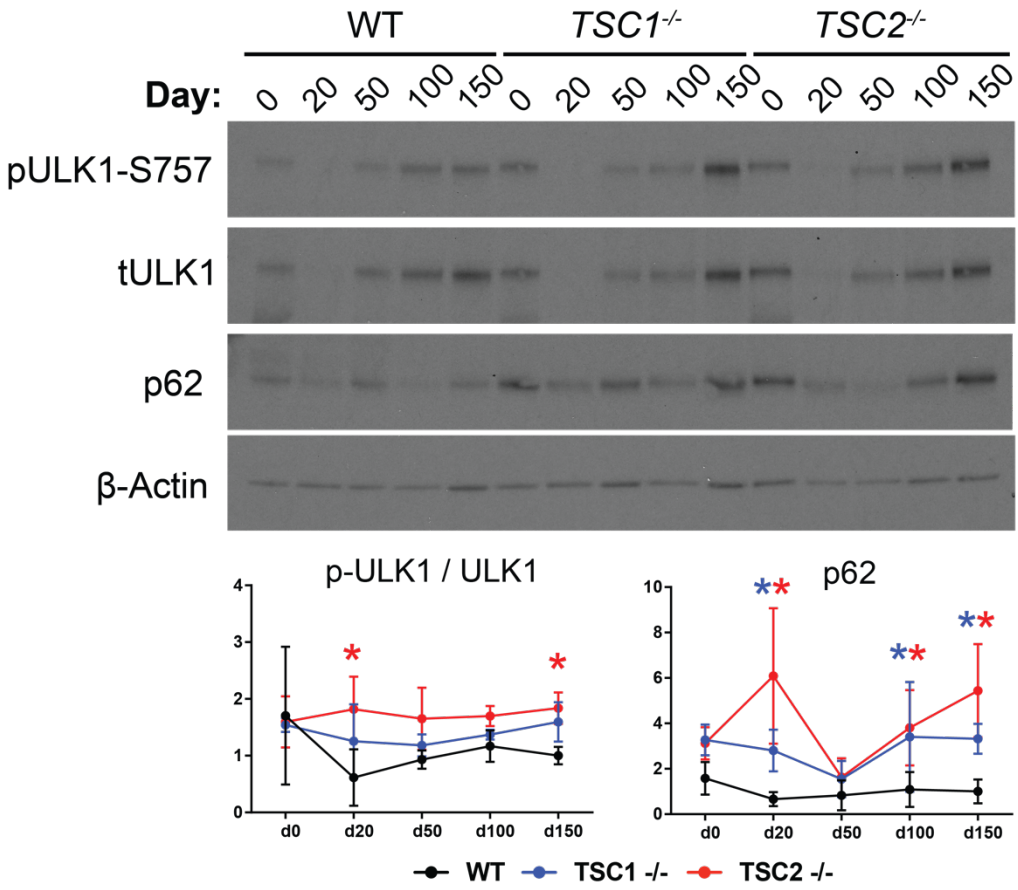

Fig. 4.3: Example western blots from hESC spheroid cultures over time (n=5 for each sample). Right, quantification of western blots for phosphorylation (Ser757) levels of ULK1 normalized to total ULK1 protein (n=5 for each sample) and p62 (n=6 for each sample). Error bars indicate S.E.M.. Asterisk indicates p <0.01 between indicated sample color and wildtype sample from a two-way ANOVA measuring across time and between genotypes.

Figure 4.4

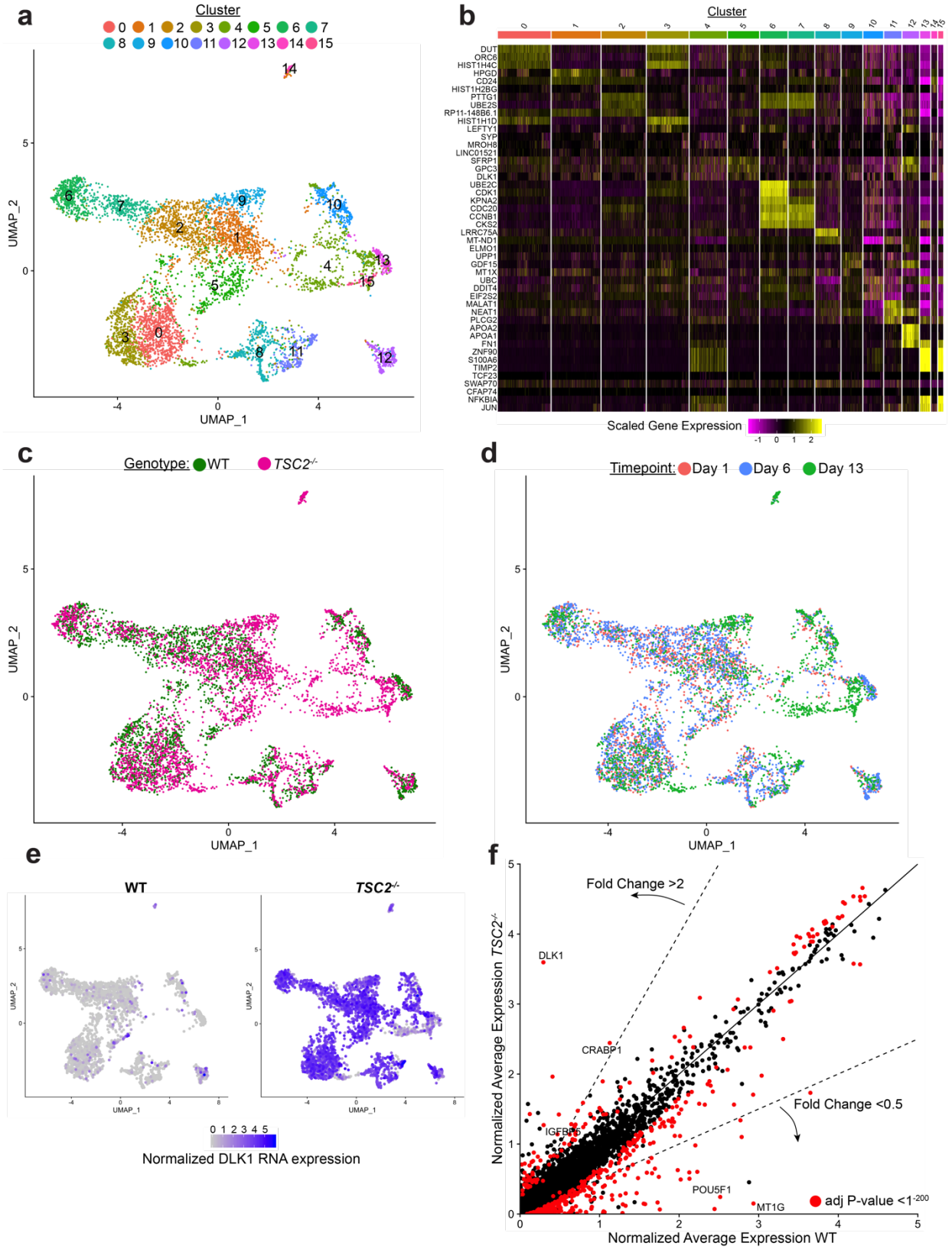
a
Cluster
0 1 2 3 4 5 6 7
8 9 10 11 12 13 14 15
UMAP_2
UMAP_1
b
Cluster
DUT
ORC6
HIST1H4C
HPGD
CD24
HIST1H2BG
PTTG1
UBE2S
RP11-148B6.1
HIST1H1D
LEFTY1
SYP
MROH8
LINC01521
SFRP1
GPC3
DLK1
UBE2C
CDK1
KPNA2
CDC20
CCNB1
CKS2
LRRC75A
MT-ND1
ELMO1
UPP1
GDF15
MT1X
UBC
DDIT4
EIF2S2
MALAT1
NEAT1
PLCG2
APOA2
APOA1
FN1
ZNF90
S100A6
TIMP2
TCF23
SWAP70
CFAP74
NFKBIA
JUN
Scaled Gene Expression
c
Genotype: WT TSC2-/-
UMAP_2
UMAP_1
d
Timepoint: Day 1 Day 6 Day 13
UMAP_2
UMAP_1
e
WT
TSC2-/-
UMAP_2
UMAP_1
0 1 2 3 4 5
Normalized DLK1 RNA expression
f
Fold Change >2
Fold Change <0.5
DLK1
CRABP1
IGFBP5
POU5F1
MT1G
adj P-value <1-200
Normalized Average Expression TSC2-/-
Normalized Average Expression WT

Fig. 4.4: (a) UMAP dimensionality reduction plot showing the clusters from all samples combined in the early time-point single cell sequencing experiments (n=1 batch, multiple spheroids per batch, for each genotype from Day 1, Day 6 and Day 13). **(b)** Heatmap showing the top 3 cluster defining genes for each cluster in **(a). (c)** UMAP plot colored by genotype. **(d)** UMAP plot colored by time-point. **(e)** Split RNA feature plot showing the normalized RNA expression of DLK1 in either Wildtype (WT) or *TSC2*$^{-/-}$ cells from early timepoints. **(d)** Scatter plot showing the normalized expression levels of all detected genes with genes of interest labeled. Red points indicate an adjusted p-value of $<1^{-200}$ when testing differential expression.

Supplementary Tables

Supplementary Table 4.1: Antibodies used in this chapter

Antibody	Host species	Company	Catalog #	Western blot dilution
TSC1	rabbit	Cell Signaling	6935S	1:1000
HK2	rabbit	Cell Signaling	2867	1:1000
EGR1	rabbit	Cell Signaling	4153	1:300
BNIP3	rabbit	Cell Signaling	3769	1:300
p-S6 (Ser240/244)	rabbit	Cell Signaling	5364S	1:2000
S6	rabbit	Cell Signaling	2317S	1:1000
p-4E-BP1 (Thr37/46)	rabbit	Cell Signaling	2855	1:750
4E-BP1	rabbit	Cell Signaling	9644	1:1000
B-Actin	mouse	Sigma	a1972	1:15000
p-EIF2α (Ser51)	rabbit	Cell Signaling	3398	1:1000
EIF2α	rabbit	Cell Signaling	5324	1:1000
p-ULK1 (Ser757)	rabbit	Cell Signaling	14202	1:1000
UK1	rabbit	Cell Signaling	8054	1:1000
p62	mouse	Abcam	ab56416	1:200

References

1. Pasca, A.M., et al., *Functional cortical neurons and astrocytes from human pluripotent stem cells in 3D culture.* Nat Methods, 2015. **12**(7): p. 671-8.
2. Blair, J.D. and H.S. Bateup, *New frontiers in modeling tuberous sclerosis with human stem cell-derived neurons and brain organoids.* Dev Dyn, 2020. **249**(1): p. 46-55.
3. O'Callaghan, F.J.K., et al., *Prevalence of tuberous sclerosis estimated by capture-recapture analysis.* The Lancet, 1998. **351**(9114).
4. Ebrahimi-Fakhari, D., et al., *Incidence of tuberous sclerosis and age at first diagnosis: new data and emerging trends from a national, prospective surveillance study.* Orphanet J Rare Dis, 2018. **13**(1): p. 117.
5. Hong, C.H., T.N. Darling, and C.H. Lee, *Prevalence of tuberous sclerosis complex in Taiwan: a national population-based study.* Neuroepidemiology, 2009. **33**(4): p. 335-41.
6. Crino, P.B., K.L. Nathanson, and E.P. Henske, *The Tuberous Sclerosis Complex.* N Engl J Med, 2006. **355**: p. 1345-56.
7. Kingswood, J.C., et al., *TuberOus SClerosis registry to increase disease Awareness (TOSCA) - baseline data on 2093 patients.* Orphanet J Rare Dis, 2017. **12**(1): p. 2.
8. Chu-Shore, C.J., et al., *The natural history of epilepsy in tuberous sclerosis complex.* Epilepsia, 2010. **51**(7): p. 1236-41.
9. Mizuguchi, M. and S. Takashima, *Neuropathology of tuberous sclerosis.* Brain Dev, 2001. **23**(7): p. 508-15.
10. van Slegtenhorst, M., et al., *Identification of the Tuberous Sclerosis Gene TSC1 on Chromosome 9q34.* Science, 1997. **277**(5327): p. 805-808.
11. Consortium, E.C.T.S., *Identification and Characterization of the tuberous sclerosis gene on chromosome 16.* Cell, 1993. **75**: p. 1305-1315.
12. Dibble, C.C., et al., *TBC1D7 is a third subunit of the TSC1-TSC2 complex upstream of mTORC1.* Mol Cell, 2012. **47**(4): p. 535-46.
13. Tee, A.R., et al., *Tuberous sclerosis complex-1 and -2 gene products function together to inhibit mammalian target of rapamycin (mTOR)-mediated downstream signaling.* Proc Natl Acad Sci U S A, 2002. **99**(21): p. 13571-6.
14. Gai, Z., et al., *Structure of the TBC1D7-TSC1 complex reveals that TBC1D7 stabilizes dimerization of the TSC1 C-terminal coiled coil region.* J Mol Cell Biol, 2016. **8**(5): p. 411-425.
15. Chong-Kopera, H., et al., *TSC1 stabilizes TSC2 by inhibiting the interaction between TSC2 and the HERC1 ubiquitin ligase.* J Biol Chem, 2006. **281**(13): p. 8313-6.
16. Saxton, R.A. and D.M. Sabatini, *mTOR Signaling in Growth, Metabolism, and Disease.* Cell, 2017. **168**(6): p. 960-976.
17. Lawrence, R.E., et al., *A nutrient-induced affinity switch controls mTORC1 activation by its Rag GTPase-Ragulator lysosomal scaffold.* Nat Cell Biol, 2018. **20**(9): p. 1052-1063.
18. Thoreen, C.C., et al., *A unifying model for mTORC1-mediated regulation of mRNA translation.* Nature, 2012. **485**(7396): p. 109-13.

19. Ruvinsky, I., et al., *Ribosomal protein S6 phosphorylation is a determinant of cell size and glucose homeostasis.* Genes Dev, 2005. **19**(18): p. 2199-211.
20. Kim, J., et al., *AMPK and mTOR regulate autophagy through direct phosphorylation of Ulk1.* Nat Cell Biol, 2011. **13**(2): p. 132-41.
21. Russell, R.C., et al., *ULK1 induces autophagy by phosphorylating Beclin-1 and activating VPS34 lipid kinase.* Nat Cell Biol, 2013. **15**(7): p. 741-50.
22. Sarbassov, D.D., et al., *Rictor, a novel binding partner of mTOR, defines a rapamycin-insensitive and raptor-independent pathway that regulates the cytoskeleton.* Curr Biol, 2004. **14**(14): p. 1296-302.
23. Fingar, D.C., et al., *Mammalian cell size is controlled by mTOR and its downstream targets S6K1 and 4EBP1/eIF4E.* Genes Dev, 2002. **16**(12): p. 1472-87.
24. Crino, P.B., *mTOR: A pathogenic signaling pathway in developmental brain malformations.* Trends Mol Med, 2011. **17**(12): p. 734-42.
25. Crino, P.B., *mTOR signaling in epilepsy: insights from malformations of cortical development.* Cold Spring Harb Perspect Med, 2015. **5**(4).
26. Reijnders, M.R.F., et al., *Variation in a range of mTOR-related genes associates with intracranial volume and intellectual disability.* Nat Commun, 2017. **8**(1): p. 1052.
27. Grabiner, B.C., et al., *A diverse array of cancer-associated MTOR mutations are hyperactivating and can predict rapamycin sensitivity.* Cancer Discov, 2014. **4**(5): p. 554-63.
28. Martin, K.R., et al., *The genomic landscape of tuberous sclerosis complex.* Nat Commun, 2017. **8**: p. 15816.
29. Rosset, C., C.B.O. Netto, and P. Ashton-Prolla, *TSC1 and TSC2 gene mutations and their implications for treatment in Tuberous Sclerosis Complex: a review.* Genet Mol Biol, 2017. **40**(1): p. 69-79.
30. Crino, P.B., *The mTOR signalling cascade: paving new roads to cure neurological disease.* Nat Rev Neurol, 2016. **12**(7): p. 379-92.
31. Qin, W., et al., *Analysis of TSC cortical tubers by deep sequencing of TSC1, TSC2 and KRAS demonstrates that small second-hit mutations in these genes are rare events.* Brain Pathol, 2010. **20**(6): p. 1096-105.
32. Takahashi, D.K., et al., ***Abnormal Cortical Cells and Astrocytomas in the Eker Rat Model of Tuberous Sclerosis Complex****.* Epilepsia, 2004. **45**(12): p. 1525-1530.
33. Lui, J.H., D.V. Hansen, and A.R. Kriegstein, *Development and evolution of the human neocortex.* Cell, 2011. **146**(1): p. 18-36.
34. Hansen, D.V., et al., *Neurogenic radial glia in the outer subventricular zone of human neocortex.* Nature, 2010. **464**(7288): p. 554-561.
35. Rowitch, D.H. and A.R. Kriegstein, *Developmental genetics of vertebrate glial-cell specification.* Nature, 2010. **468**(7321): p. 214-22.
36. Zecevic, N., F. Hu, and I. Jakovcevski, *Interneurons in the developing human neocortex.* Dev Neurobiol, 2011. **71**(1): p. 18-33.
37. Lim, L., et al., *Development and Functional Diversification of Cortical Interneurons.* Neuron, 2018. **100**(2): p. 294-313.

38. Greig, L.C., et al., *Molecular logic of neocortical projection neuron specification, development and diversity.* Nat Rev Neurosci, 2013. **14**(11): p. 755-69.
39. Bayraktar, O.A., et al., *Astrocyte development and heterogeneity.* Cold Spring Harb Perspect Biol, 2014. **7**(1): p. a020362.
40. Stiles, J. and T.L. Jernigan, *The basics of brain development.* Neuropsychol Rev, 2010. **20**(4): p. 327-48.
41. Roessmann, U. and P. Gambetti, *Astrocytes in the developing human brain. An immunohistochemical study.* Acta Neuropathol, 1986. **70**(3-4): p. 308-13.
42. Kwiatkowski, D.J., et al., *A mouse model of TSC1 reveals sex-dependent lethality from liver hemangiomas, and up-regulation of p70S6 kinase activity in Tsc1 null cells.* Hum Mol Genet, 2002. **11**(5): p. 525-34.
43. Onda, H., et al., *Tsc2(+/-) mice develop tumors in multiple sites that express gelsolin and are influenced by genetic background.* J Clin Invest, 1999. **104**(6): p. 687-95.
44. Talos, D.M., et al., *Cell-specific alterations of glutamate receptor expression in tuberous sclerosis complex cortical tubers.* Ann Neurol, 2008. **63**(4): p. 454-65.
45. Sosunov, A.A., et al., *Epileptogenic but MRI-normal perituberal tissue in Tuberous Sclerosis Complex contains tuber-specific abnormalities.* Acta Neuropathol Commun, 2015. **3**: p. 17.
46. Ruppe, V., et al., *Developmental brain abnormalities in tuberous sclerosis complex: a comparative tissue analysis of cortical tubers and perituberal cortex.* Epilepsia, 2014. **55**(4): p. 539-50.
47. Fallah, A., et al., *Predictors of seizure outcomes in children with tuberous sclerosis complex and intractable epilepsy undergoing resective epilepsy surgery: an individual participant data meta-analysis.* PLoS One, 2013. **8**(2): p. e53565.
48. Overwater, I.E., et al., *Epilepsy in children with tuberous sclerosis complex: Chance of remission and response to antiepileptic drugs.* Epilepsia, 2015. **56**(8): p. 1239-45.
49. Klawitter, J., B. Nashan, and U. Christians, *Everolimus and sirolimus in transplantation-related but different.* Expert Opin Drug Saf, 2015. **14**(7): p. 1055-70.
50. Yang, H., et al., *mTOR kinase structure, mechanism and regulation.* Nature, 2013. **497**(7448): p. 217-23.
51. Koenig, M.K., et al., *Efficacy and Safety of Topical Rapamycin in Patients With Facial Angiofibromas Secondary to Tuberous Sclerosis Complex: The TREATMENT Randomized Clinical Trial.* JAMA Dermatol, 2018. **154**(7): p. 773-780.
52. French, J.A., et al., *Adjunctive everolimus therapy for treatment-resistant focal-onset seizures associated with tuberous sclerosis (EXIST-3): a phase 3, randomised, double-blind, placebo-controlled study.* The Lancet, 2016. **388**(10056): p. 2153-2163.
53. Krueger, D.A., et al., *Everolimus for treatment of tuberous sclerosis complex-associated neuropsychiatric disorders.* Ann Clin Transl Neurol, 2017. **4**(12): p. 877-887.

54. Miller, J.M., et al., *The effects of everolimus on tuberous sclerosis-associated lesions can be dramatic but may be impermanent.* Pediatr Nephrol, 2015. **30**(1): p. 173-7.
55. Thoreen, C.C., et al., *An ATP-competitive mammalian target of rapamycin inhibitor reveals rapamycin-resistant functions of mTORC1.* J Biol Chem, 2009. **284**(12): p. 8023-32.
56. Chung, C.Y., et al., *Covalent targeting of the vacuolar H(+)-ATPase activates autophagy via mTORC1 inhibition.* Nat Chem Biol, 2019. **15**(8): p. 776-785.
57. Zhang, H., et al., *Regulation of cellular growth by the Drosophila target of rapamycin dTOR.* Genes Dev, 2000. **14**(21): p. 2712-24.
58. Loewith, R. and M.N. Hall, *Target of rapamycin (TOR) in nutrient signaling and growth control.* Genetics, 2011. **189**(4): p. 1177-201.
59. Hernandez, O., et al., *Generation of a conditional disruption of the Tsc2 gene.* Genesis, 2007. **45**(2): p. 101-6.
60. Park, S.M., et al., *Brain Somatic Mutations in MTOR Disrupt Neuronal Ciliogenesis, Leading to Focal Cortical Dyslamination.* Neuron, 2018. **99**(1): p. 83-97 e7.
61. Nguyen, L.H., T. Mahadeo, and A. Bordey, *mTOR Hyperactivity Levels Influence the Severity of Epilepsy and Associated Neuropathology in an Experimental Model of Tuberous Sclerosis Complex and Focal Cortical Dysplasia.* J Neurosci, 2019.
62. Lin, T.V., et al., *Normalizing translation through 4E-BP prevents mTOR-driven cortical mislamination and ameliorates aberrant neuron integration.* Proc Natl Acad Sci U S A, 2016. **113**(40): p. 11330-11335.
63. Lim, J.S., et al., *Somatic Mutations in TSC1 and TSC2 Cause Focal Cortical Dysplasia.* Am J Hum Genet, 2017. **100**(3): p. 454-472.
64. Eker, R., et al., *Hereditary renal adenomas and adenocarcinomas in rats.* Diagn Histopathol, 1981. **4**(1): p. 99-110.
65. Wenzel, H.J., et al., *Morphology of cerebral lesions in the Eker rat model of tuberous sclerosis.* Acta Neuropathol, 2004. **108**(2): p. 97-108.
66. Tsai, P. and M. Sahin, *Mechanisms of neurocognitive dysfunction and therapeutic considerations in tuberous sclerosis complex.* Curr Opin Neurol, 2011. **24**(2): p. 106-13.
67. Lipton, J.O. and M. Sahin, *The neurology of mTOR.* Neuron, 2014. **84**(2): p. 275-91.
68. Costa-Mattioli, M. and L.M. Monteggia, *mTOR complexes in neurodevelopmental and neuropsychiatric disorders.* Nat Neurosci, 2013. **16**(11): p. 1537-43.
69. Magri, L. and R. Galli, *mTOR signaling in neural stem cells: from basic biology to disease.* Cell Mol Life Sci, 2013. **70**(16): p. 2887-98.
70. Crino, P.B., *Evolving neurobiology of tuberous sclerosis complex.* Acta Neuropathol, 2013. **125**(3): p. 317-32.
71. Ehninger, D., et al., *Reversal of learning deficits in a Tsc2+/- mouse model of tuberous sclerosis.* Nat Med, 2008. **14**(8): p. 843-8.
72. Auerbach, B.D., E.K. Osterweil, and M.F. Bear, *Mutations causing syndromic autism define an axis of synaptic pathophysiology.* Nature, 2011. **480**(7375): p. 63-8.

73. Sato, A., et al., *Rapamycin reverses impaired social interaction in mouse models of tuberous sclerosis complex.* Nat Commun, 2012. **3**: p. 1292.
74. Tsai, P.T., et al., *Autistic-like behaviour and cerebellar dysfunction in Purkinje cell Tsc1 mutant mice.* Nature, 2012. **488**(7413): p. 647-51.
75. Takahashi, K. and S. Yamanaka, *Induction of pluripotent stem cells from mouse embryonic and adult fibroblast cultures by defined factors.* Cell, 2006. **126**(4): p. 663-76.
76. Mali, P., et al., *RNA-guided human genome engineering via Cas9.* Science, 2013. **339**(6121): p. 823-6.
77. Blair, J.D., D. Hockemeyer, and H.S. Bateup, *Genetically engineered human cortical spheroid models of tuberous sclerosis.* Nat Med, 2018. **24**(10): p. 1568-1578.
78. Chiba, K., et al., *Cancer-associated TERT promoter mutations abrogate telomerase silencing.* Elife, 2015. **4**.
79. Blair, J.D., H.S. Bateup, and D.F. Hockemeyer, *Establishment of Genome-edited Human Pluripotent Stem Cell Lines: From Targeting to Isolation.* J Vis Exp, 2016(108): p. e53583.
80. Aoto, J., et al., *Distinct circuit-dependent functions of presynaptic neurexin-3 at GABAergic and glutamatergic synapses.* Nat Neurosci, 2015. **18**(7): p. 997-1007.
81. Wang, C., et al., *Scalable Production of iPSC-Derived Human Neurons to Identify Tau-Lowering Compounds by High-Content Screening.* Stem Cell Reports, 2017. **9**(4): p. 1221-1233.
82. Tian, R., et al., *CRISPR Interference-Based Platform for Multimodal Genetic Screens in Human iPSC-Derived Neurons.* Neuron, 2019. **104**(2): p. 239-255.e12.
83. Hockemeyer, D., et al., *Efficient targeting of expressed and silent genes in human ESCs and iPSCs using zinc-finger nucleases.* Nat Biotechnol, 2009. **27**(9): p. 851-7.
84. Chambers, S.M., et al., *Highly efficient neural conversion of human ES and iPS cells by dual inhibition of SMAD signaling.* Nat Biotechnol, 2009. **27**(3): p. 275-80.
85. Zhang, Y., et al., *Rapid single-step induction of functional neurons from human pluripotent stem cells.* Neuron, 2013. **78**(5): p. 785-98.
86. Tsai, P.T., et al., *Sensitive Periods for Cerebellar-Mediated Autistic-like Behaviors.* Cell Rep, 2018. **25**(2): p. 357-367 e4.
87. Stoodley, C.J., et al., *Altered cerebellar connectivity in autism and cerebellar-mediated rescue of autism-related behaviors in mice.* Nat Neurosci, 2017. **20**(12): p. 1744-1751.
88. Sundberg, M., et al., *Purkinje cells derived from TSC patients display hypoexcitability and synaptic deficits associated with reduced FMRP levels and reversed by rapamycin.* Mol Psychiatry, 2018. **23**(11): p. 2167-2183.
89. Lancaster, M.A., et al., *Cerebral organoids model human brain development and microcephaly.* Nature, 2013. **501**(7467): p. 373-9.
90. Qian, X., et al., *Brain-Region-Specific Organoids Using Mini-bioreactors for Modeling ZIKV Exposure.* Cell, 2016. **165**(5): p. 1238-1254.

91. Kadoshima, T., et al., *Self-organization of axial polarity, inside-out layer pattern, and species-specific progenitor dynamics in human ES cell-derived neocortex.* Proc Natl Acad Sci U S A, 2013. **110**(50): p. 20284-9.
92. Chen, H.I., H. Song, and G.L. Ming, *Applications of Human Brain Organoids to Clinical Problems.* Dev Dyn, 2019. **248**(1): p. 53-64.
93. Costa, V., et al., *mTORC1 Inhibition Corrects Neurodevelopmental and Synaptic Alterations in a Human Stem Cell Model of Tuberous Sclerosis.* Cell Rep, 2016. **15**(1): p. 86-95.
94. Grabole, N., et al., *Genomic analysis of the molecular neuropathology of tuberous sclerosis using a human stem cell model.* Genome Med, 2016. **8**(1): p. 94.
95. Li, Y., et al., *Abnormal Neural Progenitor Cells Differentiated from Induced Pluripotent Stem Cells Partially Mimicked Development of TSC2 Neurological Abnormalities.* Stem Cell Reports, 2017. **8**(4): p. 883-893.
96. Nadadhur, A.G., et al., *Neuron-Glia Interactions Increase Neuronal Phenotypes in Tuberous Sclerosis Complex Patient iPSC-Derived Models.* Stem Cell Reports, 2019. **12**(1): p. 42-56.
97. Zucco, A.J., et al., *Neural progenitors derived from Tuberous Sclerosis Complex patients exhibit attenuated PI3K/AKT signaling and delayed neuronal differentiation.* Mol Cell Neurosci, 2018. **92**: p. 149-163.
98. Ebrahimi-Fakhari, D., et al., *Impaired Mitochondrial Dynamics And Mitophagy In Neuronal Models Of Tuberous Sclerosis Complex.* Cell Rep, 2016. **17**(8): p. 2162.
99. Boer, K., et al., *Inflammatory processes in cortical tubers and subependymal giant cell tumors of tuberous sclerosis complex.* Epilepsy Res, 2008. **78**(1): p. 7-21.
100. Tyburczy, M.E., et al., *Novel proteins regulated by mTOR in subependymal giant cell astrocytomas of patients with tuberous sclerosis complex and new therapeutic implications.* Am J Pathol, 2010. **176**(4): p. 1878-90.
101. Blair, J.D., et al., *Widespread Translational Remodeling during Human Neuronal Differentiation.* Cell Rep, 2017. **21**(7): p. 2005-2016.
102. Bateup, H.S., et al., *Excitatory/inhibitory synaptic imbalance leads to hippocampal hyperexcitability in mouse models of tuberous sclerosis.* Neuron, 2013. **78**(3): p. 510-22.
103. Talos, D.M., et al., *Altered inhibition in tuberous sclerosis and type IIb cortical dysplasia.* Ann Neurol, 2012. **71**(4): p. 539-51.
104. Jay, V., et al., *Cerebellar pathology in tuberous sclerosis.* Ultrastruct Pathol, 1998. **22**(4): p. 331-9.
105. Vaughn, J., et al., *MRI characterization and longitudinal study of focal cerebellar lesions in a young tuberous sclerosis cohort.* AJNR Am J Neuroradiol, 2013. **34**(3): p. 655-9.
106. Pollen, A.A., et al., *Establishing Cerebral Organoids as Models of Human-Specific Brain Evolution.* Cell, 2019. **176**(4): p. 743-756 e17.
107. Bershteyn, M., et al., *Human iPSC-Derived Cerebral Organoids Model Cellular Features of Lissencephaly and Reveal Prolonged Mitosis of Outer Radial Glia.* Cell Stem Cell, 2017. **20**(4): p. 435-449 e4.

108. Bhaduri, A., et al., *Cell stress in cortical organoids impairs molecular subtype specification.* Nature, 2020. **578**(7793): p. 142-148.
109. Yoon, S.J., et al., *Reliability of human cortical organoid generation.* Nat Methods, 2019. **16**(1): p. 75-78.
110. Birey, F., et al., *Assembly of functionally integrated human forebrain spheroids.* Nature, 2017. **545**(7652): p. 54-59.
111. Watanabe, M., et al., *Self-Organized Cerebral Organoids with Human-Specific Features Predict Effective Drugs to Combat Zika Virus Infection.* Cell Rep, 2017. **21**(2): p. 517-532.
112. Li, Y., et al., *Induction of Expansion and Folding in Human Cerebral Organoids.* Cell Stem Cell, 2017. **20**(3): p. 385-396.e3.
113. Zheng, G.X., et al., *Massively parallel digital transcriptional profiling of single cells.* Nat Commun, 2017. **8**: p. 14049.
114. Stuart, T., et al., *Comprehensive Integration of Single-Cell Data.* Cell, 2019. **177**(7): p. 1888-1902.e21.
115. Cao, J., et al., *The single-cell transcriptional landscape of mammalian organogenesis.* Nature, 2019. **566**(7745): p. 496-502.
116. Lopez, R., et al., *Deep generative modeling for single-cell transcriptomics.* Nat Methods, 2018. **15**(12): p. 1053-1058.
117. Sloan, S.A., et al., *Human Astrocyte Maturation Captured in 3D Cerebral Cortical Spheroids Derived from Pluripotent Stem Cells.* Neuron, 2017. **95**(4): p. 779-790 e6.
118. Velasco, S., et al., *Individual brain organoids reproducibly form cell diversity of the human cerebral cortex.* Nature, 2019. **570**(7762): p. 523-527.
119. Kanton, S., et al., *Organoid single-cell genomic atlas uncovers human-specific features of brain development.* Nature, 2019. **574**(7778): p. 418-422.
120. Polioudakis, D., et al., *A Single-Cell Transcriptomic Atlas of Human Neocortical Development during Mid-gestation.* Neuron, 2019. **103**(5): p. 785-801 e8.
121. van Slegtenhorst, M., et al., *Identification of the tuberous sclerosis gene TSC1 on chromosome 9q34.* Science, 1997. **277**(5327): p. 805-8.
122. European Chromosome 16 Tuberous Sclerosis, C., *Identification and characterization of the tuberous sclerosis gene on chromosome 16.* Cell, 1993. **75**(7): p. 1305-15.
123. Crino, P.B., K.L. Nathanson, and E.P. Henske, *The tuberous sclerosis complex.* N Engl J Med, 2006. **355**(13): p. 1345-56.
124. Thiele, E.A., *Managing and understanding epilepsy in tuberous sclerosis complex.* Epilepsia, 2010. **51 Suppl 1**: p. 90-1.
125. Curatolo, P., R. Moavero, and P.J. de Vries, *Neurological and neuropsychiatric aspects of tuberous sclerosis complex.* Lancet Neurol, 2015. **14**(7): p. 733-45.
126. Mohamed, A.R., et al., *Intrinsic epileptogenicity of cortical tubers revealed by intracranial EEG monitoring.* Neurology, 2012. **79**(23): p. 2249-57.
127. Jansen, F.E., et al., *Cognitive impairment in tuberous sclerosis complex is a multifactorial condition.* Neurology, 2008. **70**(12): p. 916-23.
128. Magri, L., et al., *Sustained activation of mTOR pathway in embryonic neural stem cells leads to development of tuberous sclerosis complex-associated lesions.* Cell Stem Cell, 2011. **9**(5): p. 447-62.

129. Feliciano, D.M., et al., *Single-cell Tsc1 knockout during corticogenesis generates tuber-like lesions and reduces seizure threshold in mice.* J Clin Invest, 2011. **121**(4): p. 1596-607.
130. Way, S.W., et al., *Loss of Tsc2 in radial glia models the brain pathology of tuberous sclerosis complex in the mouse.* Hum Mol Genet, 2009. **18**(7): p. 1252-65.
131. Onda, H., et al., *Tsc2 null murine neuroepithelial cells are a model for human tuber giant cells, and show activation of an mTOR pathway.* Mol Cell Neurosci, 2002. **21**(4): p. 561-74.
132. Carson, R.P., et al., *Neuronal and glia abnormalities in Tsc1-deficient forebrain and partial rescue by rapamycin.* Neurobiol Dis, 2012. **45**(1): p. 369-80.
133. Goto, J., et al., *Regulable neural progenitor-specific Tsc1 loss yields giant cells with organellar dysfunction in a model of tuberous sclerosis complex.* Proc Natl Acad Sci U S A, 2011. **108**(45): p. E1070-9.
134. Meikle, L., et al., *A mouse model of tuberous sclerosis: neuronal loss of Tsc1 causes dysplastic and ectopic neurons, reduced myelination, seizure activity, and limited survival.* J Neurosci, 2007. **27**(21): p. 5546-58.
135. Zeng, L.H., et al., *Tsc2 gene inactivation causes a more severe epilepsy phenotype than Tsc1 inactivation in a mouse model of tuberous sclerosis complex.* Hum Mol Genet, 2011. **20**(3): p. 445-54.
136. Silbereis, J.C., et al., *The Cellular and Molecular Landscapes of the Developing Human Central Nervous System.* Neuron, 2016. **89**(2): p. 248-68.
137. Dehay, C. and H. Kennedy, *Cell-cycle control and cortical development.* Nat Rev Neurosci, 2007. **8**(6): p. 438-50.
138. Florio, M. and W.B. Huttner, *Neural progenitors, neurogenesis and the evolution of the neocortex.* Development, 2014. **141**(11): p. 2182-94.
139. Ma, X.M. and J. Blenis, *Molecular mechanisms of mTOR-mediated translational control.* Nat Rev Mol Cell Biol, 2009. **10**(5): p. 307-18.
140. Inoki, K., et al., *Rheb GTPase is a direct target of TSC2 GAP activity and regulates mTOR signaling.* Genes Dev, 2003. **17**(15): p. 1829-34.
141. Huang, J. and B.D. Manning, *The TSC1-TSC2 complex: a molecular switchboard controlling cell growth.* Biochem J, 2008. **412**(2): p. 179-90.
142. Laplante, M. and D.M. Sabatini, *mTOR signaling in growth control and disease.* Cell, 2012. **149**(2): p. 274-93.
143. Au, K.S., et al., *Complete inactivation of the TSC2 gene leads to formation of hamartomas.* Am J Hum Genet, 1999. **65**(6): p. 1790-5.
144. Henske, E.P., et al., *Allelic loss is frequent in tuberous sclerosis kidney lesions but rare in brain lesions.* Am J Hum Genet, 1996. **59**(2): p. 400-6.
145. Smolarek, T.A., et al., *Evidence that lymphangiomyomatosis is caused by TSC2 mutations: chromosome 16p13 loss of heterozygosity in angiomyolipomas and lymph nodes from women with lymphangiomyomatosis.* Am J Hum Genet, 1998. **62**(4): p. 810-5.
146. Sepp, T., J.R. Yates, and A.J. Green, *Loss of heterozygosity in tuberous sclerosis hamartomas.* J Med Genet, 1996. **33**(11): p. 962-4.

147. Chan, J.A., et al., *Pathogenesis of tuberous sclerosis subependymal giant cell astrocytomas: biallelic inactivation of TSC1 or TSC2 leads to mTOR activation.* J Neuropathol Exp Neurol, 2004. **63**(12): p. 1236-42.
148. Crino, P.B., et al., *Biallelic TSC gene inactivation in tuberous sclerosis complex.* Neurology, 2010. **74**(21): p. 1716-23.
149. de Vries, P.J. and C.J. Howe, *The tuberous sclerosis complex proteins--a GRIPP on cognition and neurodevelopment.* Trends Mol Med, 2007. **13**(8): p. 319-26.
150. Goorden, S.M., et al., *Cognitive deficits in Tsc1+/- mice in the absence of cerebral lesions and seizures.* Ann Neurol, 2007. **62**(6): p. 648-55.
151. Ehninger, D., et al., *Reversal of learning deficits in a Tsc2(+/-) mouse model of tuberous sclerosis.* Nat Med, 2008. **14**(8): p. 843-8.
152. Jones, A.C., et al., *Molecular genetic and phenotypic analysis reveals differences between TSC1 and TSC2 associated familial and sporadic tuberous sclerosis.* Hum Mol Genet, 1997. **6**(12): p. 2155-61.
153. Cheadle, J.P., et al., *Molecular genetic advances in tuberous sclerosis.* Hum Genet, 2000. **107**(2): p. 97-114.
154. Dabora, S.L., et al., *Mutational analysis in a cohort of 224 tuberous sclerosis patients indicates increased severity of TSC2, compared with TSC1, disease in multiple organs.* Am J Hum Genet, 2001. **68**(1): p. 64-80.
155. Lengner, C.J., et al., *Derivation of pre-X inactivation human embryonic stem cells under physiological oxygen concentrations.* Cell, 2010. **141**(5): p. 872-83.
156. Dan, H.C., et al., *Phosphatidylinositol 3-kinase/Akt pathway regulates tuberous sclerosis tumor suppressor complex by phosphorylation of tuberin.* J Biol Chem, 2002. **277**(38): p. 35364-70.
157. Efeyan, A. and D.M. Sabatini, *mTOR and cancer: many loops in one pathway.* Curr Opin Cell Biol, 2010. **22**(2): p. 169-76.
158. Woodford, M.R., et al., *Tumor suppressor Tsc1 is a new Hsp90 co-chaperone that facilitates folding of kinase and non-kinase clients.* EMBO J, 2017. **36**(24): p. 3650-3665.
159. Capo-Chichi, J.M., et al., *Disruption of TBC1D7, a subunit of the TSC1-TSC2 protein complex, in intellectual disability and megalencephaly.* J Med Genet, 2013. **50**(11): p. 740-4.
160. Miller, F.D. and A.S. Gauthier, *Timing is everything: making neurons versus glia in the developing cortex.* Neuron, 2007. **54**(3): p. 357-69.
161. Bonni, A., et al., *Regulation of gliogenesis in the central nervous system by the JAK-STAT signaling pathway.* Science, 1997. **278**(5337): p. 477-83.
162. Au, K.S., et al., *Genotype/phenotype correlation in 325 individuals referred for a diagnosis of tuberous sclerosis complex in the United States.* Genet Med, 2007. **9**(2): p. 88-100.
163. Hockemeyer, D., et al., *Genetic engineering of human pluripotent cells using TALE nucleases.* Nat Biotechnol, 2011. **29**(8): p. 731-4.
164. Sosunov, A.A., et al., *Tuberous sclerosis: a primary pathology of astrocytes?* Epilepsia, 2008. **49 Suppl 2**: p. 53-62.
165. Cloetta, D., et al., *Inactivation of mTORC1 in the developing brain causes microcephaly and affects gliogenesis.* J Neurosci, 2013. **33**(18): p. 7799-810.

166. Tsai, P.T., et al., *Prenatal rapamycin results in early and late behavioral abnormalities in wildtype C57BL/6 mice.* Behav Genet, 2013. **43**(1): p. 51-9.
167. D'Gama, A.M., et al., *Somatic Mutations Activating the mTOR Pathway in Dorsal Telencephalic Progenitors Cause a Continuum of Cortical Dysplasias.* Cell Rep, 2017. **21**(13): p. 3754-3766.
168. Maldonado, M., et al., *Expression of ICAM-1, TNF-alpha, NF kappa B, and MAP kinase in tubers of the tuberous sclerosis complex.* Neurobiol Dis, 2003. **14**(2): p. 279-90.
169. Tyburczy, M.E., et al., *Mosaic and Intronic Mutations in TSC1/TSC2 Explain the Majority of TSC Patients with No Mutation Identified by Conventional Testing.* PLoS Genet, 2015. **11**(11): p. e1005637.
170. McConnell, M.J., et al., *Intersection of diverse neuronal genomes and neuropsychiatric disease: The Brain Somatic Mosaicism Network.* Science, 2017. **356**(6336).
171. Blair, J.D., H.S. Bateup, and D.F. Hockemeyer, *Establishment of Genome-edited Human Pluripotent Stem Cell Lines: From Targeting to Isolation.* J Vis Exp, 2016(108).
172. Mandal, P.K. and D.J. Rossi, *Reprogramming human fibroblasts to pluripotency using modified mRNA.* Nat Protoc, 2013. **8**(3): p. 568-82.
173. Cong, L., et al., *Multiplex genome engineering using CRISPR/Cas systems.* Science, 2013. **339**(6121): p. 819-23.
174. Madisen, L., et al., *A robust and high-throughput Cre reporting and characterization system for the whole mouse brain.* Nat Neurosci, 2010. **13**(1): p. 133-40.
175. Chambers, S.M., et al., *Converting human pluripotent stem cells to neural tissue and neurons to model neurodegeneration.* Methods Mol Biol, 2011. **793**: p. 87-97.
176. Saxton, R.A. and D.M. Sabatini, *mTOR Signaling in Growth, Metabolism, and Disease.* Cell, 2017. **169**(2): p. 361-371.
177. Hu, H., et al., *The C/EBP Homologous Protein (CHOP) Transcription Factor Functions in Endoplasmic Reticulum Stress-Induced Apoptosis and Microbial Infection.* Front Immunol, 2018. **9**: p. 3083.
178. Fiock, K.L., et al., *Increased Tau Expression Correlates with Neuronal Maturation in the Developing Human Cerebral Cortex.* eNeuro, 2020.
179. Zheng, X., et al., *Metabolic reprogramming during neuronal differentiation from aerobic glycolysis to neuronal oxidative phosphorylation.* Elife, 2016. **5**.
180. Foster, E.M., et al., *Clusterin in Alzheimer's Disease: Mechanisms, Genetics, and Lessons From Other Pathologies.* Front Neurosci, 2019. **13**: p. 164.
181. Yamazaki, Y., et al., *Apolipoprotein E and Alzheimer disease: pathobiology and targeting strategies.* Nat Rev Neurol, 2019. **15**(9): p. 501-518.
182. Zhao, W., et al., *Lack of CUL4B leads to increased abundance of GFAP-positive cells that is mediated by PTGDS in mouse brain.* Hum Mol Genet, 2015. **24**(16): p. 4686-97.
183. Morel, L., et al., *Intracortical astrocyte subpopulations defined by astrocyte reporter Mice in the adult brain.* Glia, 2019. **67**(1): p. 171-181.

184. Zamanian, J.L., et al., *Genomic analysis of reactive astrogliosis.* J Neurosci, 2012. **32**(18): p. 6391-410.
185. Morgado, A.L., et al., *MicroRNA-34a Modulates Neural Stem Cell Differentiation by Regulating Expression of Synaptic and Autophagic Proteins.* Mol Neurobiol, 2015. **51**(3): p. 1168-83.
186. Philippidou, P. and J.S. Dasen, *Hox genes: choreographers in neural development, architects of circuit organization.* Neuron, 2013. **80**(1): p. 12-34.
187. Zhang, Y., et al., *Purification and Characterization of Progenitor and Mature Human Astrocytes Reveals Transcriptional and Functional Differences with Mouse.* Neuron, 2016. **89**(1): p. 37-53.
188. Lin, H.H., et al., *Neuronatin promotes neural lineage in ESCs via Ca(2+) signaling.* Stem Cells, 2010. **28**(11): p. 1950-60.
189. Iwaki, T. and J. Tateishi, *Immunohistochemical Demonstration of AlphaB-Crystallin in Hamartomas of TuberousSclerosis.* Am J Pathol, 1991. **139**(6): p. 1303-1308.
190. Wang, F., et al., *Pivotal role of augmented alphaB-crystallin in tumor development induced by deficient TSC1/2 complex.* Oncogene, 2014. **33**(34): p. 4352-8.
191. Tanaka, Y., et al., *Synthetic Analyses of Single-Cell Transcriptomes from Multiple Brain Organoids and Fetal Brain.* Cell Rep, 2020. **30**(6): p. 1682-1689 e3.
192. Beaudoin, G.M., 3rd, et al., *Culturing pyramidal neurons from the early postnatal mouse hippocampus and cortex.* Nat Protoc, 2012. **7**(9): p. 1741-54.
193. Ingolia, N.T., et al., *Genome-Wide Analysis in Vivo of Translation with Nucleotide Resolution Using Ribosome Profiling.* Science, 2009. **324**(5924): p. 218-223.
194. Heiman, M., et al., *A translational profiling approach for the molecular characterization of CNS cell types.* Cell, 2008. **135**(4): p. 738-48.
195. Floor, S.N. and J.A. Doudna, *Tunable protein synthesis by transcript isoforms in human cells.* Elife, 2016. **5**.
196. Poulain, L., et al., *High mTORC1 activity drives glycolysis addiction and sensitivity to G6PD inhibition in acute myeloid leukemia cells.* Leukemia, 2017. **31**(11): p. 2326-2335.
197. Hetz, C., *The unfolded protein response: controlling cell fate decisions under ER stress and beyond.* Nat Rev Mol Cell Biol, 2012. **13**(2): p. 89-102.
198. Bernales, S., K.L. McDonald, and P. Walter, *Autophagy counterbalances endoplasmic reticulum expansion during the unfolded protein response.* PLoS Biol, 2006. **4**(12): p. e423.
199. Ebrahimi-Fakhari, D., et al., *Impaired Mitochondrial Dynamics and Mitophagy in Neuronal Models of Tuberous Sclerosis Complex.* Cell Rep, 2016. **17**(4): p. 1053-1070.
200. Eze, U.C., et al., *Heterogeneity of Human Neuroepithelial Cells and Early Radial Glia.* bioRxiv, 2020.
201. Heiman, M., et al., *Cell type-specific mRNA purification by translating ribosome affinity purification (TRAP).* Nat Protoc, 2014. **9**(6): p. 1282-91.
202. Bengtsson H., S.K., Bullard J., Hansen K., *aroma.affymetrix: A generic framework in R for analyzing small to very large Affymetrix data sets in bounded memory.* UCB-DOS Tech Report, 2008.

203. Johnson, W.E., C. Li, and A. Rabinovic, *Adjusting batch effects in microarray expression data using empirical Bayes methods.* Biostatistics, 2007. **8**(1): p. 118-27.
204. Ritchie, M.E., et al., *limma powers differential expression analyses for RNA-sequencing and microarray studies.* Nucleic Acids Res, 2015. **43**(7): p. e47.